CRANFIELD UNIVERSITY

SALEM KALIFA BRINI AHMED

A STUDY OF GAS LIFT ON OIL/WATER FLOW IN VERTICAL RISERS

SCHOOL OF ENGINEERING

PhD THESIS
Academic Year: 2013 - 2014

Supervisor: Prof. Hoi Yeung
January 2014

CRANFIELD UNIVERSITY

SCHOOL OF ENGINEERING
Department Of Offshore, Process And Energy Engineering

PhD THESIS

Academic Year 2013 - 2014

SALEM KALIFA BRINI AHMED

A study of gas lift on oil/water flow in vertical risers

Supervisor: Prof. Hoi Yeung
January 2014

This thesis is submitted in partial fulfilment of the requirements for
the degree of Doctor of Philosophy

ABSTRACT

Gas lift is a means of enhancing oil recovery from hydrocarbon reservoirs. Gas injected at the production riser base reduces the gravity component of the pressure drop and thereby, increases the supply of oil from the reservoir. Also, gas injection at the base of a riser helps to mitigate slugging and thus, improving the performance of the topside facility. In order to improve the efficiency of the gas lifting technique, a good understanding of the characteristics of gas-liquid multiphase flow in vertical pipes is very important.

In this study, experiments of gas/liquid (air/water) two-phase flows, liquid/liquid of oil/water two-phase flows and gas/liquid/liquid (air/oil/water) three-phase flows were conducted in a 10.5 m high 52 mm ID vertical riser. These experiments were performed at liquid and gas superficial velocities ranging from 0.25 to 2 m/s and ~0.1 to ~6.30 m/s, respectively. Dielectric oil and tap water were used as test fluids. Instruments such as Coriolis mass flow meter, single beam gamma densitometer and wire-mesh sensor (WMS) were employed for investigating the flow characteristics. For the experiments of gas/liquid (air/water) two-phase flow, flow patterns of Bubbly, slug, churn flow regimes and transition regions were identified under the experimental conditions. Also, for flow pattern identification and void fraction measurements, the capacitance WMS results are consistent with those obtained simultaneously by the gamma densitometer. Generally, the total pressure gradient along the vertical riser has shown a significant decrease as the injected gas superficial velocity increased. In addition, the rate of decrease in total pressure gradient at the lower injected gas superficial velocities was found to be higher than that for higher gas superficial velocities. The frictional pressure gradient was also found to increase as the injected gas superficial velocity increased.

For oil-water experiments, mixture density and total pressure gradient across the riser were found to increase with increasing water cut (ranging between 0 - 100%) and/or mixture superficial velocity. Phase slip between the oil and water was calculated and found to be significant at lower throughputs of 0.25 and 0.5 m/s. The phase inversion point always takes place at a point of input water cut

of 42% when the experiments started from pure oil to water, and at an input water cut of 45% when the experiment's route started from water to pure oil. The phase inversion point was accompanied by a peak increase of pressure gradient, particularly at higher oil-water mixture superficial velocities of 1, 1.5 and 2 m/s.

The effects of air injection rates on the fluid flow characteristics were studied by emphasizing the total pressure gradient behaviour and identifying the flow pattern by analysing the output signals from gamma and WMS in air/oil/water experiments. Generally, riser base gas injection does not affect the water cut at the phase inversion point. However, a slight shift forward for the identified phase inversion point was found at highest flow rates of injected gas where the flow patterns were indicated as churn to annular flow. In terms of pressure gradient, the gas lifting efficiency (lowering pressure gradient) shows greater improvement after the phase inversion point (higher water cuts) than before and also at the inversion point.

Also, it was found that the measured mean void fraction reaches its lowest value at the phase inversion point. These void fraction results were found to be consistent with previously published results.

Keywords:

Vertical multiphase flow, gas lift, phase inversion, void fraction, wire mesh sensor.

ACKNOWLEDGEMENTS

TABLE OF CONTENTS

LIST OF FIGURES

LIST OF TABLES

LIST OF EQUATIONS

LIST OF ABBREVIATIONS

CapWMS   Capacitance wire-mesh sensor

CondWMS   Conductive wire-mesh sensor

DP   Differential pressure

E&H   Endress and Hauser

ECT   Electrical Capacitance Tomography

ERT   Electrical Resistance Tomography

ESP   Electrical submersible pumping

GD   Gamma Densitometer

GOR   Gas oil ratio

GVF   Gas volume fraction

HG   Hard Gamma count

HZDR   Helmholtz-Zentrum Dresden-Rossendorf

ID   Internal Diameter

PDF   Probability Density Function

SG   Soft Gamma count

WC   Water cut

WMS   Wire-mesh Sensor

Nomenclature

$\left(\dfrac{dP}{dh}\right)_T$ Total pressure gradient (bar/m)

$\left(\dfrac{dP}{dh}\right)_a$ Acceleration pressure gradient, bar/m

$\left(\dfrac{dP}{dh}\right)_f$ Frictional pressure gradient, bar/m

$\left(\dfrac{dP}{dh}\right)_g$ Gravitational pressure gradient, bar/m

ρ_m Mixture density (kg/m^3)

ρ_g Gas density, (kg/m^3)

ρ_L Liquid density, (kg/m^3)

ρ_o	Oil density, (kg/m^3)
ρ_w	Water density, (kg/m^3)
g	Acceleration due to gravity, (m/s^2)
α	Gas void fraction
H_L	Liquid holdup
f	Frictional factor
f_s	The WMS system frame rate
U_m	Mixture velocity, m/s
D	Pipe diameter, m
R_e	Reynolds's number
K/D	Dimensional relative roughness
A_p	Cross-sectional area of the pipe (m^2)
A	Total cross-sectional area
U_{sg}	Gas superficial velocity, (m/s)
U_{sl}	Liquid superficial velocity (m/s)
Q_g	Actual gas flow rate (m^3/s)
Q_L	Actual liquid flow rate (m^3/s)
U_g	Actual gas velocity, (m/s)
U_L	Actual liquid velocity, (m/s)
U_o	Oil velocity (m/s)
U_w	Water velocity (m/s)
V_L	Volume of liquid, (m^3)
V_g	Volume of gas (m^3)
V	Total volume (m^3)
L_g	Length of line through the gas phase
L	Total length
s	Slip ratio
I	Mixture gamma radiation intensity
I_o	Initial intensity

I_{water}	Water flow gamma count rates
I_{Oil}	Oil flow gamma count rates
ε_w	In situ water fraction
ε_o	In situ oil fraction
γ	The attenuation coefficient of the component
μ_o	Oil viscosity, cSt (mPa.s)
μ_w	Water viscosity, cSt (mPa.s)
μ	Viscosity ratio
ρ	Density ratio
C	Inclination correction factor
N	Number of the cross section images

CHAPTER ONE

1. INTRODUCTION

1.1 Background

In contrast to single-phase flow, multiphase flow is a complex, simultaneous process of multiple fluids in the same geometry. Hence, the knowledge and prediction of multiphase flow behaviour (characteristics) is of paramount importance and determines the efficiency and effectiveness of the process and system in which multiphase flow is encountered. In industrial applications, gas-liquid, liquid-liquid and gas-liquid-liquid flows or any other combinations are frequently encountered.

In the offshore production and transportation of oil and gas resources, the conventional way to transport both produced gas and liquids is through a single flow-line (Figure 1-1) and then separate them on the plat-form or onshore. This, however, incurs challenges associated with gas/oil/water multiphase flows in pipelines. On the other hand, a riser is a very conventional geometry configuration in pipelines. The presence of multiphase flow in a riser pipe can: a) cause an increased hydrostatic pressure on the production well, which could have a number of unfavourable effects on the production and/or the oil reservoir; b) induce flow instability problems (e.g. large pressure gradient/flowrate fluctuations caused by severe slugging and hydrodynamic slugs) and may ultimately damage the pipe system itself. In order to deal with all those problems, the gas lift technique is a conventional method used in oil and gas operations.

Also, the total pressure gradient in the production riser consists of gravitational, frictional and acceleration components with the gravitational (hydrostatic) pressure drop dominating. Therefore, reduction in gravitational pressure gradient by gas aeration results in lower pressure loss and makes available enough energy for an appreciable oil production which drives the application of the gas lift technique.

Injected compressed gas affects the liquid flow in the wells and the risers in two ways: (i) the energy of expansion propels (drives) the liquid to the surface, (ii) the gas aerates the liquid to reduce its density/hydrostatic pressure (gravitational pressure gradient) which makes the liquid lighter and thus aids the fluids to reach to the top surface more easily and faster. The injected gas introduces more gas into the riser and increases the gas volume fraction (GVF) in the riser. The resultant effect is a change in the riser flow characteristics. Moreover, this method accounts for a significant portion of the energy consumption relating to oil/gas production. Thus how to improve the efficiency of the gas injection is of great interest to the oil/gas industries. To achieve this, it is necessary to obtain a better understanding of multiphase flow behaviours in a riser system under various processing conditions.
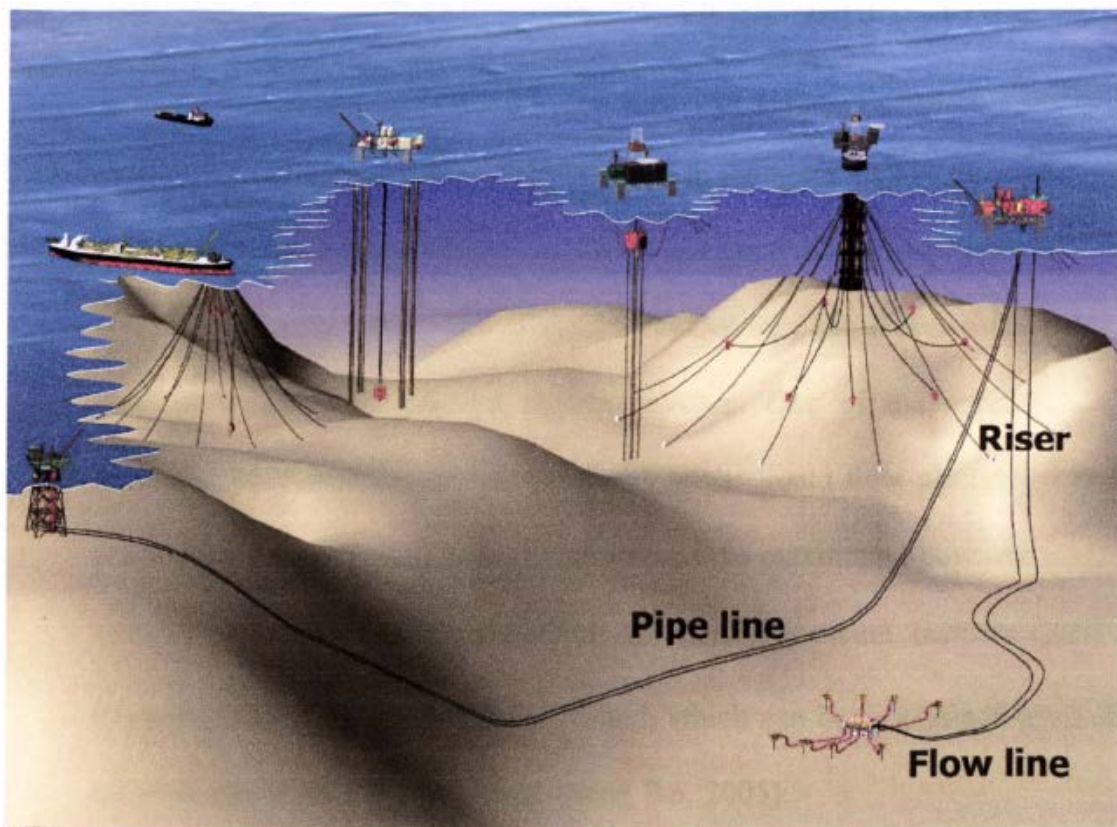
Figure 1-1: Flowline and Riser System in off-shore Production (Zangana, 2011)

.

1.2 Aim and Objectives

The importance of gas lift as a method of improving oil recovery from hydrocarbon reservoirs cannot be overemphasised. An improvement in the gas lift technique will directly lead to increased oil output. In order to improve the efficiency of the gas lifting technique, it is important to gain understanding of the characteristics of gas-liquid multiphase flow in vertical pipes.

Although some experimental studies have explored the flow behaviours of gas/liquid flows, such as gas/water and gas/oil flows, when the liquid is a single component fluid, there is evidence showing that the behaviours of gas/oil/water three-phase flow in a riser possess a variety of specific features which differ from those in gas/liquid two-phase flows.

Recent experimental works have shown that, sometimes the gas lift technique is not efficient in gas/oil/water flows. One of the reasons for this is the interplay between the individual components; another reason is the dependence of the continuous phase in the riser. When flow in the riser system changes from oil continuous flow to water continuous flow, the behaviour of multiphase flow also changes. Those specific behaviours lead to different phase distributions and frictional factors in a riser, which are extremely important for optimizing a gas-lift system design in risers/wells.

Therefore, the objective of this work is to study the behaviours of gas/liquid two-phase flows and gas/oil/water three-phase flows in a riser using the three-phase facility at Cranfield University with advanced instrumentation.

The main tasks for the study can be summarised as follows:

- Carry out a comprehensive literature review on the topic of the gas-lift technique in oil wells as well as in subsea riser systems. In addition, a literature review on two-phase (gas-liquid and liquid-liquid flows) and three-phase flows (gas/liquid/liquid, i.e. gas-oil-water) characteristics in vertical pipes will be carried out together with a review of the phase inversion phenomenon and its effect on the performance of gas lifting techniques.

- Carry out an initial experimental investigation using air-water two-phase flow in the vertical riser in order to understand the behaviour of two-phase flow and examine the data collection of the used instrumentations' response to comprehensive multiphase flow conditions.

- Investigate the phase inversion and associated phenomena that affects the performance of the gas-lift technique over a wide range of liquid flow rates and riser-base gas injection. Thus, systematic experimental work in a 52 mm internal diameter vertical riser for both oil/water and air/oil/water flows will be conducted.

- Compare this research results with that from previous vertical up flow experimental studies would be appropriate

- In order to gain information on phase fraction and distribution in the multiphase flow and flow patterns at various flow conditions, the new instrument of wire-mesh sensor (WMS) will be tested.

1.3 Structure of the thesis:

This thesis is organised as follows:

Chapter 1: introduction: this Chapter gives the background of the work and outlines the aims and objectives of the research.

Chapter 2: Literature review: this Chapter presents the concept of the gas lift technique in oil wells and risers. Relevant fundamentals of multiphase flow include the flow patterns found in vertical and horizontal pipes, and their identification methods will be defined. Commonly used techniques for phase fraction measurements are discussed. Phase inversion phenomena and their effects on multiphase flows will be highlighted. Previous research findings on the possible influences of gas injection techniques on flow characteristics will also be reviewed.

Chapter 3: Experimental Facility, Instrumentations and Data Acquisition: In this Chapter the experimental facility (the Three-Phase Test Facility at Cranfield University) includes a brief description of the 52 mm ID vertical riser and the

process is presented. This Chapter also describes the properties of fluids used, instrumentations used and data acquisition systems. Finally, the details of the experimental procedures and tests matrixes are described in this Chapter.

Chapter 4: This Chapter presents experimental results obtained from systematic experiments for air-water two-phase flows in the 52 mm riser under various conditions of riser-base gas injection. Also, experimental investigations on the effects of upstream conditions on the flow behaviour in the vertical riser section are included here. Finally, a comparison study between capacitance and conductive wire-mesh sensor measurements that were carried out on the air-water flow will be presented.

Chapter 5: More experimental results, analysis and discussion are presented in this Chapter. These are mainly about oil-water two-phase flows behaviours without gas injection and with various rates of riser base gas injection. Also, the results obtained from the WMS for oil-water and air-oil-water are included.

Chapter 6: Conclusion and Recommendations: this Chapter will present the research outputs and conclusions, and will summarise the recommendations for future research.

References are provided after Chapter 6, followed by Appendices.

CHAPTER TWO

2. LITERATURE REVIEW

This Chapter will provide the reader with an overview of the fundamentals of multiphase flow - in particular those subjects related to this study. It will also cover the concept of the gas lift technique as an artificial lift method in oil wells and riser systems, including the advantages and disadvantages of this technique. Common flow regimes encountered in vertical and horizontal flows and the methods of their identification are outlined. Also, some methods used for phase fraction measurements are presented. Moreover, the phase inversion phenomenon and its effect on gas lift efficiency are highlighted. A review of the previous research findings on the possible influences of gas injection techniques on multiphase flow characteristics is included.

2.1 Concept of Gas-lift

In general, artificial lift methods are required for oil production when reservoir pressure is inadequate to sustain oil flow to the surface, i.e. when the oil well no longer naturally flows, or when the oil production rate is too low to be economic or to enhance the production rate. These problems can be solved by the use of mechanical devices inside the oil well, such as a pump (rod pumping, electrical submersible pumping (ESP), progressing cavity or hydraulic pumping) or by decreasing the hydrostatic column in the tubing by injecting gas into the liquid column inside the production tube. Figure 2-1 shows the most popular types of artificial lift techniques including the gas lift method. Most of the artificially produced oil wells in the world employ the gas lift technique (Anon 2005). Figure 2-2 displays the participation of each artificial method in the production of a major international oil company, which clearly shows that the gas lift technique is the most used method, with about 52% of oil production from the major oil companies in the world. The technique is applicable in sandy and gassy oil wells, deviated wells, and deep wells and offshore, where other

artificial lift methods are not suitable. This makes gas lift a very flexible system (Takács, 2005).
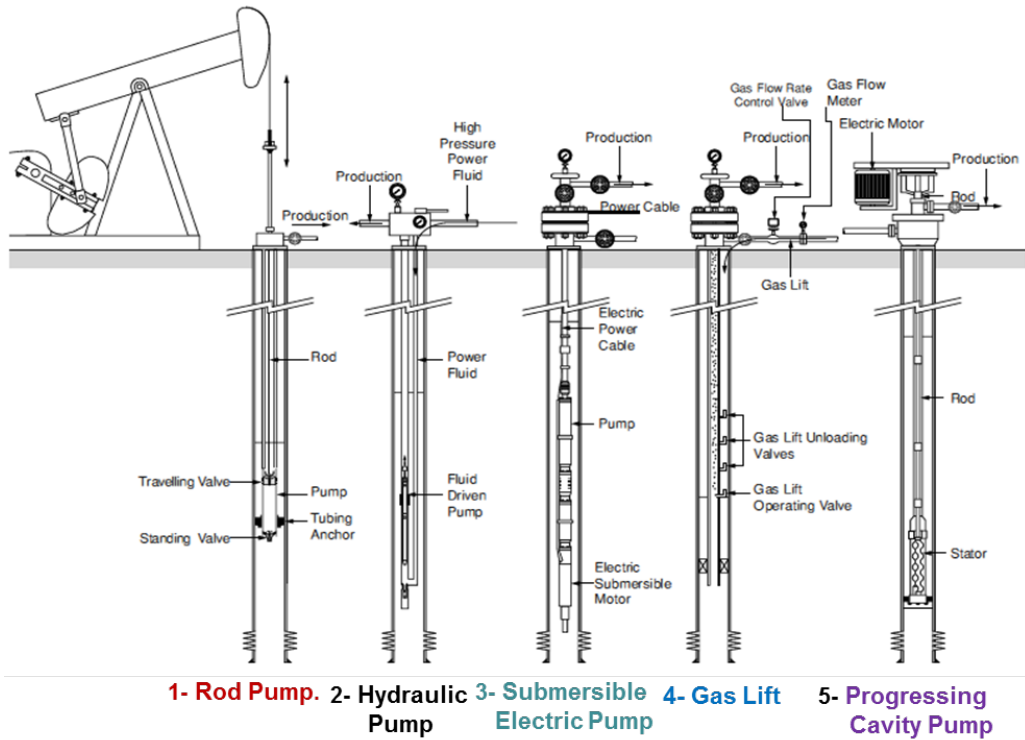
Figure 2-1: Artificial Lift Methods (Anon, 2005)
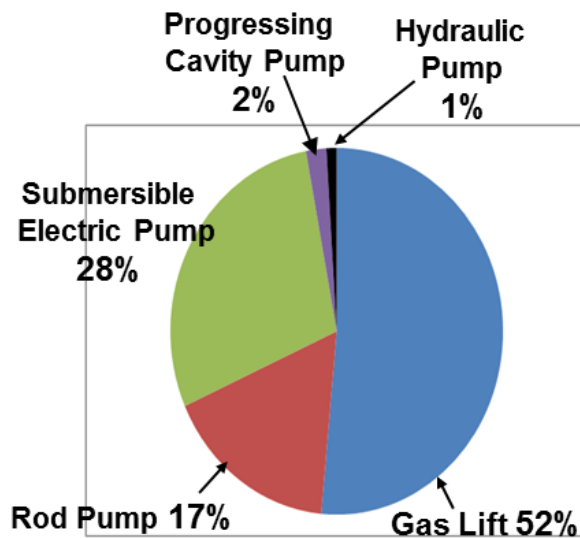
Figure 2-2: Oil Production for Major International Oil Companies (Anon, 2005)

The gas-lift is defined as a process of lifting fluids from production wells or offshore riser systems by injecting relatively high pressure pre-determined gas at selected locations very close to or at the base of the well tubing, resulting in aerating the liquid column and lowering the base pressure and hence reducing the hydrostatic head pressure in the production tube or in subsea riser lifting produced fluids to the surface. In the gas lift technique, the compressed gas can be injected continuously or intermittently into the tubing at the injection point. Continuous injection is based on continuously injecting gas into the tubing at a predetermined depth through the operating valve installed into the production tubing to reduce the pressure gradient in the tubing; whereas, the intermittent gas lift mode is operated on an intermittent basis to give time for the reservoir fluids to build up in the tubing at the bottom of the well, i.e. injection of intermittent high pressure gas into the tubing at a sufficient volume to lift the fluids' head accumulated above the injection point (Boyun et al., 2007).

Typically, the effectiveness of the gas lift technique, based on the compressed gas injection, affects the liquid column inside a production tube or the riser by providing energy of expansion which pushes the fluid in the riser to the surface. As illustrated in Figure 2-3 for gas-lift in an oil well, generally the injected gas enables the wells or risers to flow by one or more of the following processes (Anon, 2005):

a) Reducing the average fluid density above the injection point or across the riser loop, thus, enhancing the well production.

b) Partially dissolving into the produced fluids. The undissolved gas, in the form of bubbles, will expand due to reductions in the hydrostatic pressure as the fluid rises up the tubing or the riser pipe.

c) Coalescence of these gas bubbles into larger bubbles occupying a large proportion of the riser/tubing. These bubbles are separated by liquid slugs, which the gas bubbles displace to the surface.

In the case of riser base gas lift, where gas injects into the riser, the injected gas not only results in the continuous lifting of fluids to the surface, it also prevents or even eliminates the further build-up of liquid and consequent blockage to the gas flow.
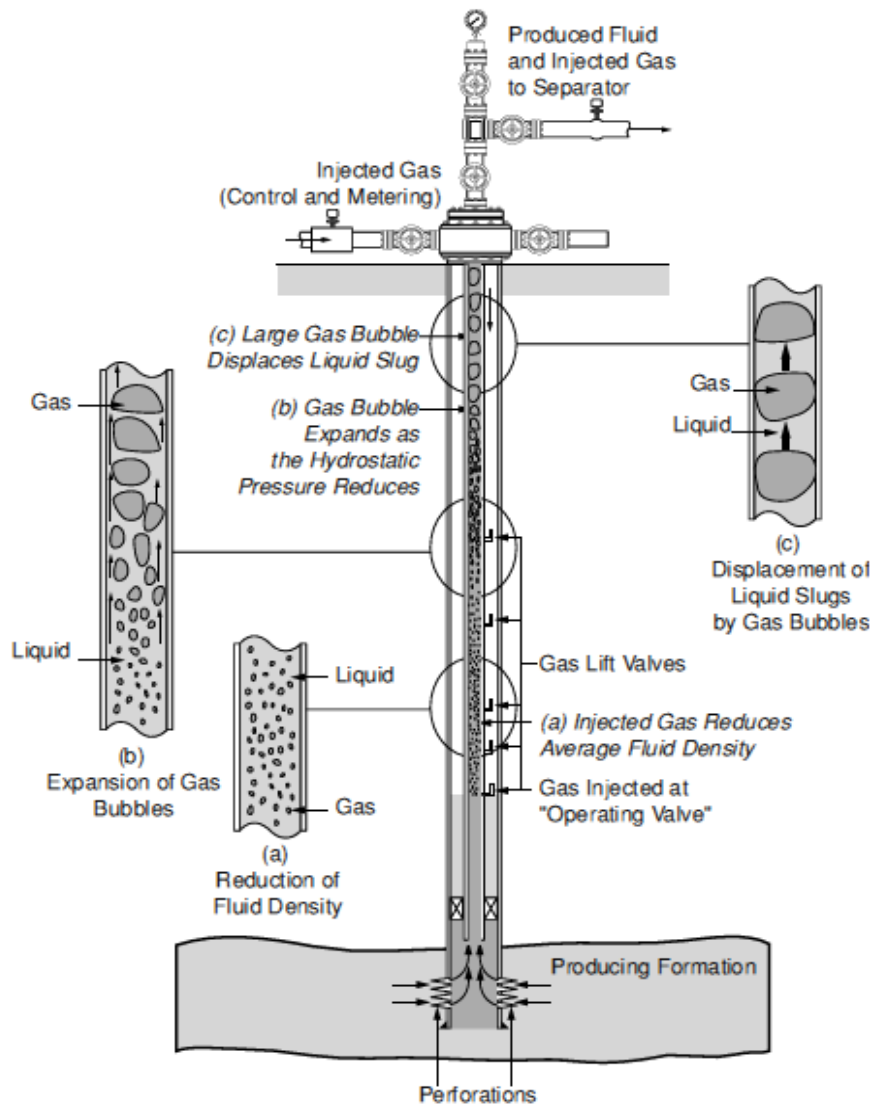
Figure 2-3: Gas-lift mechanisms in fluid flow from oil well (Anon, 2005)

In the riser base, liquid may accumulate at a low production rate and form a severe slugging flow, which is an undesired flow regime. Injected gas reduces this issue and improves the performance of the topside facility. In some cases, gas-lift at the riser base can be used to increase the possibility of blow-down for hydrate prevention (Jayawardena et al., 2007).

The gas lifting technique has many advantages over other artificial lift methods. One major advantage of gas-lift for production enhancement is that there are no moving parts in the subsea system, apart from valves and chokes. Thus, it has

relatively low maintenance costs, and is the most flexible and cost-effective artificial lift method. Gas lifting can handle a wide range of depths and flow rates and also high gas oil ratio (GOR) wells. In fact, a high GOR improves gas lifting performance rather than causing problems, as with other artificial methods (Brown, 1967). In addition, a steady flow can be achieved when gas lift is applied in offshore riser systems and it minimizes the slug sizes arriving at the topside facilities (Hill, 1990; Jansen et al., 1996). However, gas lift has the limitations of high capital cost, and requires a large space for the compressors on offshore platforms and a large supply of gas (Pots et al., 1985).

The current study will investigate multiphase flow behaviour in a 52 mm internal diameter (ID) vertical riser system based on laboratory experiments for a wider range of riser-base continuous gas injection flow rates.

2.2 Multiphase Flow

Multiphase flow is the term used to describe the simultaneous passage through a system of a stream composed of two or more phases (components). Multiphase fluid flows can be two-phase (gas-liquid, liquid-liquid, liquid-solid), three-phase (gas-liquid-liquid, gas-liquid-solid) and four-phase (gas-liquid-liquid-solid). Multiphase flow systems are of great industrial significance and are commonly found in the chemical, process, nuclear and petroleum industries. In multiphase flows, the flow behaviour is much more complex than for single-phase flow. Hence, greater knowledge and the prediction of multiphase flow behaviour (characteristics) are of paramount importance and will determine the efficiency and effectiveness of the process and/or system in which multiphase flow is encountered (Brennen, 2006).

This research study is focused on the multiphase flows encountered in petroleum production vertical risers. Emphases are placed on the gas-liquid (two-phase; air-water), liquid-liquid (two-phase; oil-water) and gas-liquid-liquid (three-phase; air-oil-water) multiphase flows. This Section will highlight the fundamentals of multiphase flows, in particular those relating to vertical flows as these have direct relevance to the current study.

11

2.2.1 Multiphase Flow Terminologies

2.2.1.1 Total Pressure Gradient

This is defined as the rate of change of pressure with distance along the pipe. The total pressure gradient $(dP/dh)_T$ is considered to be the sum of three components, gravitational $(dP/dh)_g$, frictional $(dP/dh)_f$ and acceleration $(dP/dh)_a$ pressure gradients (Brennen, 2005). Represented mathematically as:

$$(dP/dh)_T = (dP/dh)_a + (dP/dh)_f + (dP/dh)_g \qquad (2\text{-}1)$$

The gravitational part is given by $(dP/dH)_g = \rho_m \cdot g$, where ρ_m is the average mixture density, given for a homogenous mixture by the average void fraction α:

$$\rho_m = \alpha \cdot \rho_g + (1 - \alpha)\, \rho_L \qquad (2\text{-}2)$$

where ρ_g and ρ_L are the density of the gas and density of the liquid respectively. α is the gas void fraction.

The frictional component is generally given by $(dP/dh)_f = \rho_m \cdot f \cdot U_m^2 / 2D$, in which f is the friction factor, U_m is the mixture velocity and D is the diameter of the pipe. In a vertical pipe flow, the total pressure gradient can be dominated by the gravitational part, but as the mixture velocity increases the frictional component of the pressure gradient becomes more important. When the mixture flow is considered as a homogeneous dispersion in a vertical pipe, the frictional factor f can be expressed in terms of the mixture's Reynolds number R_e, using several correlations as following (Descamps et al., 2006):

- Blasius correlation for a pipe with a smooth wall

$$f = \frac{0.316}{R_e} \qquad (2\text{-}3)$$

- Haaland correlation, which is defined as

$$\frac{1}{\sqrt{f}} = -1.8 . log_{10}[\frac{6.9}{R_e} + \left(\frac{k/D}{3.7}\right)^{1.1}]$$ (2-4)

where *k/D* is the non-dimensional relative roughness
- Swamee-Jain correlation, which is defined as:

$$f = \frac{0.25}{[log_{10}(\frac{k}{3.7D} + \frac{5.74}{R_e^{0.9}})]^2}$$ (2-5)

where *k/D* is the roughness and R_e is *the* Reynolds number.

For adiabatic flows in both vertical and horizontal pipes, the acceleration pressure gradient $(dP/dh)_a$ is often very small. Thus it is usually neglected. Therefore, for the purposes of this work, the acceleration pressure gradient will be disregarded.

2.2.1.2 Superficial Velocity

This term is often used when describing multiphase flow characteristics. It is the velocity that the phase (gas or liquid) would have if it were to occupy the entire cross-sectional area A_p of the pipe. Gas superficial velocity (U_{sg}) can be determined by;

$$U_{sg} = Q_g / A_p$$ (2-6)

The superficial liquid velocity (U_{sl}) is expressed in a similar manner:

$$U_{sl} = Q_L / A_p$$ (2-7)

where Q_g and Q_L are the actual gas and liquid flow rates at pipe conditions and A_P is the cross-sectional area of the pipe.

The multiphase mixture velocity (U_{sm}) is the sum of the liquid and gas superficial velocities.

$$U_{sm} = U_{sg} + U_{sl} \tag{2-8}$$

2.2.1.3 Actual phase velocity

This is the ratio of the phase volume flow rate to the fraction of the pipe area occupied by the phase or the ratio of the phase superficial velocity to in situ void fraction (gas) or holdup (liquid).

$$U_g = \frac{Q_g}{A_g} = \frac{U_{sg}}{\alpha_g} \tag{2-9}$$

$$U_L = \frac{Q_L}{A_L} = \frac{U_{sl}}{H_L} \tag{2-10}$$

where U_g, U_L, Q_g, Q_L, U_{sg}, and U_{sl} are the actual gas velocity, actual liquid phase velocity, gas and liquid volume flow rates, superficial gas and liquid velocities respectively.

2.2.1.4 Liquid Holdup and Void Fraction

The term hold-up is often used in multiphase flow to represent the liquid fraction or the ratio of liquid volume to that of total volume of the pipe. Void fraction (α) is the ratio of the gas volume to total volume. Also, chordal void fraction is defined as the fractional length of the path through the pipe occupied by the gas phase. Both terms of void fraction and liquid holdup are important parameters used to characterise two-phase and multi-phase flow and thus provide information on the multiphase behaviour. The two terms are mathematically defined by the following relationship (Ali, 2009):

$$\alpha = \frac{V_g}{V} = \frac{A_g}{A_p} = \frac{L_g}{L} \tag{2-11}$$

$$H_L = \frac{V_L}{V} = \frac{A_L}{A_p} \qquad (2\text{-}12)$$

Here H_L is the liquid holdup and α is the gas void fraction. V_L is the volume of liquid, V_g is the volume of gas and V is the total volume. A_g and A_L are the areas occupied by gas and liquid respectively. A_p is the total cross-sectional area of the pipe. L_g is the length of line through the gas phase and L is the total length of pipe occupied by the two-phase of gas and liquid.

Liquid holdup (also called in-situ liquid fraction) depends on the flow regime, fluid properties, and pipe size and configuration. Its value can be quantitatively determined only through experimental measurements by numerous invasive or non-invasive techniques (Brennen, 2005).

2.2.1.5 Slippage

This phenomenon is important in gas-liquid flow in vertical pipes since the density differences are the greatest. Slip phenomena refers to the ability of the less dense (lighter) phase to flow at a higher velocity than the denser (heavier) phase. Under these conditions there is a slippage between the phases. If all the phases involved in the multiphase flow are flowing at the same velocity, then the flow is said to be homogeneous, also known as no-slip flow. Mathematically slip is expressed as:

$$s = \frac{U_g}{U_l} \qquad (2\text{-}13)$$

where, U_g and U_l are the gas and liquid actual velocities respectively.

For the liquid-liquid mixture flows, such as oil-water flow, the slip ratio s is defined by:

$$s = \frac{U_o}{U_w} \qquad (2\text{-}14)$$

where, U_o is the oil velocity and U_w is the water velocity. Accordingly, when oil is flowing faster, the s value is greater than 1, and conversely, when s is less than 1 the water is flowing faster than the oil.

2.2.2 Multiphase Flow regimes in pipes

The distribution of two-phase and/or three-phase flows in conduits (pipe or riser) is usually termed as a flow regime or flow pattern, which reflects the pattern and structure of the flow inside the pipe. In other words, the flow regime or pattern is the spatial arrangement of the phases flowing together through a pipe, which describes how the phases are distributed relative to one another. The flow regime classification is influenced by the operating conditions, fluid properties, flow rates, pipe geometry and pipe orientation through which the phases are flowing. Understanding which flow pattern actually exists under certain flow conditions is very important as each flow pattern results in different hydrodynamic characteristics. These characteristics further influence aspects such as pressure gradient and mass, heat and momentum transfer capabilities. Identification of which flow pattern actually exists under certain flow conditions is important in many industrial processes. Therefore, different methods have been used to identify two-phase and multiphase flow regimes in pipes. There are direct methods (visual observation and high-speed photography) and indirect techniques (void fraction fluctuations, gamma ray and tomography systems). This section provides outlines for the common flow patterns (regimes) according to the type of phase and orientation of pipe flow, and in particular gas-liquid and liquid-liquid flows in vertical and horizontal pipes.

2.2.2.1 Gas-liquid Flow Regimes

Vertical Flows

The gas/liquid flows in a vertical pipe can form various distributions depending on the physical properties of the fluids and the velocities of the phases. These distributions can exist in many configurations called flow regimes or flow patterns. As shown in Figure 2-4, four typical flow regimes have been generally distinguished in the gas-liquid two-phase flow of vertical upward flows, namely: bubbly, slug, churn, and annular flow (Hewitt, 1982; Brennen, 2005). These flow regimes occur as a progression with an increasing gas flow rate for a given liquid flow rate.
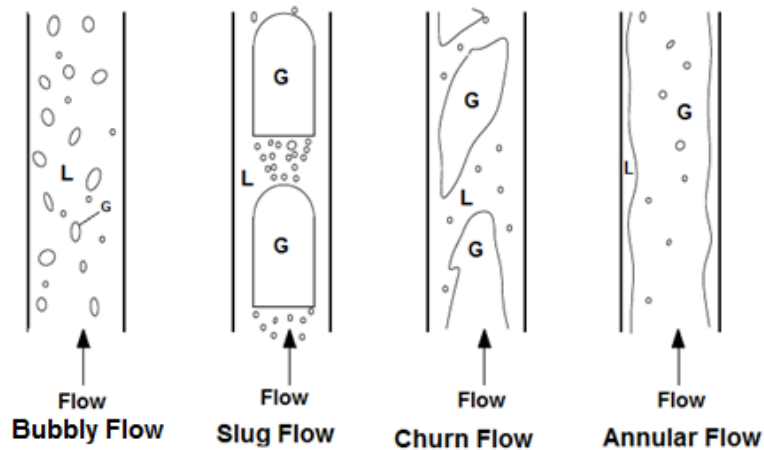
Figure 2-4: Typical flow regimes in vertical pipe, Perez (2007).

In the bubbly flow regime, small bubbles of the gas phase are dispersed in a continuous liquid phase. As the gas superficial velocity is increased, the number of gas bubbles increases and thus collisions between the bubbles occur more often to form a bubbly/slug transition flow, which is also defined as spherical cap bubbly flow, as described by some researchers (Abdulkareem, 2011). Also, when the liquid phase flows at a velocity relatively higher than the gas phase velocity, small gas bubbles are dispersed in the continuous liquid phase. This flow distribution is called dispersed bubbly flow. The gas bubbles move at the same velocity as the continuous liquid phase since gas bubbles are dispersed in the liquid and a no-slip flow occurs (Takács, 2005).

In the slug flow regime, as the gas superficial velocity is increased, the gas bubbles in the bubbly flow coalesce to form larger bubbles (large bullet shaped bubbles or Taylor bubbles) that eventually fill the entire pipe cross section. Between the large bubbles are slugs of liquid that contain smaller bubbles of entrained gas. As the gas velocity is increased, the slug/churn transition is approached. In churn flow, the larger gas bubbles in the slug flow regime become unstable and collapse due to increasing in superficial velocity, resulting in a highly turbulent intermittent flow pattern with both phases dispersed. Churn flow is also called froth slug or dispersed slug (Ali, 2009). In annular flow, the

17

gas phase becomes the continuous phase, with liquid flowing in an annulus, coating the surface of the pipe and with droplets entrained in the gas phase. The annular flow regime also has been classified as wispy annular flow and mist annular flow. A semi-annular flow regime was also observed in vertical pipes as the central gas core through the liquid on the wall was more defined with no oscillatory up and down liquid movement. However, intermittently liquid bridges were formed across the gas core and were then broken. A semi-annular flow formed between the churn and annular regimes (Spedding, 1998).

Horizontal Flows

Although this study will mainly deal with multiphase flow regimes in vertical flow, the 52 mm vertical system for this study is connected to a 40 m long upstream horizontal flowline, which may influence the flow behaviour in the vertical section. Thus common horizontal flow patterns are also briefly overviewed in this section. Several potential flow patterns, usually encountered in horizontal flow, were identified by Hewitt (1982). Figure 2-5, illustrates various flow patterns in horizontal flow: bubbly flow (exists in a continuous liquid phase with dispersed bubbles of gas, which may tend to flow at the top of the pipe), plug flow (when the gas superficial velocity is increased bubbles become larger and tend to coalesce and the forming plugs move along the top of the pipe), and stratified flow (a relatively smooth flow, at low liquid and high gas superficial velocity. The boundaries between the gas and liquid are divided in a laminar fashion (with liquid flowing at the bottom and gas flowing on the top), stratified wavy flow (when gas velocities begin to increase from the segregated flow, the gas affects the patterns of the liquid forming wavy flow in the pipe), slug flow (here the wave amplitude becomes large and touches the top of the tube forming pockets of the gas in the pipe), and annular flow (when the flow is distributed between a liquid film flowing up the wall and a dispersion of droplets flowing in the gas core of the flow).
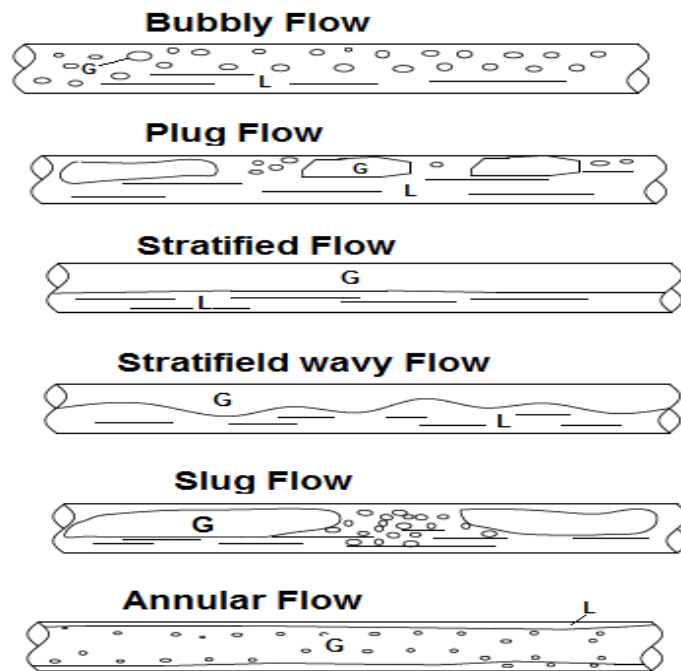
Figure 2-5: Flow regimes in horizontal gas-liquid flow, (Hernandez-Perez, 2008)

2.2.2.2 Liquid-liquid flow regimes in a vertical pipe

When two immiscible liquids flow simultaneously in a pipeline (e.g. oil-water flow), a number of different flow patterns appear reflecting how these fluids are distributed inside a pipe cross section (Ngan, 2010). In general the flow patterns of liquid/liquid oil-water flows in a vertical pipe are grouped into two major categories: a water-dominated flow (water continuous flow or oil-in-water flow) and an oil-dominated flow (oil continuous flow or water-in-oil flow). Flores et al. (1999) suggested six main flow patterns for the flow of oil and water through vertical pipes. As illustrated in Figure 2-6, three of the flows are identified as being water continuous and the other three as oil continuous. The water-dominated flows are: very fine dispersion of oil in water, dispersion of oil in water, and oil in water churn flow. The oil-dominated flows are: very fine dispersion of water in oil, dispersion of water in oil and water in oil churn flow.

19
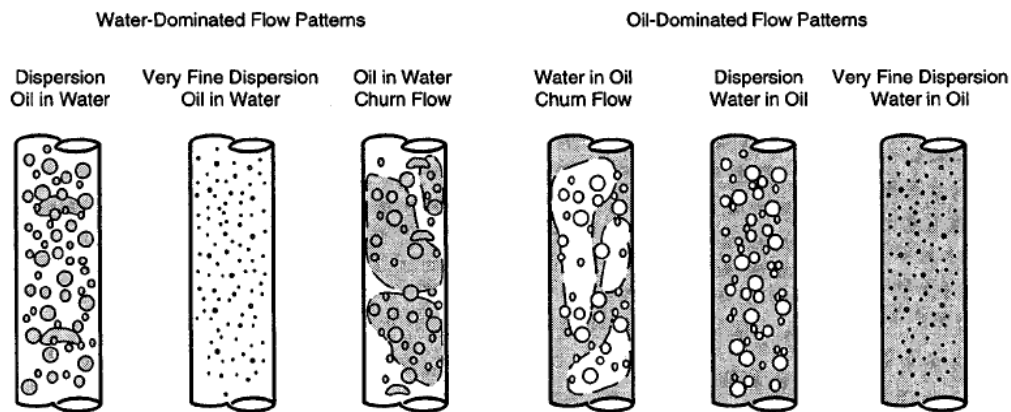
Figure 2-6: Oil-water flow patterns in vertical pipes (Flores et al., 1999)

Very fine dispersed oil in water flows:

According to Flores et al. (1999), this flow regime occurs when the oil superficial velocity is fixed and the water superficial velocity is gradually increased. This gives rise to smaller oil droplets as a result of the disintegration of larger oil droplets and globules. A further increase in water velocity results in a homogeneous flow leading to a very fine dispersed oil in water flow.

Dispersed oil in water churn flow:

This flow pattern occurs for a wide range of flow conditions in the water continuous phase region. The flow here is characterised mostly by the large oil droplets and globules observed in the oil-water dispersed flow pattern combing together due to the relatively small magnitude of the breakage forces occurring at low to medium superficial velocities of the continuous water phase. When the water velocity is increased, the size of the oil droplets may decrease. The oil bubbles in oil-water continuous flows are completely shapeless. A further increase in the oil's superficial velocity leads to the occurrence of phase inversion and then to the oil continuous flow region (Flores et al. 1999).

Water in Oil Churn Flow:

In this flow pattern, the large water bodies do not seem to have a characteristic shape. For higher oil flow rates the large water bodies observed in the water in

20

oil churn flow pattern are broken into smaller droplets. The main mechanism involved in the transition is the increase in breakage forces in direct proportion to the increase in flow rate of the continuous oil phase (Flores et al., 1999).

Dispersed Water in Oil Flow:

This flow pattern is characterised by a fairly organised and defined structure of water droplets, in some cases still of irregular shape and frequently flowing as swarms of droplets entrained near the core of the continuous oil phase. At very high superficial oil velocities, the water flows as very small droplets distributed in a continuous, fast moving, oil phase over the entire cross-sectional area of the pipe (Flores et al. 1999).

Very Fine Dispersed Water in Oil Flow:

In this flow pattern, a further increase of oil superficial velocities leads to water flows becoming very small droplets of a water phase distributed in a fast flowing oil continuous phase over the cross section of the pipe. Oil-dominated flow patterns, with the exception of the very fine dispersed water in oil flow, show significant slippage, in contrast to all the water-dominated flow patterns that show less slippage. Flores et al. (1999) also found that the frictional component of the pressure gradient indicates relatively low values for water continuous flow patterns and higher values for oil-dominated flow patterns.

2.2.3 Flow regime maps

Flow regime maps are graphical representations of occurrence ranges in which each flow regime occurs in a particular pipe system. Flow pattern maps usually contain flow regime regions separated by transition lines and result from attempts to describe and classify the various flow patterns. An understanding of which flow regime actually occurs in multiphase flows under certain flow conditions is very important as each flow regime results in different hydrodynamic flow characteristics, and consequently, these characteristics may further influence parameters such as pressure gradient, and mass and heat transfer capabilities (Abdulkadir, 2011). Therefore, several types of flow regime

maps, available from the open literature, have been established for identifying flow patterns under various flow conditions and different pipe orientations. For instance, Mandhane et al. (1974) produced a flow regimes map for gas-liquid flow in a horizontal pipe. As illustrated in Figure 2-7, the superficial phase velocities were used as mapping parameters for this flow map. The map is now the most widely accepted two-phase regime map for horizontal flows. There are also well-known flow maps for vertical multiphase flow such as those illustrated in Figures 2-8 and 2-9. The flow pattern map in Figure 2-9, generated by Hewitt and Roberts (1969) for a vertical two-phase upward flow in a vertical pipe, was validated for gas/water flow both at atmospheric pressure and high pressure systems. Also, the map is plotted in terms of the superficial momentum fluxes of the two phases $\rho_g U_{sg}^2$ and $\rho_l U_{sl}^2$, where ρ_g and ρ_l are gas and water densities, and U_{sg} and U_{sl} are the superficial velocities of gas and water.
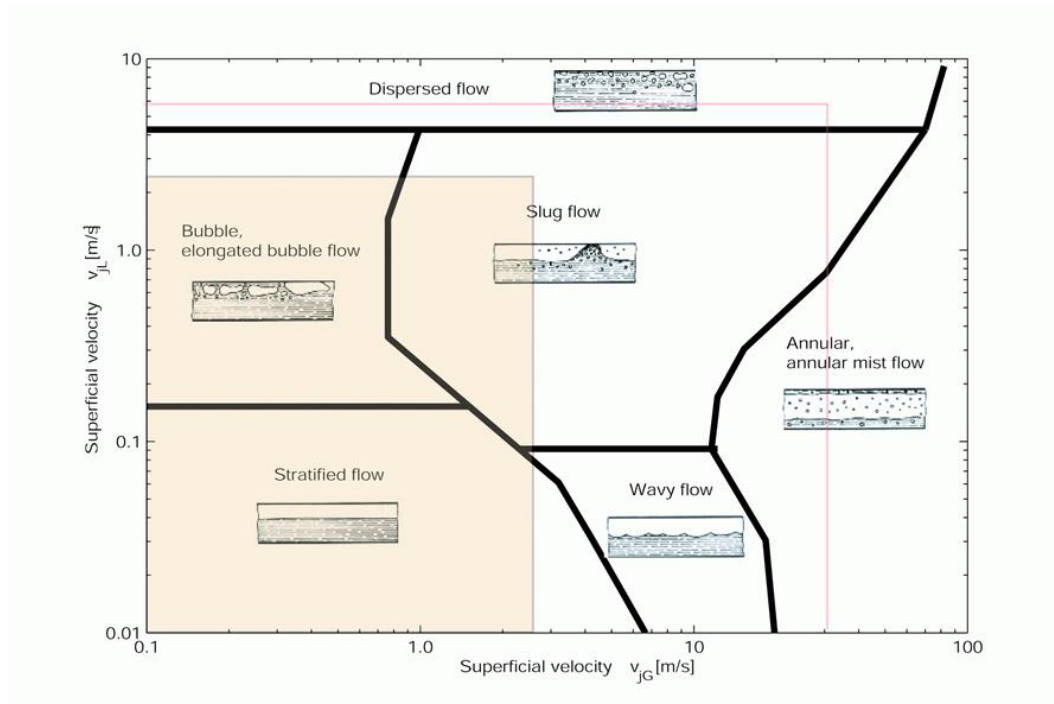
Figure 2-7: Flow regimes Map for Horizontal Flow of air-water two-phase flow in 50 mm diameter tube, Mandhane et al. (1974)
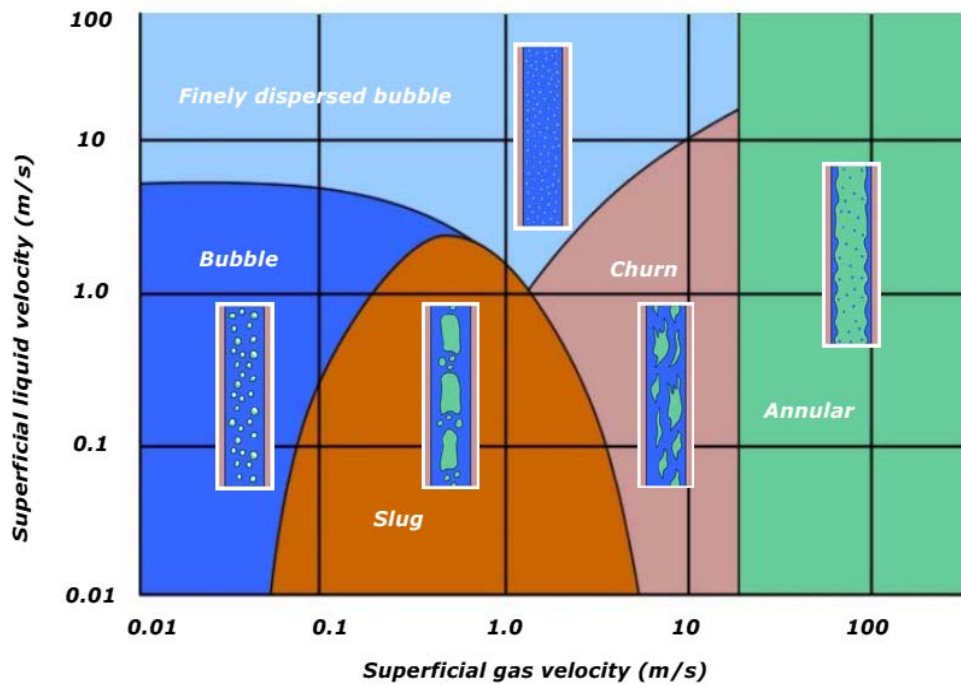
Figure 2-8: Flow patterns map for a vertically upward two-phase flow (Dykesteen, 2005)
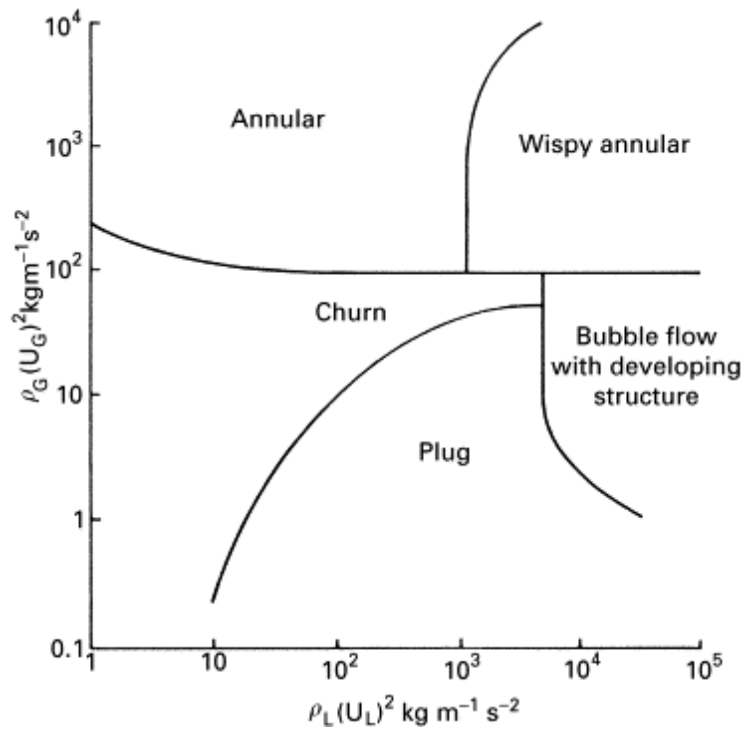
Figure 2-9: Vertical flow regime map for air-water upflow in a 3.2cm diameter tube. Hewitt and Roberts (1969)

For liquid-liquid flow in horizontal pipes, there are two flow regime maps as proposed recently by Morgan et al. (2012; 2013) involving two immiscible liquids - oil and a glycerol–water solution. As illustrated in figure 1 (Figure 10(a) for a square cross-section pipe and Figure 10(b) the circular cross-section pipe), the observed flow regimes in these maps are classified into eight distinct flow regimes which can then be grouped into four more general liquid-liquid flow types. These four are: (1) stratified flow; (2) mixed flow, which is characterised by two distinct continuous phase regions with droplets in each; (3) two-layer flow, which comprises of a dispersed region and a continuous, unmixed region; and (4) dispersed flows.

The flow regime maps relate the flow classifications to the input oil fraction and the superficial mixture velocity. However, in the regime map that was obtained for a square cross-section (Morgan et al., 2012) it is seen that stratified flows persist to considerably higher superficial mixture velocities. The transition to dispersed flow also occurs at much higher velocities in the circular geometry.

(a)   (b)
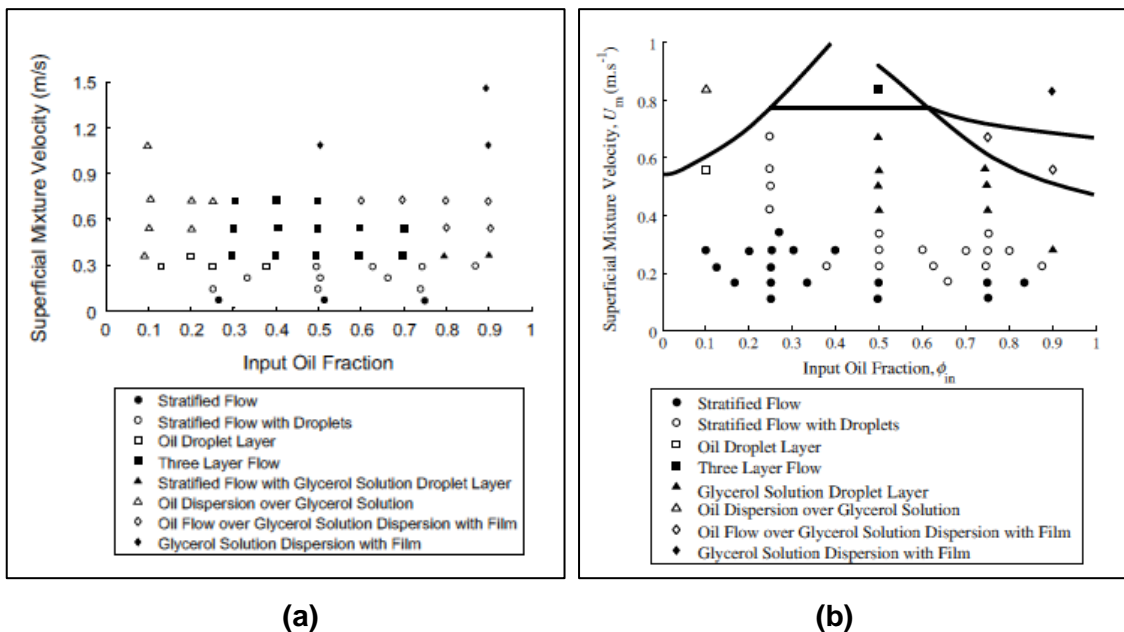
Figure 2-10: Flow regime maps proposed by Morgan et al. (2012; 2013) for horizontal flowing liquid–liquid flows, a) Square cross-section pipe, b) Circular cross-section pipe.

2.2.4 Void phase distribution characteristics in the vertical pipe

In terms of the void fraction profile of the gas-liquid flow in vertical pipes, it has different distributions depending on factors such as superficial gas velocity, bubble size distribution, pipe diameter, nature of the gas-liquid systems and flow conditions (Ali, 2009). Generally, the void fraction profile in a vertical pipe can present either as wall-peaking (higher amount of gas located near to the wall region) or core peak/centre peaking (more gas gathers around the centre). Moreover, many studies have shown that the void profile is fluids' superficial velocities dependent, i.e. at higher gas flows and low liquid flows the void distribution is core peak (central peak) but at low gas and high liquid flows where bubbly flow is formed the void distribution presents a wall peak. As the gas velocity increases the wall peak becomes much less pronounced, showing an intermediate peak before changing to core peaking profile (Olerni et al., 2013).

Serizawa and Kataoka (1988) classified the void fraction profiles in a vertical pipe into four major types: wall peaked, intermediate peak, slug peak (two peaks, one at the wall and the other at the centre) and core peak on the flow regime, as shown in Figure 2-11. They emphasized that the phase distribution of the void fraction is a function of the flow pattern and changes from a wall peak to a core peak distribution as the gas superficial velocity increases. The wall peak distribution corresponds to bubbly flow, as small bubbles tend to move close to the pipe wall and a core peak to the slug flow in conventional pipe sizes, where large bubbles tend to move towards the centre of the pipe.
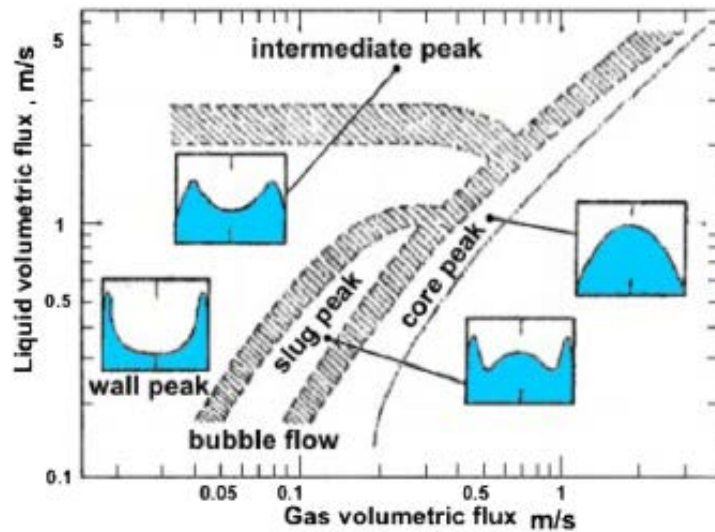
Figure 2-11: Void fraction distribution for air-water flow in vertical pipe by Serizawa and Kataoka (Olerni et al., 2013)

2.2.5 Flow regime identification

Identification of the inner structure for the multiphase flow (flow regimes) is one of the important parameters to describe the behaviour of multiphase flows in conduits. Flow regime occurrence in pipelines was traditionally identified according to visual observations performed by viewing the flow through transparent windows on the pipe wall (Bertani et al 2010). This method limits the accuracy of defining the flow regime to the judgment of the observer. Therefore, other methods have been developed for more accurate identification of multiphase flow regimes. These methods are classified into direct and indirect methods according to Bertani et al., (2010). The direct identification includes methods that involve a direct view of the flow appearance or of its distribution view through a transparent section on the pipe. These include using high speed photography/videography etc., to identify the flow pattern. Although, this method is an improvement on visual observation, it still does not give a clear delineation of the flow pattern and is therefore not good enough for the flow regime to be objectively classified. Moreover, this direct method cannot be used within real industrial pipelines that are generally not transparent.

In indirect methods, statistical analyses of reflected signals that mirror the fluctuating characteristics of multiphase flows and flow regimes can be used for identifying these flow patterns. The probability density function (PDF) is a complete probabilistic description of the instantaneous values of the sensor output signals data, which yield the PDF. It describes the probability that at a given time the signal will have the value within some defined range. Thus, signal time traces and the corresponding PDFs, have been successfully used as objective and quantitative flow pattern identification tools. Jones and Zuber (1975) found that the flow regime could be identified according to the shapes of the time trace fluctuations and the PDF. Later, Costigan and Whalley (1997) further developed the time traces and PDF methodology of Jones and Zuber and successfully classified the flow into six flow patterns: discrete bubble, spherical cap bubble (bubbly to slug transition flow), stable slug, unstable slug, churn and annular flow. The PDFs' shapes and time traces, shown in Figure 2-12 were used to classify flow patterns as follows: (i) void fraction time trace with small fluctuations and corresponding PDF shape of a single narrow tall peak at the low void fraction region, representing bubble flow; (ii) void fraction time trace with more fluctuations forming regular narrow peaks and a PDF shape of a single peak at the low void fraction, accompanied by a long tail towards the high void region representing transition bubbly-slug (spherical cap bubble); (iii) time traces void fraction with fluctuations between high and low values and corresponding PDF shape of a double peak, one at the low void fraction and the other at a higher void fraction reflecting typical slug flow; (iv) time traces void fraction trend of a high void fraction with random dips into lower void fractions and a single peak PDF shape at a high void fraction with a broadening tail towards the low void region represents churn flow; (v) approximately stable void fraction time traces at very high values and an equivalent PDF shape of a single narrow peak at the very high void fraction region, defined as annular flow.

In the current research study, the above-mentioned methods of void fraction time trace and PDFs' shapes for output signals from both a clamp-on gamma densitometer (GD) and capacitance WMS, are adapted for flow pattern identification.
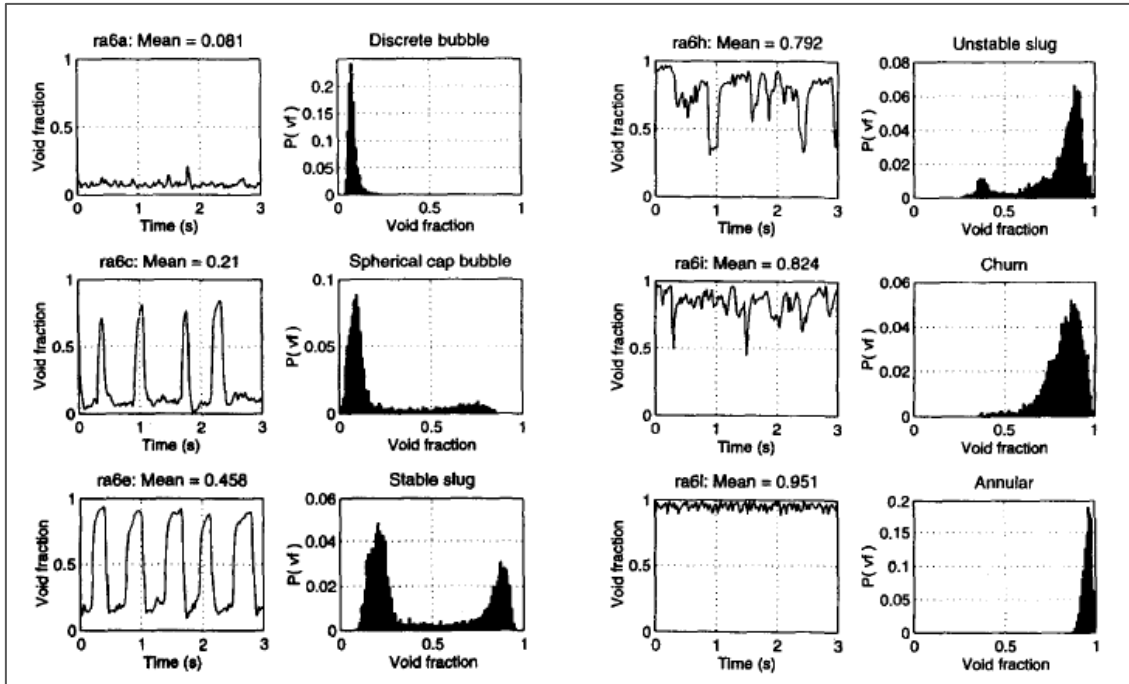
Figure 2-12: Flow regime identification, void fraction time traces and corresponding PDFs (Costigan and Whalley, 1997)

2.3 Phase Fraction Measurement

There are several techniques that have been developed for measuring gas and liquid fractions and distributions as well as identifying various flow regimes in multiphase flow in pipes. For the purpose of this study, gamma radiation attenuation techniques, Coriolis mass flow meter, wire-mesh sensor and other common techniques are briefly described next.

2.3.1 Gamma Radiation Attenuation

The principle of the gamma attenuation technique is explained by the fact that gamma rays are attenuated as they pass through media due to the interaction of their photons with the matter. The extent of this attenuation experienced by the gamma rays depends on the energy of the gamma rays and density of the absorbing media (Blaney and Yeung, 2007). Several methods of using gamma

radiation have been developed for multiphase flow measurements in pipes. The two most common methods are single-beam gamma attenuation and dual-energy gamma attenuation.

Single-beam gamma attenuation

This technique is based on the attenuation of the energy of a very narrow beam of gamma ray. As shown in Figure 2-13, the single-beam gamma densitometer consists of a gamma source and a detector unit. A collimated gamma ray is directed at the pipe with a sensor placed directly opposite the source on the other side of the pipe. The technique can be applied for gas-liquid and liquid-liquid systems. The capability of media to absorb gamma radiation is dependent on the linear attenuation coefficient γ of the absorbing material. This can be used to measure the component fraction in the volume covered by the gamma beam. The intensity of the gamma beam decays exponentially as it passes through matter, according to Beer-Lambert's law, which can be expressed as the following (Kumara et al., 2010).

$$I = I_o\ e^{-\gamma d} \tag{2-15}$$

where I_o is the initial intensity and I the intensity of the gamma radiation detected after the gamma beam has travelled through the absorbing media on length d. A gamma ray will be attenuated differently by materials according to their density. Thus, the linear attenuation coefficient of water is higher than oil and gas and it is possible to employ this variance in the attenuation of gamma rays as an indication to distinguish these phases in the pipe.
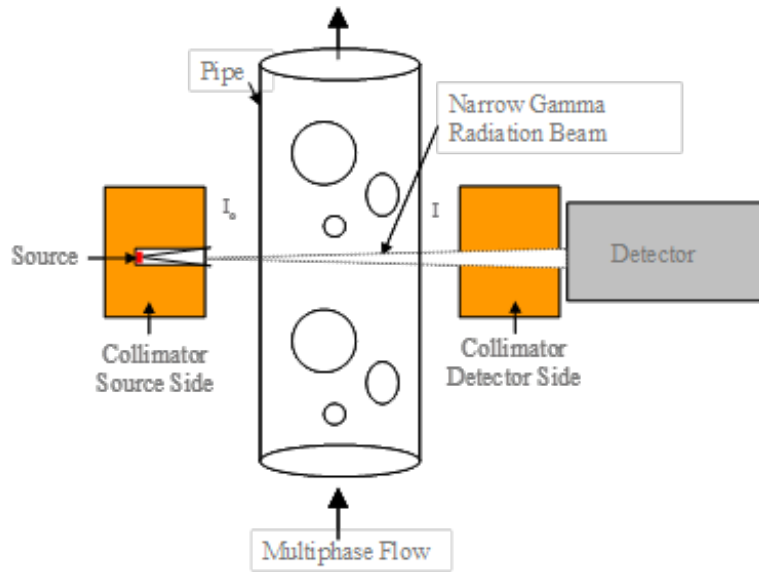
Figure 2-13: Gamma Radiation Method

Assuming the presence of a vacuum within the pipe (inner diameter D), I_E is the intensity of emitted mono-energetic photons which strike the detector. This measurement corresponds to the number of photons transmitted from the source across the air outside the pipe and through the pipe wall.

If the pipe is filled with absorbing media, the gamma beam passes the media on length $d = (1 - \alpha)D$, where α is the gas fraction. The intensity measured for a given photon energy (I) is dependent on the linear attenuation coefficient γ of the absorbing material and can be given by (Blaney, 2008):

$$I \;=\; I_E\, e^{-\gamma d} \;=\; I_E\, e^{-(1-\alpha)\gamma D} \tag{2-16}$$

Also, with the calibration measurement for a full pipe with only liquid ($d = D$ and $\alpha = 0$) and the intensity I_F is obtained by:

$$I_F \;=\; I_E\, e^{-\gamma D} \tag{2-17}$$

30

By combining the two calibration Equations, the void fraction in gas-liquid flow can be expressed as:

$$\alpha = \frac{\ln(I/I_E)}{\ln(I_F/I_E)} \tag{2-18}$$

Similarly, in the case of liquid-liquid oil-water flows, the following Equation can be used to calculate the water fraction:

$$\varepsilon_w = \frac{\ln(I/I_{oil})}{\ln(I_{water}/I_{oil})} \tag{2-19}$$

where I_{oil} and I_{water} are the calibrated values, i.e. the photon rates measured for single-phase oil and water.

Dual-energy gamma attenuation

This type of gamma attenuation technique works on the same principle as the single-beam system, but two gamma energy levels are used to measure the three components of a three-phase mixture in a pipe. For a two energy beam configuration, two independent equations will be required, one for each gamma beam energy, giving rise to two of the three equations needed to determine the phase fractions for a pipe containing a mixture of oil, water and gas in a pipe with diameter d with fractions of ε_o, ε_w and α, respectively. The third equation is simply the fact that the sum of the three-phase fraction in the pipe should be equal to unity as follows (Blaney, 2008).

$$\alpha + \varepsilon_w + \varepsilon_o = 1 \tag{2-20}$$

$$I(e) = I_0(e).\exp\left[-\sum_{i=1}^{3} \gamma_i(e).D\right] \tag{2-21}$$

where I is the measured gamma intensity, I_0 is the gamma intensity when the pipe is empty, D is the inside diameter of the pipe and γ is the attenuation coefficient of the component.

2.3.2 Electrical Process Tomography

This measurement technique for obtaining information about the phase fraction and the contents of pipelines is based on the difference in electrical properties between the measured liquid and gas phases. There are several methods of electrical process tomography depending on the property variation being considered; however, the most commonly used methods are Electrical Capacitance Tomography (ECT) and Electrical Resistance Tomography (ERT). Generally, in these techniques electrodes are arranged around the circumference of the pipe to detect signals from the phases inside the pipe (Dong et al., 2005).

2.3.2.1 Electrical Capacitance Tomography (ECT)

Electrical Capacitance Tomography is based on measuring the variations in the dielectric properties (capacitances) of the phases inside the pipe between inter-electrodes placed around the pipe. As shown in Figure 2-14a, a basic ECT system consists of twelve capacitance sensors (made up of source and detector electrodes arranged around the pipe. The technique is a non-invasive measurement method since the electrodes are not obstructing the flow inside the pipe. It is used where the phases have no electrical conductivity such as in gas/oil flows. Additionally, images can be reconstructed based on the permittivity distribution acquired from the ECT measurements through the electrodes (Dong et al., 2001).

2.3.2.2 Electrical Resistance Tomography (ERT)

ERT is also a non-intrusive measurement technique used for phase fraction, phases distribution and imaging of multiphase flows in vessels and pipes. This tomography type is suitable for applying to conductive phases (i.e. conductive phase with another phase with a different conductivity value such as air/water system) flowing through the cross section of a pipe. In the ERT system, several

electrodes are usually placed at fixed positions around the circumference of the pipe in such a way that the electrodes do not interfere with the flow but make electrical contact with the fluids within the pipeline, as illustrated in Figure 2-14(b). ERT is typically used for monitoring multiphase flows in process units on a real time basis. ERT measurements are given as resistance or conductance.
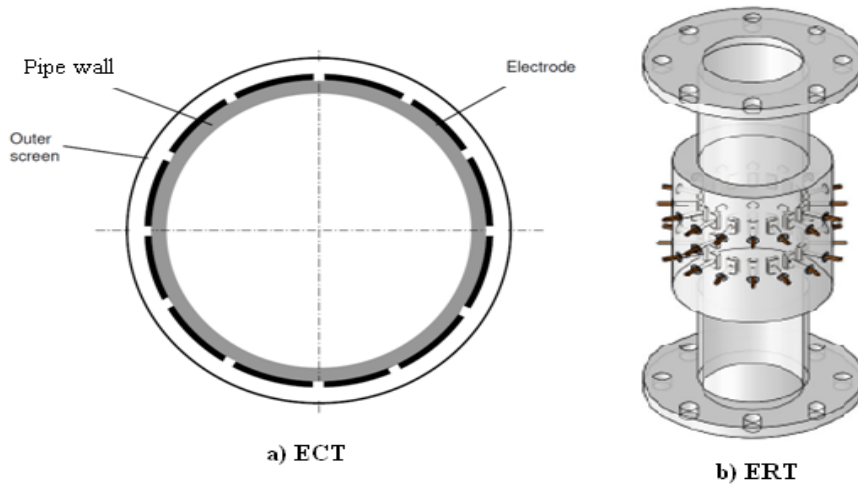
Figure 2-14: Electrical Tomography Systems, ECT and ERT

2.3.3 Wire-mesh sensor (WMS)

The WMS is a flow imaging and measuring new technique that allows the measurements of multiphase flows with high spatial and temporal resolution. This type of sensor was first introduced by Prasser et al. (1998) at Helmholtz-Zentrum Dresden-Rossendorf (HZDR), Germany. In the WMS, wire electrodes are stretched across the flow cross section with two sets of wire electrodes perpendicular to each other with a small axial separation founding a grid of electrodes, as shown in Figure 2-15. One set acts as the transmitter, while the other as the receiver. The transmitter electrodes are activated in sequence while the receiver electrodes are parallel sampled. The WMS electronics measure the local electrical properties (conductivity or permittivity) of the fluid at each crossing point of the wires by successively applying an excitation voltage to each one of the sender electrodes while keeping all other sender electrodes

at ground potential and measuring, respectively, the direct (dc) or alternating (ac) electrical current flow to all receiver electrodes synchronously. Based on those electrical measurements (conductivity or permittivity) the sensor is thus able to give information about the instantaneous phase fraction and fluids distribution across the cross section. Furthermore, the sensor measurements can provide a visualization of the different flow regimes within the pipes. There are basically two types of wire-mesh sensor: conductivity and capacitance wire-mesh sensor (Da Silva et al., 2007).
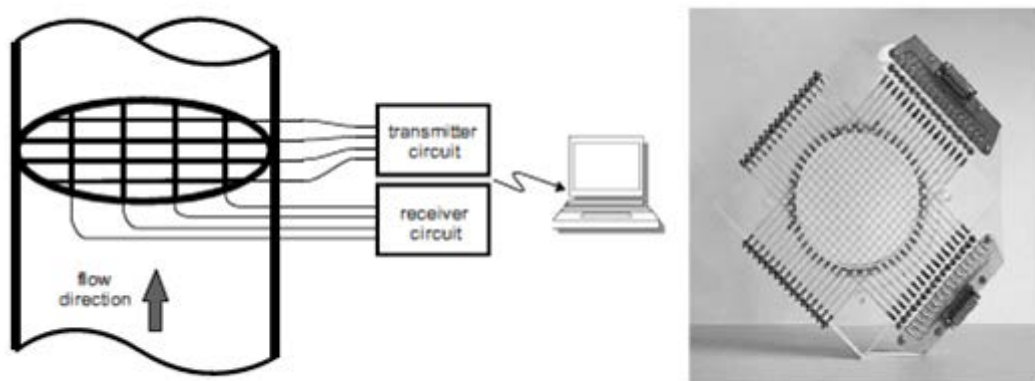
Figure 2-15: Schematics of a WMS (Da Silva and Hampel, 2013)

2.3.3.1 Conductive wire-mesh sensor

This type of wire-mesh sensor is based on conductivity measurements. It was first developed for investigations into conducting fluids. The conductive sensor measures the in-situ conductivity distribution of the fluid from the crossing points of the two sets of perpendicular wires over the cross section of the pipe. Thus it is capable of measuring a mixture flow with a conductive phase, typically gas-water and steam-water systems (Da Silva et al., 2007). However, the conductive sensor has been successfully applied in many investigations involving a two-phase flow that must include a one phase electrically conducting fluid.

2.3.3.2 Capacitance wire-mesh sensor

The capacitance WMS was developed based on direct measuring of the electrical permittivity (capacitance) of the fluid at each crossing point of the wires into the principle of the WMS, which is then related to the phase fraction and fluids distribution. The capacitance sensor was developed to allow the measurement of non-conducting fluids such as oil or organic fluids. More information about the principle of the capacitance WMS is described in detail in Da Silva et al. (2010).

In the current study, a 16 x 16 WMS with capacitance measuring electronics CAP 200 developed at Helmholtz-Zentrum Dresden-Rossendorf (HZDR) was applied to extract cross-sectional phase fractions and distributions in a vertical riser of a 52 mm internal diameter (ID) and 10.5 m long pipe.

2.3.4 Coriolis Mass Flow Meter

Principally, the flow meter is comprised of a flexible flow tube, as shown in Figure 2-16 (the shape of the tube depending on the design) and magnetic sensor. Where there is no flow through the flow meter, the measuring tube oscillates uniformly and the sensors at the inlet and outlet side of the tube record this uniform oscillation. As fluid begins to flow, additional twisting is imposed on the tube due to the fluid inertia. As a result, the inlet and outlet sections of the tube oscillate in opposite directions simultaneously. This difference in their oscillation (phase shift) is directly related to their mass flow rate. The phase shift is picked up by the sensor and used to establish the mass flow rate. As previously mentioned, the Coriolis mass flow meter can also measure the density of a fluid. The measuring tube is continuously excited at its resonant frequency. A change in the mass and thus the density of the oscillating system, results in a corresponding, automatic adjustment in the oscillation frequency. Thus the oscillation frequency is a direct measurement of the fluid's density. Both the fluid density and mass flow rate are measured simultaneously but independently (Arubi, 2011).
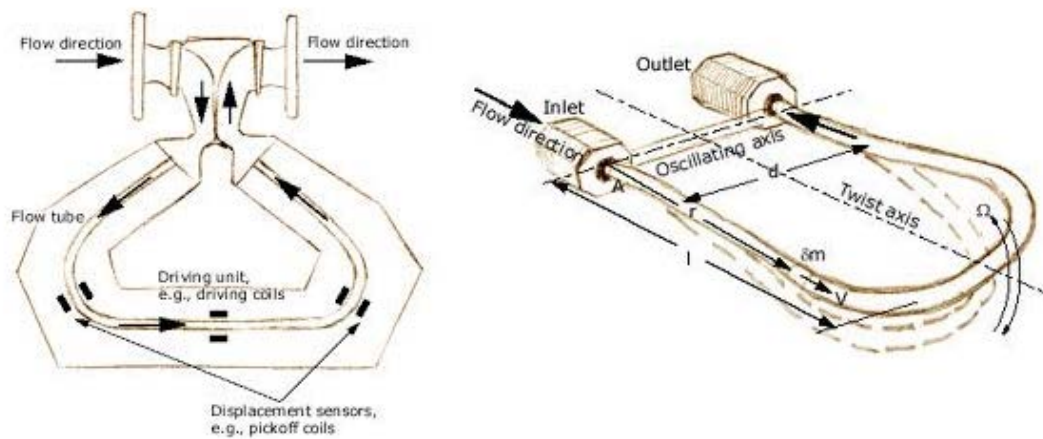
Figure 2-16: Coriolis flow meter: Principle

2.4 Phase Inversion Phenomenon

In a system of two immiscible liquids, such as oil and water flows, there are two general kinds of distribution that can be formed, depending on the conditions of the system, in which either oil drops are dispersed in a water continuous phase or water drops are dispersed in an oil continuous phase. Thus, phase inversion is defined as a phenomenon whereby the continuous phase (oil or water) inverts to become a dispersed phase and vice versa. The critical volume fraction of the dispersed phase above which this phase becomes the continuous phase is referred to as the phase inversion point (Hu and Angeli, 2006). In this section, the phase inversion process in pipelines, the parameters that were reported to effect phase inversion and the several models and correlations that have been suggested for predicting the phase inversion point will be discussed.

2.4.1 Phase Inversion in Pipeline Flow

In the oil industry, where the produced crude oil and water need to be transferred over long distances in pipelines from the reservoir to the well heads and then to the plant, the occurrence of phase inversion phenomena may result

36

in a substantial decrease of oil production and pipeline capacity. In addition, the occurrence of phase inversion in a pipeline is associated with an abrupt change of pressure gradient. Therefore, knowledge of the volume fraction where phase inversion occurs, and the inversion process itself is important. Figure 2-17 shows a schematic diagram suggested by Arirachakaran et al. (1989) to illustrate the phase inversion process in oil-water flows in a pipeline. The Figure illustrates that, when the water volume fraction is low, the mixture forms water dispersed in the oil continuous phase or water-in-oil dispersion (oil-dominated flow), where there is equilibrium between coalescence and break-up of the water drops. As the water fraction increases, more concentration of water drops can be observed until the phase inversion point, where the dispersed phase spontaneously inverts to become continuous. Then after the occurrence of phase inversion, the water drops start to coalesce and trap oil into drops. A further increase in water fraction leads to form a water continuous phase.
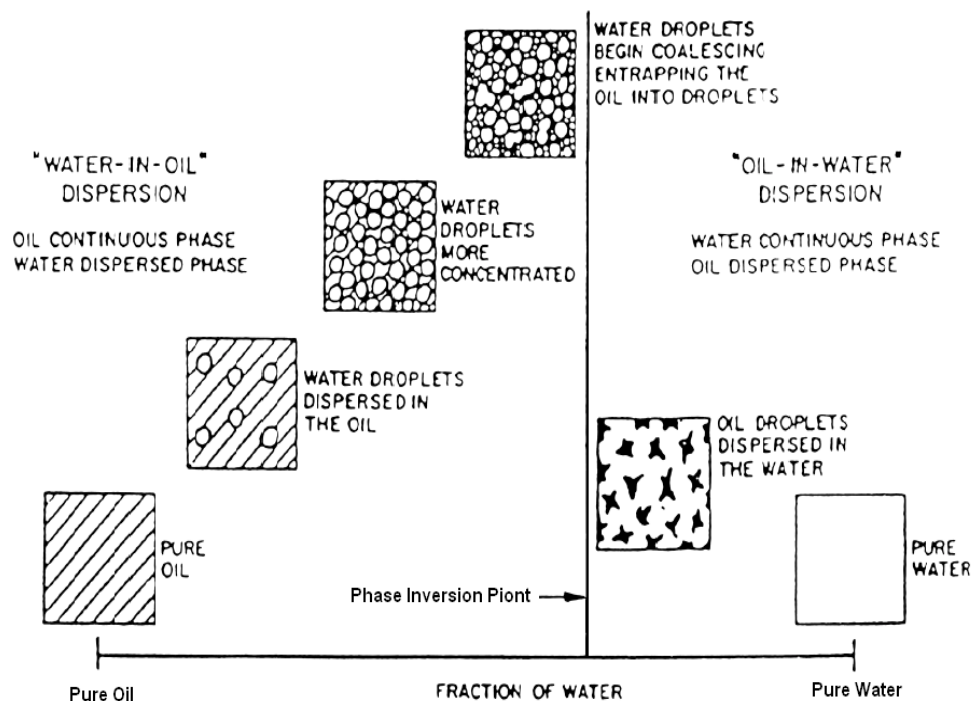
Figure 2-17: Phase inversion process for an O/W flow (Arirachakaran et al., 1989)

37

In a two-phase oil-water flow through a pipeline, phase inversion between oil and water can occur depending on the concentration (volume fraction) of the two liquids. This critical volume fraction can be affected by some physical and physicochemical parameters, such as liquids properties and initial conditions (Angeli, 1996). In order to acquire knowledge about phase inversion and associated phenomena, many experimental studies have been conducted in pipe flows, either in horizontal pipes (for instance, Angeli and Hewitt, 1998; Ioannou et al., 2005; Ngan, 2010) and vertical pipe (for instance, Descamps et al., 2006; Hu and Angeli, 2006; Xu et al., 2010). Many of those researchers found that the occurrence of phase inversion and the changes in phase continuity are usually associated with substantial changes in the rheological properties of the mixture dispersion and the accompanying pressure drop due to forming a high and effective viscosity of the mixture.

Descamps et al. (2006) studied experimentally the phase inversion for an oil and water flow through a vertical tube. Their results showed that, for an oil and water vertical upward flow, the frictional pressure gradient led to a peak at the phase inversion point. The growth of the effective viscosity increased with increasing mixture velocity. The point of phase inversion was always close to an input water fraction of 30%, independent of the direction of change in water fraction during the experiments (from oil to water or from water to oil).

In the current research, efforts were made to identify the phase inversion point and its effects on the pressure gradient experimentally for oil-water flow first and then for air-oil-water flows in a 10.5 m vertical riser in different flow patterns.

2.4.2 The parameters affecting the occurrence of phase inversion

There are several parameters that influence the occurrence of phase inversion; these parameters include physical properties (fluid viscosity, density and interfacial tension), inlet conditions and Flow geometry (Ngan, 2010).

Liquids properties:

In terms of system properties factors, fluids viscosities have been reported in many studies to be an important factor affecting phase inversion. For instance, Arirachakaran et al. (1989) from their experimental data on phase inversion in pipelines with different viscosity oils found that the critical water fraction that corresponded to the occurrence of phase inversion was dramatically reduced with an increase in oil viscosity. Similarly, Ioannou (2006) observed that the more viscous oil tended to invert at a higher oil fraction. The viscosity effect was also confirmed more recently by Wang and Gong (2009) when they concluded from their work on high viscosity mineral oil-water flow through a horizontal pipe that phase inversion for an oil phase with high viscosity occurs much earlier than for low viscosity oil, and the critical inversion point tends to be delayed with increases in the experimental temperature.

Fluids' densities do not affect phase inversion significantly, particularly when the density difference between the two liquids is small, but will influence the homogeneity of the dispersion. On the other hand, systems with a large density difference between the phases show an increased tendency to invert (Ngan 2010).

Also, the interfacial tension was reported to have an influence on phase inversion. However, Yeh et al. (1964) suggested that interfacial tension plays a small role in phase inversion in the absence of other forces, as it will cause inversion to occur at 50% of volume fraction. On the other hand, Luhning and Sawistowski (1971) found that interfacial tension can affect the phase inversion since it affects drop size and interfacial area. Later, Clarke and Sawistowski (1978) confirmed the change in the interfacial area during phase inversion and showed that the width of the inversion ambivalent region is significantly affected

by interfacial tension, and that lowering the interfacial tension will widen the region. More recently, Ioannou et al. (2005) investigated the influence of pipe wettability on phase inversion by using stainless steel and plastic pipes. The results showed that phase inversion of oil-in-water flows would happen at a higher input oil fraction when using the plastic pipe, than in the stainless steel pipe at the same velocity (Ngan 2010).

Inlet conditions:

The inlet conditions (i.e. how the two fluids are introduced into the pipe), can affect the phase inversion appearance. This was examined in the experiments conducted by Piela et al. (2006, 2008) when two ways of introducing the fluids into the test pipe were investigated. In one of their experiments, the continuous phase was introduced in the pipe loop and wetted the pipe wall. The dispersed phase was then injected into the loop and a particular volume of mixture removed to ensure a constant mixture velocity of fluid in the system. The dispersed phase fraction was gradually increased with the continuous injection of the dispersed phase until phase inversion occurred. In the direct experiment, the two fluids were introduced as two separate continuous phases and subsequently mixed within the test pipe. The input flow rates of the two phases were adjusted to maintain a constant mixture velocity. From the experimental outcome, the critical fraction of the dispersed phase for inversion can be significantly higher for the continuous experiment than for the direct one. This suggests that phase inversion can be postponed or avoided by altering the inlet conditions (Ngan, 2010).

Flow geometry:

In pipeflow, it is possible that obstacles present at the wall could cause the dispersed phase to be separated out behind the obstacle due to the recirculation of the fluid. The separation of these drops could possibly have an influence on the coalescence rate and hence on phase inversion.

Hossain et al. (1983) examined the relationship between the dispersion wedge geometry and phase inversion in mixer-settlers. Here, the dispersion wedge is

the shape of the dispersion band which is distributed in the form of a wedge between the two separated phases in a settler. They found that phase inversion is accompanied by either an increase or decrease in the dispersion wedge length, thus affecting the effective settler length. In industrial settlers which seldom operate under steady-state conditions, there is enhanced mutual phase entrainment since the design of the settler involves the dispersion wedge extending across the entire length of the settler. Minimum entrainment is obtained, on the other hand by ensuring phase stability (Yeo et al., 2000).

2.4.3 Predicting the Phase Inversion Point

In designing pipelines, separation facilities and multiphase pumps, phase inversion is a key factor to be considered because of associated changes to the rheological properties of the dispersion and the accompanying pressure drop due to the high effective viscosity of the mixture (Angeli, 1996; Brauner and Ullmann, 2002; Wang and Gong, 2009; Xu., 2007). Thus, an investigation of phase inversion in pipelines can help to improve the pipe design to facilitate the transportation of multiphase mixtures.

Based on the many experimental studies into oil-water flows, several models and correlations have been suggested for predicting the phase inversion point.

Yeh et al., (1964) suggested a correlation to determine the point of phase inversion as a function of the viscosities of fluids, as given below:

$$\varepsilon_w = 1 \Big/ \left(1 + \left(\frac{\mu_o}{\mu_w} \right)^{0.5} \right) \qquad (2\text{-}22)$$

where ε_w is the water fraction at the phase inversion point. μ_w and μ_o are the water and oil viscosities, respectively.

Arirachakaran et al. (1989) suggested an empirical model also includes the viscosity effect on the phase inversion point as follows:

$$\varepsilon_w = 0.5 - 0.1108 \log \frac{\mu_o}{\mu_w} \tag{2-23}$$

where ε_w is the water fraction at the phase inversion point. μ_w and μ_o are the water and oil viscosities, respectively.

Decarre and Fabre, (1997) established the following correlation to estimate the phase inversion point based on the properties (density and viscosity) of the continuous and dispersed phases:

$$\varepsilon_w = 1/(1 + \left(\frac{\mu_o}{\mu_w}\right)^{(1/6)} \cdot \left(\frac{\rho_o}{\rho_w}\right)^{(5/6)}) \tag{2-24}$$

where μ_o and μ_w are the viscosities of oil and water, respectively, and ρ_o and ρ_w are oil and water densities, respectively.

Chen (2001) developed a correlation for the critical water fraction, where the point of phase inversion takes place, based on Arirachakaran et al. (1989) and experimental results. In Chen's correlation, the oil-water density ratio was taken into account and is given as:

$$\varepsilon_w = 0.3788 - 0.1108 \log \left(\frac{\mu_o}{\mu_w}\right) - 9.6533 \left(\frac{\rho_w - \rho_o}{\rho_w}\right) + 2.4841 \left(\frac{\rho_w - \rho_o}{\rho_w}\right) \tag{2-25}$$

where, ρ_o and ρ_w are densities of the pure oil and water, respectively. μ_o the viscosity of oil and μ_w the water viscosity.

Brauner and Ullmann (2002) proposed a model that is quite similar to that of Decarre and Fabre (1997) for predicting the critical fraction; based on minimum changes in system energy, the oil and water phases and system temperature are almost constant at phase inversion as given below:

$$\varepsilon_w = 1 - (\rho \cdot \mu^{0.4}/(1 + \rho \cdot \mu^{0.4})) \tag{2-26}$$

where ε_w is the water fraction, ρ the density ratio $\frac{\rho_o}{\rho_w}$ and μ the viscosity ratio $\frac{\mu_o}{\mu_w}$

Another correlation based on the momentum equation for stratified flow was suggested by Nädler and Mewes (1997) to determine the point of phase inversion. They presumed there to be no slip between two fluids and the interfacial tension was neglected.

$$\varepsilon_w = \cfrac{1}{1 + k_1 \left[\cfrac{C_o \; \rho_o^{(1-n_o)} \; \mu_o^{n_o}}{C_w \; \rho_w^{(1-n_w)} \; \mu_w^{n_w}} \; (D \; U_m)^{(n_w - n_o)} \right]^{1/k_2}} \qquad (2\text{-}27)$$

where ρ_o is oil density, ρ_w is water density, D is the pipe diameter, U_m is the oil-water mixture velocity, C and n are the parameters used in the Blasius fraction factor correlation ($C \, R_e^{\,n}$). k_1 and k_2 are empirical parameters. K_1 reflects the wall-liquids contact perimeter and k_2 accounts for the flow regime in each of the phases.

The aforementioned correlations have been used in the literature to predict the phase inversion point in oil-water flow systems. Therefore, some of these equations will be used to estimate the critical input water fraction theoretically and compare it with the tested experimental results in the present work.

2.5 Influence of gas injection on flow Characteristics in pipes

In the petroleum industry, oil-gas-water three-phase vertical flow often occurs. For instance, the gas-lift technique is often applied in oil wells and subsea risers. There are recent experimental works showing that for various reasons sometimes gas lift is not efficient in three-phase flows. One of the reasons for this is the interplay between the oil and water and this depends on which is the continuous phase when phase inversion occurs. When the flow in the riser system changes from oil continuous to water continuous flow, the behaviour of the multiphase flows also change. As previously discussed, this is reported to have significant consequences for the pressure gradient that accompanies phase inversion. However, there are many researchers who have investigated oil-water liquid-liquid flows and the phase inversion phenomenon in horizontal and vertical pipes, but little work has been done concerning the influence of gas injection on this phenomenon and particularly investigations into the pressure gradient characteristics.

Nädler and Mewes (1995) performed experiments on the flow of two immiscible liquids and investigated the influence of inserting low percentages of gas into a horizontal pipe. The experiments were carried out in a horizontal pipe with an inner diameter of 59 mm and a total length of 48 m. The results of their experiments indicated that drag reduction was possible by injecting gas into laminar flow mixtures of oil and water. Both water-dominated and oil-dominated flow systems could be distinguished in the aerated slug flow regime of the three-phase flow. According to their experimental data, they suggested that the pressure drop of the three-phase flow should be estimated by the pressure drop of the two-phase flow of water and air in a water-dominated system and by the pressure drop of oil and air in an oil dominated system.

Xu et al. (2009) have also investigated the influence of gas injection into an oil-water flow in horizontal pipe. Their study emphasised the influence of gas injection on the average in-situ oil fraction. They found that injected gas has a considerable influence on the in-situ fraction. An increase in the rate of gas

injection leads to a decrease in the local oil fraction, i.e. the in-situ oil fraction with gas injection decreases to a greater extent than that without gas injection, at the same input liquid flow rates.

Descamps et al. (2006, 2007) carried out experimental investigations on the influence of gas injection on phase inversion and the associated pressure gradient increase during the phase inversion of oil-water vertical flows. They used low injected gas flow rates (max GVF = 9.52%) where only two flow regimes of dispersed flow and slug flow were formed. Their results showed that with gas injection the pressure gradient of the three-phase flow was always smaller than for the case of oil-water two-phase flow, except at the point of phase inversion where the pressure gradient could be even higher than for the oil-water flow. They also found that air injection did not significantly change the critical concentration of oil and water where phase inversion occurs.
Moreover, their results showed that the sharp increase of mixture viscosity at phase inversion is still noticeable, and is responsible for a dramatic increase of the friction component of the pressure gradient in a vertical pipe flow.

Recently, Xu et al. (2012) carried out experimental work in a vertical pipe to study the influence of gas injection on pressure gradient. Their work was restricted to bubbly flow (with a low gas flow range of 0 - 0.85 m/s) with continuous liquid (oil or water). Their results showed that gas injection has little effect on phase inversion as it is still taking place at the same oil volume fraction before injecting the gas. The average in-situ gas fraction reached its lowest value around the phase inversion point. In comparison to the oil-water flow, the presence of gas decreased the gravity pressure gradient considerably and the total pressure gradient was also reduced. However, when the input oil fraction was close to the phase inversion point, the contribution of frictional and gravity terms to the total pressure gradient became more equalised, hence the total pressure gradient in a three-phase flow could be higher than that in an oil-water flow around the phase inversion region.

In order to extend the knowledge of the influences of gas injection on the flow characteristics of oil-water flows in vertical pipes, the current study carried out

such an investigation in a 52 mm vertical riser using a wide range of injected gas flow rates (up to 100 sm^3/h, equivalent to ~ 6.30 m/s gas superficial velocity), which had not been tested before. These flow conditions were expected to form several types of flow regimes in the riser, which may then show different behaviours of gas injection on oil-water flows. Moreover, in order to gain information about the flow behaviour at various flow conditions, advanced instrument of capacitance WMS and conventional clamp-on gamma densitometer were tested.

CHAPTER THREE

3. EXPERIMENTAL FACILITY, INSTRUMENTATIONS and DATA ACQUISITIONS

This Chapter presents a detailed description of the experimental facilities and rig used to study the flow behaviour present in a vertical pipe. An overview of the three-phase facility is given in Section 3.1. A detailed description of the 2 inch test rig (52 mm vertical riser) and the modifications made to the system to accommodate the proposed experiments for this study are presented in Section 3.1.3. The test fluids and their properties are given in Section 3.1.5. The instrumentation used and data acquisition systems are highlighted in Sections 3.2 and 3.3, respectively. Furthermore, the details of the experimental procedures and tests matrixes will be described in Section 3.4.

3.1 Description of the Experimental Facility

The experiments of this work were performed in the three-phase test facility in the Flow Laboratory, Offshore, Process and Energy Engineering Department at Cranfield University, United Kingdom. In the three-phase test facility, there are two, 52 mm and 102 mm flow loops. However, in this study all the experimental work was carried out using only the 52 mm flow loop riser system. Figure 3-1 shows the schematic of the three-phase test facility flowline including the 52 mm riser system. The three-phase test facility is a high pressure, automatically controlled test facility, which is able to supply, measure and control oil, water and air flows to the test rigs. The test facility can be divided into four areas as illustrated in Figure 3-1: the fluid supply and metering area, the valve manifold area, the test area and the separation area.

3.1.1 Fluid Supply and Metering Area

Oil and water are pumped from their 12.5 m^3 storage tanks using their own multistage Grundfos CR90-5 pumps (each of which is designed to supply a

maximum flow rate of 100 m^3/h at 10 barg). Start-up, speed control and shutdown of these two pumps are achieved remotely using the Emerson DeltaV control system. The air is delivered by a compressor (Atlas Copco Electonikon GA75) and stored in a large air receiver to reduce the pressure fluctuation from the compressor, before entering the flowline. The air from the receiver passes through filters and then a cooler where debris and condensates are stripped out. The supplied air is metered by two Rosemount Mass flow meters, one for metering lower air flow rate from 0 - 120 sm^3/h and a larger one which can measure higher air flow rate from 120 - 4,250 sm3/h. Apart from these two gas flow meters another flow meter is also installed near the 52mm riser base to measure the injected air. This flow meter is an Endress and Hauser Vortex flow meter with an accuracy of ±0.25%.

3.1.2 Valve Manifold Area

The three-phase rig is built with enough flexibility so that various parametric effects can be studied by changing or modifying the setup. Thus, the supplied fluids can be mixed before entering the test rigs loops at the valve manifold area, which is designed to mix and distribute fluids to test rigs in the three-phase facility. The main purposes of the valve manifold area are as follows:

- Supplying water and/or oil to 52 mm ID flow loop and 101 mm ID flow loop exclusively.

- Providing the accessibility of the main air supply to 52 mm flow loop and 101 mm flow loops. Thus air can be injected into the risers' systems either at the horizontal section, which is at the upstream of the risers' bases or at the risers' bases.

3.1.3 Test Rig Description

The 52 mm (2 inch) riser in the multiphase test facility is made up of NB schedule 10 stainless steel. It consists of a 40 m long horizontal flow-line, connecting to a 10.5 m height vertical pipe.
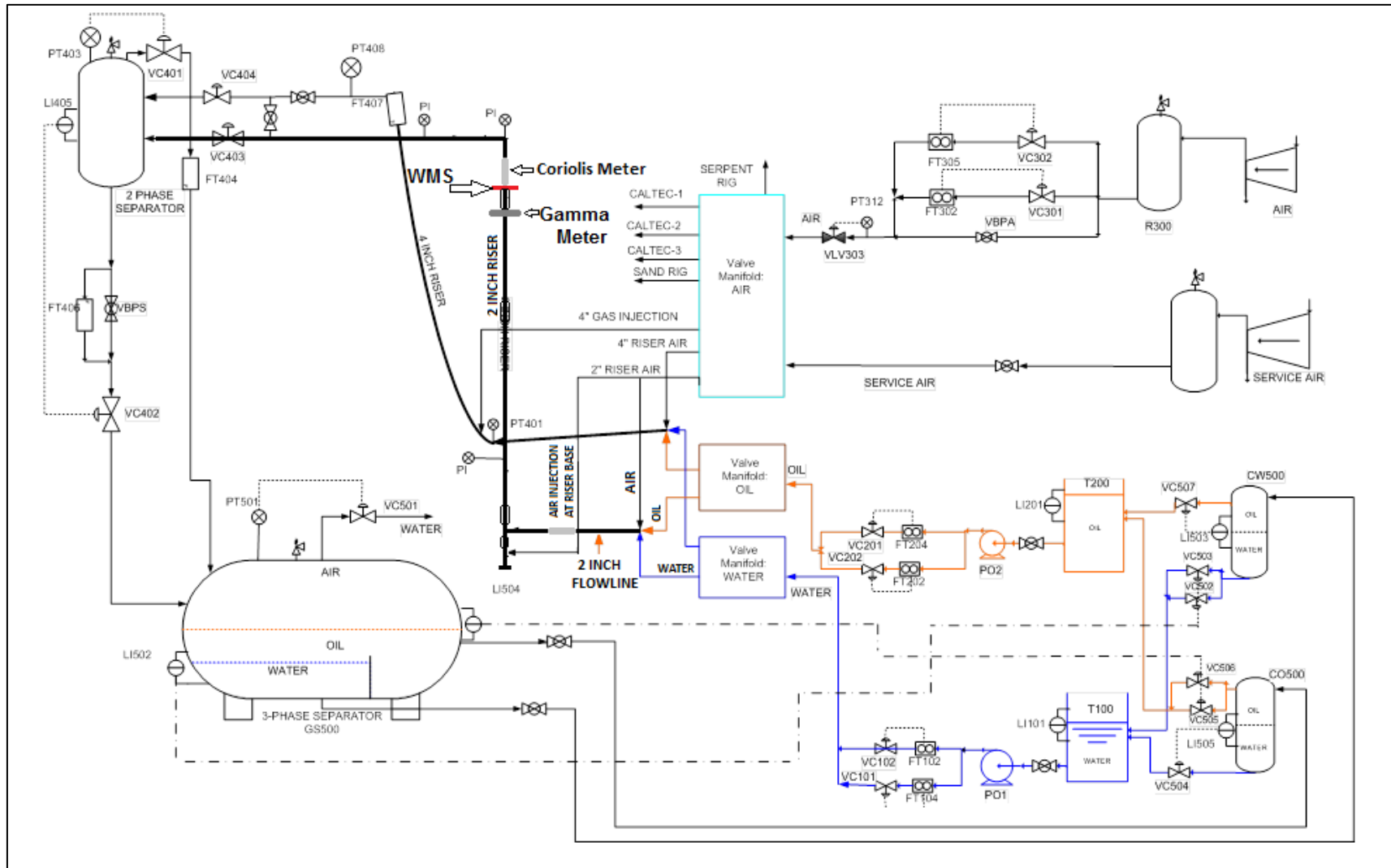
Figure 3-1: Schematic of the Three-Phase Test Facility in the Flow Laboratory (Yeung and Lao, 2013)

As illustrated in Figure 3-2, the vertical stainless steel riser has four transparent Perspex sections of lengths of 30 cm, 60 cm, 20 cm and 40 cm. They are installed at locations ~0.01, 0.5 m, 5.5 m and 9 m above the riser base (where the gas injection points are located), respectively. Through these sections, visual observation of the flow can be made. The riser outlet is connected to a two-phase vertical separator, where the air and liquid are separated. Several instruments are installed along the riser to study the multiphase flow characteristics inside the riser. A 2 inch control valve is installed between the riser and the two-phase top separator, which is used for the purpose of controlling the flow conditions in the test section.

As shown in Figure 3-2 (at the left hand side of the Figure), the 52 mm riser in the three-phase facility was slightly modified to accommodate the proposed experimental work in this study. Four calibrated flush mounted pressure transducers are installed along the vertical section of the riser at different axial distances to obtain a pressure gradient profile by monitoring the differential pressure (DP) along the 52 mm vertical riser. Two Rosemount 3051pressure transducers are installed in the riser system at distances of 1.6 m and 9.10 m from the riser base. Also, two Druck PMP 1400 pressure transducers are installed in the middle part of the riser at 4.35 m and 5.75 m from the riser base. This arrangement of the transducers forms three DP measurement sections with axially separated distances of 2.76 m, 1.38 m and 3.26 m long (bottom, middle and the top section, respectively). The outputs of these pressure transducers are all recorded in the Labview data acquisition system.

Also, two Coriolis meters made by Endress and Hauser (E&H) are fitted on the 52 mm rig system. One is installed in the horizontal section of the flow loop about 1.2 m before the riser base and the other at the top of the vertical riser. The specifications and operating conditions of the 52 mm riser test loop are summarised in Table 3-1.

Moreover, a 16 × 16 WMS was recently installed in the 52 mm vertical riser at a distance of 9.5 m (~183D) from the riser base. In-line filter for the 52 mm flow loop was also installed downstream of the horizontal flowline. The filter is used to ensure clean fluids in the flowline so that the WMS would not be damaged by

particles. A clamp-on gamma densitometer supplied by Neftemer Ltd is also installed near the riser top at about 9 m (~173D) from the riser base and 0.5 m below the WMS.
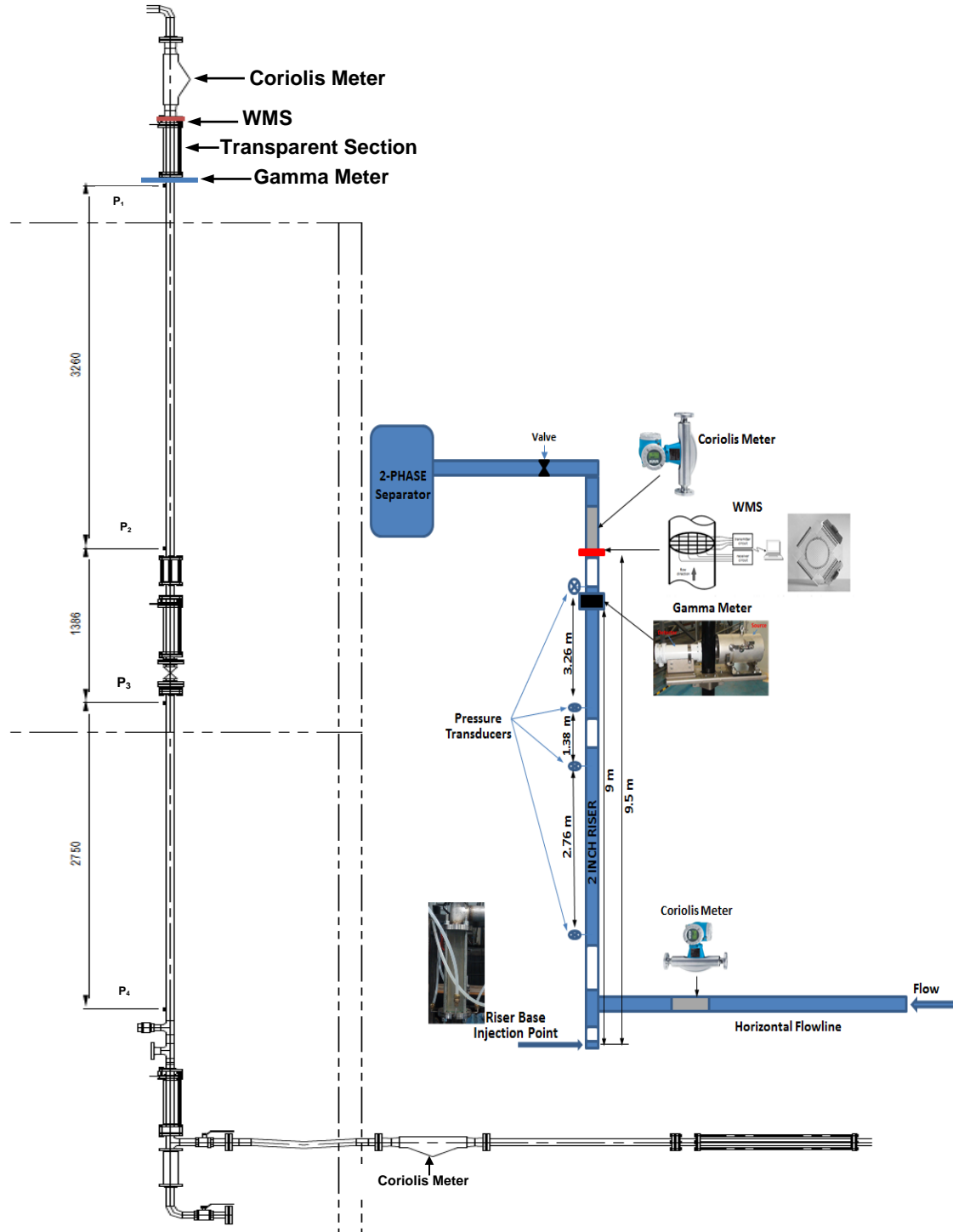
Figure 3-2: The 52 mm riser with the existing instruments: The left hand side of the Figure shows a drawing of a modified riser system.

Figure 3-3: Actual picture of the 52 mm riser rig in the flow laboratory

3.1.4 Separation Area

This area consists of two main separators: Two-phase vertical separator and 3-phase horizontal separator. When exiting the test rigs, the liquid and air mixture is separated into air and liquid (oil and/or water) in a two-phase vertical separator, where the air and liquid are separated. The liquid mixture from the two-phase separator goes into the three-phase horizontal separator where it is gravity separated into respective phases. The pressure, oil/water interface level and gas/liquid interface level in the 3-phase separator are controlled by means of a pressure controller and two level controllers, managed by the DeltaV control system the remaining air is then discharged to the atmosphere. The oil and water enters their respective coalescers where they are further separated from the other phase. The oil and water then enter their respective storage tanks.

Further description and details of the full operating procedure of the three-phase test facility can be found in Yeung and Lao (2013).

Table 3-1: Summary of specification and operating conditions for 3-phase facility

Parameter	52 mm riser loop
Diameter of flow loop & riser	2 inch (52 mm) NB Schedule 10
Length of flow loop	10.5 m vertical pipe/40 m flowline
Inclination of flow loop	0°
Shape of riser	vertical
Pressure rating of flow loop	20 barg
Temperature rating test facility	0 - 80°C
Duty of water pump	100 m^3 /hr @ 10 barg
Duty of oil pump	100 m^3 /hr @ 10 barg
Duty of air compressor-1# (Atlas Copco Electonikon GA75)	570 m^3 /hr FAD @ 7 barg
Range of inlet water flow meter 1" Rosemount 8742 Magnetic flow meter 3" Foxboro CFT50 Coriolis meter	0 - 7.36 kg/s (Accuracy of ± 0.20 %) 0 - 30 kg/s (Accuracy of ± 0.15%)
Range of inlet oil flow meter 1" Micro Motion Mass flow meter 3" Foxboro CFT50 Coriolis meter	0 - 9.47 kg/s (Accuracy of ± 0.50%) 0 - 30 kg/s (Accuracy of ± 0.15%)
Range of inlet air flow meter ½" Rosemount Mass flow meters 1" Rosemount Mass flow meters	0 - 150 sm^3 /hr 100 - 4250 sm^3 /hr (Accuracy of ± 0.90 %)

3.1.5 Experimental Fluids

The fluids used for this research work are air (as the gas), and Dielectric oil Rustlick EDM-250 (non-hazardous liquid with a density of about 810 kg/m^3 and viscosity at about 7.2 mPa.s at around 21°C) and tap water as the liquids. The temperature in the riser system for all experiments was observed to be around 21°C (+/- 4°C). The physical properties of used water and oil are summarised in Table 3-2. Because there were no available data in the literature about how the viscosity and density of the dielectric oil changes with temperature, initial tests were carried out to study the variation of the oil viscosity and density with possible changes in temperature. A bench test using a calibrated Brookfield viscometer (a copy of the calibration certificate is included in Appendix A) was performed to obtain viscosity measurements at different temperatures. As can be seen in Figure 3-4, an exponential trend line was used to generate an equation that can be applied to predict how the dielectric oil's viscosity changes with temperature.

In addition, experimental data for oil only flows in the three-phase facility were examined to ascertain how oil density changes with temperature. Density readings at the inlet Coriolis meter for different oil flow rates were recorded and the results plotted against the temperature, as shown in Figure 3-5. A linear trend line was used to generate an equation that can predict how the dielectric oil density changes with temperature. Thus, these equations will be used to determine in-situ oil viscosity and density at a particular temperature during the test experiments involving oil flow.

Table 3-2: The physical properties of the liquids used in the 3-phase rig

Property	Water	Oil	Air
Density, kg/m^3	998	810 @ ≈21°C	1.225 @ ≈21°C
Viscosity, mPa.s	1	7.2@ ≈21°C	0.0185
Boiling point (°C)	100	273	-
Relative permittivity	80	2.3	1
Conductivity, µS/cm	310 (540)	N/A	0
Surface tension, mN/m	71(32)	19	-
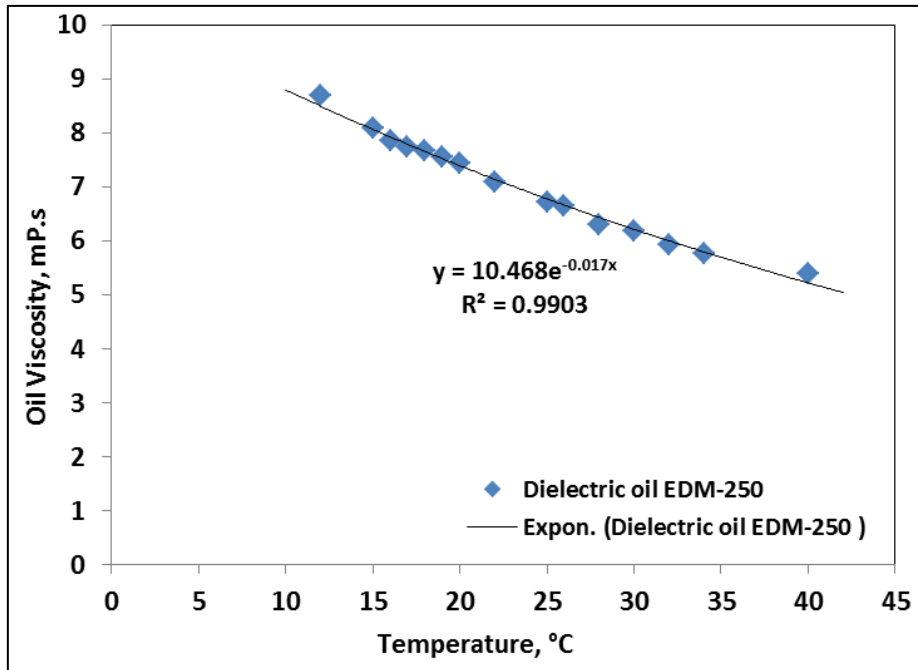
Figure 3- 4: Dielectric Oil EDM 250's viscosity changes with temperature
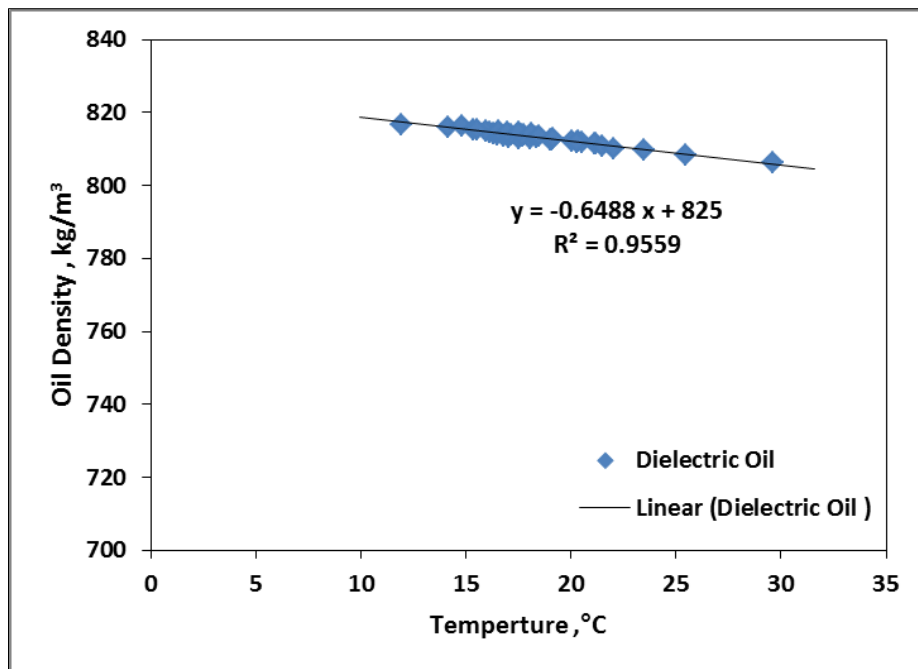
Figure 3-5: Dielectric Oil EDM 250's density changes with temperature

3.2 Instrumentation

3.2.1 Pressure transducers

As previously mentioned, in order to monitor the pressure gradient across the 52 mm riser, four mounted pressure transducers are installed along the vertical section of the riser at different axial distances. The two Rosemount pressure transducers with a range of 0 - 7 barg with an accuracy of ±0.15% were also installed on to the riser system at distances of 1.6 m (~30D) and 9.1 m (~175D) from the riser base. The two Druck PMP 1400 pressure transducers with a range of 0 - 2.5 barg, an output voltage of 0 to 5 volts and a nominal accuracy of ±0.15% are installed at distances of 4.35 m (~84D) and 5.75 m (~110D) from the riser base. Prior to installing these pressure transducers, they were individually calibrated. The output voltage from the pressure transducers is shown in a linear relationship with the pressure, as can be seen in Figure 3-6. The calibration results (slope and offset) for each pressure transducer were programmed into the Labview Data Acquisition system. The outputs of these pressure transducers were all recorded in the Labview system at a frequency of 1,000 Hz and the recording rate was 100 Hz.
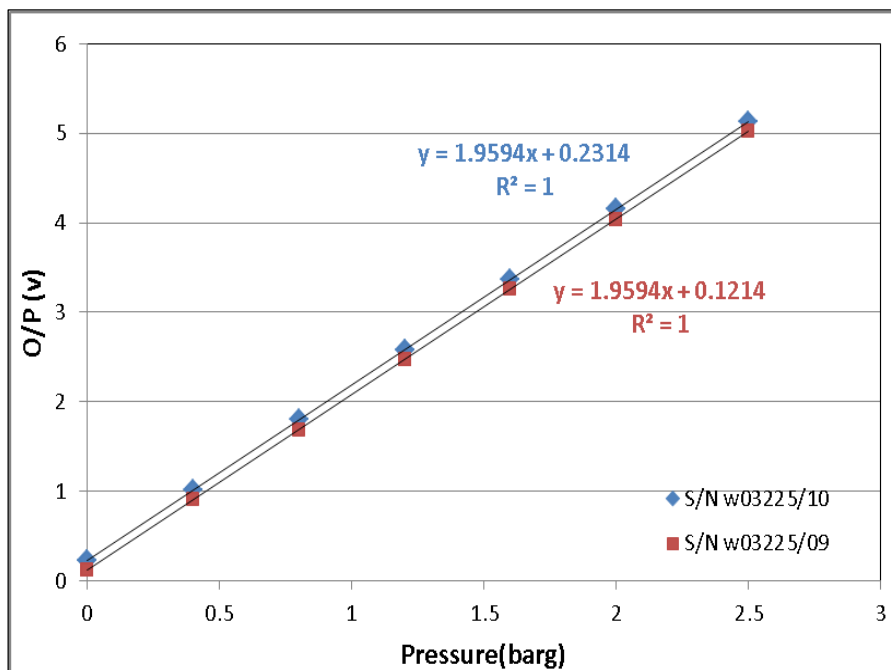
Figure 3-6: Pressure Calibrations for two Druck Pressure Transducers.

57

3.2.2 Coriolis Mass Flow meters

The 52 mm vertical riser is utilised by two Endress and Hauser (E&H) Coriolis mass flow meters (Promass 83F). A typical image for an E& H Coriolis flow meter is illustrated in Figure 3-7. One Coriolis is located at the top of the vertical riser section and the other on the horizontal flowline near to the riser base in order to measure the oil-water mixture mass flow and density, so that phase slips in the vertical riser can be estimated by comparing mixture densities from the Coriolis meter at the riser base and the existing meter at the riser top. This type of Coriolis flow meter is configured to give the fluid mass flow rate (proportional to the phase difference between two sensors mounted on the measuring tube to register a phase shift in the oscillation), fluid density (proportional to resonance frequency of the measuring tube) and temperature (measured with temperature sensors) simultaneously. It has a wide range of process conditions during measuring operations: measured fluid temperatures up to 350 °C, line pressures (up to 100 bars) and mass flow measurement (up to 2200 t/h). The outputs of the Coriolis mass flow meters in this experimental work were also recorded through the Labview system at scan and recording rates of 1000 Hz and 100 Hz, respectively. The basic measurement principles of the Coriolis mass flow meters were described in Section 2.3.4.

Figure 3-7: E&H Coriolis Mass Flow Meter

3.2.3 Capacitance Wire Mesh Sensor (CapWMS)

In the capacitance wire-mesh sensor instrument, the electronics measure the electrical capacitance (permittivity) of the fluid at each crossing point of the grid formed by the wires, which is then related to a fluid phase. The transmitter electrodes are activated in sequence while the receiver electrodes are parallel sampled. The WMS electronics measure the local permittivity of the fluid in each crossing point by successively applying an excitation voltage to each one of the sender electrodes while keeping all other sender electrodes at ground potential, and then measuring, respectively, the direct or alternating electrical current flow to all receiver electrodes synchronously. Based on these measurements, each crossing point of the transmitter and receiver electrodes is scanned individually, generating a matrix in the x–y plane depending on the size of the sensor. Accordingly, the average phase fraction and fluids distribution at any point within the cross section of the sensor in the pipe is estimated (Da Silva et al., 2007).

In the current study, a 16 × 16 wire mesh sensor (WMS) based on permittivity measurements was employed to determine the void fraction/liquid holdup, phases distribution and flow patterns identification inside the 52 mm vertical riser. Thus, the WMS system CAP200 and its associated softwares that were recently developed at Helmholtz-Zentrum Dresden-Rossendorf (HZDR) were used to extract and analyse the cross-sectional phase distribution in the 52 mm riser. The sensor was installed at the top part of the vertical riser at a distance of 9.5 m (~182D) from the riser base, where the flow is considered as fully developed. The electronics box of the wire mesh sensor CAP200 system is designed to be able to produce up to a 10,000 frames/s. The sensors are constructed to operate under temperatures up to 180°C and pressures up to 7 MPa (HZDR, 2012). Figure 3.8 shows an actual image for the CAP 200 capacitance electronic box (marked (a)) and the 16 x 16 WMS (marked (b)) that were used in this work and installed at the top of the riser. Also, the design drawing for the 16 x 16 WMS used is provided in Appendix A-2.
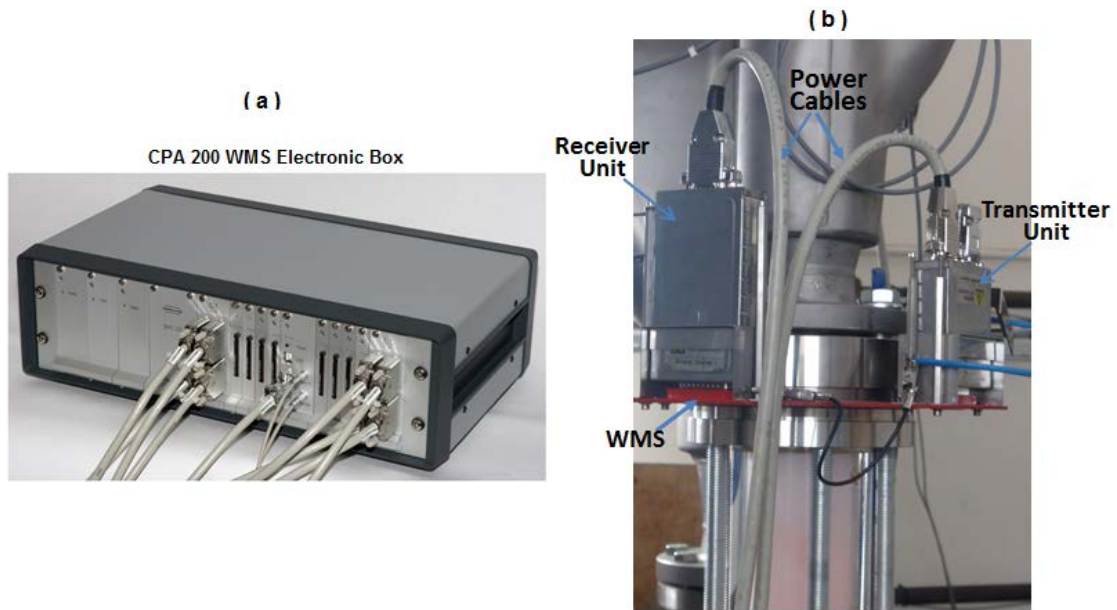
Figure 3-8: Wire-mesh sensor (WMS), a) Capacitance WMS electronic box, b) WMS installed in the riser and connected to the electronic box

Wire-Mesh Sensor (WMS) measuring procedure:

After connecting the electronic device, switch on the WMS CAP200 basic device.

- Start the WMS CAP200 software.
- After the system configuration, the WMS CAP200 main screen is displayed as shown in Figure 3-9.
- Activate the Online button.
- Load a pre-created mask.
- Adjust Offset and Gain sliders to take the calibration process to achieve the highest possible contrast between the smallest and largest electrical permittivity values used in the experiments. The calibration data for the lowest and highest electrical permittivity should be acquired, as mentioned below, by filling the complete cross section with the specific fluids. The max. Gain value should be less than 90%; Offset should be adjusted to be above zero level (approx. 5%).
- Set the frequency and measurement duration (1,000 Hz/30 sec).
- Deactivate the Online button and press the Start button.

- Measurement status displayed via the progress bar's Measurement, Download and Check, are also displayed.
- Press the Save As button to save the measurement data.
- Convert the data to raw data using the WMS Data-converter.
- Finally, use an associated WMS framework to obtain output WMS data. Figure 3-10 illustrates a schematic of the WMS CAP200 and the procedure to gain the output data.
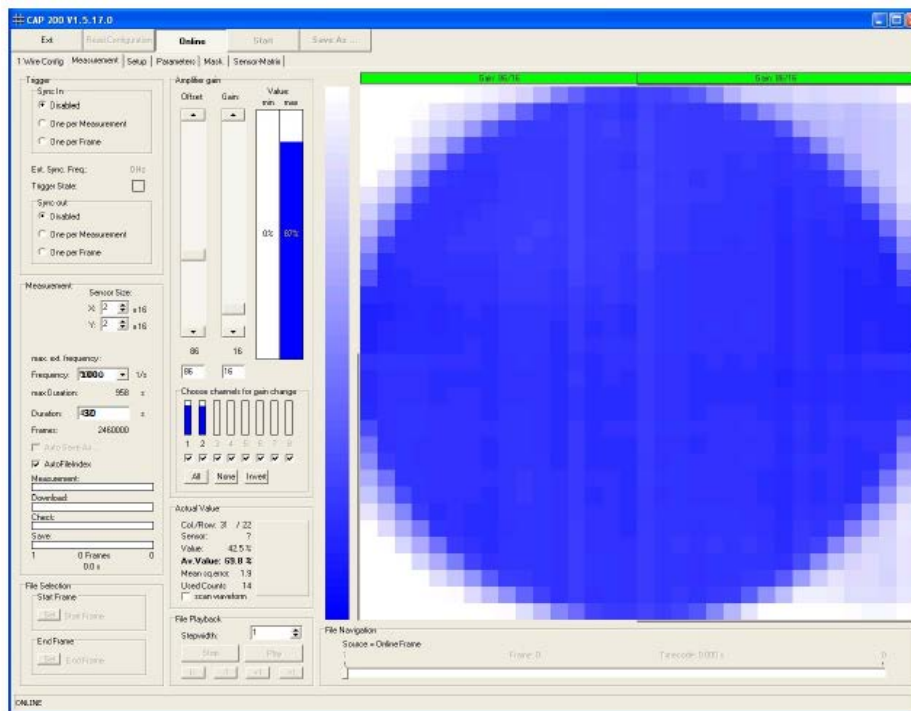
Figure 3-9: WMS CAP200 data acquisition program
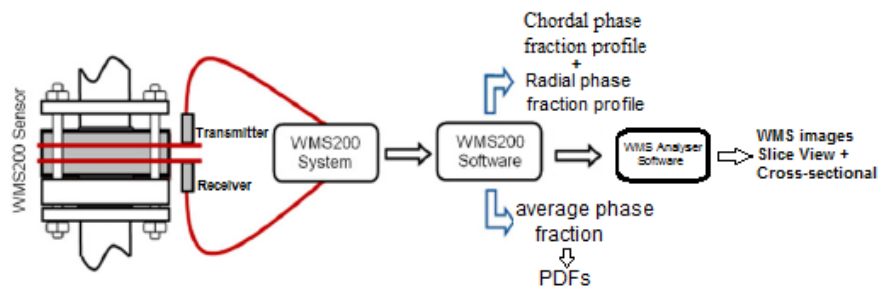
Figure 3-10: Schematic of the WMS CAP200 measurement.

For the graphical presentation of the WMS data, different visualization methods were extracted. These included phase fraction distribution along a central chord of the cross section. Additionally, axial coloured sliced view movies and cross-sectional images were produced by using courtesy software (wire-mesh analyser v1.4) developed recently by Dr. Marco Da Silva's Group at Universidade Tecnológica Federal do Paraná. The produced images were reconstructed as a cross section image and X and Y axially slice views as shown in Figure 3-11. Image X is obtained by stacking cross section images and then axially slicing in a 0°-180° direction, similarly for image Y along the 90° - 270° direction. In order to give near reality geometries of phase structures in the pipe at different mixture superficial velocities, the number of cross section images *N* was used to reconstruct the axially slice images, which is given by:

$$N = \frac{f_s \cdot \mathrm{L_p}}{\mathrm{U_{sm}}} \qquad (3\text{-}1)$$

where, f_s is the WMS system frame rate, i.e. 1,000 frame/s; $\mathrm{L_P}$ is the pipe section length represented by the axial sliced images, i.e. 1 m; and $\mathrm{U_{sm}}$ is the mixture velocity at the respective flow conditions.

It is essential that a calibration process for the WMS is performed under static conditions. In the case of air-liquid experiments, two reference settings were acquired for the calibration: pipe empty as the low reference measurement and pipe full of static liquid as the high reference measurement. Likewise, prior calibration with the riser full of static oil only, then full of static water, was carried out for the oil-water experiments. All the wire mesh sensor measurements were obtained at a frequency of 1000 for a 30 second experimental measurement period.
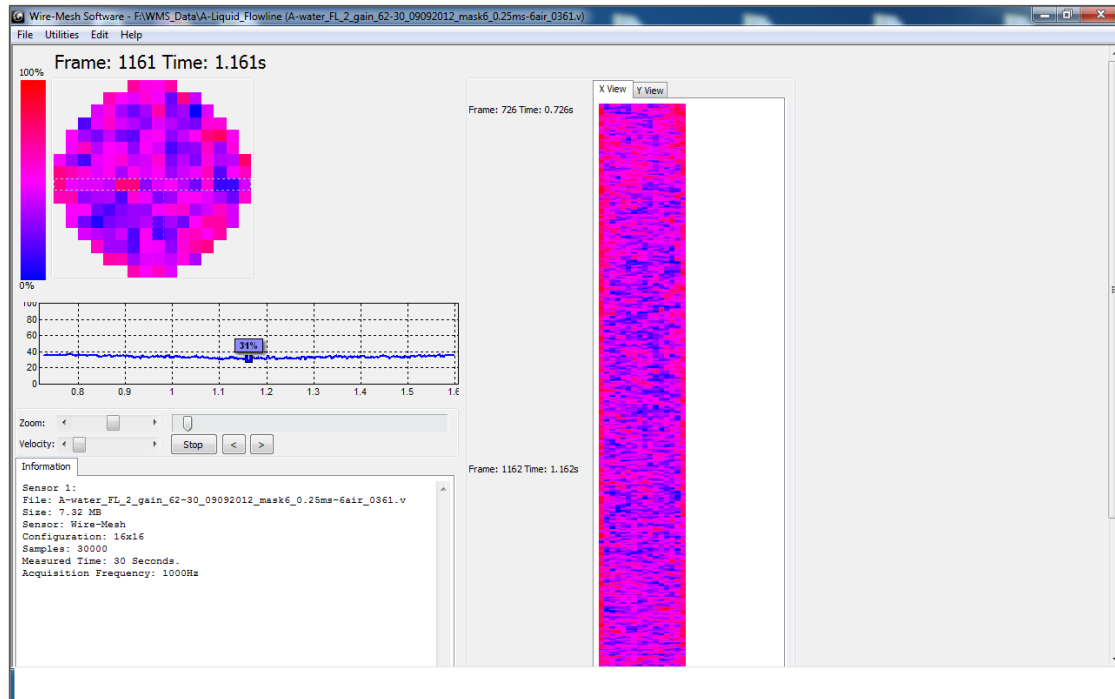
Figure 3-11: Wire-mesh sensor visualization software

3.2.4 Gamma Densitometer:

A Gamma densitometer generally consists of a single beam gamma source and detector units, as shown in Figure 3-12, for the clamp-on gamma densitometer available in the Flow Laboratory. A collimated gamma ray is directed at the pipe with a sensor placed directly opposite the source on the other side of the pipe. The general principles of Gamma densitometers are described briefly in Chapter 2, Section 2.3.1.

In the present study, gamma densitometer units, supplied by Neftemer Ltd were installed at the top part of the 52 mm vertical riser at 9 m (~173D) from the riser base. The gamma densitometer source emits direct high-energy photons (named the hard spectrum counts) and scattered radiation (the soft spectrum counts) for multiphase flow measurement. Received gamma counts at a sampling rate of 250 Hz were transferred to a local PC, where the obtained data were saved and processed.
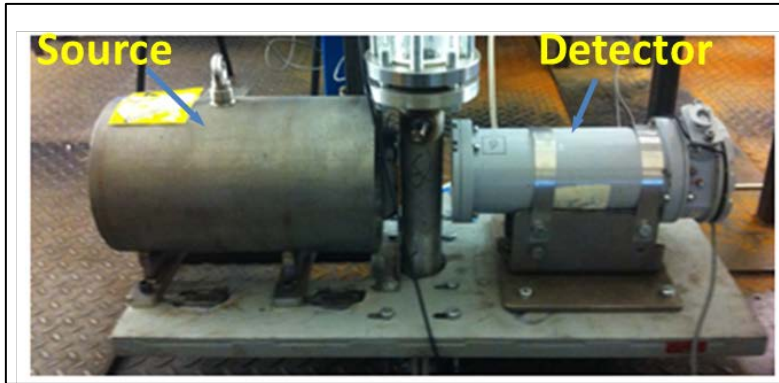
Figure 3-12: Gamma Densitometer in the flow laboratory

The gamma phase fractions (gas void fraction and oil or water fraction) were determined using Equation 2-18 for void fraction in gas-liquid flows and Equation 2-19 for water fraction in oil-water flows. Therefore, calibrations for the gamma meter with air (empty pipe), oil only and water only were carried out for about 30 minutes in static conditions before and after any of the experimental running. Then the collected gamma count rates were averaged to give calibration values for hard and soft gamma counts of each test fluid. The average gamma count values for calibration tests of experiments were plotted against the attenuating fluids (air, oil and water) densities as shown in Figure 3-13. It is clearly shown that gamma count decreases in an approximately linear trend with increasing attenuating fluid density for both hard and soft counts. The hard and soft energy gamma counts show different behaviours of attenuation with increasing density. Thus, the gamma densitometer demonstrated that it was functioning appropriately and exhibited the expected response to fluids of differing densities, which gives confidence and reliability to the data that were measured by the gamma meter.

For the current study, approximately five minutes of actual measurement time was adopted for each test point of all experiments of mixture flows in the 52 mm riser. Also, one of the fascinating uses of gamma densitometer is for flow pattern identification (Blaney and Yeung, 2008). Thus, the output time-varying gamma count signals and the corresponding probability density function (PDF) were used for identifying flow patterns.
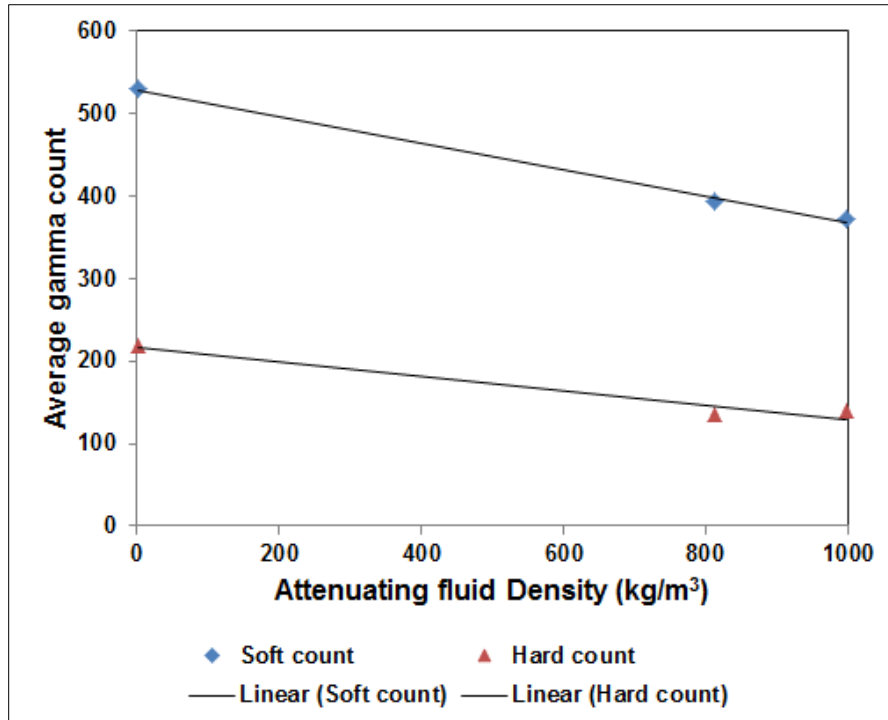
Figure 3-13: Average Gamma Counts as a Function of Fluid Density

3.3 Data Acquisition Systems:

Experimental data in this study were obtained through several separate data acquisition systems. The output signals for each measurement device transferred to these systems using stand-alone PCs where signals being converted into physical values resulted. These systems include:

3.3.1 Delta-V System: By using this system all the processes in the three-phase facility are controlled and monitored remotely. This automation system consists of controllers that control the air, water and oil flow rates to the desired flow rates into the three-phase facility. Figure 3-12 shows the metering area in the DeltaV system. The connected instrumentations in the test facility are interfaced via Fieldbus and PROFIBUS with the DeltaV automation system which is configured to record the connected instruments' output values at a frequency of 1 Hz. The obtained data are stored in the DeltaV historian from where they can be downloaded after the experiments. Further details about the DeltaV system for the 3-phase facility can be found in Yeung and Lao (2013).
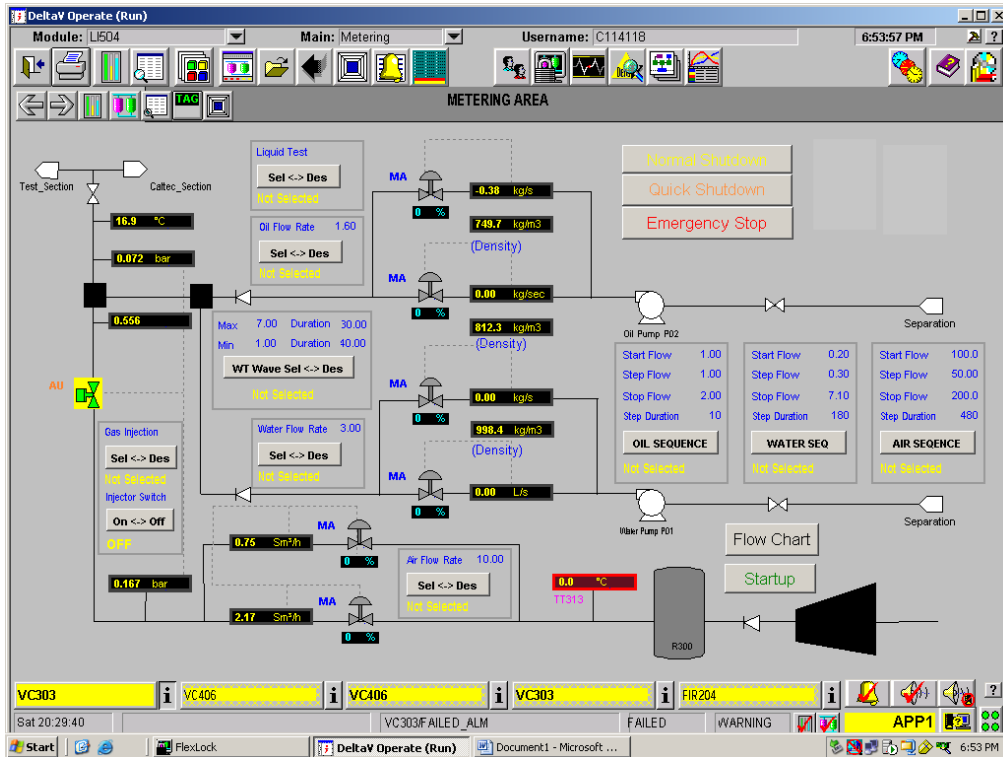
Figure 3-14: DeltaV System Showing the Metering Area.

3.3.2 Labview System: This includes a computer program which was written in Labview. This program is used to record the output signals from the devices such as both Coriolis mass flow meters (fluids density, mass flow rate and temperature measurement) and all pressure transducers installed along the 52 mm rig. The outputs of the gas flow meter for the air inlet to the riser base are also recorded in the Labview program. This Labview program is written as three subdivisions: data acquisition, viewing and saving. The obtained data are read from the channels in the form of output sensor voltages and then converted to values based on the calibration results obtained for each measurement device and save data to text file at a chosen rate. For the experiments in the current study, Labview data scan rate, recording rate and recording duration for each test point were set at 1,000 Hz, 100 Hz and 3 minutes, respectively.

3.3.3 Neftemer Ltd proprietary system: This data acquisition system was used to obtain data from the gamma densitometer installed at the top part of the 52 mm riser. The main part in this system is an ICP I-7188D programmable

66

logic controller (PLC) where the raw densitometer signal is processed into a gamma count signal at a sample rate of 250 Hz before being stored in two separate files: one for the high-energy (hard) counts and the other for the low-energy (soft) gamma counts. The raw data files can then be exported into a Microsoft Excel spreadsheet for further processing.

3.4 Experiment Procedure

Several sets of experimental campaigns for gas-liquid, liquid-liquid and gas-liquid-liquid flows were carried out using the 52 mm riser within the three-phase facility in the Flow Laboratory.

3.4.1 Test Matrix

Firstly, a set of experiments for initial tests of gas-liquid (air-water) two-phase flows was carried out. These experiments of air-water flows were conducted by keeping the liquid superficial velocity constant (water flow of 0.25, 0.5, 1, 1.5 and 2 m/s) in the 52 mm riser and varying the air injection to the vertical section via four uniformly distributed inlets at the riser base. At each constant liquid (water) superficial velocity, varied values of air volumetric flow from 1.50 Sm^3/h (U_{sg} ~ 0.1 m/s) to 100 Sm^3/h (Usg ~ 6.25 m/s) were supplied to the measurements section in the vertical riser. The superficial gas velocities were calculated at the operating conditions of pressure and temperature at the highest part of the riser where the main instruments are located. In order to investigate the effects of the upstream conditions on the flow behaviour in the vertical riser section (presented in Chapter 4, Section 4.2), two different configurations of gas injection on water flows were examined: (i) circumferential injection to the vertical section via the riser base; (ii) gas injection on the horizontal flowline at 40 m upstream of the riser base.

Secondly, systematic experiments of liquid-liquid (oil-water) two-phase flows without gas injection at different values of fixed mixture superficial velocities and different water and oil concentrations were conducted in the riser system. These

experiments were followed by a further long campaign of experiments for air-oil-water where a continuous air flow was injected through the riser base using a wide range of injected air flow rates.

The experiments for oil-water flow were conducted on the simultaneous upflow of the two liquids by keeping the total mixture superficial liquid velocity constant (i.e. oil superficial velocity + water superficial velocity = constant, whenever the input water cut (WC) changes, the total mixture's liquid superficial velocity needs to be adjusted to keep it fixed in the riser system) and changing the input water cut (WC) in steps from 0 - 100%. In these tests, different values for mixture superficial liquid velocities of 0.25, 0.5, 1, 1.5 and 2 m/s were tested. At each flow rate the water cut varied from 0 - 100% at 13 different values (i.e. input water cuts = 0, 10, 20, 30, 40, 42, 45, 50, 60, 70, 80, 90 and 100%).
The average water and oil fractions (in-situ fractions) for each test point of oil-water two-phase flows experiment were determined by (i) using gamma counts from the gamma densitometer applying Equation 2-19; (ii) Coriolis density measurements considering the measured mixture density and oil and water densities using the following Equation;

$$\varepsilon_{\mathrm{w}} = \frac{\rho_{\mathrm{mix}} - \rho_{\mathrm{o}}}{\rho_{\mathrm{w}} - \rho_{\mathrm{o}}} \tag{3-2}$$

where ρ_{mix}, ρ_{o} and ρ_{w} are the mixture, oil and water densities respectively obtained from the horizontal and vertical Coriolis meters at test temperature. From the results of the phase fraction (oil and water fractions), the slip ratio was calculated by using Equation (2.14).

In the experiments for air-oil-water flows, the oil and water were supplied at a constant total mixture superficial velocity and the water cut was varied using the same values as in the oil-water tests. Continuous air injection at the riser base was varied for each oil-water mixture flow at the fixed water cut. A wide range of air injection flow rates of 1.5, 3, 6, 10, 15, 20, 25, 30, 40, 50 and 100 sm^3/h was used. The gas superficial velocities were also calculated at the operating

conditions of the highest part of the riser where instruments (gamma densitometer, wire-mesh sensor and the Coriolis flow meter) are installed.

Each experiment (i.e. each test point at a particular water cut and/or air flow) from the planned test matrixes was conducted at least twice to ensure the reproducibility of the experiments. At each test point, the flows were allowed to stabilize for approximately 25 minutes before any measurement was taken.

Prior to running the experiments and starting up the three-phase facility, the instrumentations (WMS and gamma densitometer) were calibrated at atmospheric pressure as described in Section 3.2.3 for WMS and in Section 3.2.4 for gamma meter. Also, the pressure readings for the pressure transducers were obtained before starting up the system and they applied as zero points to correct the obtained pressure measurements.

An Emerson DeltaV system was used to control the flow rate remotely from the control room. Prior to the pumping of fluids, the system was pressurised to 1 barg using air. For the purpose of this study, the system was allowed about 25 minutes to stabilize before data readings for any flow condition were taken by the data Acquisition Systems. The temperature of the mixture of fluids in the test section was always at around 21°C (±4 °C).

3.4.2 Determination of Inlet Parameters:

The air flow rate was metered at standard conditions near the compressor and at the riser base by two Rosemount mass flow meters. The effect of the local pressure in the test section was considered and the air was treated as an ideal gas. The air superficial velocity at the top of the vertical riser was then calculated as:

$$U_{sg} = \frac{Q_g}{A_P} = \frac{P_{std} \cdot T_t}{P_t \cdot T_{std}} \cdot \frac{Q_{std}}{A_P}$$

(3-3)

where Q_g and Q_{std} are the air volume flow rates at test section conditions and volume flow rate at standard conditions, respectively. T_t and T_{std} are the test section and standard temperatures. P_t and P_{std} are average pressures of the actual test and standard pressure, respectively. A_P is the area of the riser pipe.

The oil and water are supplied individually from their storage tanks using their own multistage pumps. The water flow rate (Q_w) is metered by a 1" Rosemount Magnetic flow meter (up to 7.36 l/s) before entering the 52 mm riser system. Thus, the water superficial velocity can be determined as:

$$U_{sw} = \frac{Q_w}{1000 \, . \, A_P}$$

(3-4)

where, Q_w is the water flow rate (l/s) and U_{sw} is the water superficial velocity (m/s).

On other hand, the oil mass flow rate (Q_o) is metered by a Micro Motion Mass flow meter (up to 9.47 kg/s). Hence, the oil superficial velocity can be calculated as:

$$U_{so} = \frac{Q_o}{\rho_o \, . \, A_P}$$

(3-5)

where Q_o is the oil mass flow rate (kg/s), ρ_o is the oil density (kg/m^3) at the riser temperature and A_p is the area of the pipe (m^2).

3.5 Chapter summary

This Chapter has presented details of the three-phase test facility that was used for this research work. The 52 mm diameter vertical riser flow loop system used in this study, as well as the working fluids and their physical properties were described in detail. An overview of the instrumentation used was presented. The calibration processes for each instrument and how the data were acquired from these instruments was discussed. The procedures undertaken to achieve test matrixes and acquire the experimental data were also discussed.

CHAPTER FOUR

4 GAS-LIQUID TWO-PHASE FLOW IN VERTICAL RISER

In this Chapter the results obtained from a series of laboratory experiments in air-water two-phase flow under riser base gas injection will be presented and discussed. Results from an investigation into the effect of gas injection location on flow patterns and phase distributions occurring in the 52 mm diameter vertical riser will be also presented. The comparison study between capacitance and conductive wire-mesh sensor measurements that were carried out on the air-water flow will be highlighted. These experiments were performed on the 52 mm ID vertical riser flow system which is available within the three-phase facility in the Flow Laboratory at Offshore, Process and Energy Engineering Department at Cranfield University.

4.1 Gas-Liquid Flow Characteristics

In this Section, the results for air-liquid (air-water) characteristics under riser base gas injection will be presented and discussed. Results obtained from different methods of determining void fraction/liquid holdup and flow pattern measurements that were carried out on air-water flow will also be discussed. Pressure gradient characteristics over the vertical riser will be also presented.

4.1.1 Void fraction:

Several experiments for air-water flows were carried out in the 52 mm diameter riser. The experiments were carried out at various air superficial velocities in the range of ~ 0.1 - 6.25 m/s (corresponding to an injected air flowrate range of 1.5 - 100 sm^3/h) at each constant water superficial velocity of 0.25, 0.5, 1, 1.5 and 2 m/s. Determination of the void fraction at each test point of the air-water experiments was performed at the top of the riser using the outputs data from the instrumentations of the capacitance WMS and the clamp-on gamma densitometer. The mean cross-sectional void fraction was obtained directly from

the capacitance WMS by considering the acquired time series of the cross-sectionally averaged void fraction. In the case of the gamma meter, the void fraction was calculated from the average of obtained hard and soft gamma counts for each test point. Figure 4-1 shows how the mean void fraction, measured by the two measuring techniques increases systematically with increasing air superficial velocity at each constant liquid superficial velocity. This trend is explained by the fact that an increase in the gas flow rate increases bubble production, which results in an increase in the void fraction. On other hand, the measured void fraction decreases with an increase of water flow rates. This is due to the increase in the amount of liquid in the pipe causing the decrease in gas void fraction (increase in holdup).
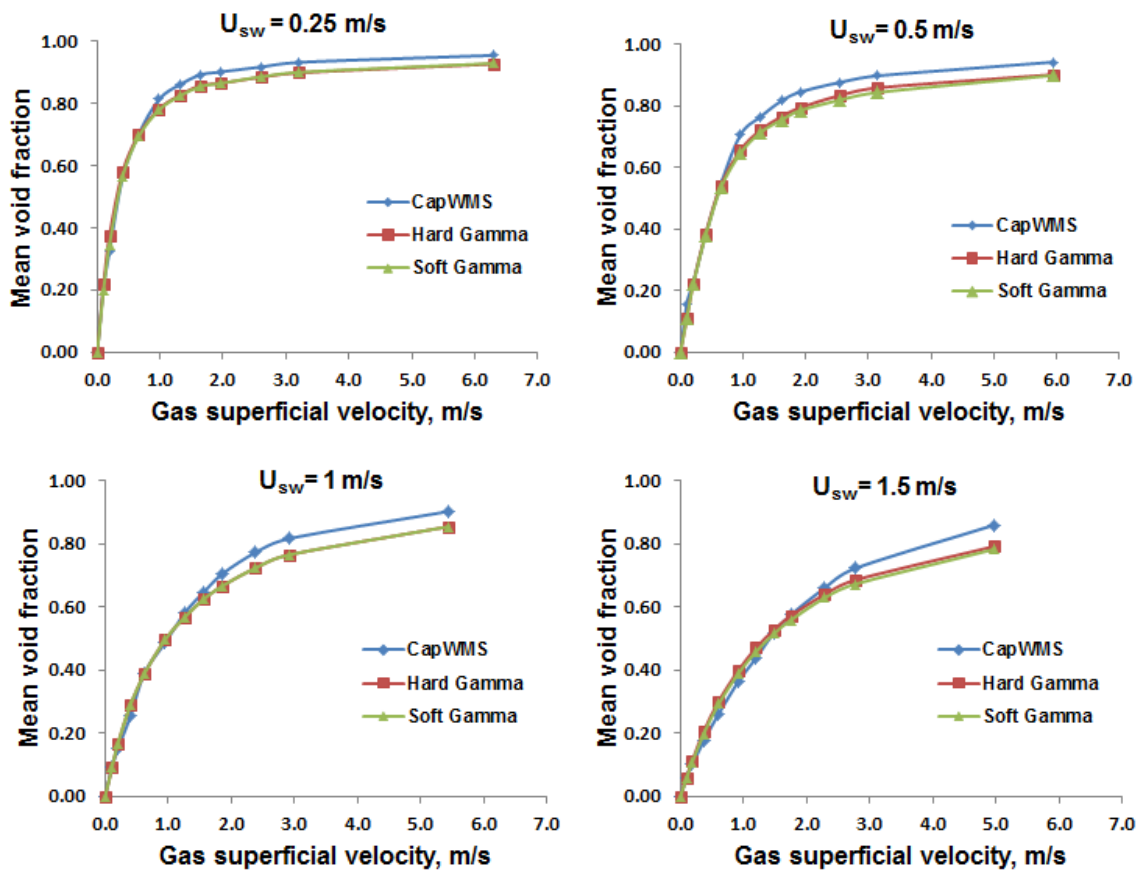
Figure 4-1: Variation of void fraction with superficial gas velocity at different liquid superficial velocities

In general, the above figures illustrate good agreement between the hard gamma and soft gamma void fraction results. However, capacitance WMS void fraction results were particularly consistent with gamma voids (hard and soft) at lower gas superficial velocities. But at higher gas superficial velocities, the capacitance WMS void fractions were slightly higher than the gamma measurements. This slight deviation at higher gas flow rates is probably due to the difference in the performances of the devices at high void fraction. Additionally, the WMS gives the cross-sectional void fraction, which is based on averaging the local void at each crossing point of the grid in the sensor cross section, while the gamma densitometer measures the void fraction averaged over a single beam or chord through the cross section.

4.1.2 Flow patterns

Several experiments for air-water flows were carried out in the 52 mm diameter vertical riser. For each flow condition studied in these experiments, its flow pattern in the riser was identified. This was performed at the top of the riser by using a combination of i) visual observation, ii) the void fraction time traces and corresponding probability density function (PDFs) signatures that were obtained from WMS and gamma densitometer data, and iii) visualization provided by wire mesh sensor data (integrating data that can produce slice views and cross section movies to see the flow as it would be seen if the pipe were transparent). The use of visual observation for determining flow patterns usually has the limitations of being subjective and can lead to differences in the interpretation of flow patterns. In addition, when it comes to usage within actual industrial pipelines (these are generally not transparent), the visual method of observation cannot be employed. However, since each flow pattern has a characteristic signal trace, the use of time traces and corresponding PDFs for obtained signals analysis will give a simple quantitative means for the determination of flow patterns inside the pipeline. As a result of this, the time series and corresponding PDFs of the obtained signals fluctuations for air-water flows have been adopted for objective and quantitative flow pattern identification. Time traces and the corresponding PDFs have been used to classify the flow patterns

inside pipes by many researchers, for example Costigan and Whalley (1997) and Omebere-Iyari and Azzopardi (2007). Also, the use of gamma raw signal analysis gives a simple quantitative means for the determination of flow patterns in multiphase flows and was therefore considered to be desirable (Blaney and Yeung, 2007).

In this research work, simultaneous measured data (at the top part of the 52 mm vertical riser) by both the capacitance WMS and gamma densitometer at each flow condition for air-water experiments were used to generate corresponding PDF functions of the recorded signals. The PDFs' shapes were used in this research work to classify flow patterns inside the pipes. For example, Figure 4-2 shows the void fraction time series and the corresponding PDF that was obtained from Capacitance WMS data for air-water flow at a constant liquid superficial velocity of 0.25 m/s and lower riser-base injected gas superficial velocity of about 0.1 m/s (air flow rate of 1.5 sm^3/h). It can be seen that the void fraction time trace (Figure 4-2(a)) for this flow condition centres around a low cross-sectional average void fraction of about 18.5% with very small fluctuations (standard deviation of ±2%) corresponding to the passage of small bubbles in the liquid's structure, which indicates a typical bubbly flow regime. The corresponding PDF (Figure 4-2(b)) for this air-water flow condition presents a single, narrow, tall peak for the relatively low main void fraction. This peak ranges between 0.14 and 0.25 void fractions, indicative of the small fluctuations around the mean value. The single narrow peak for this PDF's shape is also a characteristic of bubbly flow regime. These time traces and the PDF that is obtained from the WMS data for this air-water flow condition align with those extracted from the gamma densitometer output signals (soft and hard gamma counts) as shown in Figure 4-3 (a) and (b). The raw signal for both gamma output signals (soft and hard counts) also show small fluctuations (standard deviation of ±8% and ±10% for hard and soft counts, respectively) indicative of bubbly flow pattern. In addition, the PDF signature for the soft gamma count signal shows a narrow single peak in the lower gamma count region (290 to 360), confirming the occurrence of bubbly flow pattern inside the riser.
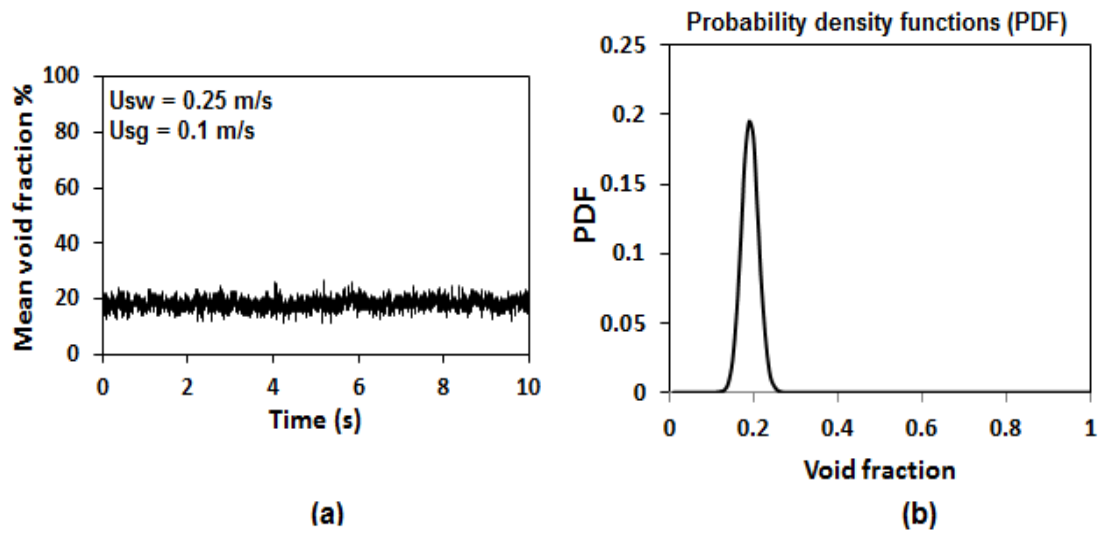
Figure 4-2: WMS output data for air-water flow at U_{sl} = 0.25 m/s and U_{sg} = 0.1 m/s, a) Void fraction time series, b) probability density function

Figure 4-3: Gamma densitometer signals for air-water flow at U_{sl} = 0.25 m/s and U_{sg} = 0.1 m/s, a) Gamma counts time series, b) PDF for gamma count

By increasing the gas superficial velocity to about 0.98 m/s (injected air flow of 15 Sm^3/h) at the same water flow of 0.25 m/s, the flow pattern inside the riser is transferred to a slug flow regime. This is indicated by the time traces and PDFs obtained from the wire mesh sensor (WMS) and gamma densitometer (GD) as illustrated in Figures 4-4 and 4-5, respectively. From these Figures, it can be seen that the time series and PDFs both show similar trends for this flow condition. The void fraction time traces for the capacitance WMS measurement in Figure 4-4 (a) and gamma counts in Figure 4-5 (a) show fluctuations with distinct peaks and troughs, which are produced by the alternate passing of relatively larger gas bubbles in the measurement section in the riser. This is an indication of a slugging system. As illustrated in Figures 4-4 (b), and 4-5 (b), the PDFs' shapes display shorter peaks than the PDFs in the previous condition with the progressive development of a second peak. The PDFs also show larger ranges for void fraction and soft gamma count (broader distribution) when compared to a gas superficial velocity of 0.1 m/s. The shape of the PDFs for this flow condition implies that there is a slug flow in the riser.

Figure 4-4: WMS data for air-water flow at U_{sl} = 0.25 m/s and U_{sg} = 0.98 m/s, a) Void fraction time traces, b) probability density function (PDF)

Figure 4-5: Gamma Densitometer Signals for air-water flow at U_{sl} = 0.25 m/s and U_{sg} = 0.98 m/s, a) Gamma counts time traces, b) PDF for soft gamma count.

When the gas superficial velocity is increased to 3.22 m/s (riser base injected air flow of 50 Sm^3/h) with the same water flow of 0.25 m/s in the riser system, the PDFs from the wire mesh sensor and gamma densitometer result in slight similar shapes for this flow condition. As can be seen from Figure 4-6(b), the PDF from the wire mesh sensor shows a main peak at a higher void fraction region (average void fraction of about 89%), with a small tail extending towards the lower void fraction, signifying a churn flow regime. In Figure 4-6(b), the PDF's plot of the soft gamma count, obtained from the gamma densitometer, for this flow condition is presented. As can be seen, there is a broad single peak, which tilts towards the high gamma count range, with a corresponding tail towards the lower counts (the tail ranges from about 300 to 370 gamma counts), indicating a churn flow pattern in the riser.
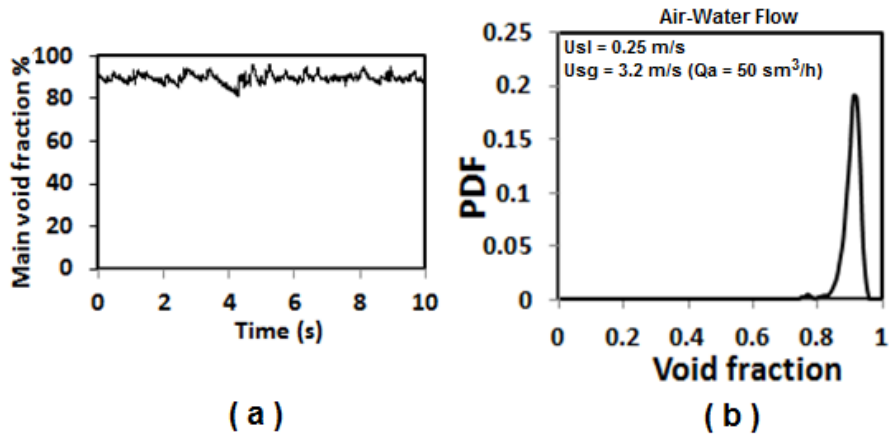
Figure 4-6: WMS data for Air-water flow at U$_{sl}$ = 0.25 m/s and U$_{sg}$ = 3.22 m/s, a) Void fraction time traces, b) Probability density function (PDF)
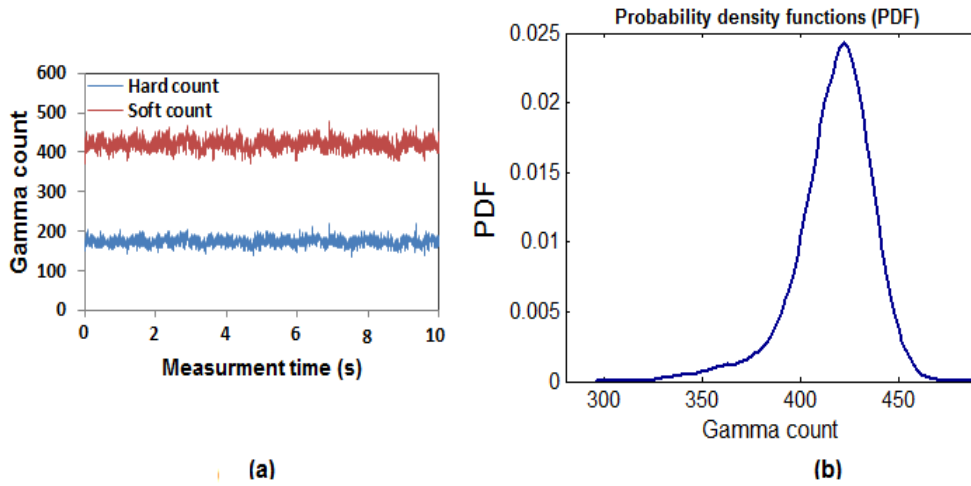
Figure 4-7: Gamma Densitometer signals for air-water flow at U$_{sl}$ = 0.25 m/s and U$_{sg}$ = 3.22 m/s, a) Gamma counts time traces, b) PDF for soft count

At the highest superficial gas velocity of about 6.28 m/s (riser-base injected air flow rate of 100 sm^3/h), the void fraction time series obtained by the wire mesh sensor show an almost stable void fraction (standard deviation of ±0.65%) with a high main void value of 0.96, reflecting an annular flow pattern inside the riser (see Figure 4-8 (a)). The corresponding PDF shape in Figure 4-8 (b) shows a tall, very narrow, single peak situated in the highest void fraction region (void fraction for the peak ranging between 0.93 and 1), indicating an annular flow pattern. This observation is consistent with the shapes of the raw data time traces and PDF for gamma counts that were obtained from the gamma

densitometer measurement. The gamma counts, plotted as a function of time, show very low fluctuation signals for both soft and hard counts (standard deviation of ±9% and ±11% for hard counts and soft counts, respectively) as can be seen in Figure 4-9 (a). The measured values of the void fraction are about 93% for both hard and soft counts. The PDF shape of the soft gamma count shows a single dominant peak in the high gamma count region (380 to 480) as illustrated in Figure 4-9 (b). This distribution for the PDF also indicates annular flow for this flow condition.

(a)

(b)
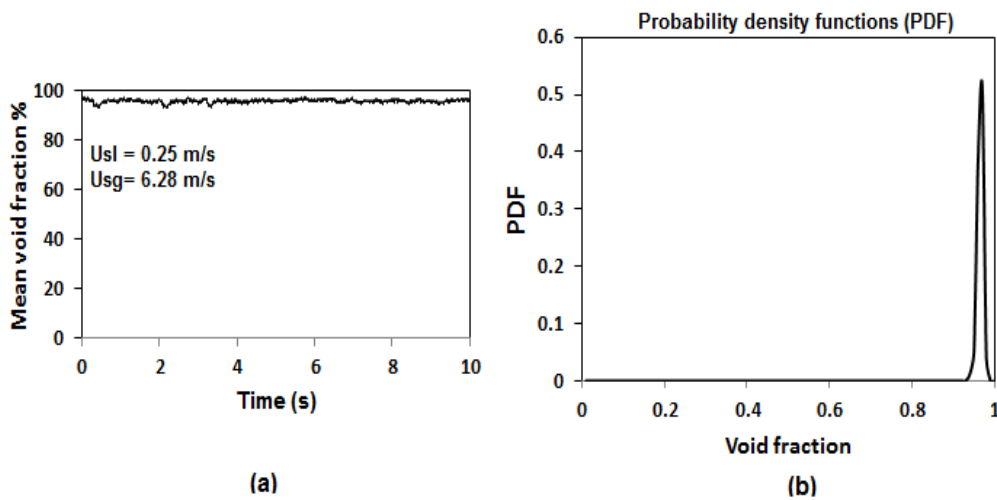
Figure 4-8: WMS results for Air-water flow at U$_{sl}$ = 0.25 m/s and U$_{sg}$ = 6.28 m/s, a) Void fraction time traces, b) Probability density function (PDF)

(a)

(b)

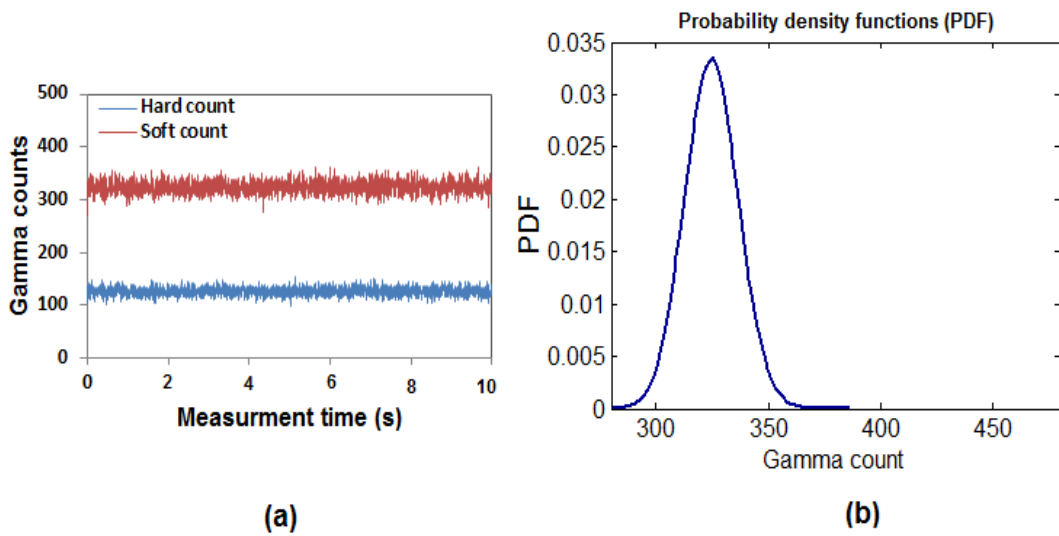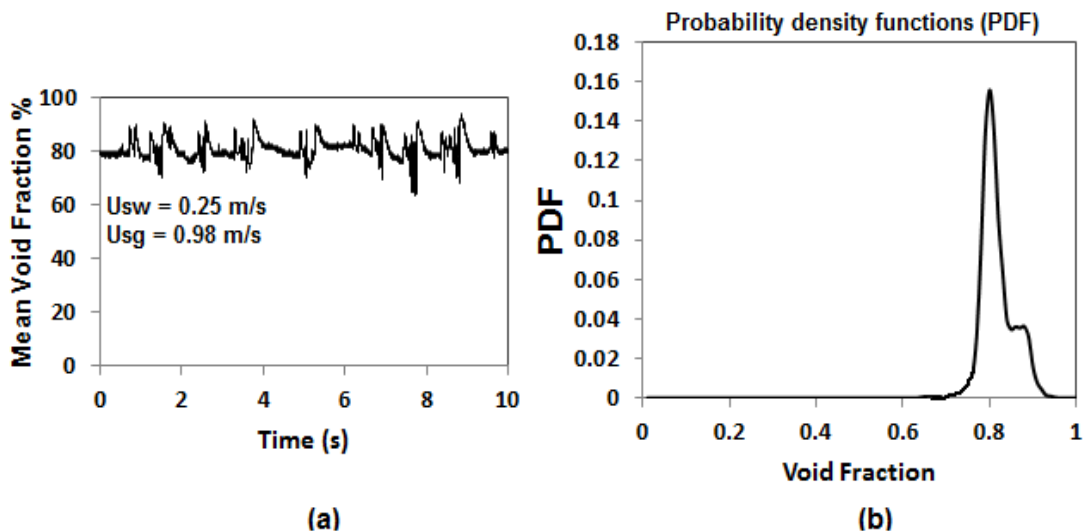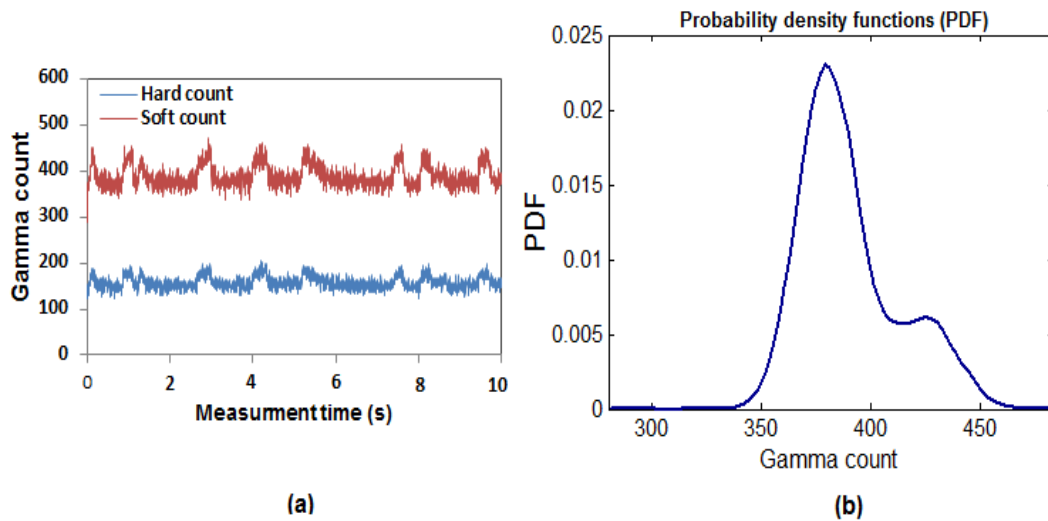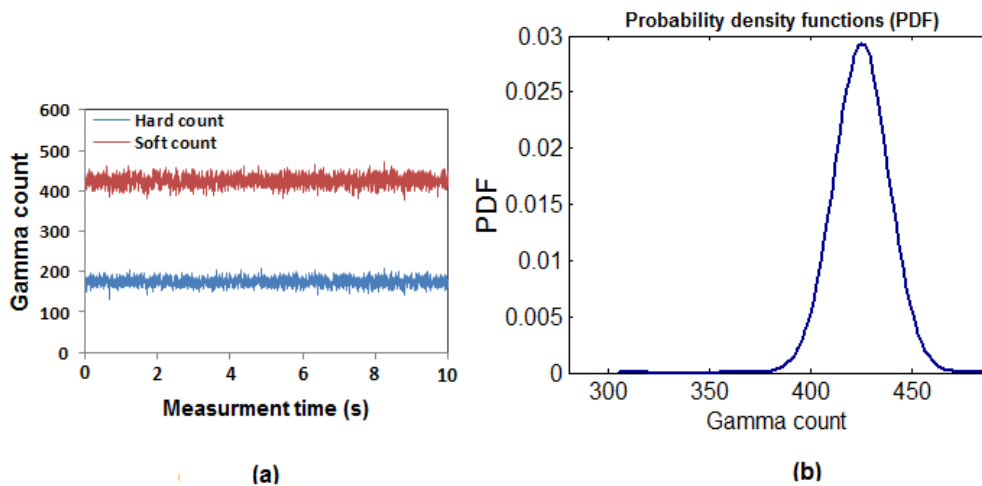**Figure 4-9: Gamma Densitometer signals for air-water flow at U$_{sl}$ = 0.25 m/s and U$_{sg}$ = 6.28 m/s, a) Gamma counts time traces, b) PDF for soft count**

4.1.3 Visualization Images for Two-Phase Flow by WMS Data

In addition to the above-mentioned methods using void fraction time series and corresponding probability density functions (PDFs) for flow regime identification, visualization (the cross-sectional images and slice views) provided by the capacitance wire mesh sensor was also used to confirm the flow patterns that were encountered inside the riser.

Figure 4-10 shows an example of slice views and cross-sectional images of the void fractions data that were obtained from the capacitance wire mesh sensor for constant liquid velocity of 0.25 m/s and various gas superficial velocities (red colour indicates the gas phase and blue represents the liquid phase; the colour scale displays permittivity values). Additional snapshot images for more flow conditions are given in Appendix B-1. The images in Figure 4-10 indicate the various flow regimes encountered with an increase in gas superficial velocities at constant water superficial velocity. It is concluded that these results support the air-water results presented earlier in Section 4.1.2. At a gas superficial velocity of about 0.1m/s, it is clear that the flow pattern in the riser is bubbly flow for the air-water flow. When the gas velocity is increased to 0.98 m/s, slug flow patterns were visualized for the air-water at the top of the riser. Relatively large pockets of gas, sometimes with small gas bubbles in a liquid structure, can be envisaged for this flow condition of air-water. At the highest gas superficial velocity of about 6.28 m/s (injected air flow rate of 100 Sm^3/h), the air-water flow is observed to change to annular flow. These results are almost in agreement with the corresponding time traces and PDFs' results for the same flow conditions presented in the previous Section.
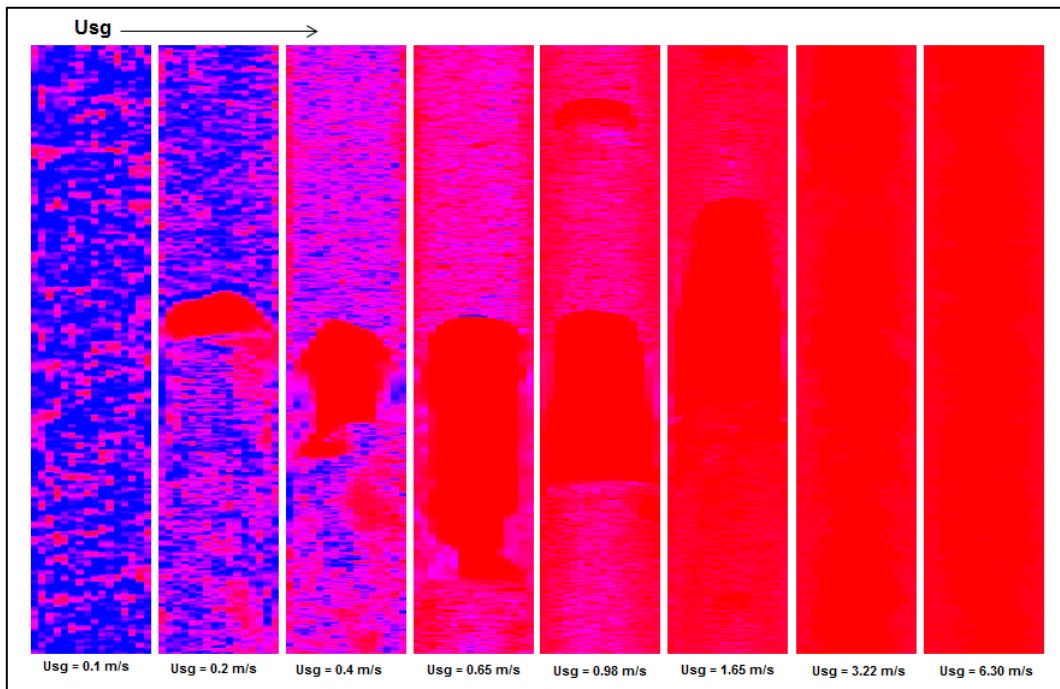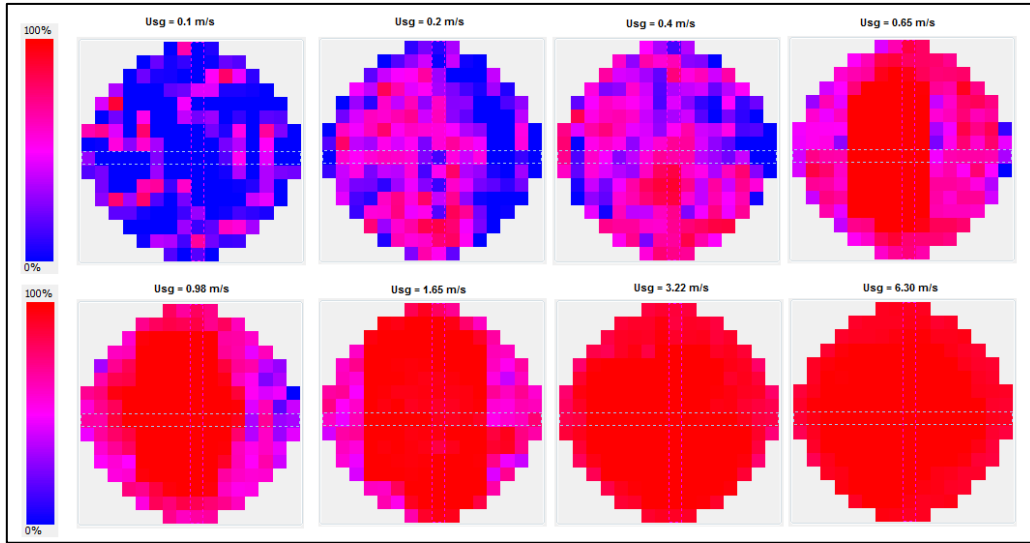
Figure 4-10: Cross-sectional and slice images acquired with the WMS at a constant liquid superficial velocity of 0.25 m/s and various gas flows

4.1.4 Flow pattern map

As previously mentioned, the flow pattern for each flow condition in these experiments was identified. As a result, a flow pattern map was produced for air-water flows under riser base gas injection. This flow regime map is plotted in terms of local superficial gas and liquid velocities on the axes. The flow characteristics identified in this part of the current study are within bubbly, bubbly to slug transition (spherical cap bubbly), slug, churn and annular flows. Figure 4-11 represents a flow regime map for the tested air-water flows. Solid lines indicate bounders between the flow regime regions. For air-water flow, bubbly flow was identified at liquid superficial velocity of 0.25 m/s and gas superficial velocity of about 0.1 m/s (air flow rate of 1.5 Sm^3/h). At the next higher gas velocity of about 0.2 m/s, for the same liquid velocity of 0.25 m/s, air-water moves into bubbly to slug transition (spherical cap) flow. With an increase of gas superficial velocity to ~0.98 m/s (injected air flow rate of 15 sm^3/h), the flow tends to form slug flow. At the highest gas velocity of about 6.28 m/s, air-water flows are showing annular flow characteristics, as discussed above. The obtained flow regime map for these pressurised tests was in agreement with that generated by Hewitt and Roberts (1969) in Figure 2.9, which was validated for gas/liquid upward flow in a vertical pipe at high pressure systems. However, some regimes observed in Hewitt and Roberts map were not seen in the current study.
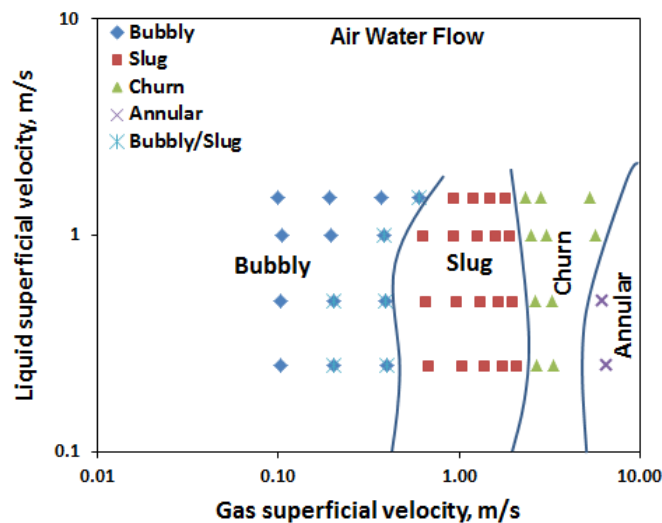
Figure 4-11: Flow regime map for air-water flows in 52 mm vertical riser

4.1.5 Phase Fraction Distributions:

An advantage of the wire mesh sensor (WMS) is that it can also provide very detailed information about the distribution of the liquid and gas phase in the two-phase flow in the pipe cross section. Figure 4-12 illustrates the chordal void fraction distribution in the pipe cross section for air-water flow at several tested constant liquid superficial velocities of 0.25, 0.5, 1 and 1.5 m/s and various superficial gas velocities for each liquid superficial velocity. The void distributions were generated by the capacitance WMS measurements for each flow condition at about 9.5 m (~183D) from the gas injection point into the riser. The chordal void fraction distributions were made by averaging the mean void fractions measured at each crossing point belonging to the four centrelines' sixteen wires (1 - 16), going from 180° to 0° (left to right) over the 52 mm diameter vertical riser cross section. It can be seen from Figure 4-12, that at lower gas superficial velocities, the chordal void fraction distribution of air-water flow for the lower injected air flows (where flows were indicated as bubbly and bubbly-slug transition flow regimes) is nearly flattened around the pipe centre with a slight decrease at the pipe wall. It can also be observed that at lower liquid superficial velocities of 0.25 and 0.5 m/s the void fraction profiles appear to have a more flattened profile (almost intermediate peak distribution) round the pipe centre compared to the higher water flows of 1 and 1.5 m/s. As air and water superficial velocities increase, the void fraction profiles become gradually higher void values around the pipe centre (core-peaking profile). At higher gas superficial velocities, the void fraction profiles show clearly the maximum values around the pipe centre and these centreline values also increase with increasing gas superficial velocity. It can be concluded that the phase distribution was core peak void fraction distribution in most of the cases; however, at flow conditions of lowest gas superficial velocities and lower water flow rates of 0.25 and 0.5 m/s it showed an almost intermediate peak.
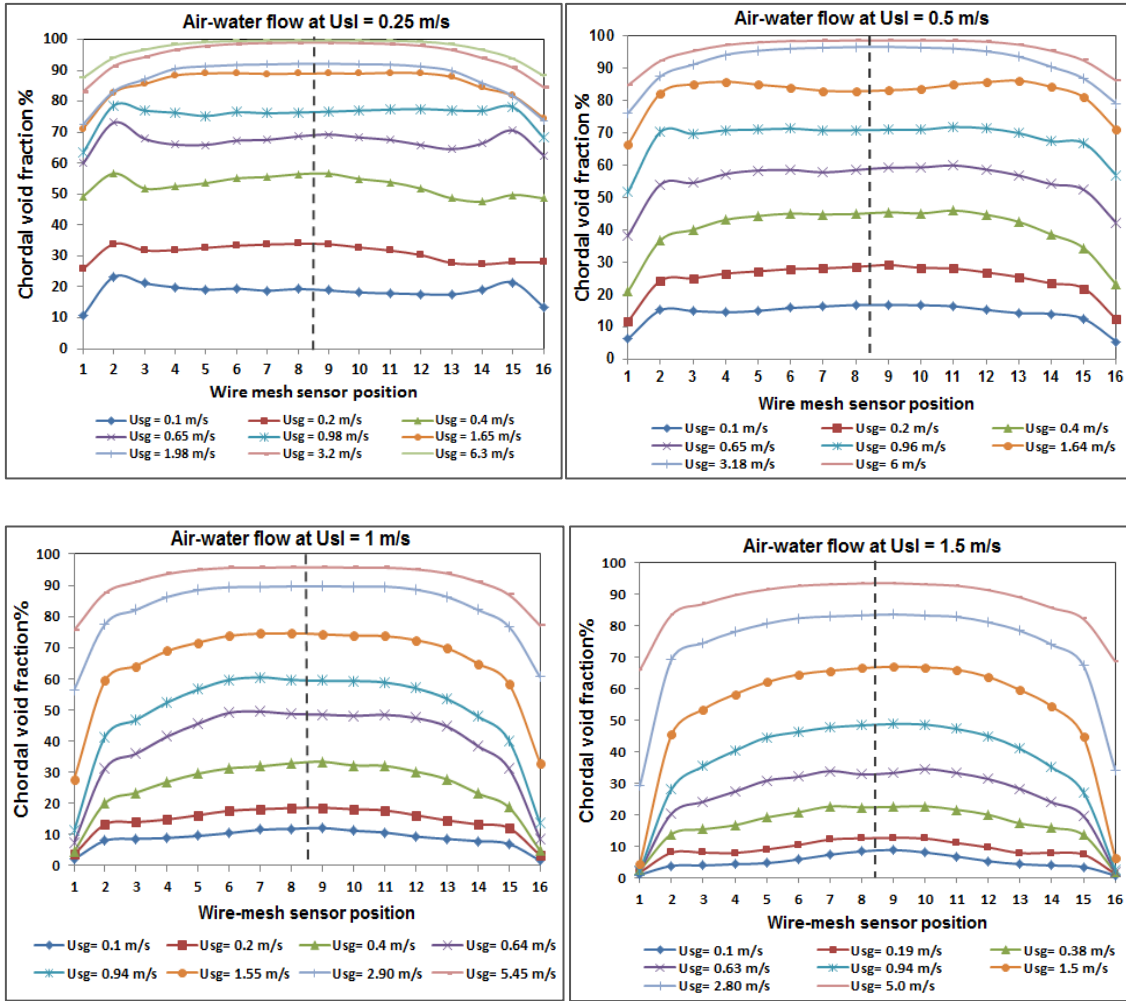
Figure 4-12**: Chordal void fraction distribution for air-water flow.**

4.1.6 Pressure Gradient for Two-phase Air-Water Flow in the Riser

For a two-phase mixture fluid flow in a vertical pipe, the total pressure gradient is equivalent to the sum of the gravity pressure gradient part and the frictional pressure gradient part. For this air-water experimental work, the total pressure gradient was measured with the aid of pressure transducers installed along the vertical riser system as described in Chapter 3 (Experimental Facility).

Figure 4-13 shows the total pressure gradient measured for different liquid superficial velocities as a function of various local gas superficial velocities for air-water upflow. It can be seen that there is a decrease in the total pressure gradient due to an increase in gas superficial velocity, which suggests an

increase in the effectiveness of the gas lifting. The observed decrease in the total pressure gradient can be explained by the fact that the flow in the riser is gravity dominated, i.e. the major contributor to total pressure gradient in a vertical pipe is the gravity pressure gradient ($\rho_m \cdot g$). Moreover, the increase in gas superficial velocity will promote an increase in the void fraction inside the riser, thereby reducing the mixture fluid density as a result of a decrease in the liquid holdup. Consequently the total pressure gradient for the air-water system decreases with an increase in gas superficial velocity. It can also be observed that the rate of the decrease in the total pressure gradient at lower gas superficial velocities is higher than that measured at the higher gas superficial velocities. This is due to a gradual rise in mixture velocity and the air-water mixture flow becoming more turbulent. As a result, the frictional pressure gradient contribution thus becomes more influential in the determination of total pressure gradient. At constant injected gas flow rate, the total pressure gradient increases with increasing liquid superficial velocity. This is because liquid holdup inside the riser increases with escalating mixture liquid superficial velocity at constant gas flow rate. Additionally, the increase of the total pressure gradient is due to promoting the fractional gradient with the increasing flow rate.
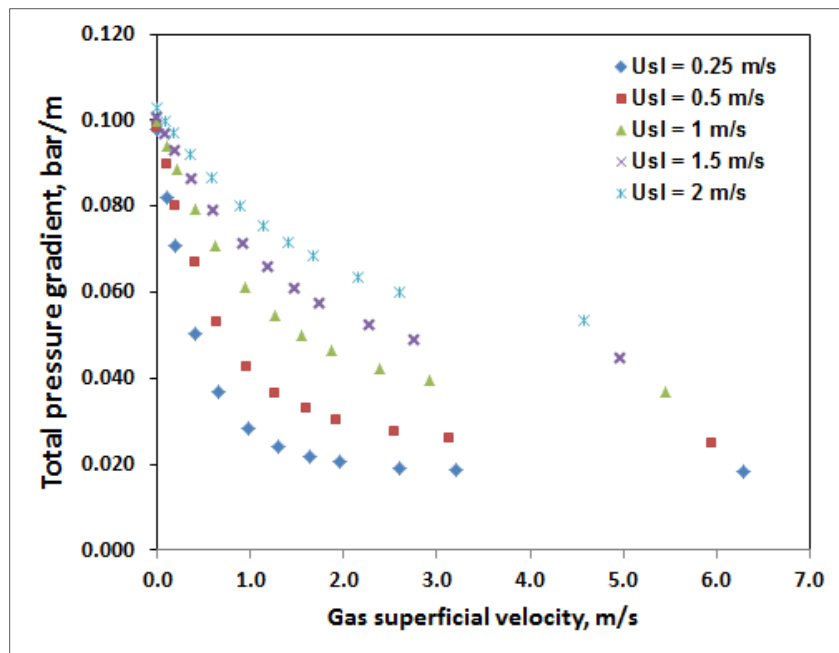
Figure 4-13: Air-water flow: Total pressure gradient as a function of local gas superficial velocity

The frictional pressure gradient was also determined from the measured total pressure gradient (i.e. by subtracting the gravity term from the measured total pressure gradient). The obtained frictional pressure gradient as a function of superficial gas velocity for several constant water superficial velocities is shown in Figure 4-14. Due to an increase in gas superficial velocity at constant liquid superficial velocity, the frictional pressure gradient is observed to increase. It is also observed that the frictional pressure gradient increases with a rise in liquid superficial velocity for the same gas flow rates. This is because the rise in liquid velocity will increase the mixture velocity and thus the flow becomes more turbulent and as a result, the frictional pressure gradient contribution increases.
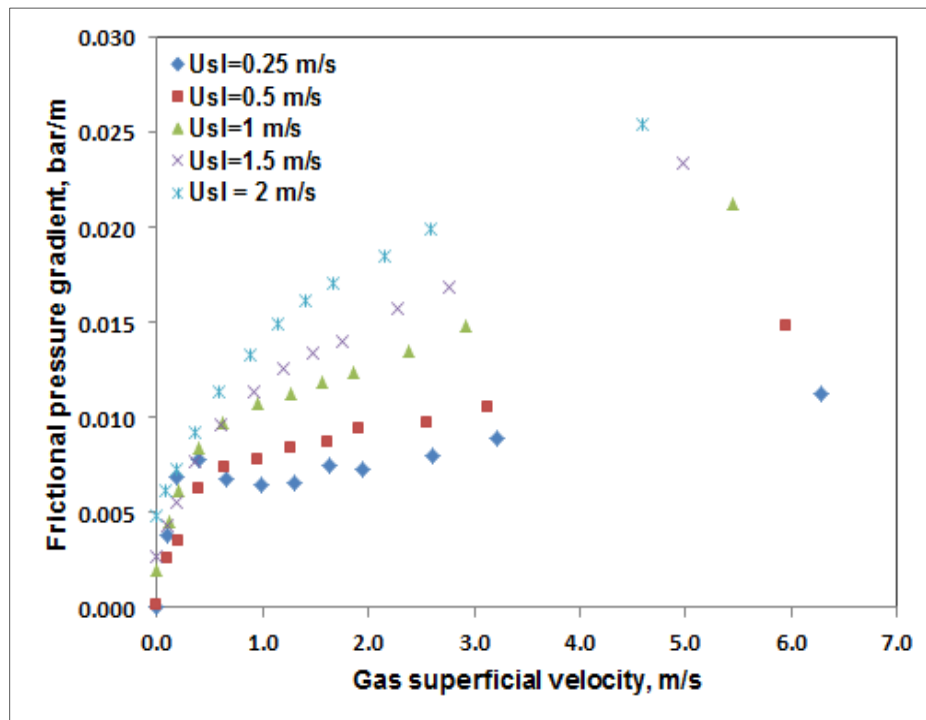
Figure 4-14: Air-water flow: Frictional pressure gradient as a function of local gas superficial velocity

4.2 Effects of Air Inlet Condition on Two-phase in Vertical Riser

Despite many studies having investigated gas-liquid two-phase flow characteristics in vertical pipes (Szalinski et al., 2010), these studies do not include the effect of the flow path which is typical for certain applications such as gas injection in deep vertical risers. There was an attempt to investigate the upstream effects in flow patterns using the same riser that was used in this study with gamma densitometer measurements. The results suggested there were no observable inlet effects at low gas throughput as similar flow patterns were indicated. However, slightly dissimilar flow regimes were observed at higher air and water superficial velocities (Arubi, 2011). Those results suggested that, in order to gain a better understanding of the effect of gas injection configuration on the flow in risers, a more extensive investigation using an advanced measurement technique might be necessary. Therefore, the results from the investigation on the effect of gas injection location on air-water flow patterns and phase distributions occurring in a 52 mm diameter vertical riser using a wire-mesh sensor will be presented in this section. The experiments were performed with two different gas injection configurations, namely riser base gas injection and horizontal flowline inlet gas injection. From these configurations, the entrance effect on the two-phase flow characterises in the riser was studied. In these experiments, the 16 x 16 capacitance WMS was used to obtain comprehensive information of the flow regime, phase fraction fluctuation and phase distribution in the riser. In order to properly investigate the effect of inlet conditions on flow behaviours occurring in the riser, the results of the selected cases for air-water flow under both gas inlet conditions will be considered.

At gas superficial velocity of about 0.4 m/s (air flow rate of 6 Sm^3/h) and water superficial velocity of 1 m/s, the case of a typical bubbly flow pattern was observed inside the riser when the gas was injected through the flowline. On the other hand, a bubbly to slug transition flow pattern (or what some researchers have referred to as spherical cap bubbly flow) was observed when the same amount of gas (U_{sg} = 0.4 m/s) was introduced at the riser base with the same

loading of water of 1m/s. This can be seen clearly from the extracted images (cross-sectional images and slice view) that were obtained from the capacitance WMS data for this condition presented in Figure 4-15 (red indicates the gas phase and blue the water). It is clear that from the obtained cross-sectional images and slice views for this flow condition, the flow pattern is bubbly for flowline gas injection and is bubbly to slug flow pattern when gas is injected at the riser base. The difference in flow patterns for this flow condition was also identified from the shapes of the cross section void fraction time series and their corresponding PDFs. Figure 4-16 shows the time traces and PDFs for gas injection in the flow line case (Figure 4-16 (a)) and at the riser base (Figure 4-16 (b)) for the same flow condition (U_{sl} = 1m/s and U_{sg} = 0.4m/s (air flow rate 6 Sm^3/h)). The void fraction time trace for flowline injection has an averaged value of about 22% with very small fluctuations (standard deviation of 1.5%), corresponding to bubbly flow regime.
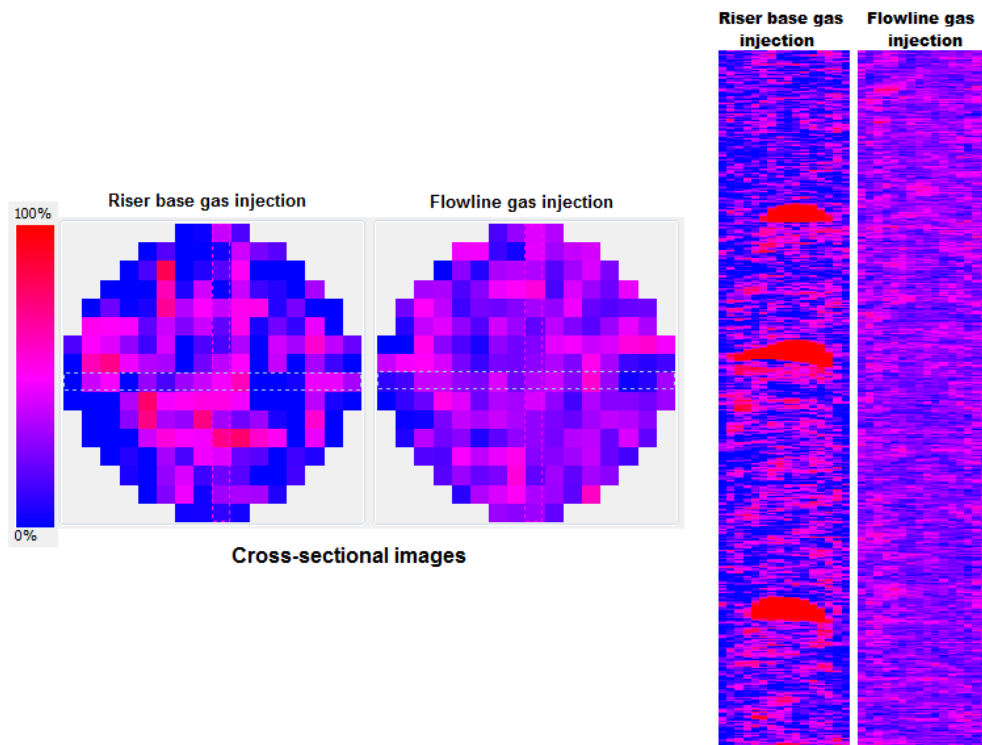
Figure 4-15: Cross-sectional images and slice views for air-water flow at U_{sl} = 1m/s and U_{sg} =0.4m/s

The corresponding PDF presents a tall narrow single peak which is also a characteristic of typical bubbly flow. However, the shapes of the time trace and PDF for the same flow condition for gas injection at the riser base were different, as can be seen in Figure 4-16 (b). The void fraction time trace shows sharp and narrow peaks. This time the trace shape shows more fluctuations than in the flowline gas injection case (standard deviation of 1.5%). The corresponding PDF presents a shorter and broader single peak with a tail extending towards the high void fraction region. These characteristics indicate a bubbly-slug transitional flow for this flow condition.
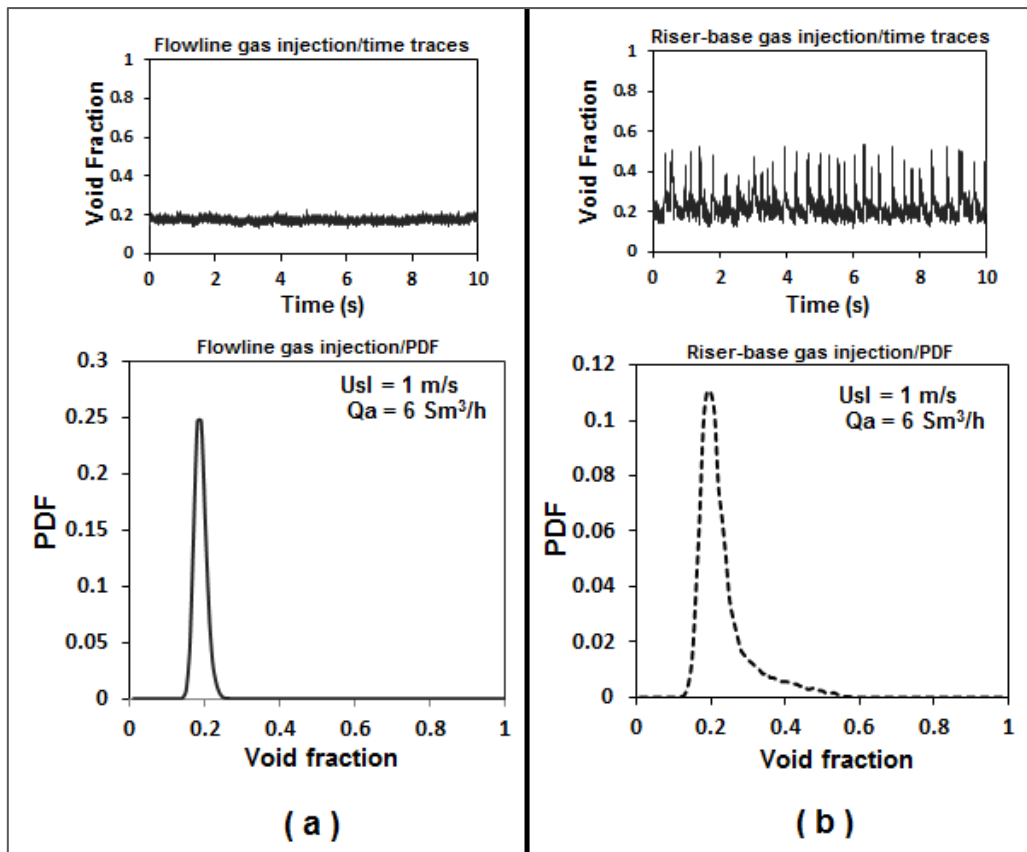
Figure 4-16: Time traces and PDFs,

a) Riser base gas injection, b) Flowline gas injection

When the gas superficial velocity is increased to 1.55 m/s (equivalent for air flow rate of 25 Sm^3/h) at the same water superficial velocity of 1 m/s, the flow patterns inside the riser were discovered to be a slug flow regime for both gas inlet configurations. This can be seen from the images (cross-sectional images and slice view) obtained from the wire mesh sensor output data as illustrated in Figure 4-17. Relatively large pockets of gas (but with their length still less than the pipe diameter), with small gas bubbles in the water's structure can be observed for both gas inlet configurations at the same gas and water flow condition. However, riser base gas injection for this flow condition has shown higher slug frequency than the flowline gas injection case in the pipe, which can be observed from the number of air slugs in the images. The change from bubbly flow in the previous condition to slug flow at this flow condition (U_{sg} = 1.55 m/s) is due to the coalescence of gas bubbles, which leads to the creation of a slug flow. The slug flow in the horizontal line may also help to create this slug flow inside the vertical riser in the flowline gas injection case.
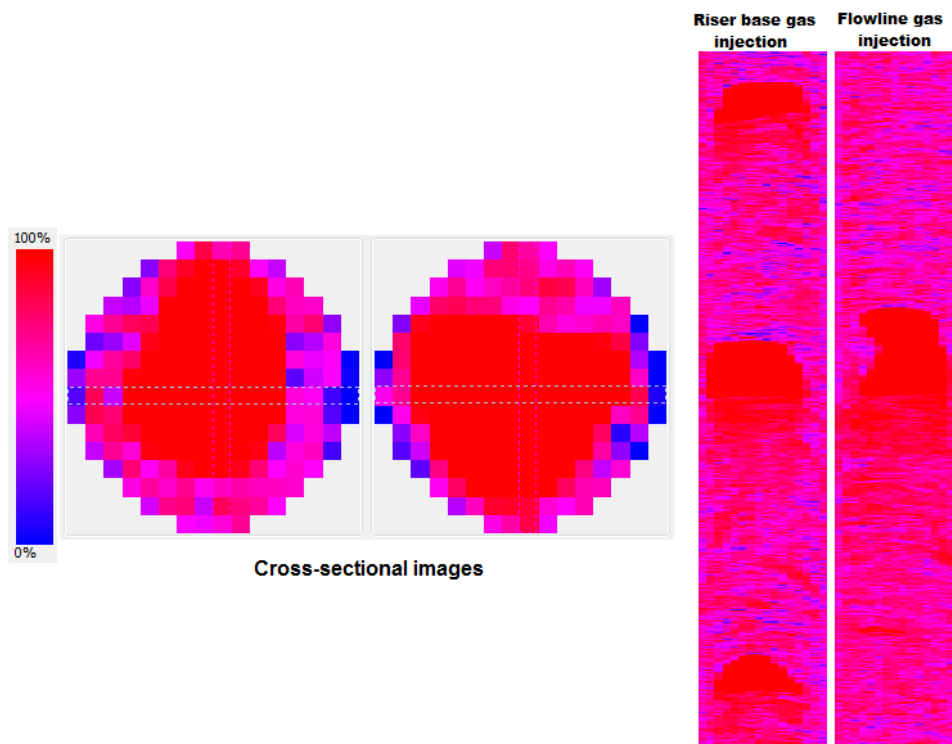
Figure 4-17: Cross-sectional images and slice views for air-water flow at U_{sl} = 1m/s and U_{sg} = 1.55 m/s

Figures 4-18(a) and 4-18(b) show the void fraction time series and the corresponding PDFs for the riser base gas injection case and flowline gas injection, respectively. Both the void fraction time traces indicate the flow regimes as slug flow. However, the time trace for flowline gas injection shows fluctuations at the lower frequency (about 1 Hz) than at that for riser base injection (approximately 3 Hz). This result supports the slice view results in Figure 4-16. The PDFs' thus have nearly similar shapes for this flow condition under the two gas injection configurations. The PDFs' shapes show almost two peaks, which imply slug flow.
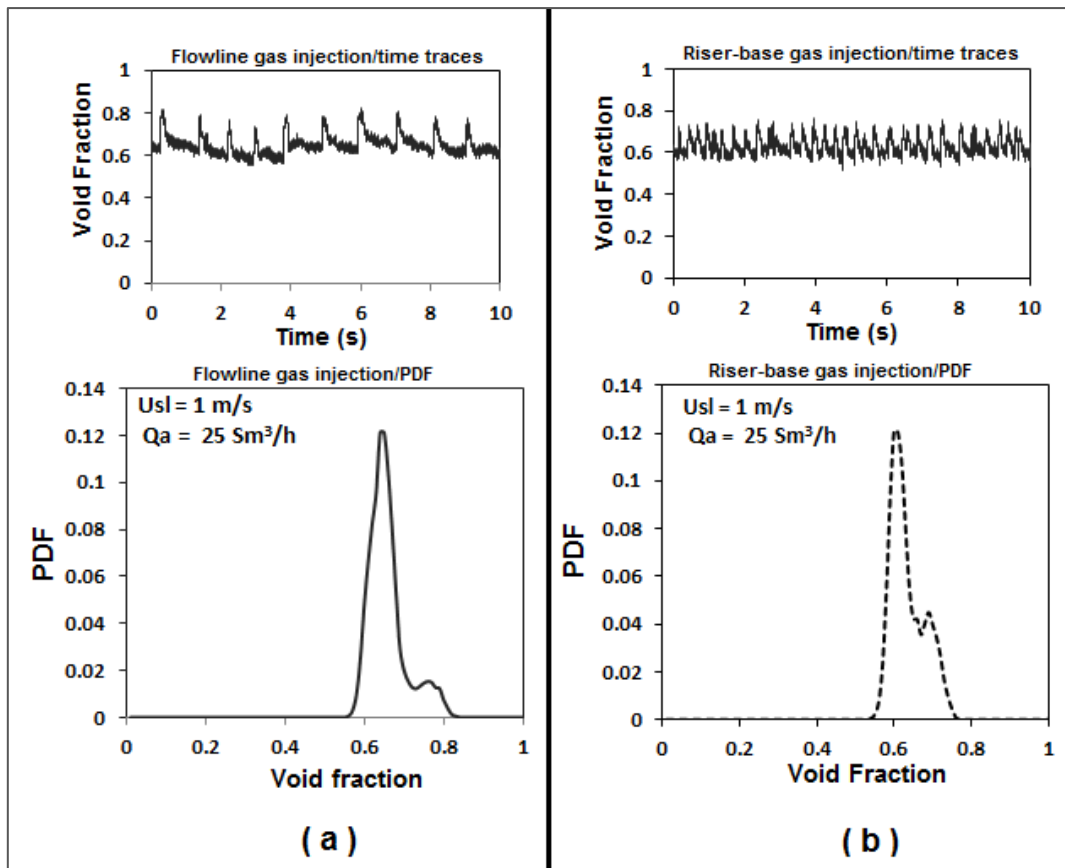
Figure 4-18: Time traces and PDFs,

a) Riser base gas injection, b) Flowline gas injection

At the highest local gas superficial velocity of about 5.45 m/s (gas flow injection of 100 sm^3/h), intermittent gas cores were observed inside the riser for both gas inlet configurations as shown in Figure 4-19. However, the gas core for the flowline gas injection case occupies more space in the riser than the riser-base gas injection. The observed flow can be classified as a churn to annular flow regime. The void fraction time traces and PDFs for both cases of gas injection are shown in Figures 4-20 (a) and (b). There is a noticeable difference in time trace as its trend shows less fluctuation for riser base gas injection around an average void fraction value of about 90% for both cases. This can be seen in Figure 4-20. For this flow condition, the PDF geometries display slight dissimilarity in shape and a difference in their heights. The PDFs' shapes are in the form of narrow peaks with tails towards the left with a difference in height along the tails. The narrow peaks are situated in the direction of the highest void fraction region. This observation is almost consistent with the images in Figure 4-19. The PDFs' shapes for this flow condition all reflect almost churn to annular flow regimes for both gas injection configurations.
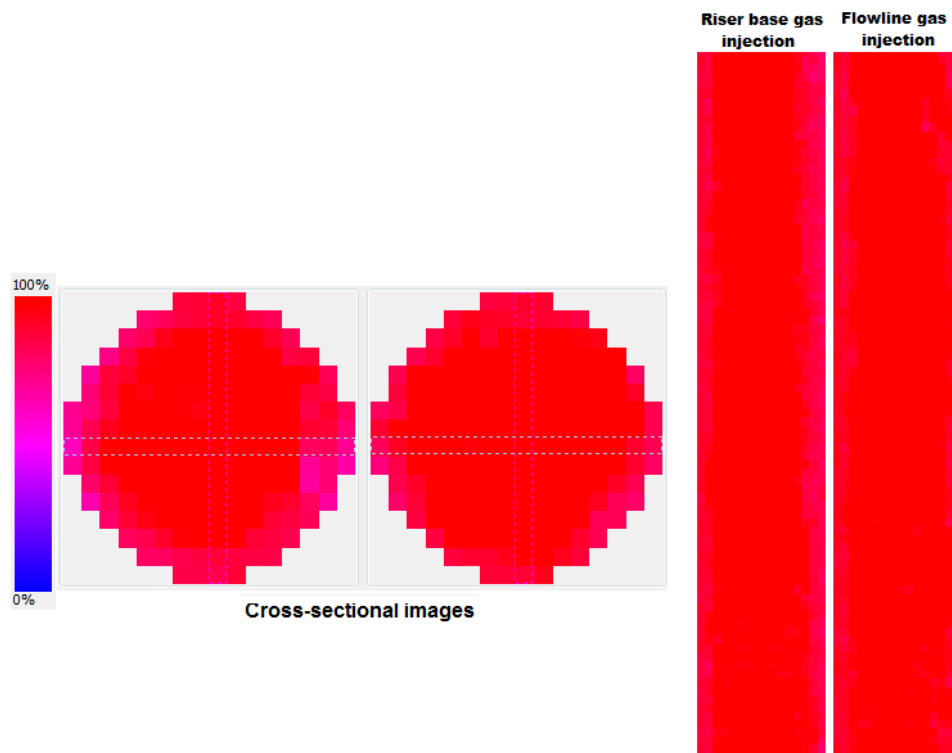
Figure 4-19: Cross-sectional images and slice views for air-water flow at U_{sl} = 1m/s and U_{sg} = 5.45 m/s
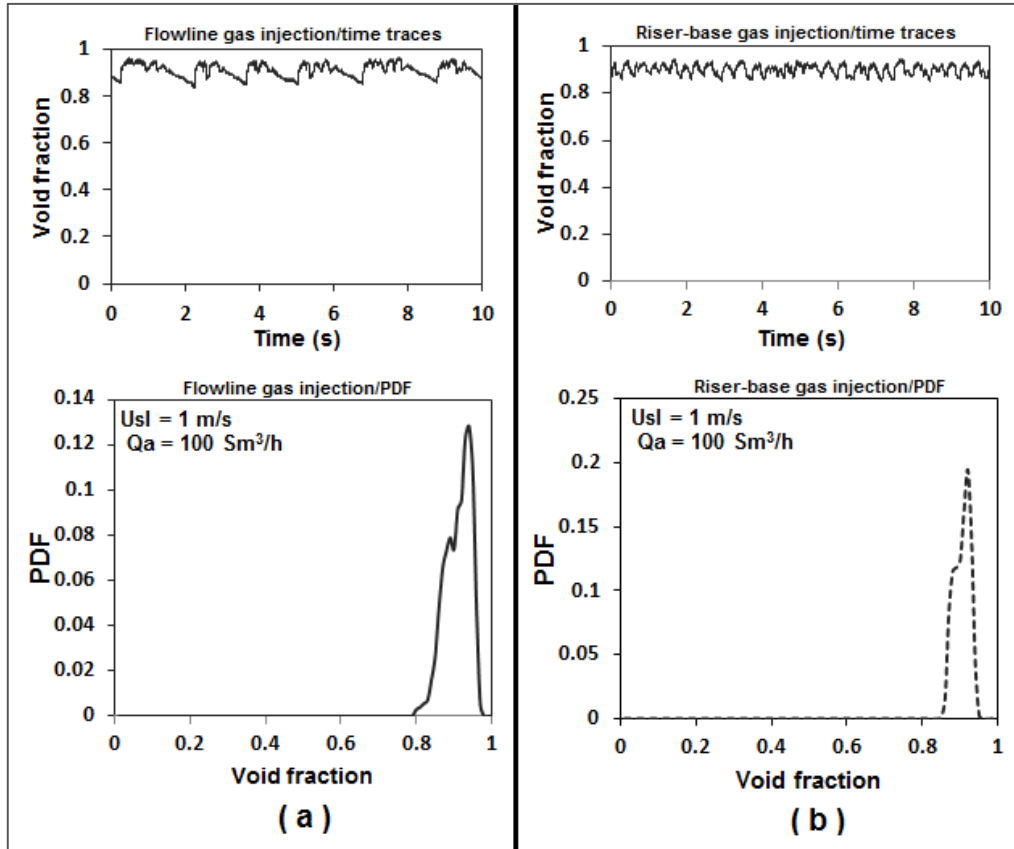
Figure 4-20: Time traces and PDFs for U_{sl} = 1m/s and U_{sg} = 5.45m/s; a) Riser base gas injection, b) Flowline gas injection

As previously mentioned, the WMS can provide very detailed information about the distribution of the liquid and gas phase in the two-phase flow inside the pipe. This can be achieved by measuring the chordal void fraction over the cross section of the pipe. Figure 4-21 shows chordal void fraction distributions for both injection configurations (i.e. riser base gas injection and upstream horizontal flowline gas injection) at liquid superficial velocity of 1 m/s and several air superficial velocities.

At lower gas superficial velocities (0.4 m/s ≤ U_{sg} ≤ 0.95 m/s) it can be observed that the two gas inlet configurations exhibited different void fraction values and distributions inside the riser. For the case of gas injection through the flowline, the distribution of higher void fraction is near the pipe wall (wall-peaking), and a decrease of void fraction is towards the pipe centre. This indicates wall-peaking bubbly flow for this flow configuration. A higher chordal void fraction distribution

around the pipe centre (core-peak void distribution) is found for riser base gas injection under the same flow conditions of low air flows. The dissimilarity in void profiles in the vertical section caused by the different gas injection configurations at these lower gas superficial velocities is explained by the influence of the flow regime encountered in the horizontal flowline when gas injects through the flowline. Based on visual observation via the window installed in the horizontal pipe and also according to Mandhane et al. (1974), the identified horizontal flow regime for this flow condition (U_{sl} =1m/s and U_{sg} = 0.4m/s) is bubbly/elongated bubbly flow which may help in creating a smoother flow with small air bubbles and consequently contribute to form wall-peak bubbly flow in the vertical pipe for upstream horizontal flowline gas injection.

At higher gas superficial velocity ($U_{sg} \geq 1.55$ m/s) it can be observed that the void fraction generally increases due to the increase in superficial velocity. The general trend of void distribution at the higher air flows shows core-peak distribution for the two gas injection configurations. However, it is still a slightly more flattened void fraction existence around the centre of the pipe for the case of upstream horizontal flowline gas injection.

The findings in this part of the current work show that, in some multiphase applications that utilise gas-lift or gas injection, the location of the injection point could impact on the phase fraction measurements and distributions.
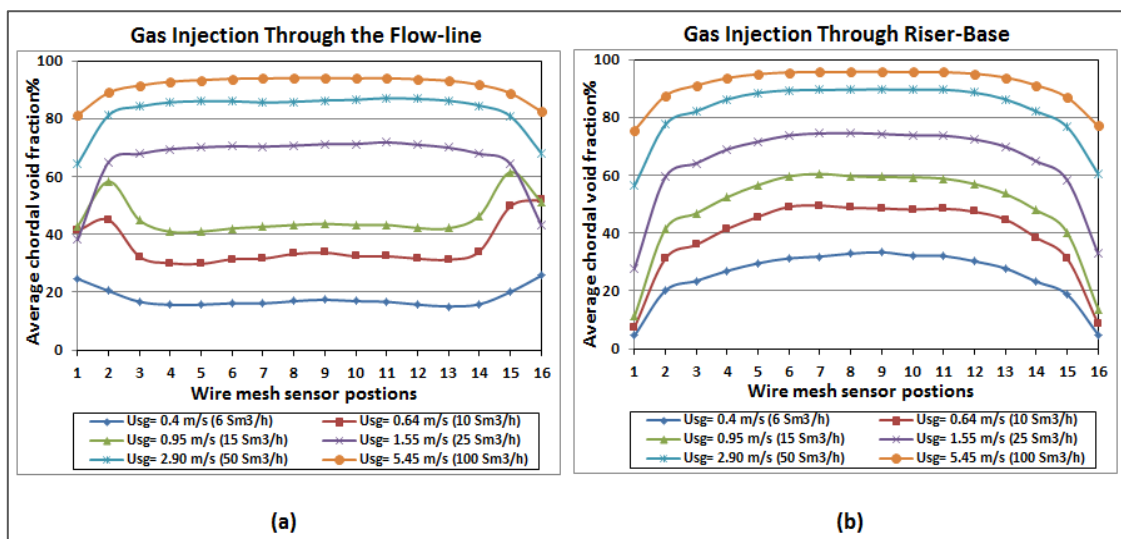
Figure 4-21: Chordal void fraction distribution in the riser's cross-sectional: a) Flowline gas injection, b) Riser base gas injection

4.3 Comparison between Capacitance and Conductive WMS

A comparison between the capacitance and conductive wire-mesh sensor measurements for air-water flow has been carried out at the top of the vertical riser. The comparison was performed for air superficial velocities values that are equivalent to air flow rates of 1.5, 6, 10, 15, 25, 50 and 100 sm^3/h, while a superficial water velocity was kept fixed at 0.25 and 1 m/s. These flow conditions are capable of establishing various flow regimes. The measurements for the capacitance WMS were carried out by using a CAP 200 electronics unit. While the conductive WMS measurements were performed by using SGITT100 conductive electronics unit, which was loaned out from HZDR for a short period. Both measuring electronic units were operated at a frequency of 1,000 Hz over a time period of 30 sec. In addition to the obtained visualization images, time series of the averaged cross section void fraction and local Chordal void fraction distributions are used for this comparison. Figure 4-22 shows a compression between the mean void fraction measured by the capacitance WMS and that measured by the conductive WMS for the same air-water flow conditions. The solid line in the Figure indicates the ideal concordance. It was found that the main void fraction values obtained from conductive WMS and capacitance WMS are reasonably close, with a small percentage difference ranging between -2% to +5% for liquid superficial velocity of 0.25 m/s and between +0.1% to +6% for liquid superficial velocity of 1 m/s. the positive difference depicts the capacitance mean void fraction is the higher value.

The time series of cross-sectional void fraction and corresponding PDFs that were extracted from both wire mesh sensors were tested to identify the flow patterns inside the riser. Table 4-1 shows typical results obtained via wire mesh sensors (CapWMS & CondWMS) for several selected test points at the same flow conditions including various air superficial velocities at a fixed liquid superficial velocity of 1 m/s. From the represented results it can be seen that at a liquid superficial velocity of 1 m/s and gas superficial velocity of 0.1 m/s (air flow rate of 1.5 sm^3/h), both conductive WMS and capacitance WMS identify the flow regimes as bubbly flow.

95
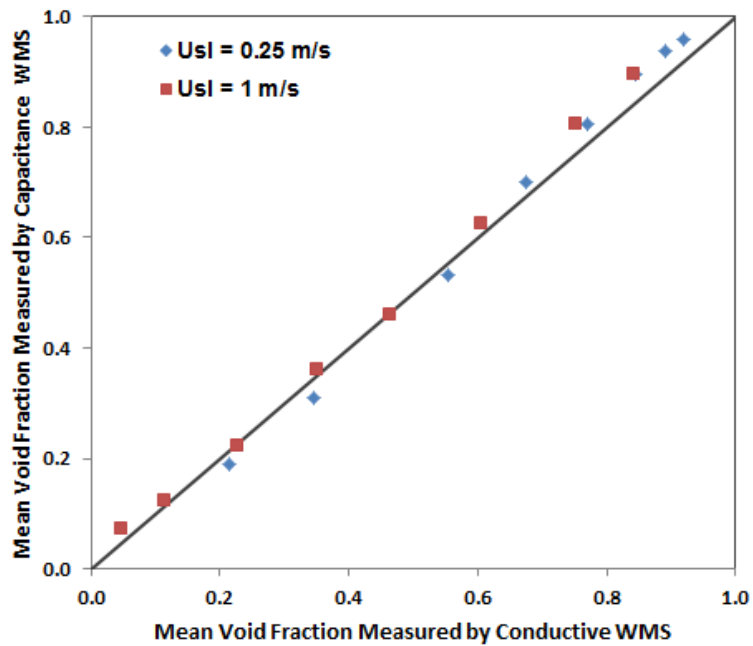
Figure 4-22: Mean void fraction measured by the CondWMS against that measured by the CapWMS.

The time series of the cross-sectional averaged void fraction for this flow condition from both CapWMS and CondWMS shows the obtained signals centre around low average void fraction values with very small fluctuations (standard deviation of ±1.8% and ±1.9% for conductive and capacitance WMS, respectively). The corresponding PDFs present narrow single peaks with the same height at the lower void fraction region for both CondWMS and CapWMS, which also indicate bubbly flow pattern.

At gas superficial velocity of about 0.4 m/s (water superficial velocity was maintained at the same 1 m/s), the shape of time series and the corresponding PDFs for both wire-mesh sensors' measurements also show an almost similar trend. The time traces show fluctuations with sharp and very narrow peaks and the PDFs' shapes show a broader peak with a long tail extending towards the higher void fraction region, which indicate spherical cap bubbly flow for this flow condition by both wire-mesh sensors.

Upon increasing the gas superficial velocity to 1.55 m/s (air flow rate of 25 Sm^3/h), the flow pattern inside the riser indicated as bubbly/slug transition flow by both capacitance and conductive WMS measurements, as indicated from the obtained time series of void fraction and PDF shapes. The mean void fraction time traces for wire-mesh sensors show fluctuations with distinct peaks and troughs. The PDF' shapes for this condition generally shows almost two peaks (tall peak with progressive development of a second peak) by conductive WMS as well as capacitance WMS. However, the PDF from the conductive WMS' data still shows a slight higher peak than that from the capacitance WMS data.

At higher gas superficial velocity of about 3 m/s (air flow rate of 50 Sm^3/h), the void fraction time traces and PDFs shapes for both cases of conductive WMS and capacitance WMS show slight dissimilarity. The time series void fraction for capacitance WMS shows slightly less fluctuation than the conductive measurement, as can be seen in Table 4-1. Accordingly, the PDFs' geometries display a little dissimilarity in shape and in their heights, although both measurements' results indicate almost the same flow pattern of slug flow inside the pipe.

At the highest gas superficial velocity of about 5.45 m/s (air flow injection of 100 sm^3/h), the PDF for this flow condition provided by conductive WMS data also shows a slightly different shape from that produced by capacitance WMS data, i.e. double peaks provided by conductive WMS, which indicates slug flow, whereas, higher single peak with the bulge towards the low void region is provided by the capacitance WMS measurements, indicating a churn flow pattern.

Generally, the obtained result therefore shows that both instruments (capacitance and conductive wire-mesh sensors) predict almost similar flow regime signatures.

Table 4-1: Time series and PDF of void fraction for Capacitance and Conductive WMS

U$_{sg}$, m/s	Conductive WMS		Capacitance WMS	
0.1				
0.4				
1.55				
3.0				
5.45				
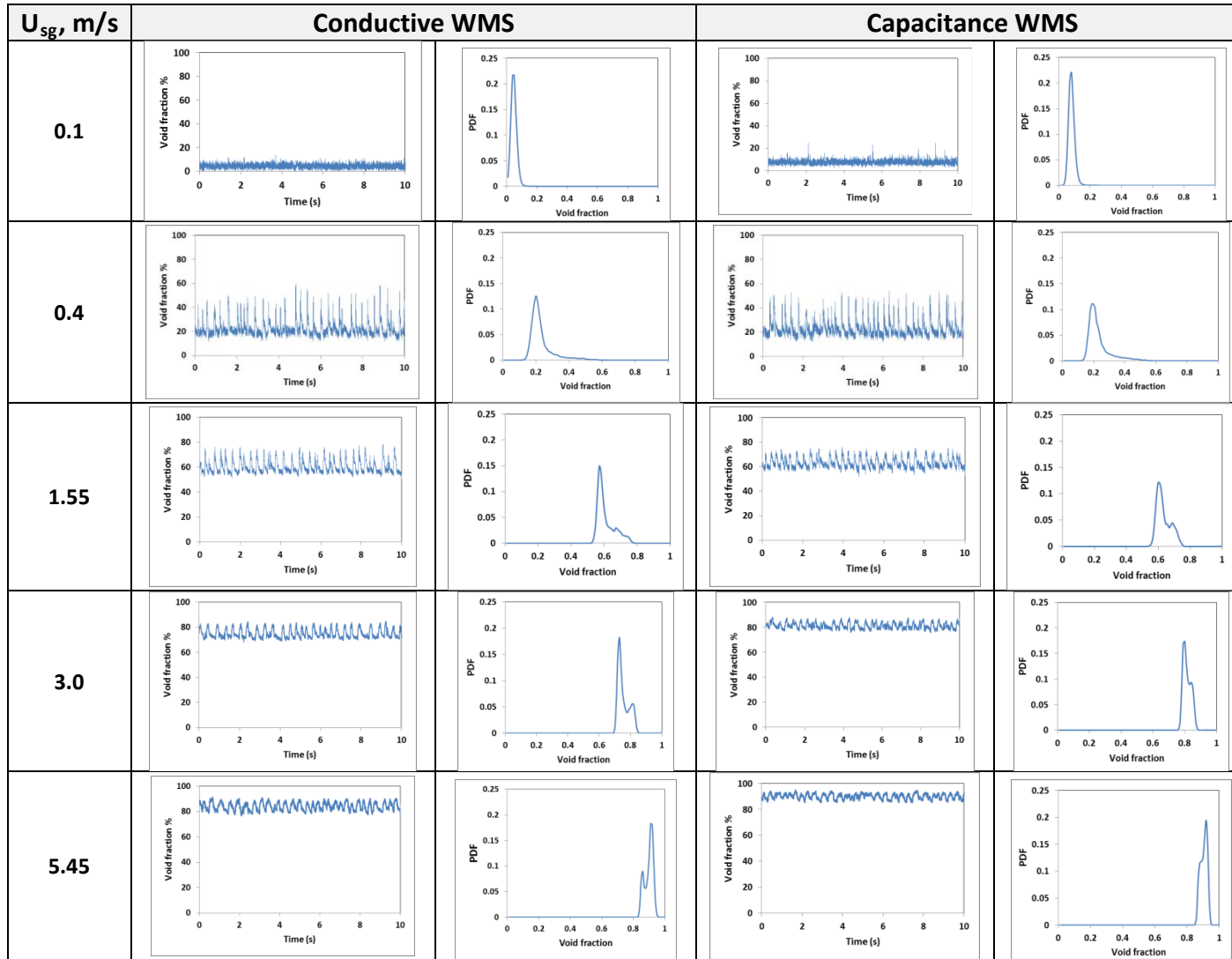
In addition to using average cross-sectional void fraction time series and the corresponding PDFs for flow regime identification, the visualization images (the slice views) provided by wire mesh sensors were also compared in terms of identifying the flow patterns that were encountered inside the riser. Figure 4-23 shows axially slice views images of the void fractions data that were obtained from the conductive (Figure 4-23 (a)) and capacitance (Figure 4-23 (b)) WMS for the same flow conditions (red colour indicates gas phase and blue represents water phase). At a gas superficial velocity of about 0.1m/s, the flow appears as small bubbles flowing within the liquid structure, which reflects bubbly flow. At gas superficial velocity of 0.4 m/s, both wire-mesh sensors show small bubbles with bubbles of a larger size, but not as large as the pipe diameter, which is described as transition flow or spherical cap bubble. At gas superficial velocity of 1.55 m/s, a bit larger bubble is formed and starts to lead towards forming an almost slug flow. At the higher gas flow of 3 m/s, the image extracted by the conductive WMS measurement shows a long and large gas bucket in the centre of the pipe, while the image from the capacitance WMS displays an intermittent gas core as churn flow. At the highest gas superficial velocity of 5.45 m/s, the capacitance WMS image shows the flow is almost churn to annular flow, whereas, the gas core occupied the centre of the pipe.

The visualization images are almost in agreement with the corresponding time traces and PDFs' results for the same flow conditions presented in the previous section. However, the slight dissimilarity between the indicated flow patterns at the highest gas flows is also observed from the extracted images from the conductive WMS and the capacitance WMS for the same flow condition of 5.45 m/s gas superficial velocity.

Usg = 0.1 m/s   Usg = 0.4 m/s   Usg = 0.95 m/s   Usg = 1.55 m/s   Usg = 3.0 m/s   Usg = 5.5 m/s

Usg →

Conductive WMS images

(A)

Usg = 0.1 m/s   Usg = 0.4 m/s   Usg = 0.95 m/s   Usg = 1.55 m/s   Usg = 3.0 m/s   Usg = 5.5 m/s

Usg →

Capacitance WMS images
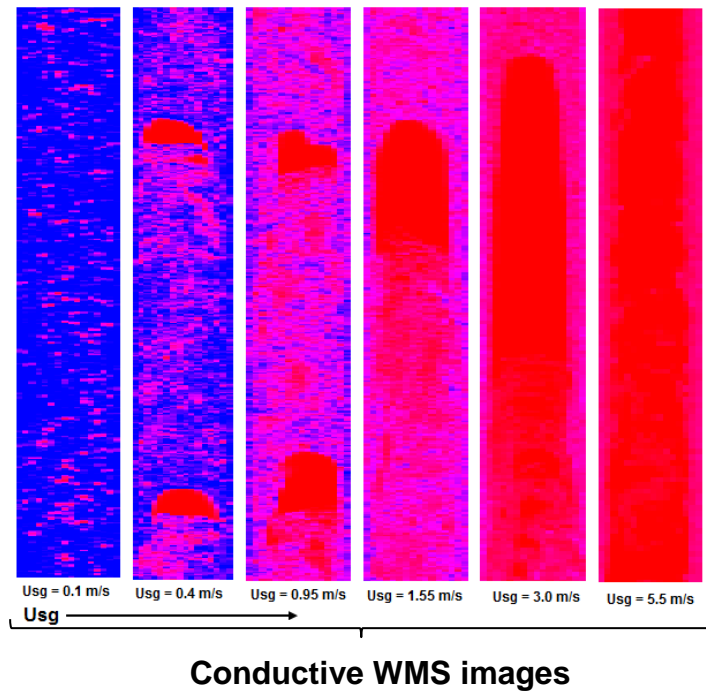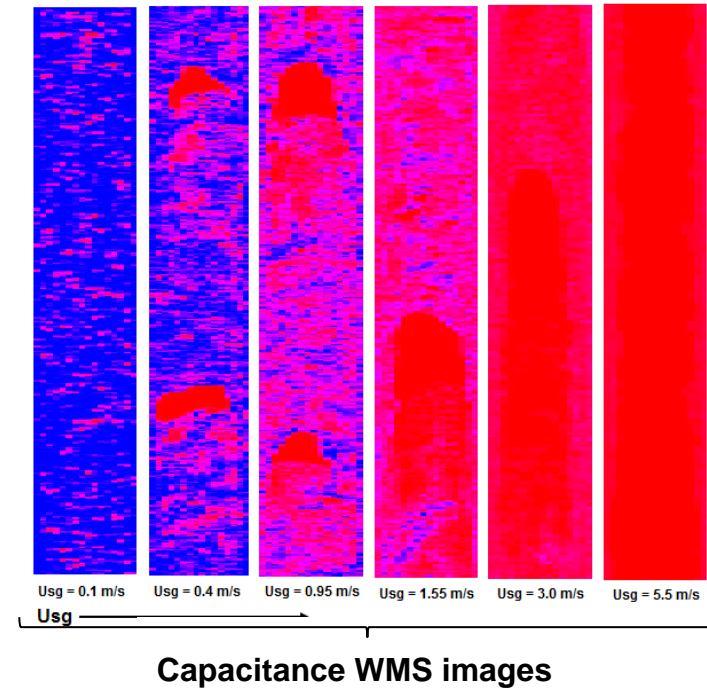
(B)

Figure 4-23: Slice view images of the air-water two-phase flow at constant water velocity of U_{sl} = 1 m/s

100

The void fraction distributions for the compared flow conditions were analysed for both the conductive and capacitance wire mesh sensors data. The average chordal void fraction distributions were made by averaging the void fractions measured at each crossing point belonging to the four centrelines sixteen wires (1 – 16), going from 180° to 0°(left to right) and from 270° to 90° over the cross section of the vertical riser. The results are illustrated in Figures 4-24 for conductive WMS and Figure 4-25 for capacitance WMS measurements at fixed water superficial velocity of 1 m/s and several air superficial velocities.

In all cases (conductive and capacitance WMS, U_{sl} =1 m/s and U_{sl} = 0.25 m/s), these results show a general trend that the time-averaged chordal gas fraction profiles have maxima distributions located around the pipe centre (core-peaking profile) and these values increase with increasing gas superficial velocity. Also, at the low gas superficial velocities (where bubbly flow was indicated) the average choral void fraction profiles appear more flattened over the pipe cross-section, compared to those of higher superficial velocities.

Although, the conductive measurements itself displays similar distribution in both directions (0° to 180° and from 270° to 90°), they still show slight differences against the capacitance WMS results. These differences between conductive void distributions and the capacitance void distributions clearly appear towards the pipe wall. This observation may suggest that, deeper investigations, including comparison with other reliable instruments, are suggested to be carried out in the future by following researchers.

(a)   (b)
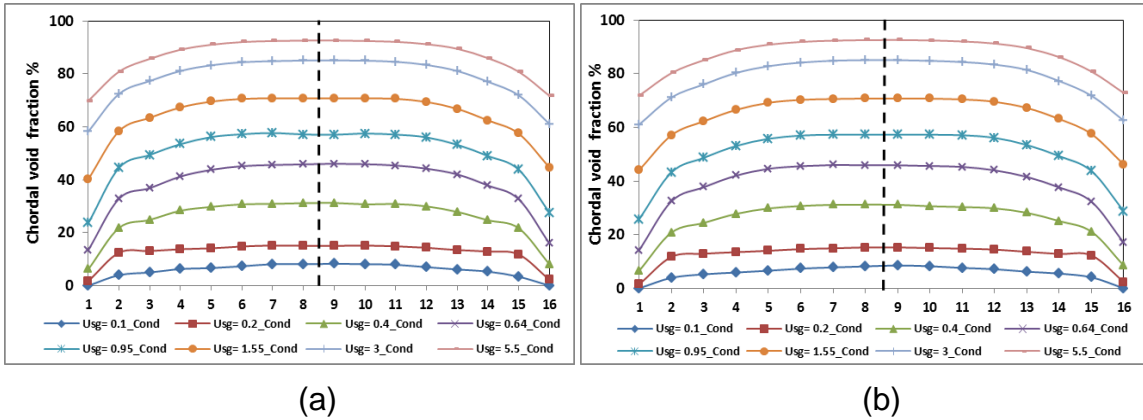
Figure 4-24: Conductive WMS at U_{sl} = 1 m/s: chordal void fraction distribution going from a) 90° to 270°, b) 180° to 0°

(a)   (b)
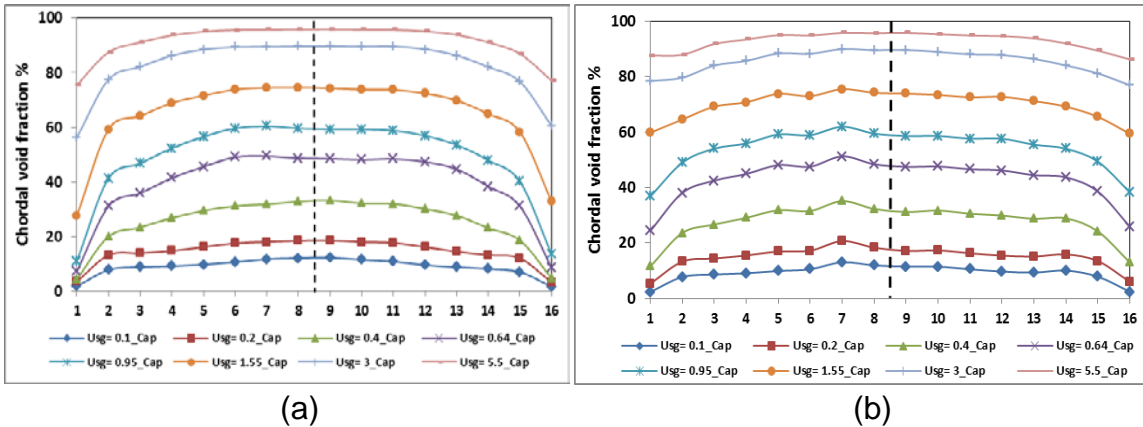
Figure 4-25: Capacitance WMS at U_{sl} = 1 m/s: chordal void fraction distribution going from a) 90° to 270°, b) 180° to 0°

4.4 Chapter summary

In this Chapter, various results obtained from air-liquid two-phase flows in a 52 mm diameter and 10.5 m long vertical riser were presented and discussed.

In additional to the visual observation, the time traces and corresponding PDFs of the obtained signals fluctuations from both the WMS and clamp-on gamma densitometer for air-water flows have been adopted for objective and quantitative flow pattern identification. The flow characteristics identified in this study were within bubble, bubbly to slug transition (spherical bubbly), slug,

102

churn and annular flows. The capacitance WMS showed high performance as its obtained data are consistent with those obtained simultaneously by the gamma densitometer in terms of flow pattern identification and void fraction measurements. However, the WMS showed greater ability for providing useful information about flow patterns, phase fraction and phase fractions distribution. Thus, the qualitative and quantitative results from the tests of air-water two-phase flows showed that the WMS is a valuable technique with which to investigate multiphase flows.

The behaviour of the total pressure gradient along the vertical riser has shown a significant decrease as the injected gas superficial velocity increased. Also, the rate of drop in total pressure gradient at the lower injected gas superficial velocities is higher than that for higher gas superficial velocities. On the other hand, the deduced frictional pressure gradient was found to increase as the injected gas superficial velocity increased.

The entrance effect on the two-phase flow characteristics in the 52 mm diameter vertical riser was also studied. The advanced technique of capacitance WMS was used to obtain comprehensive information of the flow regime, phase fraction fluctuation and phase distribution at the top of the riser. The experiments were conducted with two different gas injection configurations, namely riser base gas injection and horizontal flow-line inlet gas injection. The considered results for the two inlet configurations exhibited differences in flow patterns, void fraction values and distributions inside the riser. This dissimilarity is due to the effect of flow behaviour in the horizontal flowline that influences the vertical riser behaviour. These findings show that, in some multiphase applications that utilise gas-lift or gas injection, the location of the injection point could impact on the phase fraction measurements and distributions.

A comparison between capacitance and conductive wire mesh sensor measurements has been carried out at the top of the riser. The comparison has been conducted for various superficial air velocities with a fixed superficial water velocity of 0.25 and 1 m/s. Data including time traces of the averaged void

fraction, and its PDFs and chordal void fraction distributions, are used for this comparison.

The time traces of the averaged void fraction and its PDFs generated from the CapWMS and CondWMS show similar tendencies, particularly at lower gas superficial velocity. Similar observations were found for the visualization method by the both instruments, i.e. flow regimes for the same flow conditions of air-water are observed to be the same at lower gas superficial velocities and a little different at the highest gas superficial velocity. The void fraction distribution results for capacitance and conductive WMS showed slight differences near to the pipe wall. Thus, further investigations are recommended to be carried out in the future.

The valuable qualitative and quantitative results from the capacitance WMS for air-water two-phase flows in the 52 mm vertical riser are encouraging for trying to use the instrument to investigate the oil-water two-phase flow and air-oil-water three-phase flows in the current study.

CHAPTER FIVE

5 INFLUENCE OF GAS INJECTION ON OIL-WATER FLOW

In this Chapter, the results of a series of experiments on oil-water two-phase upflow are shown, analysed and discussed. Also, experimental results corresponding to riser base gas injection on oil-water flow in the riser will be presented and discussed. The results of liquid-liquid (oil-water) flows are demonstrated to help in the interpretation of the oil-water experiments with a riser base gas injection at a wide range of air flow rates, which will also be presented in the following Section of this Chapter. In addition, the results for oil-water and gas-oil-water data that were acquired by the capacitance wire-mesh sensor will be shown in this Chapter.

5.1 Liquid-liquid/Oil-Water Flow in a Vertical Riser

The liquid-liquid experiments were conducted in the three-phase facility (described in Chapter 3) using the 52 mm ID vertical riser. Tap water and dielectric oil EDM-250 were used as the water and oil phases respectively with their properties as illustrated in Table 3-2. The experiments generally were performed by keeping a simultaneous oil-water upflow at constant mixture superficial velocity and changing the input water cut from 0 - 100% and vice versa (Oil superficial velocity + Water superficial velocity = constant, whenever the input water cut changes, the total mixture liquid superficial velocity needs to be adjusted to keep it fixed in the riser system). The experiments were conducted at each constant superficial velocity from two different routes, starting from pure oil single-phase to pure water single-phase and from water single-phase to oil single-phase, respectively. The tests were performed for several values of constant mixture superficial velocity: 0.25 m/s, 0.5 m/s, 1 m/s, 1.5 m/s and 2 m/s. At each phase fraction in a particular mixture velocity (i.e. a test point), the flow was allowed to stabilize for approximately 25 minutes before

any measurement was taken. Each experiment was conducted at least twice to ensure the reproducibility of the experiments and that it was good.

Firstly, in order to check the quality of the data collected from the instruments in the three-phase system for the targeted tests of oil-water experiments, initial tests with only single-phase of pure water and pure oil were pumped separately through the riser system at different liquid superficial velocities of 0.25, 0.5, 1, 1.5 and 2 m/s. The in-situ liquid mass flowrate and density of the fluid at different locations of the flow-loop were measured simultaneously by inlet flow meters (recorded by the DeltaV system), near to the riser base horizontal Coriolis meter and then by the vertical Coriolis meter at the top of the riser (recorded simultaneously by the Labview system). The average values for the obtained mass flow rates of water flows and oil flows single-phase are represented in Figures 5-1 and 5-2, respectively. It can be observed that the average readings of the mass flow rates for each liquid superficial velocity were close, with only small differences (not more than 0.12%).
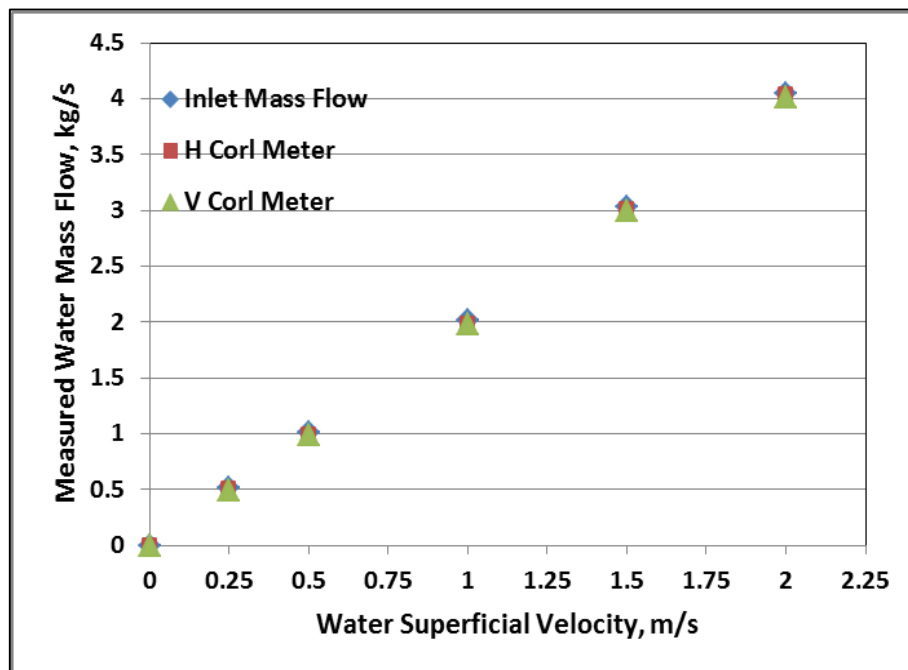
Figure 5-1: Water Mass Flow rates Measured Simultaneously by Different Flow Meters installed in the Riser System
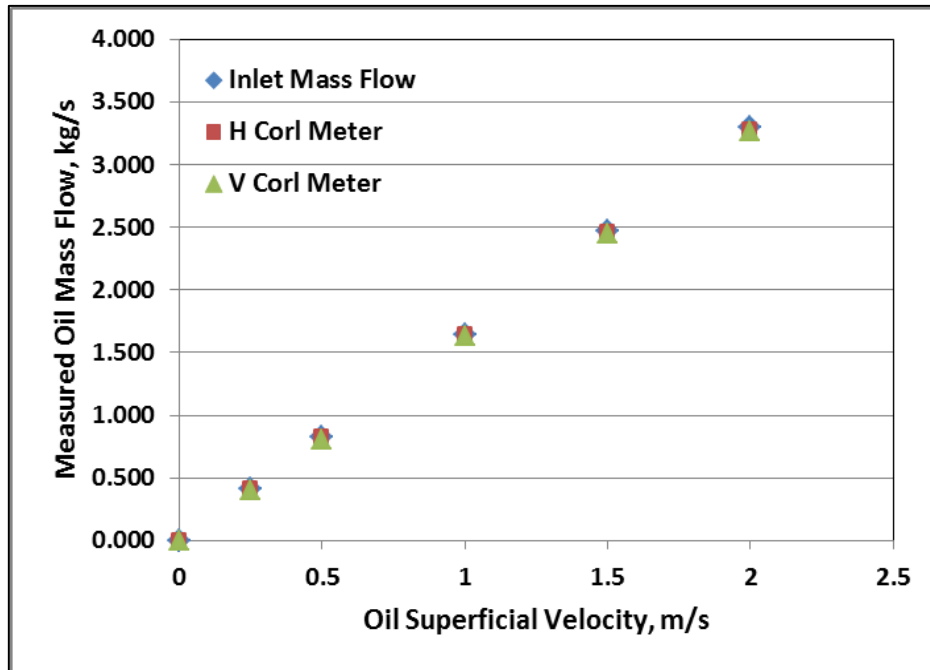
Figure 5-2: Oil Mass Flow rate Measured Simultaneously by Different Flow Meters installed in the Riser System

Similarly, the density measurements obtained from both Coriolis meters and the inlet flow meter were recorded simultaneously. The average values of density at each test point for several liquid superficial velocities of water only and oil flow only are shown in Figure 5-3. From the plot in Figure 5-3 it can be observed that the metering densities by the Coriolis mass flow meters (horizontal and vertical) are relatively the same density metering as the inlet flow meter for both water and oil. The agreement between the readings of these flow meters was very good with differences of not more than 0.14%. Moreover, the measured densities were close to the standard densities of oil and water used for the experiments. These results give confidence and reliability to the mass flow rate and density that were measured by the flow meters used.
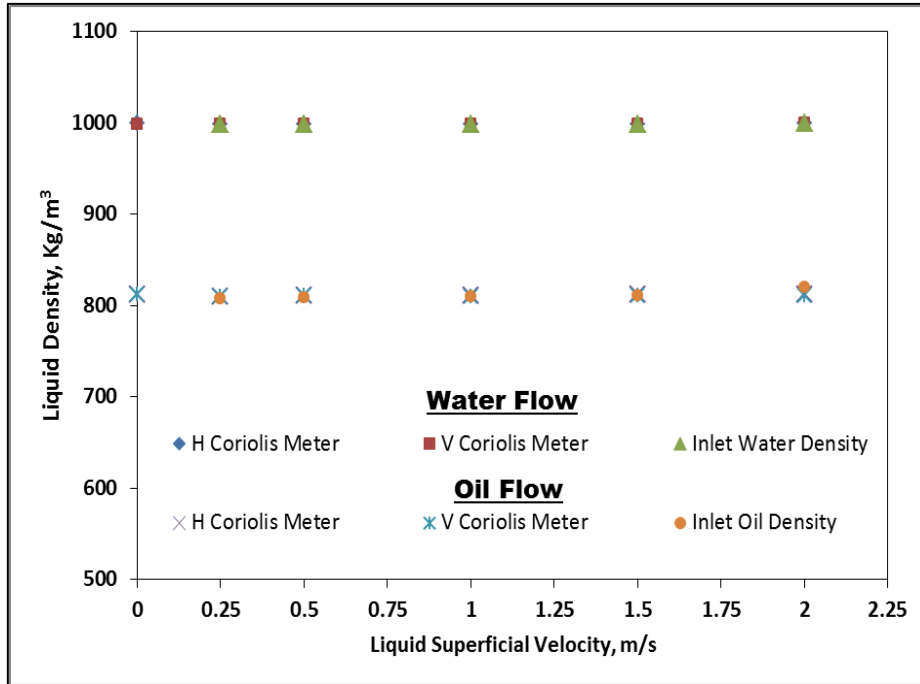
Figure 5-3: Density Measurement for Single-phase Flows

Likewise, total pressure gradients across the vertical riser were determined for single-phase flow of water and oil at different values of liquid superficial velocities. For most of these flow conditions the flow was turbulent, with the Reynolds number ranging between 3×10^3 and 1×10^5. Only the flow rates corresponding to low oil flow only of 0.25 m/s were classified as laminar flow with oil flow Reynolds number of 1.330×10^3. Thus, the Haaland correlation (Equation 2-4) and Swamee - Jain correlation (Equation 2-5) were used to calculate the frictional pressure gradient part.

The single-phase experimental results for the total pressure gradient that were measured across the riser sections were compared with the calculated pressure gradient, as can be seen in Figure 5-4(a) for pure water and 5-4(b) for pure oil. The average value of measured water or oil density at the horizontal and vertical Coriolis mass flow meters was used to calculate the hydrostatic pressure gradient. The results show that the measured total pressure gradient is close to the calculated total pressure gradient.

108
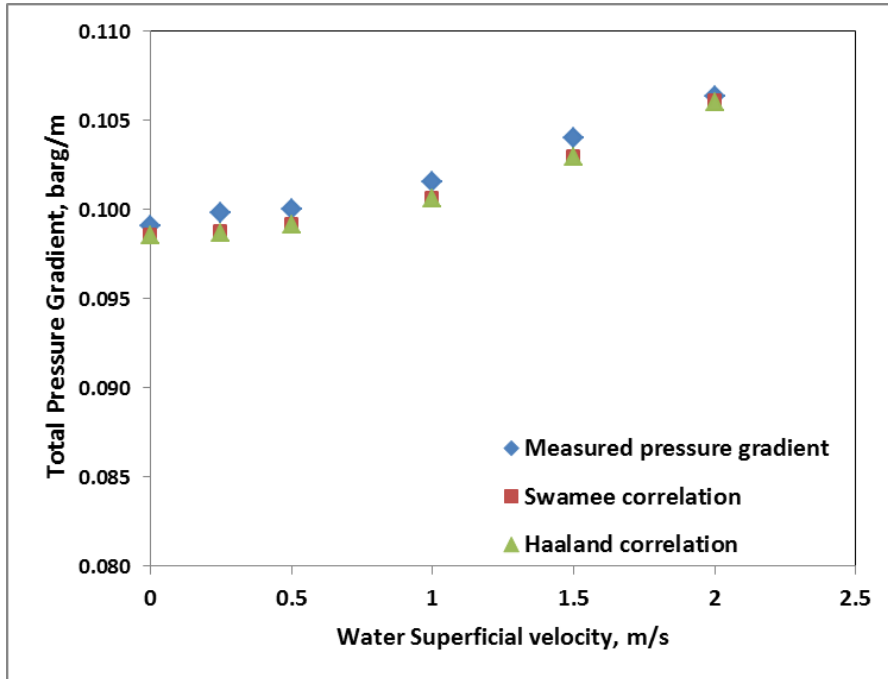
(a)
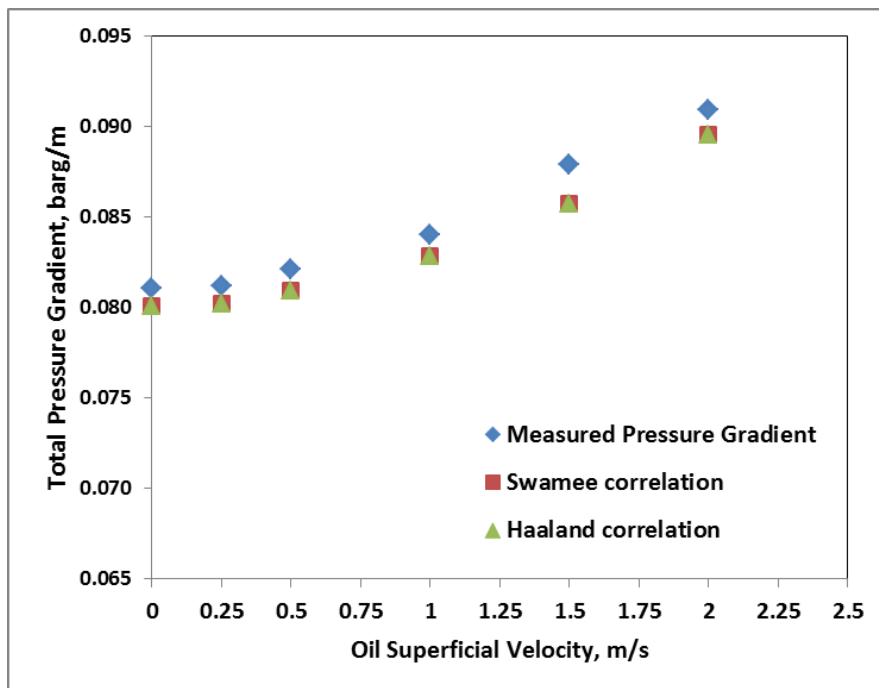
(b)

Figure 5-4: Total Pressure Gradient for Single-Phase Flow of:

a) Water flow, b) Oil flow

5.1.1 Flow patterns of Oil-Water in the Vertical Riser

The flow characteristics of oil-water flow in the 52 mm vertical riser for various liquid throughputs and different water cuts were firstly visually (recorded videos) observed through the transparent Perspex sections along the riser. The mixture flow exhibited that as the water cut increases the oil-water flow pattern changes gradually from oil-dominated (water dispersed phase) to water-dominated (oil dispersed phase) and vice versa. The observed flow patterns generally can be distinguished into less homogeneous (almost dispersed) mixture flows at lower mixture superficial velocity of 0.25 m/s, almost homogeneous flows at higher mixture superficial velocities of 0.5 m/s and homogeneous (well mixed) flows for U_{sm} > 0.5 m/s. Snapshots of the flow regimes for different mixture flow rates at different water and oil cuts are shown in Figure 5-5. At a lower oil-water mixture superficial velocity of 0.25 m/s and low water cuts, the observed flow regime is water dispersed in oil with some water phase moves close to the pipe wall. As the water cut increases the flow gradually becomes water-dominated and the flow pattern changes from water dispersed in oil to oil dispersed in water. Gradual replacement of the water phase close to the pipe wall by oil can also be observed as the input water fraction increases. Also, when the mixture of liquid throughput increases (as can be seen from the exemplary experimental test points corresponding to the mixture superficial velocities of 0.5 and 1 m/s), the oil-water mixture becomes more homogeneous which aids the homogenization of the mixture and results in the flow changes from dispersed to finely dispersed flow characteristics. The transition from dominated oil flow to a water continuous phase associated with viscous flow can be observed at input water cuts of 0.4, 0.42 and 0.45 (0.4 ≤ input water cut ≤ 0.45). This may lead to identifying the occurrence of a phase inversion point around those water cut points. At higher oil fraction, the whole pipe is completely dominated by the oil continuous phase. With an oil continuous phase, the water phase cannot be easily seen.The visual images did not provide clear information on the oil-water phase distribution in the pipe. Therefore, attempts were made to use a capacitance wire-mesh sensor to visualize and reconstruct the phase distribution across the pipe cross section. The wire-mesh sensor results will be discussed in the following section.
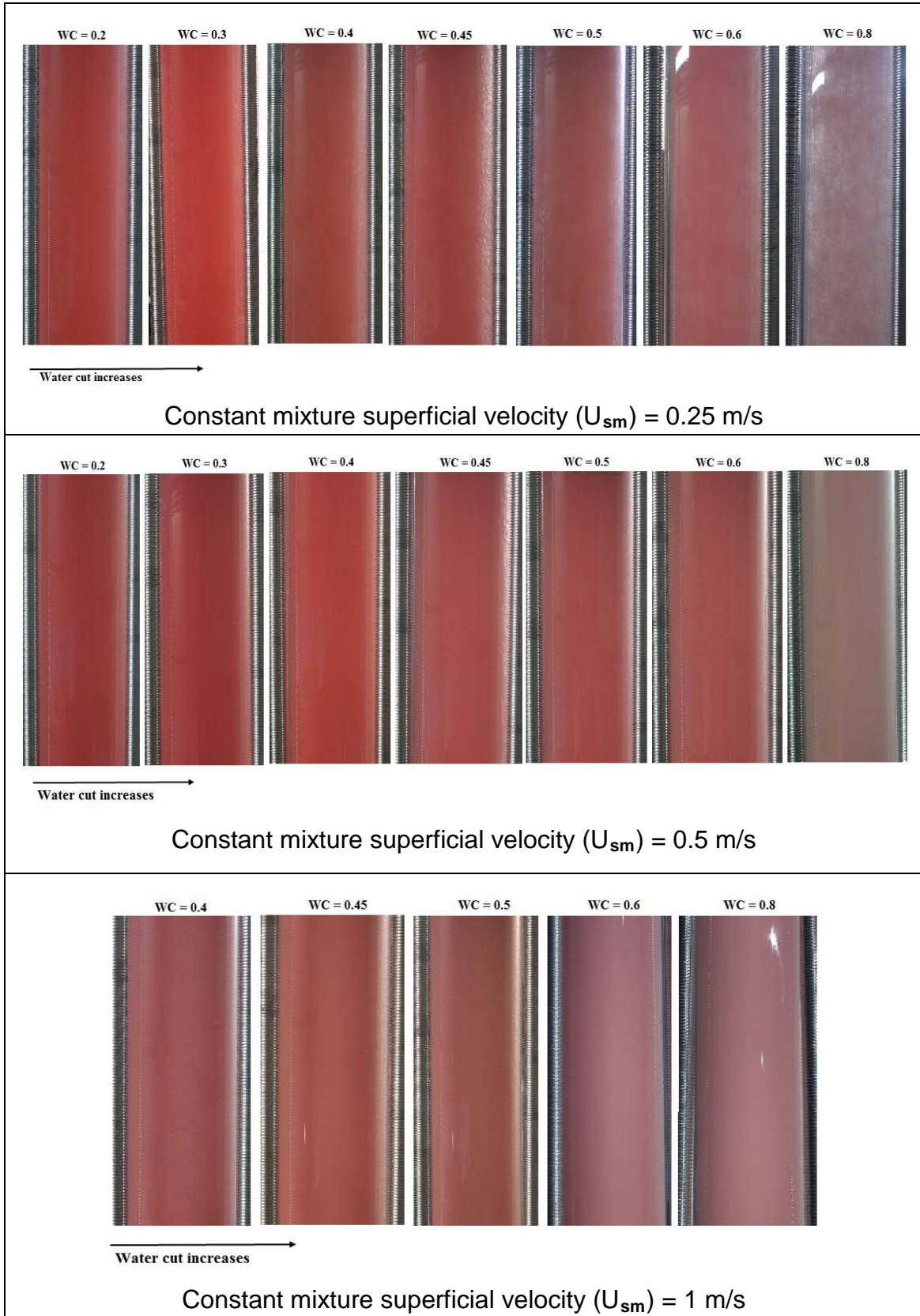
Figure 5-5: Oil/Water Flow Characteristics at Different Water Cuts and Different Liquid Throughputs.

5.1.2 Wire-Mesh Sensor Measurement for Oil-Water Upflow:

The use of a WMS for investigating the characteristics of liquid-liquid oil-water flows has been reported in a some previous studies (Rodriguez et al. (2011); Da Silva et. al. (2011). However, these investigations were carried out for the oil-water flows in horizontal pipes. The implementing of the WMS for oil-water flow in vertical flow, to the author's knowledge, has not been previously reported. Thus, further attempts have been carried out in the current study on the possibility of obtaining useful information about the oil-water upflow characteristics inside a 52 mm vertical riser under different oil and water concentrations using capacitance WMS. The measurements were conducted simultaneously along with the other instrumentations, i.e. Coriolis flow meters and a single-beam gamma densitometer. Also, the capacitance wire-mesh sensor (WMS) measurements were performed close to these instrumentations, at a location of approximately 9.5 m (~182D) from the riser base. The measurements were conducted for constant mixture superficial velocities of 0.25, 0.5, 1 and 1.5 m/s. Only data for the oil-water mixture flow when the flow was in a water-dominated phase (beyond input oil fraction of about 40% for U_{sm} = 0.25 m/s and 0.5 m/s and 55% for U_{sm} = 1 and 1.5 m/s) were analysed. Prior to the beginning of the experiments, the WMS electronics box described in Chapter three was connected to the sensor to take the WMS measurements of the flow conditions. Then, a calibration was performed (as explained in Chapter 3) with oil only and water only as references. The data were taken at a data acquisition frequency of 1000 Hz over an interval of 30 seconds. There were no data to be extracted when the mixture flow was in the oil continuous phase.

5.1.2.1   WMS Visualization Images

In the current study, efforts were made to obtain results from the capacitance wire mesh sensors about the phase fraction distributions in oil-water experiments. As previously mentioned, these results were acquired only when the flow was water-dominated inside the riser system. Figure 5-6 shows cross-

sectional images for oil-water upflow for mixture velocities of 0.25, 0.5, 1 and 1.5 m/s at various input oil fractions. The water phase is represented in blue while the oil phase is represented in red. It can be observed from the cross-sectional images, that the flow at these mixture superficial velocities is oil phase dispersion in water continuous. Moreover, the oil phase tends to flow near to the pipe wall, whereas higher water concentration appears around the pipe centre. As the mixture superficial velocity increases from 0.25 to 0.5 m/s, the flow appears to become more homogeneous but it still shows higher oil fraction moves near the pipe wall and still greater water moves around the centre with some oil phase flowing within. This can also be observed clearly from the corresponding axial slice images in Figure 5-7 (red indicates oil and blue represents the water phase). As the input oil cut rises, more oil is observed to be distributed all over the cross section of the riser.

In the case of higher mixture superficial velocities of 1 and 1.5 m/s, the wire-mesh sensor provided data for a wider range of input oil fraction [10% - 55%] (i.e. 45% ≤ input water cut ≤ 90%). Figure 5-8 shows example cross-sectional tomographic (a) and axial slice views (b), obtained by the capacitance WMS measurements that were performed at a mixture superficial velocity of 1 m/s with different mixture concentrations within the aforementioned oil fraction range. Additional cross sectional and vertical slice images for more flow oil-water flow conditions are given in Appendix B-2. In general, when the superficial mixture velocity increased, both the fluids, i.e. oil (red colour) and water (blue colour) tended to homogenize and the small oil drops were finely dispersed in continuous water flow because of the breakup of oil drops induced by enhanced turbulent energy. It can also be observed from the obtained images at low oil fraction that a higher presence of this oil still tends to flow near to the pipe wall, whereas the region around the pipe centre appears to remain dominated by the water phase with the oil phase flowing within. As the input oil fraction increases the WMS images clearly show a gradual increase for the oil content and distribution throughout the cross section. With a further increase in oil fraction to 55% (i.e. 45% input water cut where phase inversion is expected to occur), the

113

oil phase tends to draw towards the centre of the pipe, forming a mixture with a high concentration of oil phase around the pipe centre.

	Oil fraction = 0.1	Oil fraction = 0.2	Oil fraction = 0.3	Oil fraction = 0.4
0.25 m/s				
0.5 m/s				
1 m/s				
1.5 m/s				
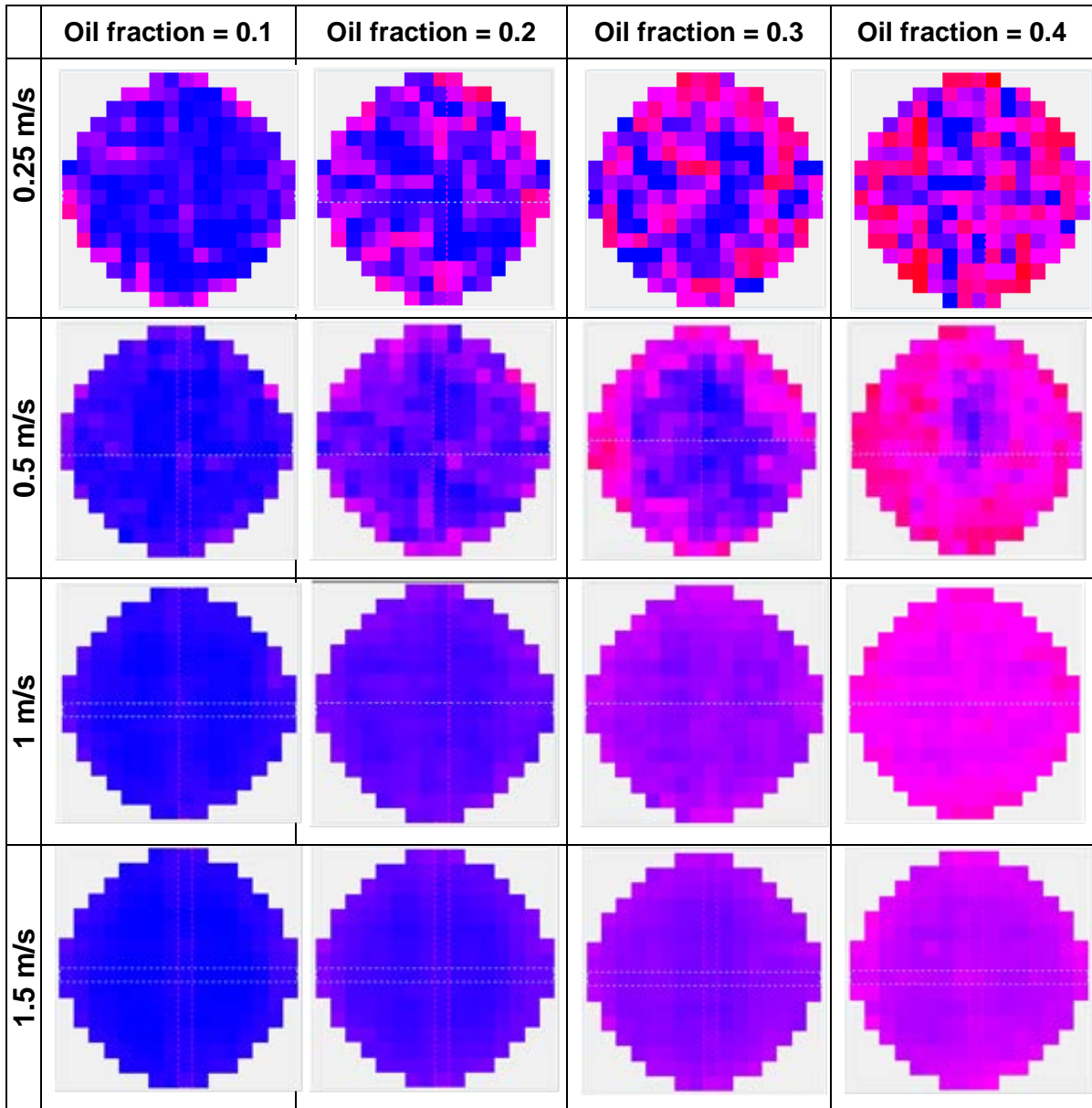
Figure 5-6: Cross-sectional images acquired by the WMS for oil-water flows at several values of constant mixture liquid superficial velocities.
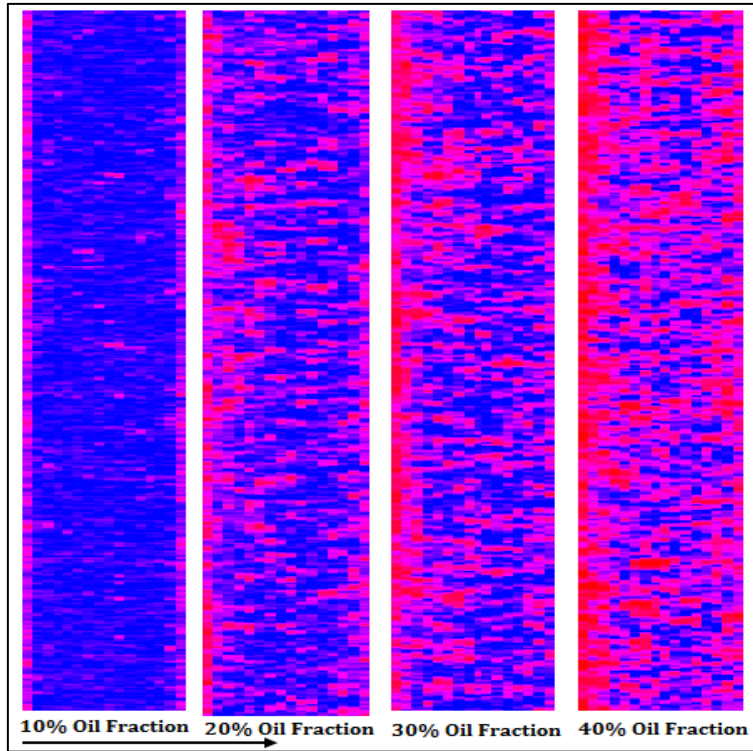
(a)
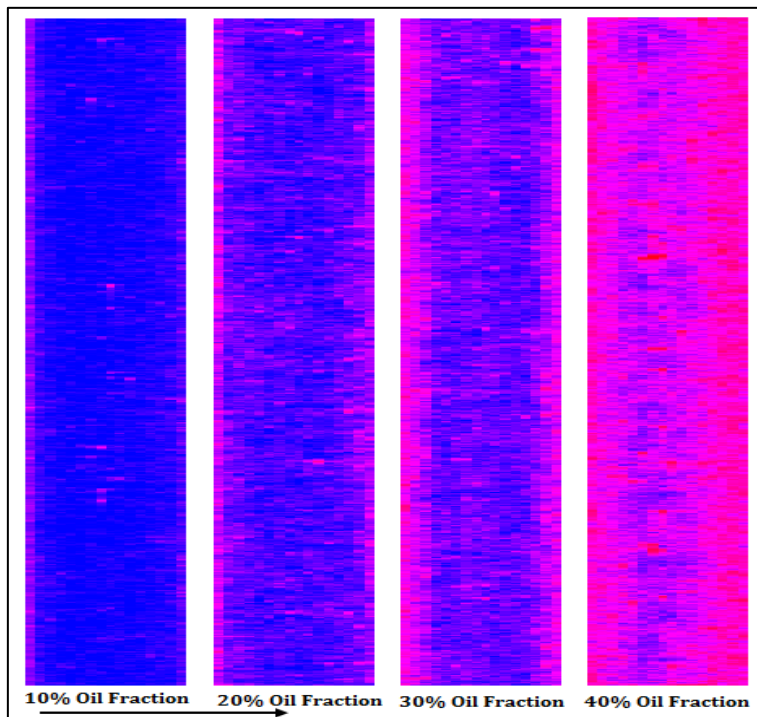
(b)

Figure 5-7: Slice view images via WMS for oil-water flow at mixture velocity of a) 0.25 m/s, b) 0.5 m/s
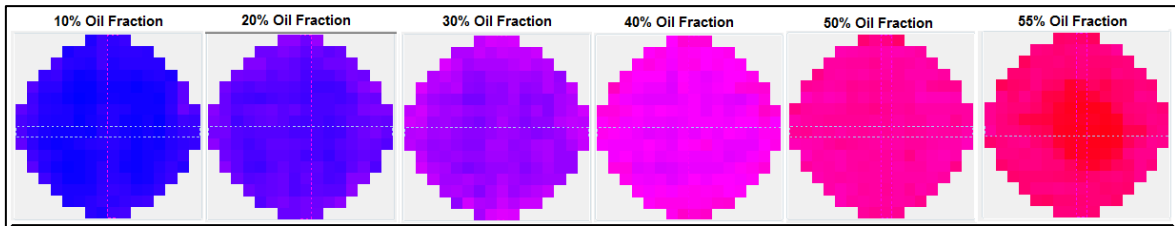
(a)
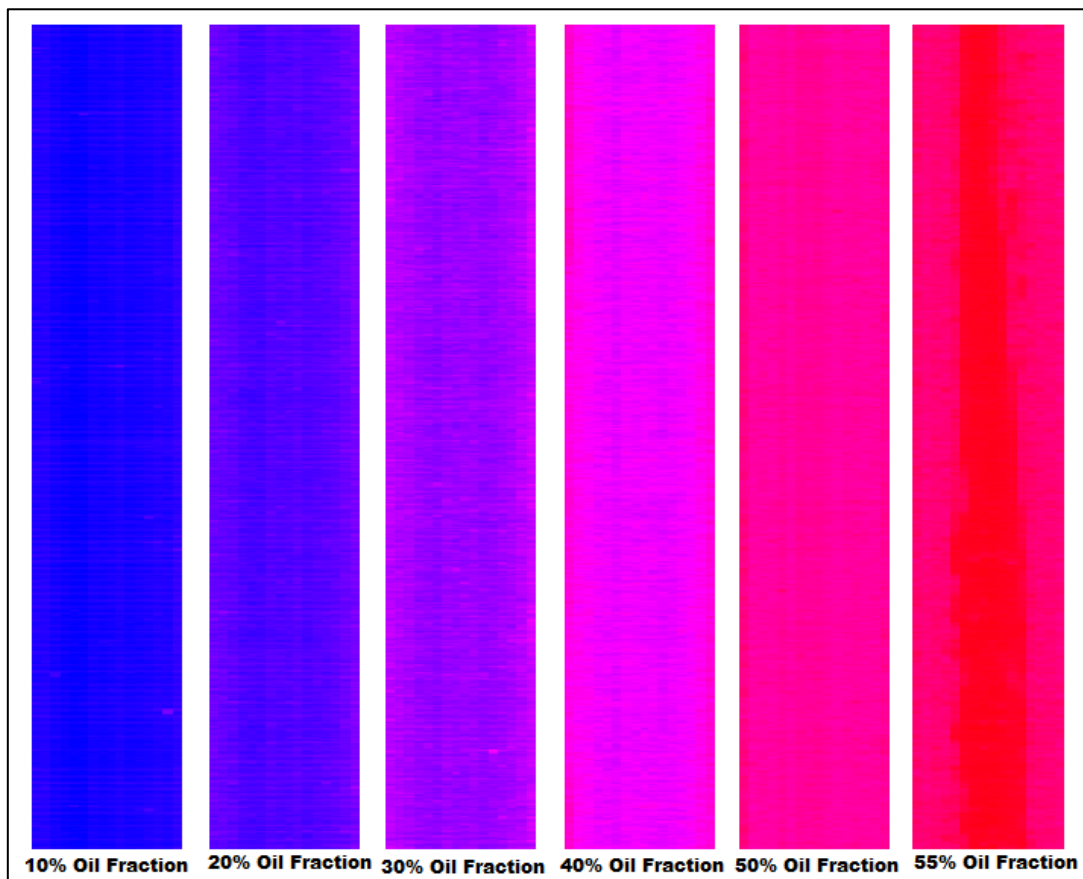
(b)

Figure 5-8: Visualization acquired with the WMS for oil-water flow at mixture superficial velocity of 1 m/s. a) Cross-sectional images, b) Slice views

5.1.2.2 Oil-Water Phase Distributions in Vertical Riser

Further details can be also provided by the WMS about the distribution of the oil and water phases inside the pipe. The chordal oil fraction distributions over the riser's cross section were made by averaging the measured average oil fractions at each crossing point belonging to the four centrelines of the sixteen wires (1 - 16), going from 180° to 0°(left to right) and in the direction from 270° to 90°.

Figures 5-9 (a and b) display the averaged chordal oil fraction for obtained data by the WMS at a constant mixture superficial velocity of 0.25 m/s at four different input oil fractions within the water continuous flow. These results show a general trend for the time-averaged chordal oil fraction profiles that are a higher amount of oil fraction flows near to the pipe wall, and present a clear decrease of oil fraction around the pipe's centre (wall-peaking oil phase fraction profiles), which is consistent with the corresponding obtained images illustrated previously in Figures 5-7 and 5-8. However, oil fraction profiles for this mixture superficial velocity are not a uniform (shown as asymmetrical) oil distribution over the pipe's cross section, as observed from the chordal phase distribution in Figure 5-9 (b). Thus, the phase distribution output data for lower mixture flows indicates that the dispersion distribution is not uniform and there is a higher amount of oil flow near to the pipe wall.

Figures 5-10(a) and (b) also show typical chordal oil fraction distributions for a higher oil-water mixture superficial velocity of 1 m/s and various input oil fractions. The chordal oil distribution result at each oil-water flow condition was also averaged in directions from 180° to 0° and from 270° to 90° over the pipe's cross-section. It can be observed that the phase distribution over the cross section tends to be more uniform with slight wall-peaks for the oil profile compared with the lower mixture superficial velocity of 0.25 m/s. It can be seen that for lower oil flow rates, the oil phase fraction profile shows a slight wall peak. With an increase of oil flow rates, the oil phase tends to distribute over the cross section of the test section, and the oil phase chordal fraction profiles display a slight wall peaking, with a relatively flat plateau around the core of the

test section. A similar observation for average oil fraction radial profile (wall-peak profiles at low oil concentrations) has also been reported by Zhao et al (2006) when they applied a double-sensor conductivity probe to study the characteristics of oil-water upflow in 40 mm ID stainless steel vertical pipe using tap water and white oil (density is 824 kg/m^3 at 20°C and viscosity is 4.1 mPa.s at 40°C) as experimental fluids.

At a higher oil flow rate (typically oil fraction = 55%, i.e. 45% input water cut), the average chordal oil concentration profile started to become core-peaking, compared with a lower oil fraction at the same mixture superficial velocity of 1 m/s. This supports what was previously observed from the obtained WMS reconstructed images (cross-sectional and slice views) at this flow condition.
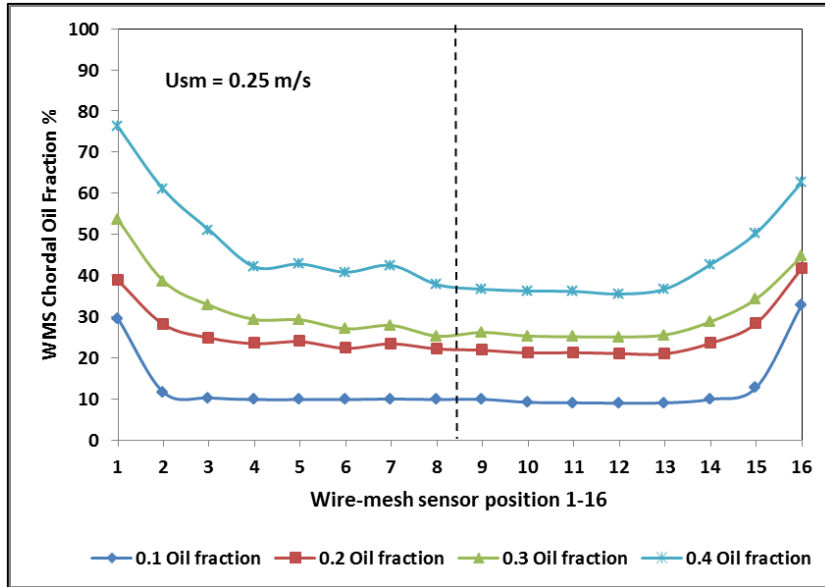
(a)
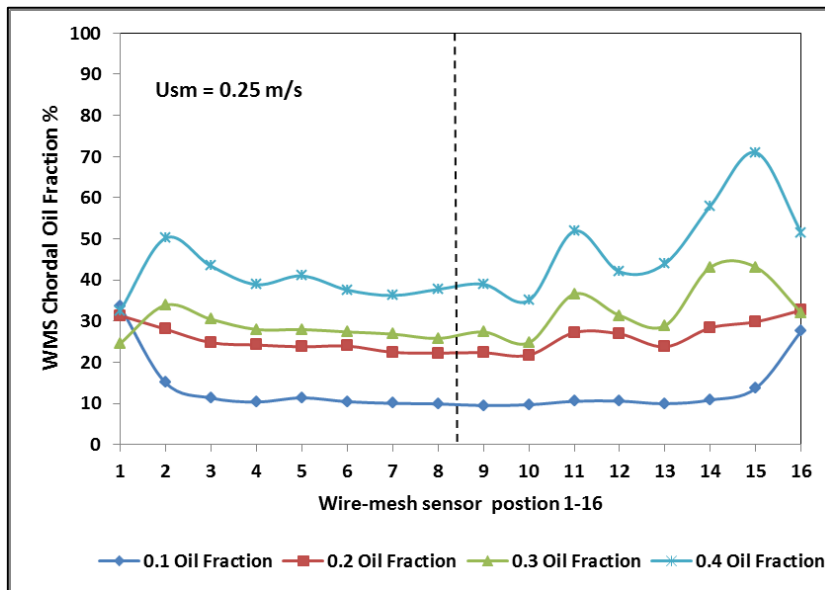
(b)

Figure 5-9: WMS Measurements at U$_{sm}$ = 0.25 m/s: Chordal Oil Fraction Distribution, a) going from left to right 180° to 0°, b) 90° to 270°.
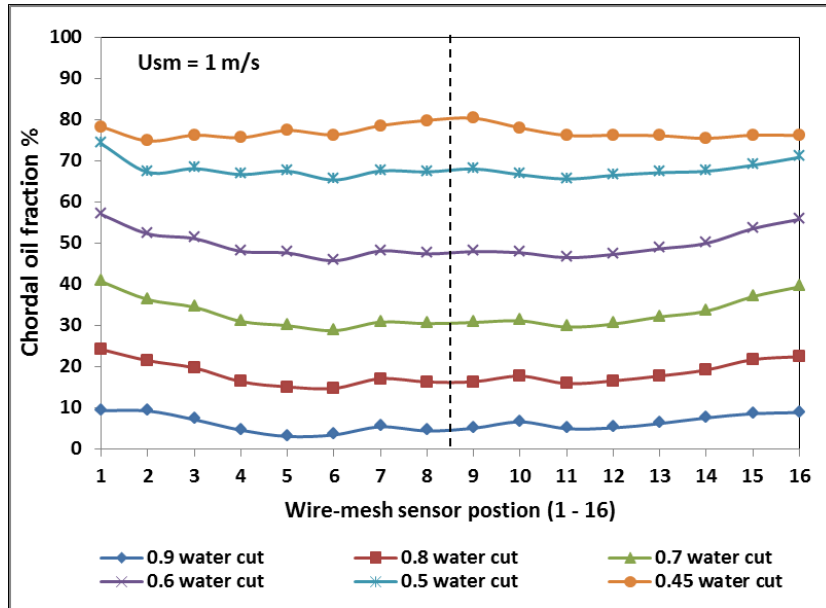
(a)
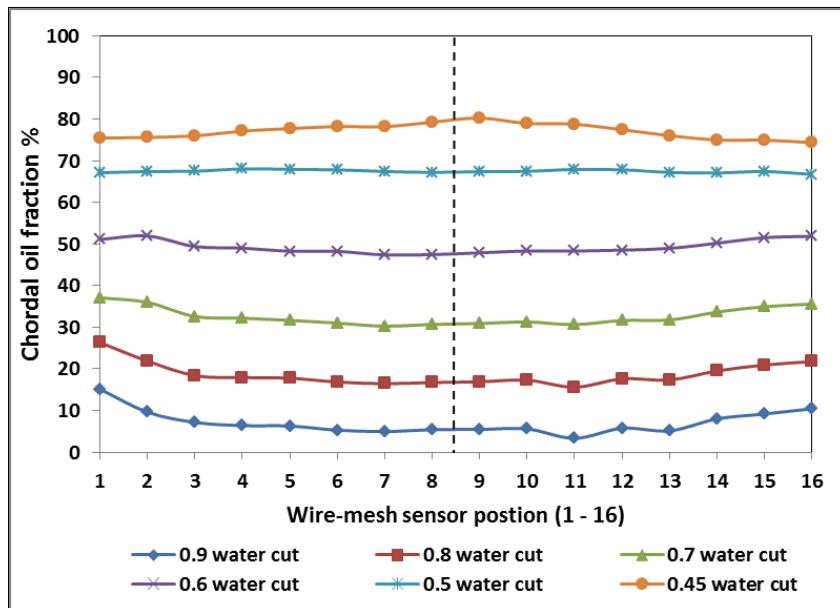
(b)

Figure 5-10: WMS Measurements at U_{sm} = 1 m/s: Chordal Oil Fraction Distribution, a) going from left to right 180° to 0°, b) 90° to 270°.

5.1.2.3 Probability density function (PDF)

The PDFs corresponding to the time series of the obtained oil volume fraction data were also generated for mixture flow conditions. In Figure 5-11 the PDF is shown for different mixture superficial velocities (U_{sm}) of 0.25, 0.5, 1 and 1.5 m/s. In general, the PDFs show a single peak shape for the measurements of all the mixture flow rates. However, the lower the superficial mixture velocity, the broader the shape of the PDF peak and vice versa. Also, it can be observed that as the mixture superficial velocity increases, the PDF peak becomes thinner and higher in amplitude. Thus, the broadening of the PDF's peak indicates the homogeneity level of the mixture in the riser. Accordingly, at the lower mixture superficial velocity of 0.25 m/s where the flow was observed to be a dispersed flow with less homogeneity, the PDF is characterised by a broader peak. At higher superficial velocities of 1 and 1.5 m/s where the flow was indicated to be more homogeneous, the PDF geometry in Figure 5-11 displays narrows peaks with high amplitude. Theses PDFs results are in good agreement with findings by Rodriguez et al. (2011) that describing oil-water horizental flow patterns. Also, the same trend was observed by Costigan and Whalley (1997) for gas/liquid dispersed flow who reported that the narrow peaks are indicated when small bubbles are somewhat uniformly distributed in the liquid continuum.
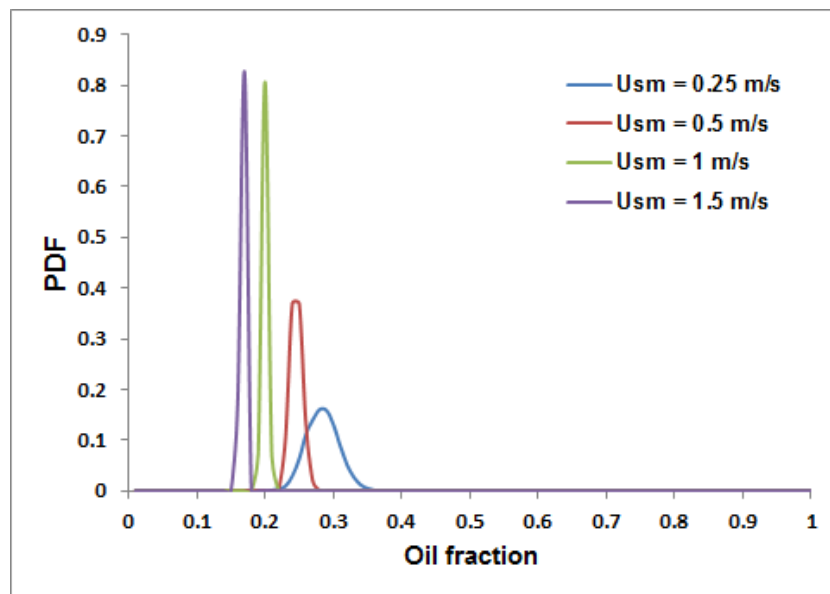
Figure 5-11: WMS results: PDF for different oil-water mixture superficial velocities

PDFs corresponding to time series for various oil fractions at the fixed mixture superficial velocity of 1 m/s are also demonstrated in Figure 5-12. All the PDFs produced (except the PDF for the input oil fraction of 55%) show an essentially similar shape of a narrow, tall single peak distribution, which indicates a homogeneous dispersion oil-in-water flow, according to Rodriguez et al. (2011). However, this is not the case at an input oil fraction of 55% where phase inversion was indicated to occur. The PDF shape is significantly different from the others. It shows a broader and shorter main peak with a small second peak at the right hand side. This unambiguous change in the PDF's character is attributed to the possible influence of the capacitance wire-mesh sensor signals by the high viscous mixture that forms at the phase inversion point. The analysis of the obtained data (PDFs for the time series averaged oil fraction distribution along with extracted images) has provided some details about the behaviour of oil-water dispersed upflow at the inversion point.

Thus, these interesting and promising initial findings for the WMS data in oil-water flows and particularly at phase inversion could lead to a better understanding of the local phase distributions during inversion after further investigation is carried out.
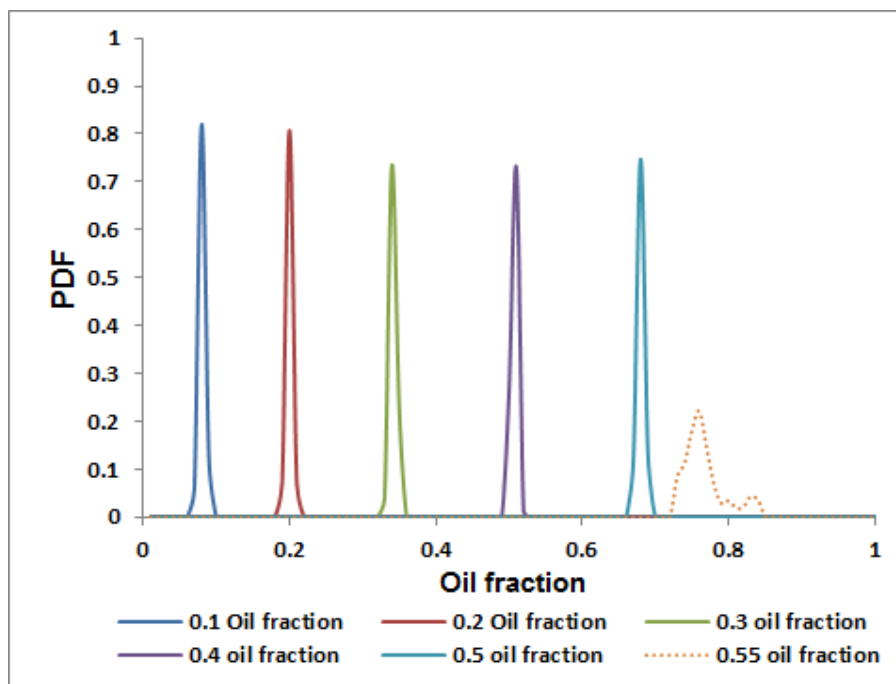
Figure 5-12: PDFs for constant mixture superficial velocity (U$_{sm}$) of 1 m/s

5.1.3 Density Measurement for Oil-Water Mixture Flow

The experimental data for oil-water mixture density were also obtained simultaneously by both horizontal, near to the riser base, Coriolis meters and the vertical top Coriolis meters. Additionally, oil-water mixture densities were calculated based on holdup measurements from gamma densitometry where both hard and soft gamma counts were used for this purpose. An example of typical results for average oil-water mixture densities measured simultaneously via Coriolis meters (horizontal and vertical meters) and the mixture density calculated from the hard and soft gamma counts as a function of input water cut (the input water cut is defined as $WC = Q_w/(Q_w + Q_o)$, where Q_w and Q_o are the volumetric flow rates of water oil and phases) for experiments of fixed mixture superficial velocities of 0.25 and 1 m/s, are presented in Figure 5-13. It can be observed that from the illustrated results the density generally increases linearly with increasing water fraction. This behaviour, because more water (higher density phase) is added into the system, makes the density of the fluid mixture greater. At each phase fraction for the higher constant mixture superficial velocity of 1 m/s, the mixture densities obtained from the Coriolis meters and the Gamma densitometer, are all very close, as displayed in Figure 5-13(a). It was found that the mixture densities obtained from Coriolis meters' measurements at each water cut value agreed well with the gamma meter results and showed very close mixture density results. But this was not exactly the case for the lower mixture superficial velocity of 0.25 m/s, illustrated in Figure 5-13(b), where average values for density results in vertical orientation are slightly higher than those obtained by the horizontal Coriolis meters, as can be seen in Figure 5-14(b). This is due to the phase slip effect (phase slip results are discussed in Section 5.1.5), which is usually more pronounced at lower flows and becomes less and less effective as the mixture superficial velocity increases.

However, the current study objectives place greater emphasis on the flows in the vertical test section than in the horizontal test section. It was also observed that there are slight deviations between the density results for the vertical Coriolis and gamma meters, which were both performed at the top part of

vertical riser section. This is probably due to the influence of the slip effects at these flow conditions, which were expected to be higher at the Coriolis meter section due to the vertical distance (about 0.5 m) between the meters (Coriolis meter located a little further up than the gamma meter).
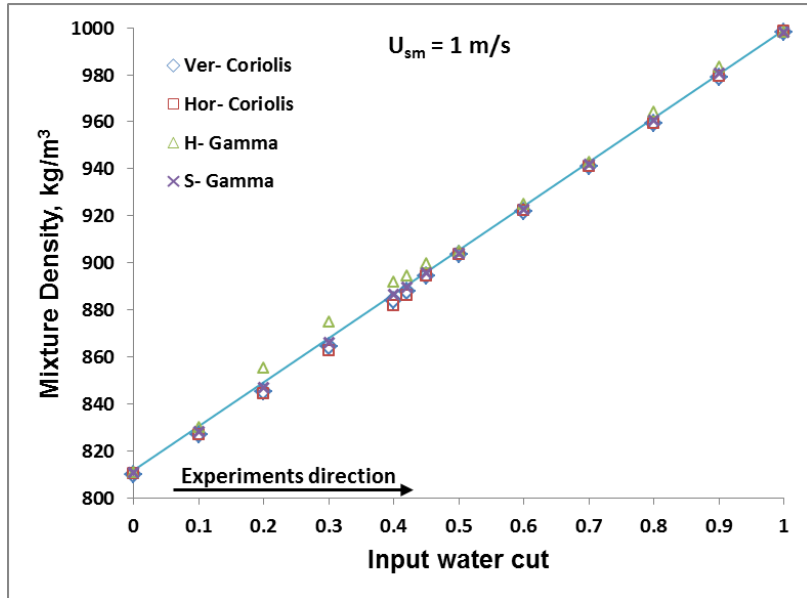
(a)
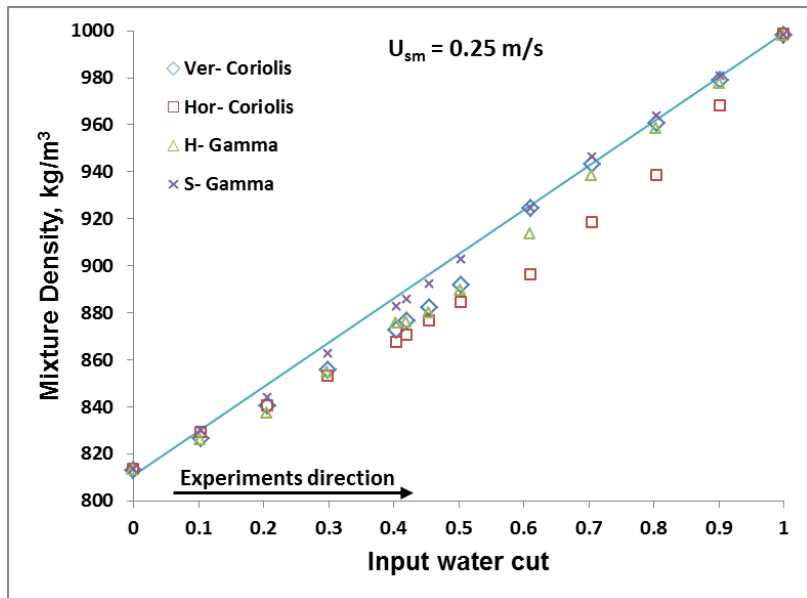
(b)

Figure 5-13: Oil-Water mixture density measurements at a) constant superficial velocity of 1 m/s, b) constant superficial velocity of 0.25 m/s

Further investigation into the results of mixture densities obtained from the Coriolis meters for a series of oil-water experiments at different fixed mixture superficial velocity values with various phase fractions starting from pure oil to pure water are also presented in Figure 5-14. The obtained density results in the figure generally show a similar trend to those in Figure 5-13, whereby the oil-water mixture density averaged values increase with an increasing input water cut for each constant mixture superficial velocity. As previously mentioned, this behaviour is due to the fact that as more water (higher density phase) is added into the system; it makes the density of the fluid mixture higher. It can be also observed that at input water cuts below around 0.5, the oil-water mixture densities obtained by the vertical Coriolis meter increase as the mixture superficial velocities increase (mixture velocity dependency). This trend for the mixture densities at a particular water cut can be observed only for the oil continuous flow region; it is not the case when the flow is water continuous. The measured mixture densities for all mixture superficial velocities at the same input water cut show almost the same density average values. This is because the increase in the mixture velocity usually leads to the mixture becoming more homogeneous which results in a decreased slip effect. Also, the consistency in density results obtained by the vertical Coriolis meter at higher water cuts is due to the fact that flow homogeneity increases with increasing liquid flow rate and water cut. Likewise, the performance of the Coriolis meter could have an influence on the obtained trend of density results, as it has been reported that their performance increases with higher mass flow and increased line pressure (Arubi, 2011). On the other hand, the behaviour of the mixture density in the horizontal Coriolis meter was slightly different from that in the vertical pipe, particularly at the lower flow rate of 0.25 m/s. It was found that at lower input mixture flow rate, the horizontal Coriolis density is slightly lower than that of the vertical Coriolis. This dissimilarity is also attributable to the effect of slip and to the different local flow patterns occurring in horizontal and vertical pipe sections at these flow conditions. However, as required by the project objectives greater emphases are placed on the flows in the vertical test section than in the horizontal test section.

When the oil-water experiments were carried out in the direction from continuous water flow to oil continuous flow, the average results of the density measurements showed exactly the same trend. These results are shown in Figure 5-15.
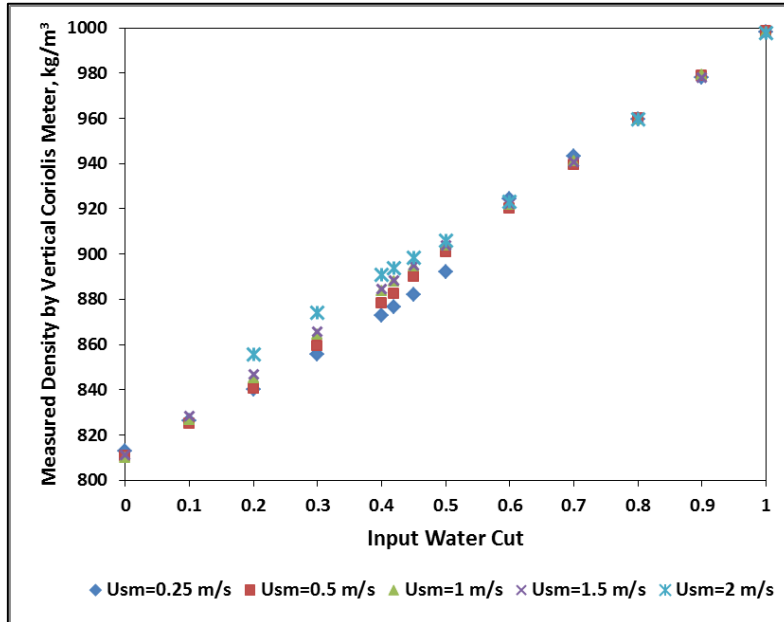
(a)
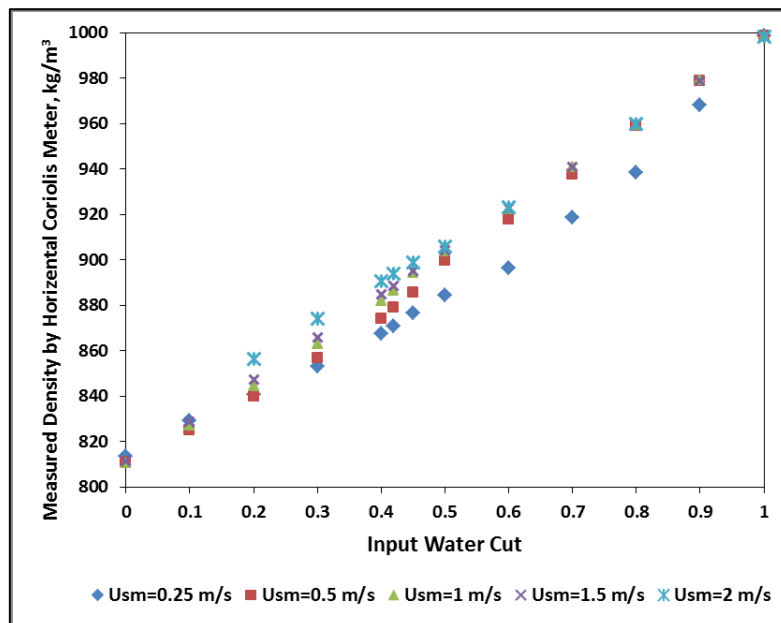
(b)

Figure 5-14: Oil-Water Mixture Density Measured by a) Vertical Coriolis Meter, b) Horizontal Coriolis Meter: The experiments were conducted from Oil to Water
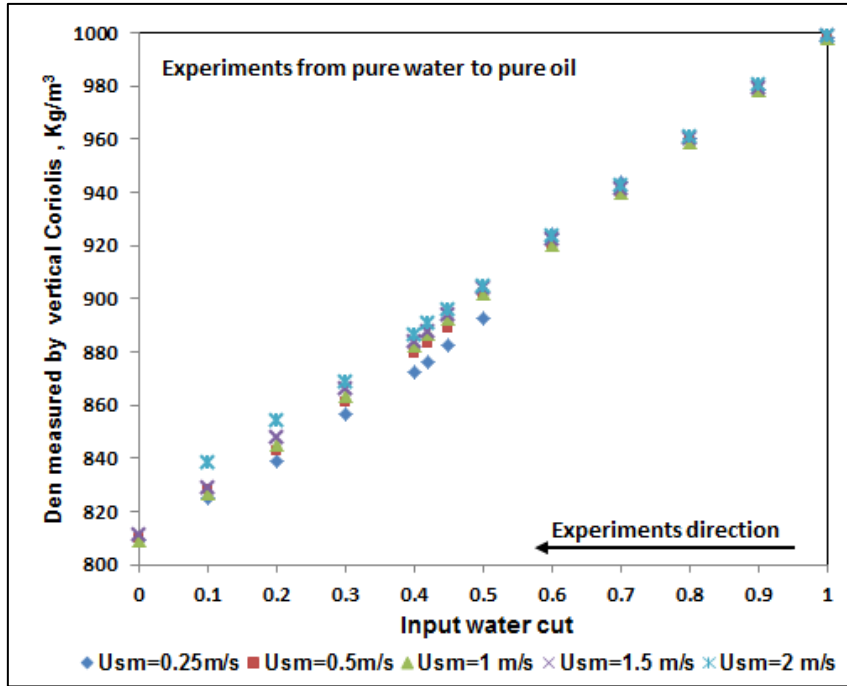
(a)
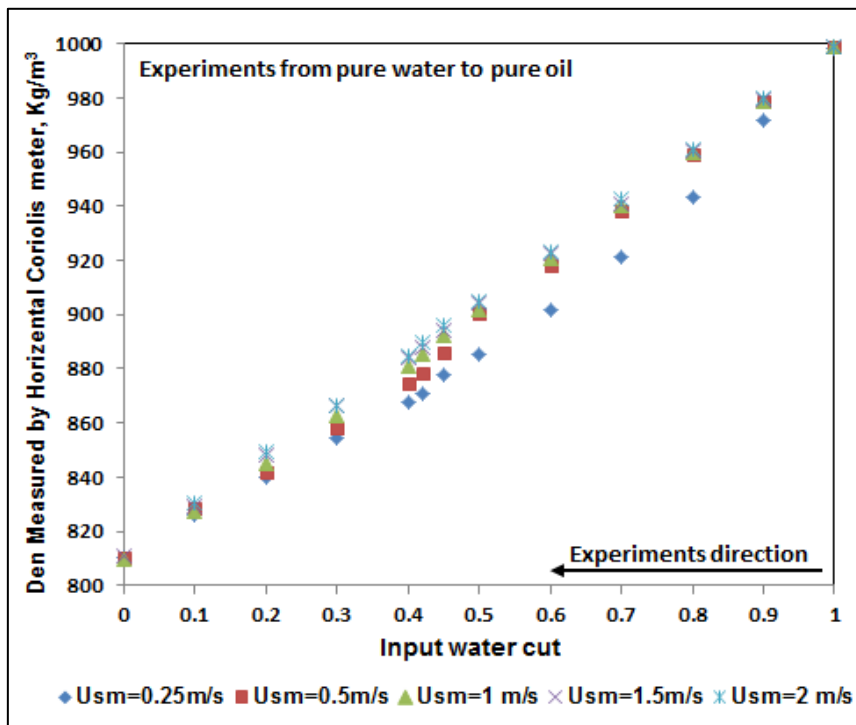
(b)

Figure 5-15: Oil-Water Mixture Density Measured by a) Vertical Coriolis Meter, b) Horizontal Coriolis Meter: The experiments were conducted from water to oil

5.1.4 In-situ oil/water Phase Fraction

The average in-situ water and oil fractions were firstly determined from vertical Coriolis density measurements for each oil-water experiment test point using Equation (3-2). It is interesting to compare these measured in-situ values with the input liquid cuts, as shown in Figure 5-16, whereby the in-situ water fraction is plotted against input water cuts for five different set of mixture velocities (i.e. 0.25, 0.5, 1, 1.5 and 2 m/s). At low mixture superficial velocity the in-situ water fractions are less than the input water cuts values particularly when input water cut values are at 50% and below. It can be also observed that at lower water cuts, the in-situ water fraction is strongly affected by the mixture velocity. The in-situ water fractions values increase and approach the input values as the mixture flow increases within the oil continuous region. This is attributed to the fact that as the mixture velocity increases; the liquid-liquid mixture becomes more homogeneous and has less slip effect. Also, the difference in local flow patterns and phases distributions at each of these flow conditions could result in increasing the in-situ water fraction with increasing mixture velocity. When the flow is water continuous the in-situ water and input water cuts' average values are almost the same. This is due to the fact that mixture flow homogeneity also increases with increasing water fraction.
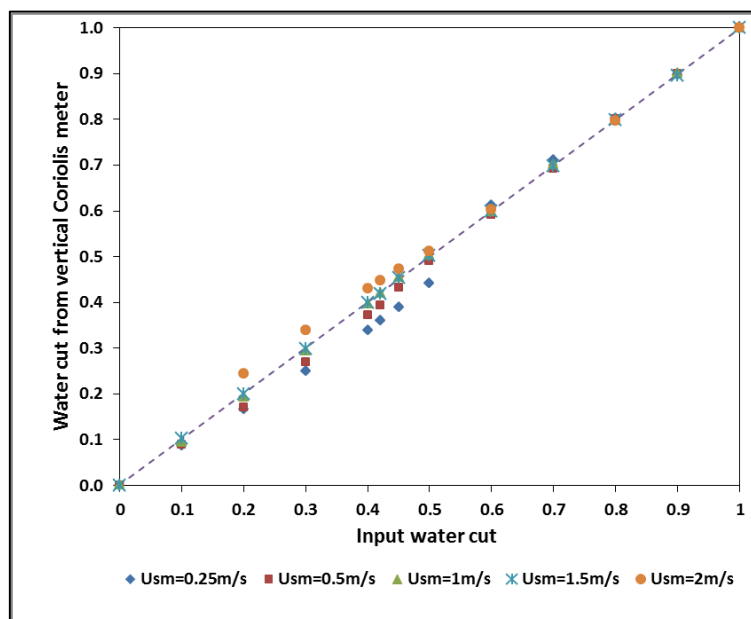
Figure 5-16: Water Cuts Obtained by Vertical Coriolis against Input Water Cuts

Also, from the extracted data by the capacitance wire-mesh sensor, the fraction of each phase in a pipe cross section can be estimated. In the oil-water experiments for this study the wire-mesh sensor measurements were conducted at the top part of the riser when the mixture flow was water continuous flow. Thus, Figure 5.17 shows the averaged oil fractions measured simultaneously by the capacitance wire-mesh sensor, Coriolis mass flow meter and gamma densitometer (determined by using average gamma counts in Equation 2-19) against the input oil fraction across a range of input phase fractions at a mixture flow velocity of 0.25 (Figure 5-17(a)) and 1 m/s (Figure 5.17-b). The solid line indicates the ideal concordance. The dashed lines represent a deviation of 25% and 27% for constant superficial velocity of 0.25 m/s and 1 m/s, respectively. The disparity in deviations is possibly due to lesser range of obtained data for the superficial velocity of 0.25 m/s than that corresponding to the mixture velocity of 1 m/s. Also, it may be as a result of a possible influence of the different flow pattern in WMS performance. The cross-sectional average oil fractions measured by capacitance WMS in most cases were higher than those measured by the Coriolis mass flow meter and gamma densitometer. Consequently, poor agreement is found between the capacitance WMS oil fraction measurement and Coriolis mass flow meter and Gamma densitometer measurements.

(a)   (b)
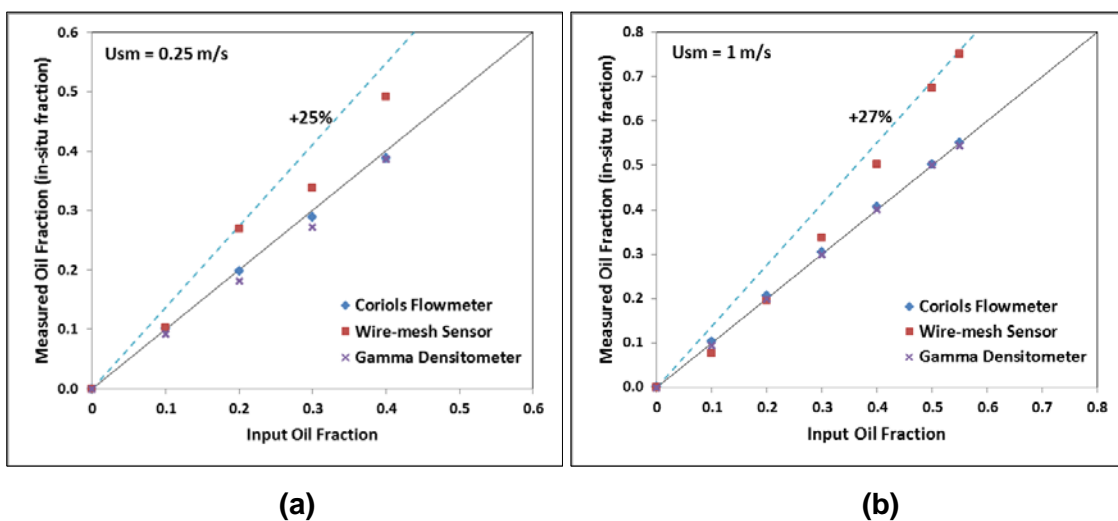
Figure 5-17: Measured oil holdup against input oil fraction across a range of input phase fractions at a) U_{sm} = 0.25 m/s, b) U_{sm} = 1m/s

5.1.5 Phase Slip between Oil and Water in 52 mm Vertical Riser

The relative movement (slip) between oil and water in a 52 mm flow loop and its effect based on the difference between the average in situ velocities of oil and water will be investigated in this Section. From the experimental results for the phase fraction (in-situ phase fraction/liquid holdup) obtained from the Coriolis meters, the slip ratio was calculated by using Equation (2-14). Accordingly, the slip ratio value is greater than 1 when oil is travelling faster than water and is less than 1 when water is travelling faster than the oil. A slip value of unity depicts a no-slip flow, i.e. oil and water move at the same velocity. The farther the slip's value is from 1, the greater the slip effect.

In order to investigate how slip ratio changes at the vertical Coriolis over the whole range of the input water and oil cuts within several fixed mixture superficial velocities for oil-water experiments tested in the current work, firstly the slip ratio bias, i.e. slip ratio – average (slip ratio) was plotted against the input water cut, as exhibited in Figure 5-18. It can be observed that the phase slip was largely predominant at the lower mixture liquid flow rates.

Interestingly, at the lower mixture velocities of 0.25 and 0.5 m/s, the dispersed phase travels faster than the continuous phase, i.e. when the mixture flow is oil continuous, water tends to slip over the oil while at low oil fractions (water continuous), oil tends to slip over the water. This is because the lesser the area the oil or water contains the higher its velocity and the faster it moves. Also, this could be due to the effect of geometry of the riser system as there is a long length horizontal line which could induced phase separation which needs time to readjust after entering the vertical pipe. As the mixture's superficial velocity increases, both fluids tend to homogenize, therefore move approximately at the same velocity and thus the slip ratio values are close to unity. Moreover, it can be observed from the figure that, particularly at lower mixture flows, the difference between continuous and dispersed phase velocities gradually decreases (i.e. slip becomes close to unity) as the flow approaches the phase inversion. This is consistent with the findings of Hu, (2006) in an upward oil-water two-phase flow in a 38 mm ID stainless steel vertical pipe.

130

Figure 5-19 shows the slip ratio at the vertical Coriolis mass flow meter for different mixture velocities as a function of a mixture of Reynolds numbers ($Re = \rho_m U_m D / \mu_m$). It can be also shown that the slip phenomenon is more predominant at lower mixture Reynolds numbers (lower mixture liquid flow rates). As the mixture velocity and Reynolds number increase, the slip ratio values decrease and move close to unity (slip ratio value = 1). This can be explained by the fact that the increase in Reynolds number, as a result of increasing mixture velocities, leads to mixtures becoming more homogeneous and hence a mixture of fluids moves almost at the same velocity (i.e. slip ratio close to 1).
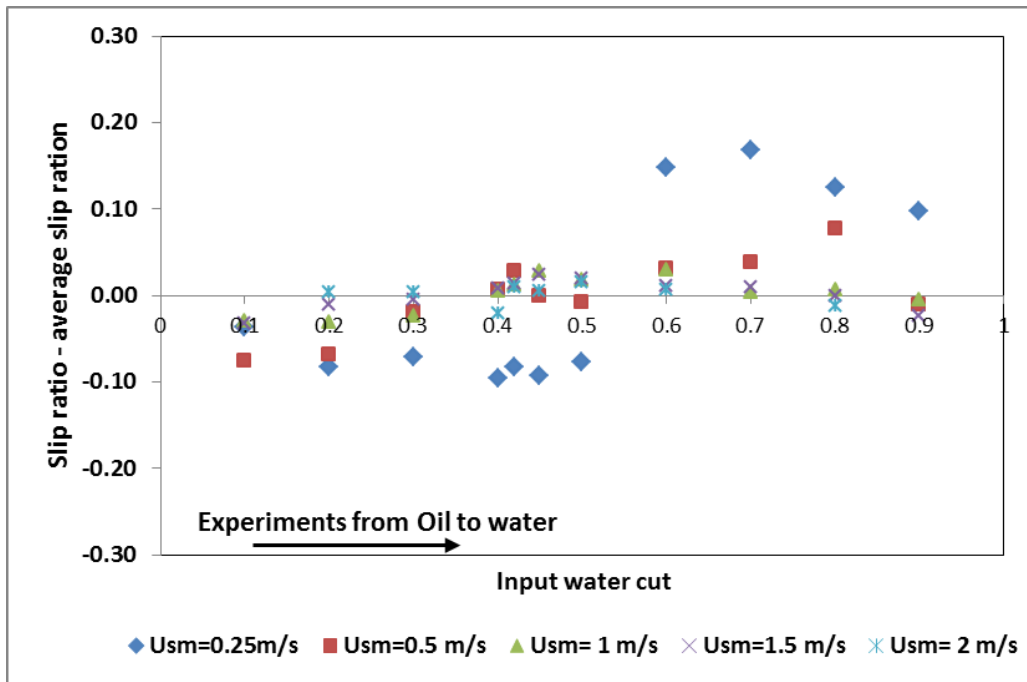
Figure 5-18: Slip ratio for different oil-water mixture superficial velocities
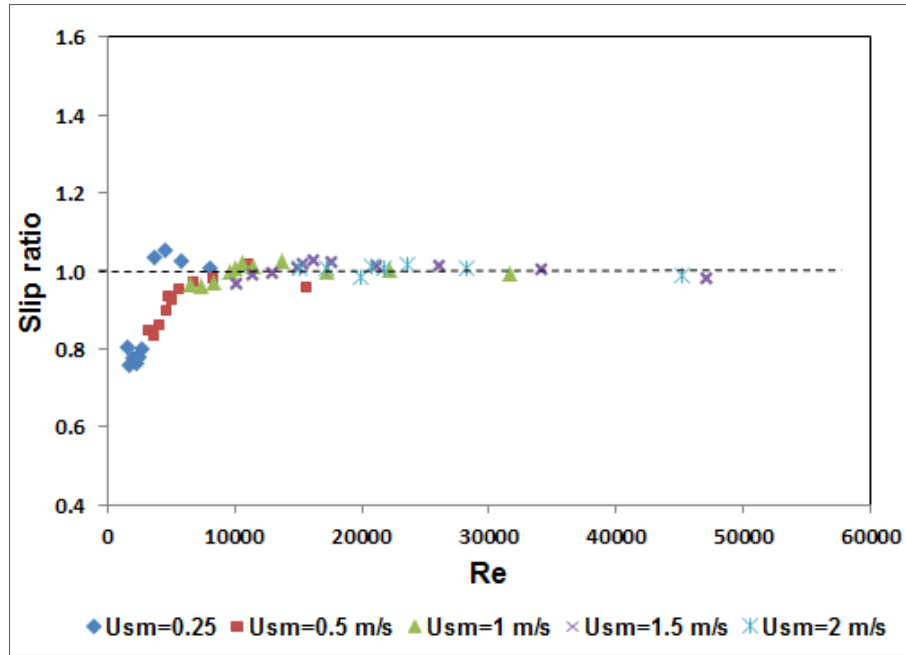
Figure 5-19: Slip ratio against Reynolds number for different mixture velocities

5.1.6 Total Pressure Gradient for Oil-Water Flow in Vertical Riser

In this study, analysis of measured oil-water pressure data along the 52 mm ID vertical riser was carried out to identify the phase inversion point (whereby the dispersed phase becomes the continuous phase and vice versa) and to understand its effect in multiphase flow in the riser pipe. Based on the literature, the phase inversion is often accompanied by a peak in pressure drop (Angeli and Hewitt, 1998; Arirachakaran et al., 1989; Descamps et al., 2006; Ioannou et al., 2005). At the phase inversion, oil and water form a particularly viscous mixture leading to a high fraction with the pipe wall and thus to a high pressure gradient (Brauner, 1998). Thus, in this experimental study, the peak in pressure gradient can be used as an indication of the phase inversion point. For this purpose, the pressure data for oil-water flow (in both directions of the experiments, i.e. from pure oil to pure water and vice versa) measured by pressure transducers at different axial distances were used. These pressure data were recorded over three minutes for each test point at specific water and oil fractions after a period of stabilization. Figures 5-20 and 5-21 depict the average obtained results for total pressure drop along the vertical riser sections

132

(bottom 2.76 m, middle 1.38 m and top 3.26 m sections) which are plotted as a function of input water fraction for exemplary experiment sets corresponding to constant oil-water mixture superficial velocity of 0.25 and 1 m/s, starting from the oil continuous phase. The total pressure drop across the riser sections shows increasing magnitude with increasing water cut and decreasing pressure drop with decreasing water cut. It can be observed that the total pressure drop in general demonstrates density dominated behaviour, with a linear increase from low to higher water cut pressure and vice versa. This is because the gravitational pressure drop is directly proportional to the mixture fluid's density, which increases with increasing water cut and vice versa. It can be observed from the plot of higher mixture superficial velocities of 1 m/s (Figure 5-21) across all riser sections, that there is a relatively sharp increase (peak) in the total pressure drop around the point of the 0.42 input water cut, indicating the occurrence of phase inversion at that point of the water cut. Also it was found that phase inversion happens simultaneously across the whole test section, as was observed over all the riser sections (bottom 2.76 m, middle 1.38 m and top 3.26 m). The peak points were not conspicuous at the lower mixture velocity of 0.25 m/s. This is as a result of the frictional pressure contribution at the phase inversion not being high enough to produce the peak.
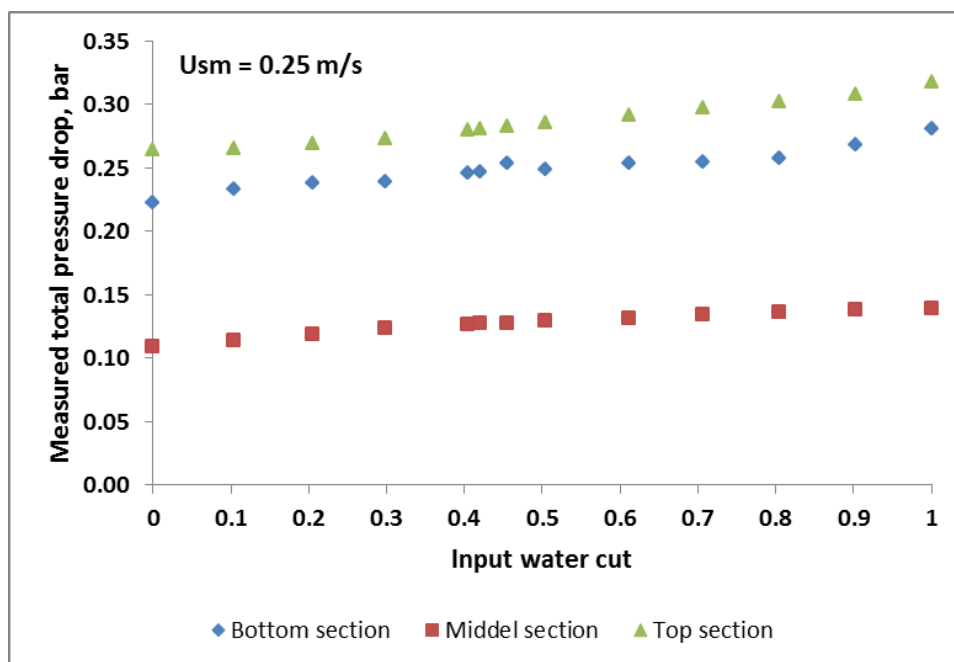
Figure 5-20: Total pressure drop along the 52 mm riser against input water cut
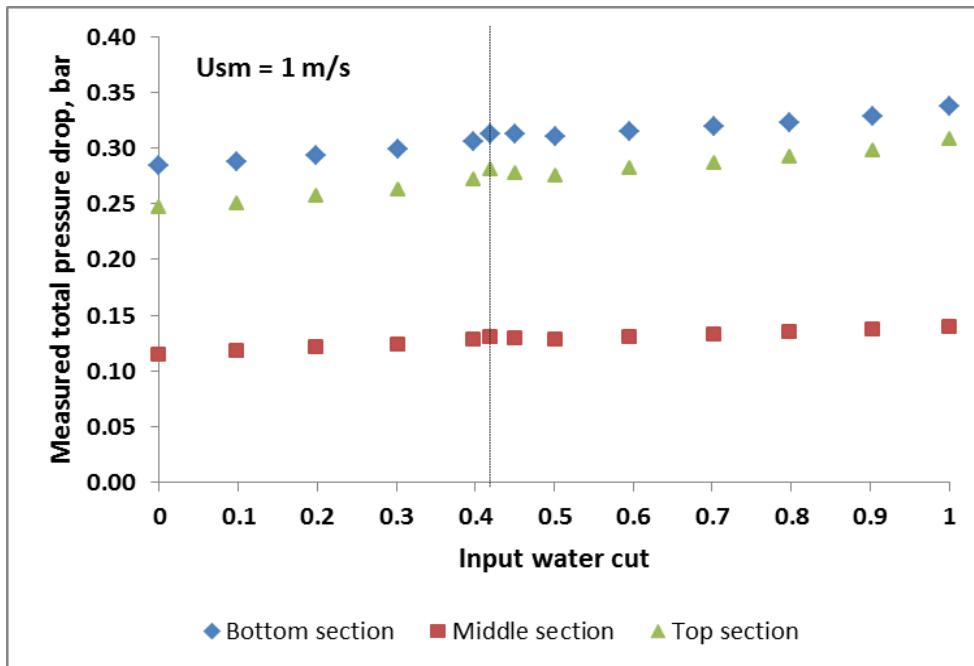
Figure 5-21: Total pressure drop along the vertical riser against input water cut: the vertical dotted line indicates the phase inversion point

In order to confirm the phase inversion point, pressure results for all oil-water experiments that were performed at several mixture superficial velocities were interpreted. Thus, the total pressure gradient was estimated for each flow condition by total pressure drop across the bottom, middle and top sections along the vertical riser. Figure 5-22 presents the average total pressure gradient measured over the middle part (an axial distance of 1.38 m between two pressure transducers) of the vertical riser for various mixture superficial velocities of 0.25, 0.5, 1, 1.5 and 2 m/s, starting from the oil continuous phase (as indicated by the direction of the arrow) as a function of the input WC. Each data point at a specific phase fraction is an average of the pressure gradient for the measurement of each test point. For the lower mixture superficial velocities of 0.25 and 0.5 m/s, the total pressure gradient demonstrates a typical linear trend of an increase from low to higher WC pressure. This pressure gradient behaviour is due to the fact that the gravitational pressure gradient is directly proportional to the mixture fluid density, as can be detected from the definition of Equation 2-1. Therefore, as the WC among the mixture flow increases, the

134

mixture density increases and the gravitational pressure gradient will increase accordingly; this leads to a gradual increase of the total pressure gradient. The total pressure gradient for the lowest mixture superficial velocity (U_{sm}) of 0.25 m/s was at some points higher than that of U_{sm} = 0.5 m/s. This can be attributed to the phase slip, which is more significant at the lower mixture velocity. For the higher mixture flow rates of 1, 1.5 and 2 m/s, the total pressure gradient data show a peak around a point of input WC of 0.42. It is also observed from the plot that the pressure gradient peak during phase inversion is more strongly enhanced at high mixture velocities than at low mixture velocities. The pressure gradient peak during phase inversion is attributable to the increase in effective viscosity of the mixture around the phase inversion, which subsequently leads to an increase in the frictional pressure gradient contribution. The effective viscosity of the mixture was also reported to increase with the increasing mixture velocity, particularly during phase inversion in the pipe (Descamps et al. 2006). The phase inversion point always takes place at a point of WC of 42%. Previous works have indicated that the phase inversion point is independent of mixture velocity (Arirachakaran et al., 1989; Descamps et al. 2006; Ioannou et al., 2005) which would agree with the current findings for the tested higher mixture velocities.
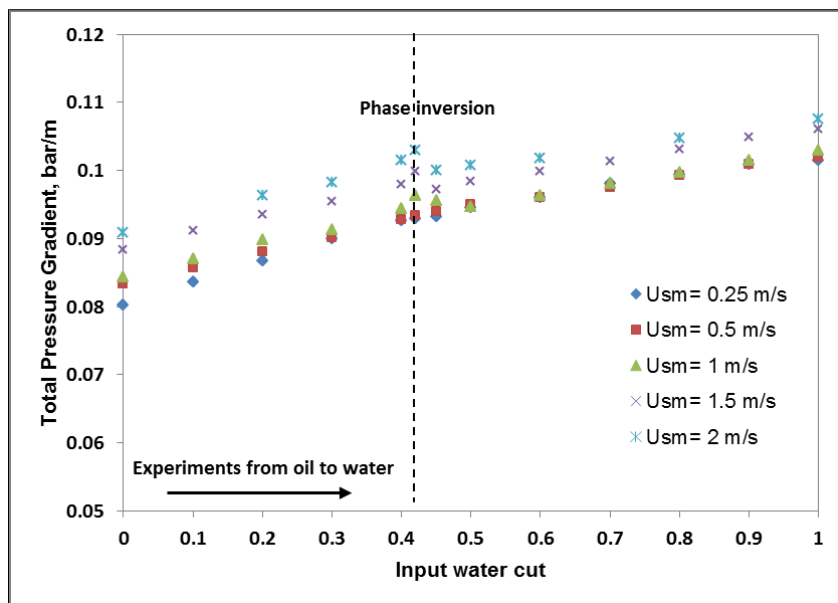
Figure 5-22: Total Pressure Gradient as a Function of Input Water Cut for Oil-Water Flow for Various Mixture Velocities

135

During the indicated phase inversion, the determined total pressure gradient over the riser shows considerable fluctuations. This can be seen from Figure 5-23, in which the pressure gradient across the middle part of the riser is shown as a function of time, as an example of the mixture superficial velocity of 1 m/s when experiments are conducted in the direction from the oil continuous phase to water continuous. As the input WC increases in steps from 0.2 to 0.3 and 0.4, the pressure gradient tends to increase because of the rise in mixture density due to increased WC and, accordingly, the gravitational pressure will increase, which leads to a gradual increase in total pressure gradient and obviously the flow moves gradually toward water-dominated flow. However, the pressure gradient near to phase inversion at the 0.40 input WC shows a slightly higher fluctuation compared to the lower water cuts of 0.2 and 0.3, as can be seen from the presented data. At the input WC of 0.42, where phase inversion takes place, the total pressure gradient reaches its highest with strong fluctuation with an immediate decrease in the pressure gradient after 0.42 of WC, before rising gradually again due to completion of the inversion process. As the input WC increases after the inversion point, the oil-dominated flow totally converts to water-dominated flow and the pressure gradient steadily increases. Additionally, it can be observed from Figure 5-24 that the pressure gradient data around the phase inversion point show a range of input phase fractions (0.4 - 0.45) where the pressure gradient is fluctuating noticeably.
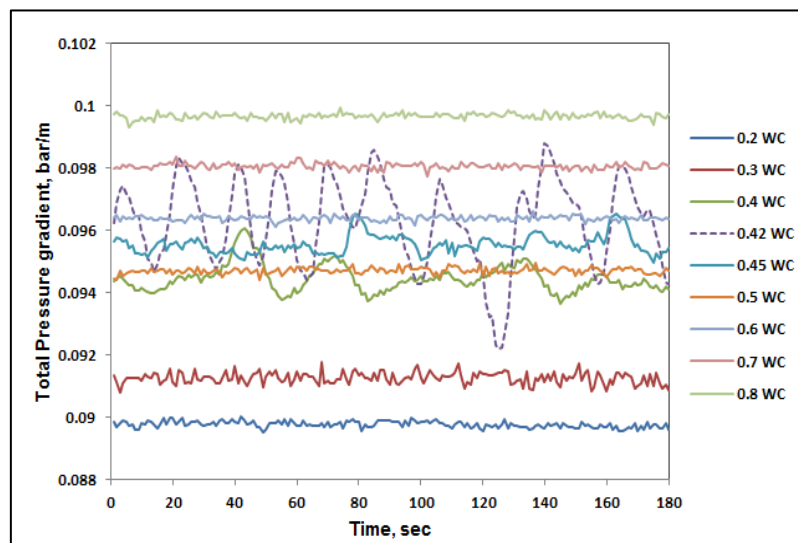
Figure 5-23: Pressure gradient as a function of time for mixture velocity of 1 m/s.

It is of interest to investigate whether the experiment route (i.e. starting from the oil phase as being continuous, to water continuous and vice versa) can influence the occurrence of the phase inversion point. As an example, the total pressure gradient results for a mixture superficial velocity of 1 m/s in the two experiment directions are shown in Figure 5-24. It can be seen that there is a slight difference in the phase inversion point between the two experiments' routes. When the experiments were carried out from a pure oil to pure water direction (indicated by the unfilled symbols), the average total pressure gradient data is peaked at 0.42 input WC, which indicates the phase inversion point at that water fraction value. On the other hand, for the opposite experiments corresponding to the same mixture velocity of 1 m/s starting from water to oil continuous (indicated with full symbols in the Figure), the phase inversion point took place at an input WC of 0.45 (i.e. a step forward of 3% in the phase fraction was observed between the two experimental routes). This difference in phase inversion occurrence could be due to temperature variation during the two sets of the experiments. Figure 5-25 shows how temperatures at the riser base and riser top changed during the two routes (starting from oil to water then from water to oil) for corresponding experiments of constant mixture superficial velocity 1 m/s. The slight increase in temperature inside the riser system during the experiments is attributed to the length of time the system had been continuously operating, which may have led to a gradual increase in the temperature of fluids inside the three-phase system. Correspondingly, the increase in the system temperature causes a reduction in fluids viscosities (in particular oil viscosity) and viscosity ratio. The explanation for the temperature effect on phase inversion was investigated by Wang and Gong (2009) for oil-water in a horizontal pipe and they found that the inversion point tends to be delayed with the increase in experimental temperature.
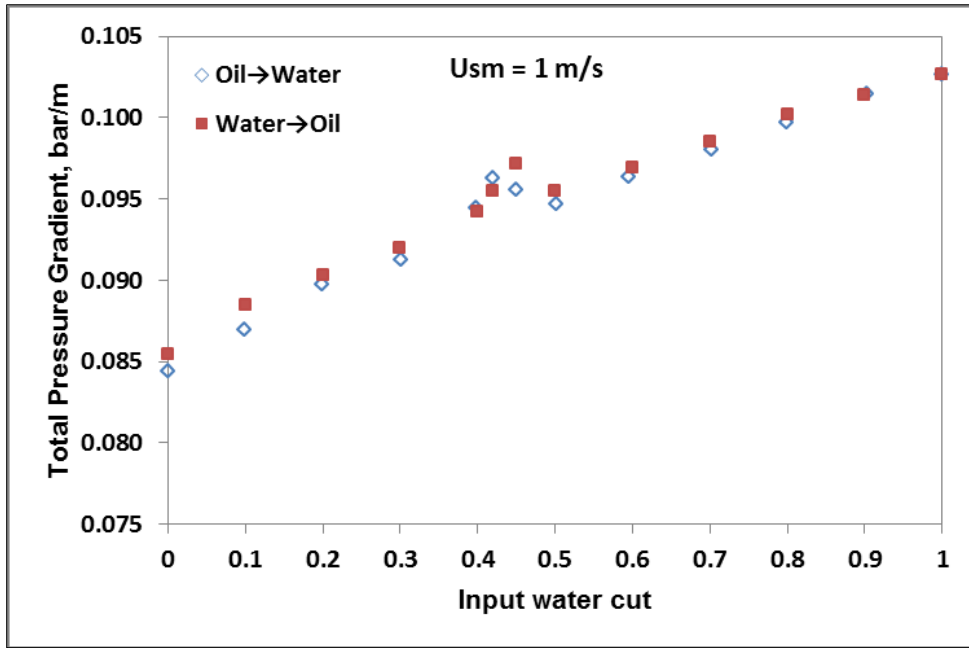
Figure 5-24: Oil-Water Experiments Start from Oil to Water (O→W) and from Water to Oil (W→O)
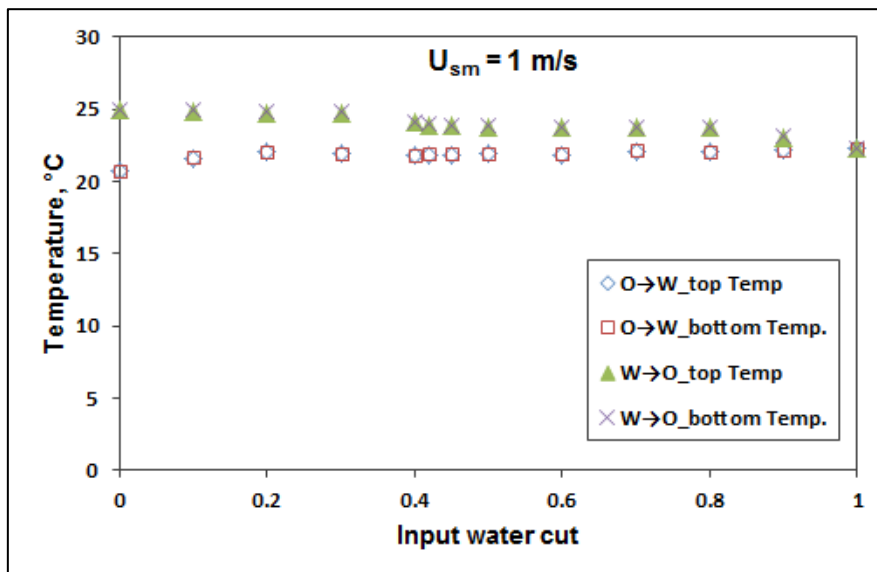
Figure 5-25: Temperature variations during oil-water experiments starting from oil to water (O→W) and from water to oil (W→O) at constant mixture velocity of 1 m/s

5.1.7 Frictional Pressure Gradient for Oil-Water in Vertical Riser

The frictional pressure gradient can be determined by subtracting the gravitational pressure gradient across the vertical riser from the measured total pressure gradient. The obtained results of the frictional pressure gradient as a function of the input water cut for all tested mixture superficial velocities of 0.25, 0.5, 1, 1.5 and 2 m/s are displayed in Figure 5-26. It can be observed from the figure that, for this study, the frictional pressure gradient for lower mixture superficial velocities of 0.25 and 0.5 m/s does not play a significant role in the total pressure gradient around phase inversion. However, it still shows small peaks around a phase inversion of 42% input water cut. The frictional pressure gradient for mixture superficial velocities of 1, 1.5 and 2 m/s, slightly increases with the increasing water cut until it reaches a point where an abrupt increase in frictional pressure gradient is observed. This increase in frictional pressure gradient corresponds to a water cut of about 42%. The frictional pressure gradient starts to decrease immediately after it hits maximum, with increased water cut and the flow becomes water-dominated to the single-phase water value. The presented data exhibit a distinct behaviour for the frictional pressure gradient associated with the phase inversion point (42% water cut in this work). It also confirms that the frictional pressure drop at phase inversion is higher than that at the oil continuous and water continuous phases. The possible reason is that at the phase inversion as one phase changes from dispersed to continuous and vice versa, the interfacial energy between the oil and water is reduced. This leads to an increase in equivalent mixture viscosity which in turn increases the frictional pressure gradient. Therefore, the behaviour of the frictional pressure drop around the phase inversion point observed in this work agrees with the results presented by Descamps et al. (2006).
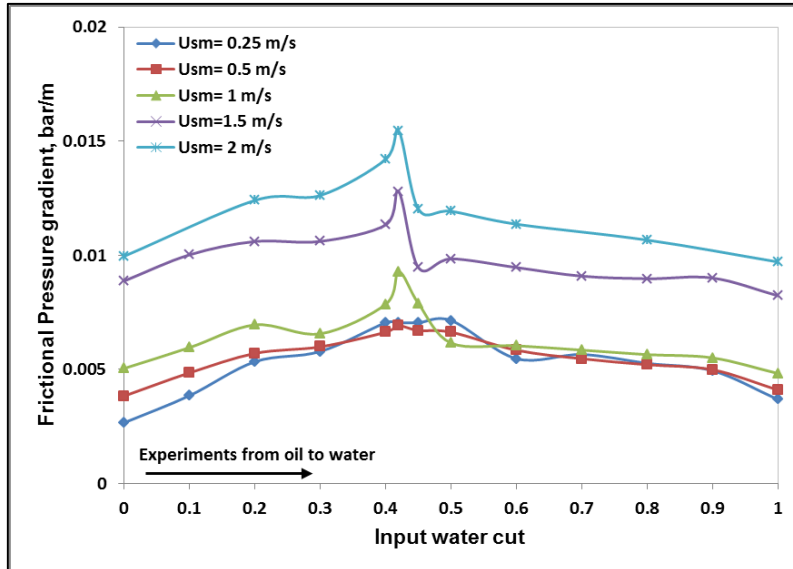
Figure 5-26: Frictional pressure gradient as a function of input water cut at different mixture superficial velocities

5.1.8 Inversion Point Prediction

The phase inversion point indicated in this work was compared with some correlations from the available literatures, as shown in Table 5. 1, Where μ_w and μ_o are the water and oil dynamic viscosities. ρ and μ are, respectively, the density ratio between oil and water and the kinematic viscosity ratio between oil and water. A look at the table shows that all five researches have different predicted values whilst implementing different inversion models. Arirachakaran et al (1989) have the highest predicted value of 58% followed by Chen (2001). Decarre & Fabre (1997), Brauner & Ullman (2002) and Yeh et al. (1964) follow respectively. It can be seen that although some values of the phase inversion point (ε_w) are close (Decarre & Fabre and Chen; Chen and Arirachakaran et al.), but the value predicted by Brauner and Ullmann's (2002) model (43%) is the closest to the inversion points obtained by our experiments in this work. This could be because their model is based on minimizing the liquid-liquid system's total energy.

Table 5-1 Prediction of the Phase Inversion Point

Authors	Inversion point model	Predicted value
Arirachakaran et al. (1989)	$\varepsilon_w = 0.5 - 0.1108 \log\left(\frac{\mu_o}{\mu_w}\right)$	0.58
Yeh et al. (1964)	$\varepsilon_w = 1 / \left(1 + \left(\frac{\mu_o}{\mu_w}\right)^{0.5}\right)$	0.36
Brauner & Ullmann. (2002)	$\varepsilon_w = 1 - \rho.\mu^{0.4}/(1 + \rho.\mu^{0.4})$	0.43
Decarre & Fabre. (1997)	$\varepsilon_w = 1/(1 + \mu^{(1/6)}.\rho^{(5/6)})$	0.50
Chen (2001)	$\varepsilon_w = 0.3788 - 0.1108 \log\left(\frac{\mu_o}{\mu_w}\right)$ $-9.6533\left(\frac{\rho_w - \rho_o}{\rho_w}\right) + 2.4841\left(\frac{\rho_w - \rho_o}{\rho_w}\right)$	0.54

5.2 Oil-Water Flow with Riser Base Air Injection

Three-phase flows are more complex to handle than single and two-phase flows in pipes. Thus, the knowledge and identification of multiphase flow behaviour is of paramount importance and determines the effectiveness of the process and/or system in which multiphase flows are encountered (Descamps et al., 2006). In this Section, the characteristics and experimental results of air-oil-water flow in the 52 mm internal diameter vertical riser under various flow rates of continuous air injection at the riser base will be discussed. These experiments were carried out by keeping the oil-water total mixture superficial velocity constant and changing the input WC in steps within a range from 0 - 1 with varying gas injections from 0 - 100 sm^3/h (0, 1.5, 3, 6, 10, 15, 20, 25, 30, 40, 50 and 100 sm^3/h). The output results for the influence of this wide-ranging set of injected air flow rates should add a contribution to our understanding of the influence of gas injection on phase inversion under different three-phase flow regimes (i.e. from bubbly to an annular flow regime). Also, an attempt to use capacitance wire-mesh sensor (CAP 200) to investigate the three-phase upflow will be reported here and preliminary results discussed. Thus, the experimental results and discussion for air-oil-water results will be presented in this Section.

5.2.1 Air-Oil-Water Flow Characterisation

For each flow condition of oil-water with air injection studied in these experiments, the flow pattern in the riser was identified. This was performed by using a combination of i) visual observation (recorded videos to support the other identification methods), and ii) the probability density function (PDF) signatures obtained from the gamma densitometer data. Additionally, an attempt to use data obtained simultaneously from the capacitance wire-mesh sensor at the top part of the riser, has been carried out in order to obtain useful information about the air-oil-water flow characteristics in the riser. Some qualitative results and visualization provided by the wire-mesh sensor data (integrating data that can produce slice view and cross-sectional movies to see the flow as it would be seen if the pipe were transparent) will be presented later in Section (5.2.4). Based on the literature, the use of PDFs analysis can give more understanding of the determination of encountered flow patterns when air is presented in multiphase flow (Blaney and Yeung, 2007) and was, therefore, considered desirable to be used to verify the air-oil-water flow in the same way as for air-water two-phase flows in this study. Based on the above-mentioned identification technique, several flow regimes have been characterised for acquired gamma counts in the studied experiments of gas-oil-water flows in the vertical riser section, namely bubbly, bubbly/slug, slug, slug/churn, churn and churn/annular. For instance, Figure 5-27 displays probability density function (PDF) profiles for the gamma densitometer's signals corresponding to various values of riser base injected gas superficial velocities at a fixed mixture liquid superficial velocity of 1 m/s at 42% input water cut (at phase inversion point). PDFs corresponding to other mixture liquid flows at other phase fractions and gas superficial velocities are given in Appendix C. At the lower injected air superficial velocity of about 0.1 m/s that is equivalent to a gas flow rate of 1.5 sm^3/h, the PDF shape (marked (a) in Figure 5-27 consists of a single mean peak associated with a tail extended towards the high gamma counts region between about 420 and 500. The mean peak reflects the higher fluid density of liquid (mixture of oil and water). The tail is due to the passage of a relatively small amount of gas phase flowing within the liquid. This shape of PDF is

indicative of a bubbly to slug transition flow pattern (spherical cap bubbly flow). This flow behaviour was also visually observed via the transparent Perspex section as small bubbles were flowing upward within the liquid body and sometimes these bubbles formed relatively larger ones, which indicates that the flow is moving gradually from bubbly to form slug flow. As the injected gas superficial velocity is increased to about 0.38 and 0.65 m/s (air flow rate of 6 and 10 sm^3/h) the basic PDF's shape (marked (b) and (c) in Figure 5-27) is conserved but a second peak at a higher gamma count region starts developing, which also still indicates a bubbly-slug transition flow pattern. The second peak becomes gradually larger as the air injection increases which is indicative of a developing slug flow regime.
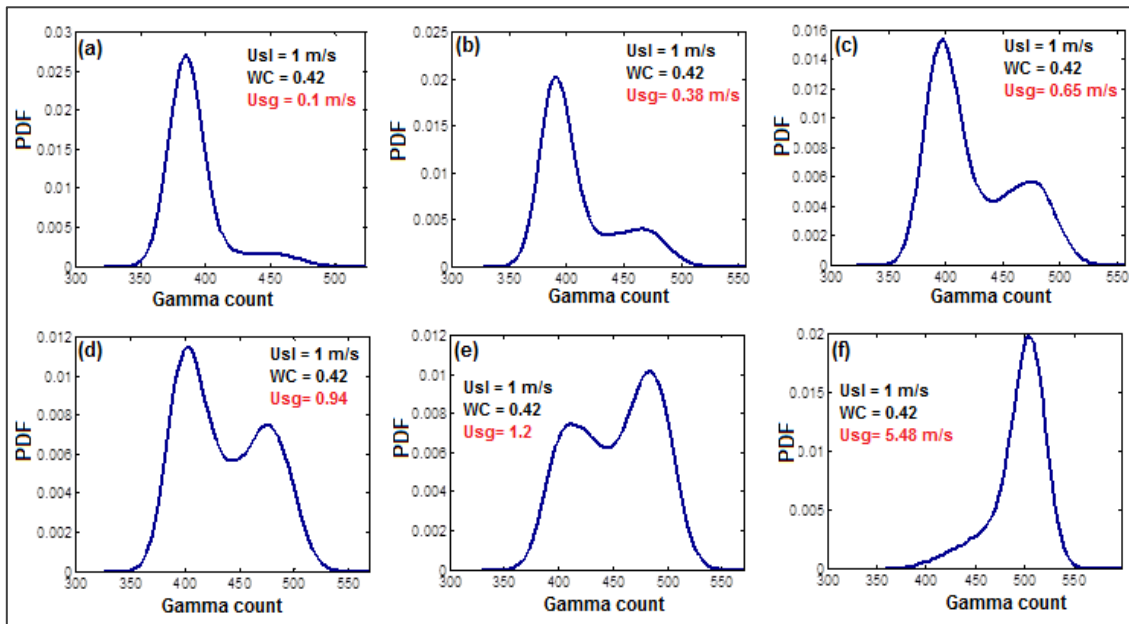
Figure 5-27: PDF Plots of gamma count data for various air flows at a mixture liquid flow of 1 m/s and water cut of 42%

With the same mixture liquid loading and the same water fraction but higher injected gas superficial velocities of 0.94 and 1.2 m/s (15 and 25 sm^3/h), the PDF shapes (marked (d) and (e) in Figure 5-27) are distinctly different with a twin peak indicating a slug flow in the riser for these flow conditions. The lower gamma count peaks correspond to a mixture liquid slug while the high gamma count peaks are for the equivalent gas body. Then, at the highest gas superficial velocity of ~5.48 m/s that corresponds to a gas flow injection of 100 sm^3/h (marked (f) in Figure 5-27), where the gas phase dominated the multiphase flow in the riser, the PDF's geometry for this flow condition has a single broad peak at a higher count region in the range of 450 to about 550, with a short tail towards the lower gamma counts, representing a churn flow pattern.

From the obtained results of the three-phase experiments it was also observed that, the increase in water cut has an effect on the flow patterns inside the riser. Figure 5-28 depicts PDF profiles for the gamma densitometer' signals are those corresponding to flow conditions of various values of water cut at a fixed mixture liquid superficial velocity of 0.25 m/s and constant riser-base injected gas superficial velocity of about 0.1 m/s (air flow rate of 1.5 m/s). It can be clearly observed that the flow pattern gradually changes from spherical cap bubbly flow at the lower water cut of 0.2 (the flow is oil continuous) to typical bubbly flow at the higher water cut of 0.8 where the flow is water continuous. These flow pattern changes that were observed by increasing the water cut are due to the gradual transition from oil continuous flow to water continuous, which leads to a gradual increase in the fluidity of the mixture flow (i.e. lowering mixture viscosity). Accordingly, the interaction behaviour between the gas and the mixture liquid will be different within both regions. Additional flow conditions showing how the gas/oil/water flow pattern changes with increasing water cut and injected gas superficial velocity at constant mixture superficial velocity of 0.25 m/s, are given in Table 5-2.
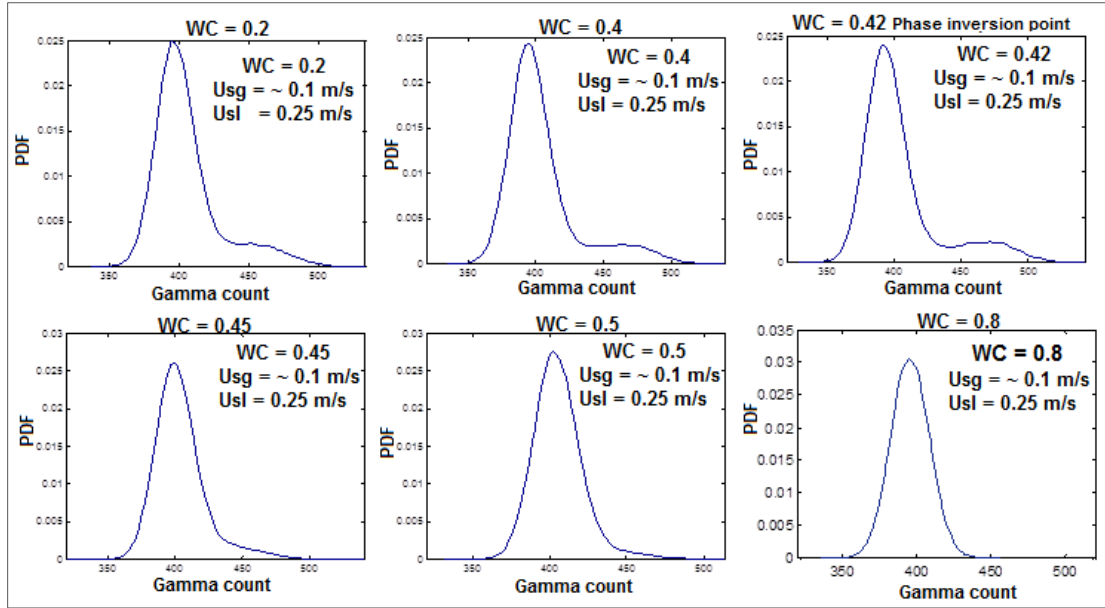
Figure 5-28: PDF Plots for different values of water cut at a mixture liquid flow of 0.25 m/s and air flow of 1.5 sm³/h

Table 5-2: PDF profiles of gamma count signals for air-oil-water flow tests at fixed mixture liquid superficial velocity of 0.25 m/s

Q_a	WC = 0.2	WC = 0.4	WC = 0.42	WC = 0.45	WC = 0.5	WC = 0.8
1.5 sm³/h						
3 sm³/h						
6 sm³/h						
25 sm³/h						

146

100 sm³/h
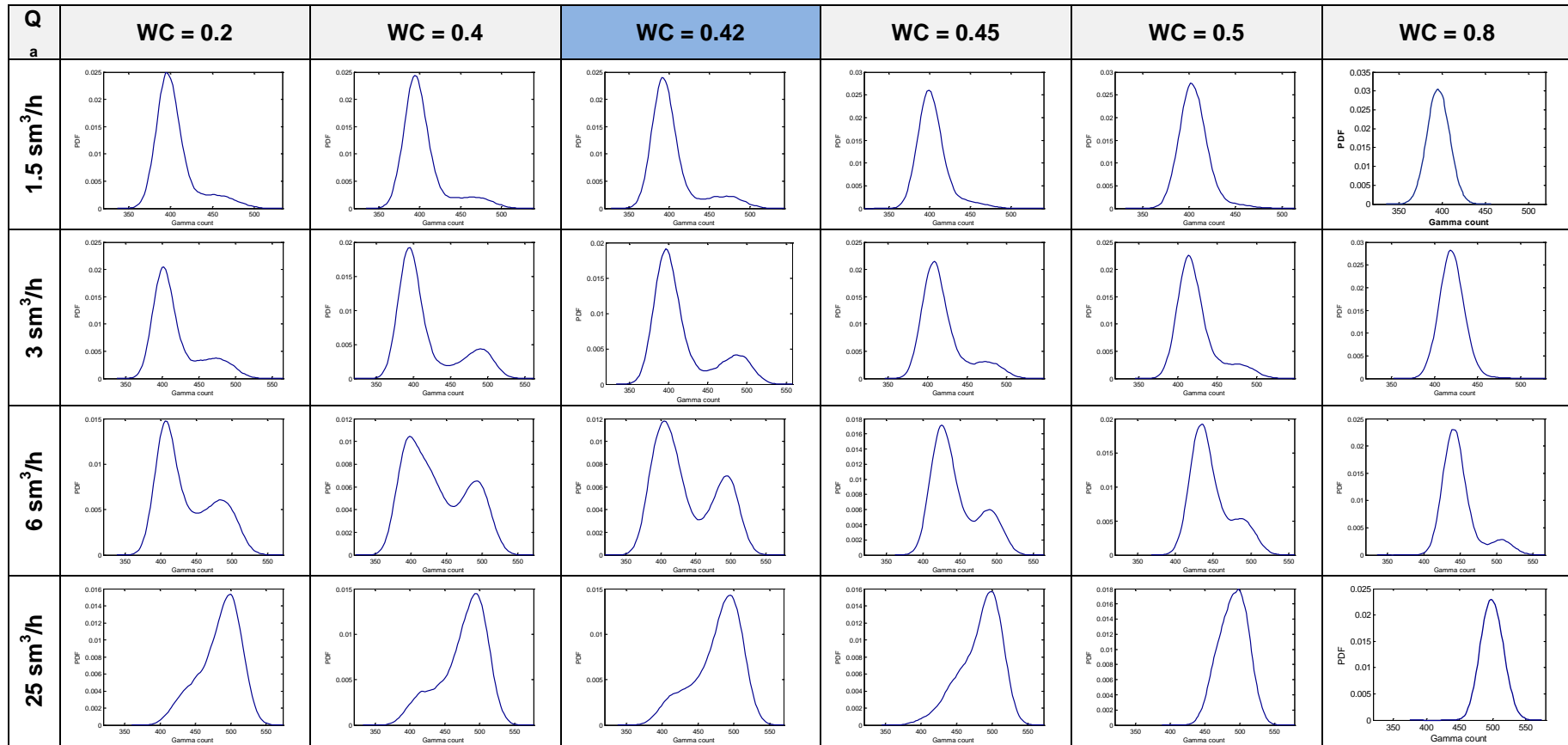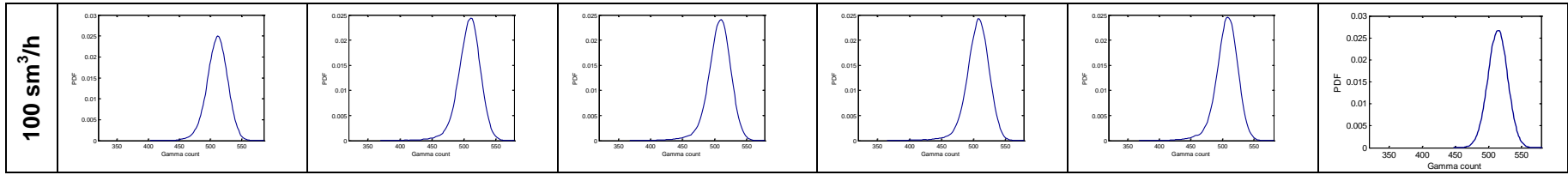
5.2.2 Total Pressure Gradient for Oil-Water with Air Injection

The total pressure gradient across the vertical riser was determined for each test point at various values of gas injection superficial velocity. In Figure 5-29, the total pressure gradient across the vertical riser, measured for several values of constant mixture liquid velocities (0.25, and 1 m/s) at various injected gas superficial velocities, is shown as a function of the input water fraction.

For the lower constant mixture liquid superficial velocity of U_{sl} = 0.25 m/s in Figure 5-29(a), there are eight values for the riser base injected gas velocity of U_{sg} = 0.09, 0.19, 0.4, 0.64, 0.96, 1.6, 3.16 and 6.20 (air flow rate of 1.5, 3, 6, 10, 15, 25, 50 and 100 sm^3/h) at several values of input water cut. While for the mixture liquid superficial velocity of U_{sl} = 1 m/s in Figure 5-29(b) there are ten values for the injected gas superficial velocity of U_{sg} = ~0.1, 0.19, 0.4, 0.65, 0.96, 1.2, 1.56, 1.8, 2.95 and ~5.48 (air flow rate of 1.5, 3, 6, 10, 15, 25, 30, 40, 50 and 100 sm^3/h). As can be observed from the plot, gas injection at the riser base has a significant influence on the pressure gradient over the riser. The total pressure gradient across the vertical riser was found to be lower than the liquid-liquid mixture flow without air injection (zero value for air injection velocity). Also, the total pressure gradient gradually decreases with the increasing gas injection, which suggests a general increase in the effectiveness of the gas lifting. The achieved decrease in total pressure gradient is due to the fact that when air is introduced at the riser base, the injected air bubbles aerate the liquid mixture column inside the riser making it lighter (reducing mixture density), consequently reducing the hydrostatic pressure gradient.

At a constant air injection rate, the total pressure gradient shows a gradual growth with the increase of water cut up to 0.42 (phase inversion point), leading to a pressure gradient peak at that point. For input water cut values greater than 0.42, the total pressure gradient tends to decline gradually. This case is more clearly visible for a higher constant mixture liquid velocity of 1 m/s. This decline in total pressure gradient is due to a decrease in the mixture's viscosity, which leads to a reduction in the frictional pressure gradient correspondingly, and then the total pressure gradient reduces subsequently.

The total pressure gradient for a flow mixture of 0.25 m/s behaves slightly differently, where a pressure peak did not appear at the lower air injection rates. The pressure gradient peak at the phase inversion point starts to be formed at the higher injected air rates. This is because of higher friction when more air is injected into the riser. Interestingly, the results of the total pressure gradient for the oil/water mixture flow under riser base gas injection showed that, with the increase of water cut greater than the phase inversion point (water continuous region), the riser total pressure gradient tends to decrease, which also suggests a better gas lifting efficiency for water continuous than oil continuous flow. This is as a result of mixture viscosity redaction, which leads to a reduction in the frictional pressure gradient and consequently the total pressure gradient reduces. Also, the sequence change in the mixture flow patterns after phase inversion influences the reduction in total pressure gradient.

Moreover, from the pressure gradient data presented in Figures 5-29(a) and (b), it was observed that the pressure gradient peak (which indicates the phase inversion point at 0.42 input water cut) at the higher air superficial velocities (equivalent to air flow rates of 50 and 100 sm^3/h) was shifted slightly forward to take place at the 0.45 input water cut. This change in phase inversion point might be due to the influence of changes in the flow patterns at these flow conditions of higher air injection, where churn and annular flow were identified. Figure 5-30 shows the behaviour of the total pressure gradient for different oil-water mixture superficial velocities at the particular input water concentration of 0.8, as a function of various injected gas superficial velocities. A general decreasing in the total pressure gradient for the three-phase flow can be observed due to an increase in gas superficial velocity. The detected decrease in the total pressure gradient can be explained by the fact that the mixture flow in the riser is gravity dominated, i.e. the major contributor to total pressure gradient in a vertical section is the gravity pressure gradient ($\rho_m \cdot \mathrm{g}$). In addition, the increase in gas superficial velocity will promote an increase in the void fraction inside the riser, thereby reducing the mixture fluid density as a result of a decrease in the liquid hold up. Consequently the total pressure gradient for the three-phase system decreases with an increase in gas superficial velocity.
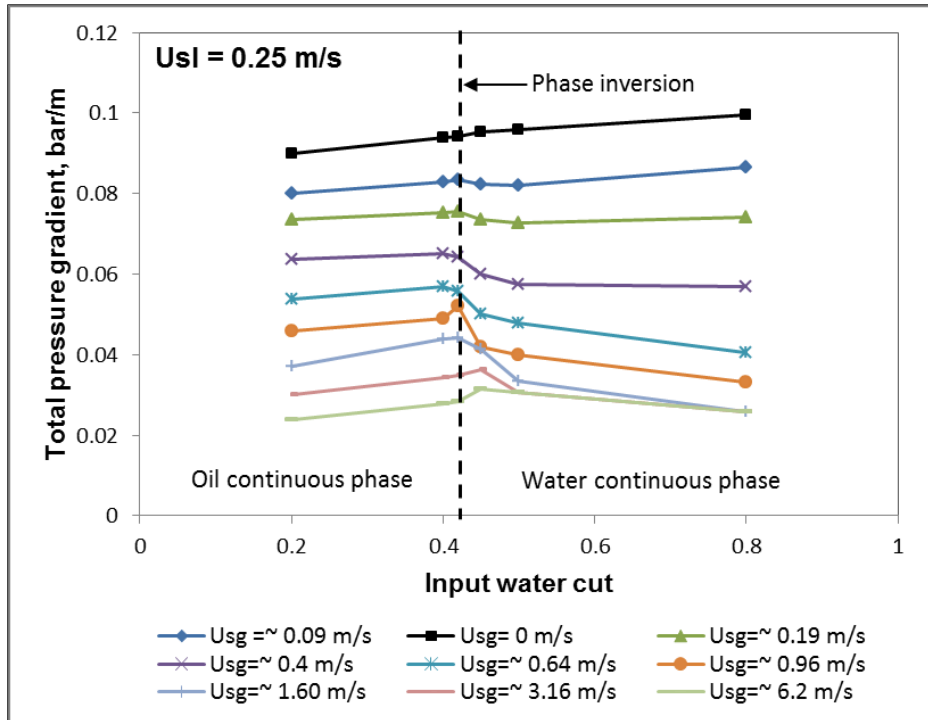
(a)
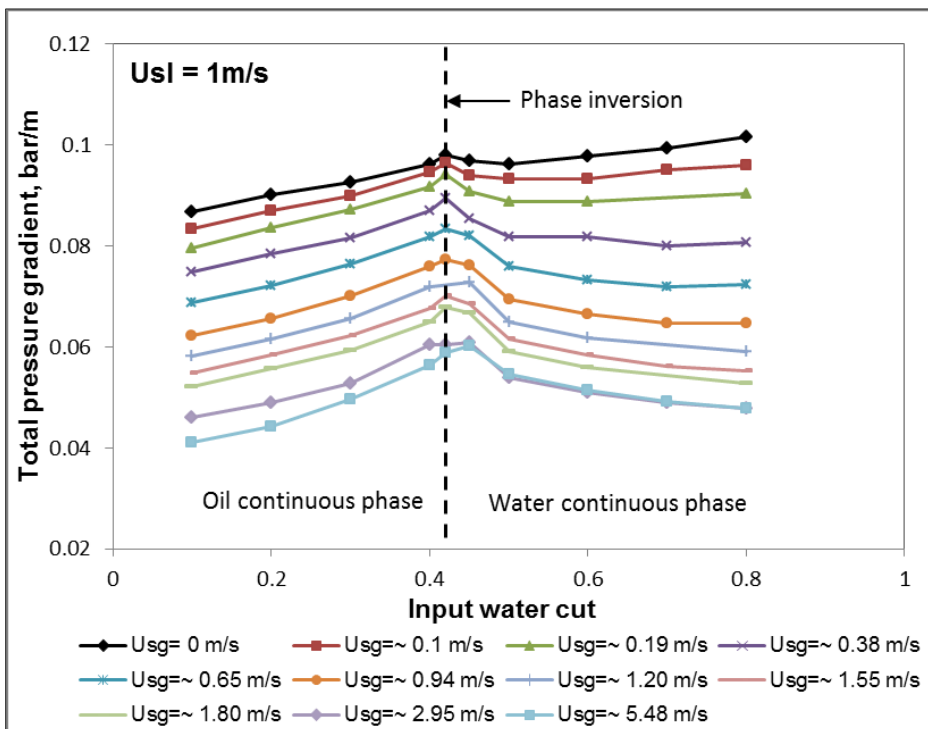
(b)

Figure 5-29: Total Pressure Gradient as a Function of Water Fraction for Air-Oil–Water Flows for a Mixture Liquid Velocity of (a) 0.25 m/s, (b) 1m/s
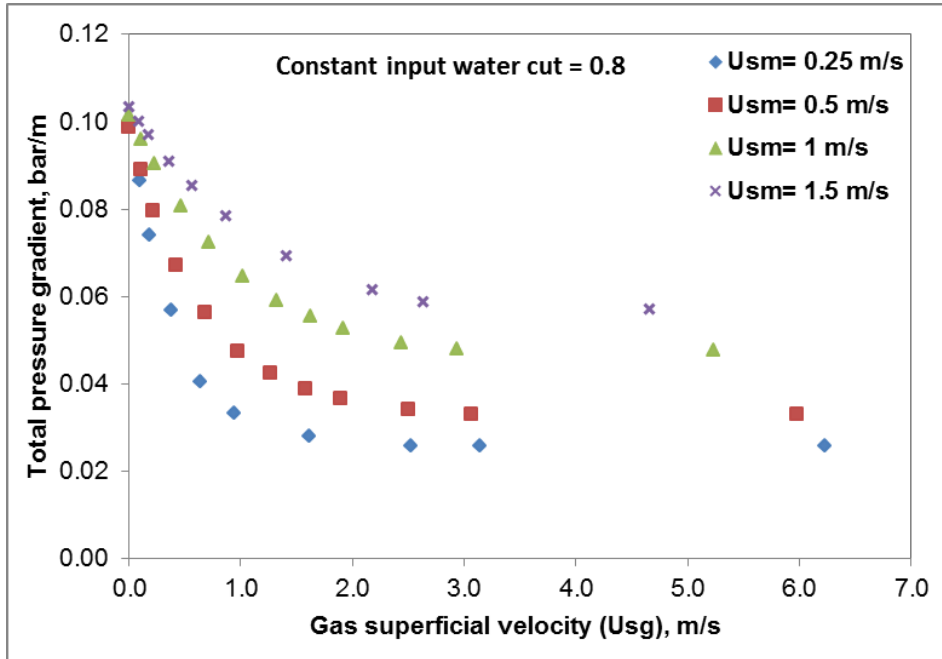
Figure 5-30: Total Pressure Gradient versus Air superficial velocity for several mixture liquid superficial velocities.

5.2.3 Average void fraction for Air-Oil-Water flow

The mean gas void fraction was determined for each test point of air-oil-water experiments by using the obtained average gamma counts in Equation 2-18. A mixture of oil and water was treated as a single liquid phase and the calibration procedure for the pipe full of liquid and empty was considered.

Figure 5-32 shows the changes of mean void fraction at each fixed input gas flow rate with increasing input water cut at constant mixture liquid superficial velocity of 1 m/s. It can be observed that the measured mean void fraction reaches its lowest value at the phase inversion point (input water cut of 42% for lower injected gas flow rates and 45% for highest injected gas flow rates of 50 and 100 Sm^3/h). These interesting findings of void fraction behaviour at phase inversion are in consistent with previous results for three-phase bubbly flow (U_{sg} < 0.85 m/s) in vertical pipe (Xu et al., 2012).
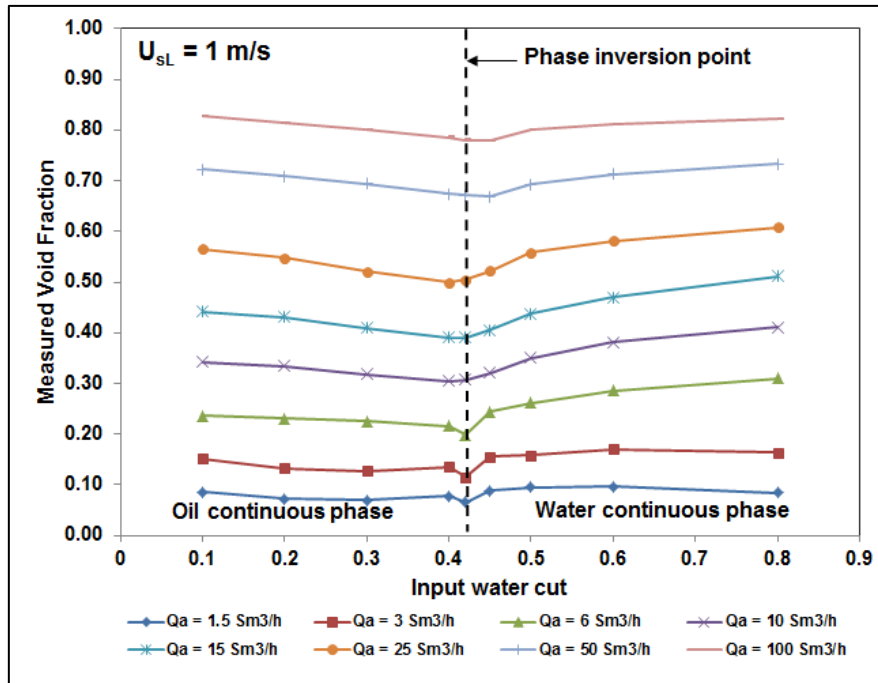
Figure 5-31: Average in situ air fraction against input water cut at fixed mixture liquid superficial velocity

5.2.4 WMS Measurements for Air-Oil-Water Three Phase Flow

The use of a WMS for investigating three-phase flow is a new topic and has been only initially reported by Da Silva et al. (2013). However, their preliminary investigations were carried out to visualise three-phase with air, silicone oil and water first in static and second in dynamic flow conditions. Their initial obtained results showed valuable images for the three-phase. Also, the presence of the emulsion and its separation process was captured by the sensor in their work.

In the current study, further attempts are made to use the capacitance WMS to acquire useful qualitative information about the characteristics of air-oil-water three-phase upflow inside the 52 mm vertical riser under different flow conditions of gas superficial velocity and input water cuts within fixed liquid superficial velocities. The WMS measurements were conducted simultaneously along with the other instrumentations during the three-phase experiments. Data

for water continuous flow conditions with various flow rates of riser-base air injection were acquired. Prior to the starting of the experiments of oil-water with riser base air injection, a two calibration series of measurements were performed for the capacitance WMS with an empty pipe and with the riser full of water as low and high permittivity references, respectively. The WMS measurements were performed at a data acquisition frequency of 1000 Hz over an interval of 30 seconds for each particular test point. During the measurements of the three-phase, it was difficult to recognise each phase individually within the three phases. The WMS was only able to discriminate between two media with different permittivity values in coloured images. It was almost discrimination between air (lower permittivity value of 1) and water/oil mixture (highly water-dominated).

Figures 5-32 and 5-33 depict the cross-sectional images and slice views measured by the WMS for three-phase at mixture liquid superficial velocities of 0.25 m/s and 1 m/s (input water cut = 0.8) and different air flow rates. Red colour indicates the gas phase and blue represents the mixture liquid; a colour scale is used for permittivity values. At the lowest gas superficial velocity of about 0.1m/s (air flow rate Q_g = 1.5 sm³/h), it can be observed that the flow pattern in the riser is bubbly flow. When the air flow is increased to 6.0 sm³/h, slug flow patterns were visualized for mixture liquid superficial velocity of 0.25 m/s. Relatively large pockets of gas, with small gas bubbles in a liquid structure, can be envisaged for this flow condition of air-water. Whereas, a spherical cap flow pattern was visualized for liquid superficial velocity of 1 m/s and the same amount of air 6.0 Sm³/h. At injected gas flow rate 10 sm³/h, a slug flow regime with a larger amount of gas phase was identified when the liquid superficial velocity was kept at 0.25 m/s but the flow pattern is still shown as bubbly/slug flow for higher liquid superficial velocity of 1 m/s. At gas flow rate of 15 Sm³/h, the flow pattern for liquid superficial velocities of 0.25 m/s (Figure 5-33) and 1 m/s (Figure 5-34) can be seen as slug flows.

At further increase of gas flow rate of 25 Sm³/h, the three-phase flow at mixture liquid superficial velocity of 0.25 m/s is observed to change to churn flow. On

other hand, slug flow regime is still identified for flow condition of liquid superficial velocity of 1 m/s and the same gas flow rate of 25 Sm^3/h.

These qualitative results of the three-phase flow and its structure can encouraging for using the capacitance WMS for further three-phase measurements such as phase fraction estimation and distributions.
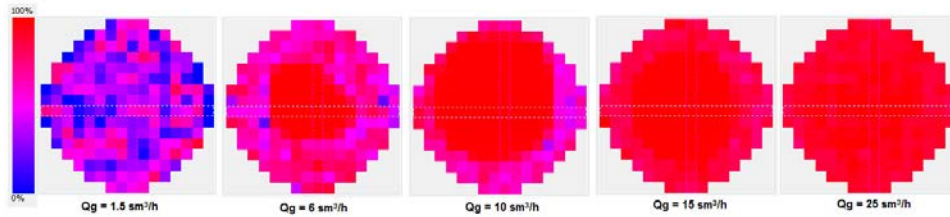
(a)
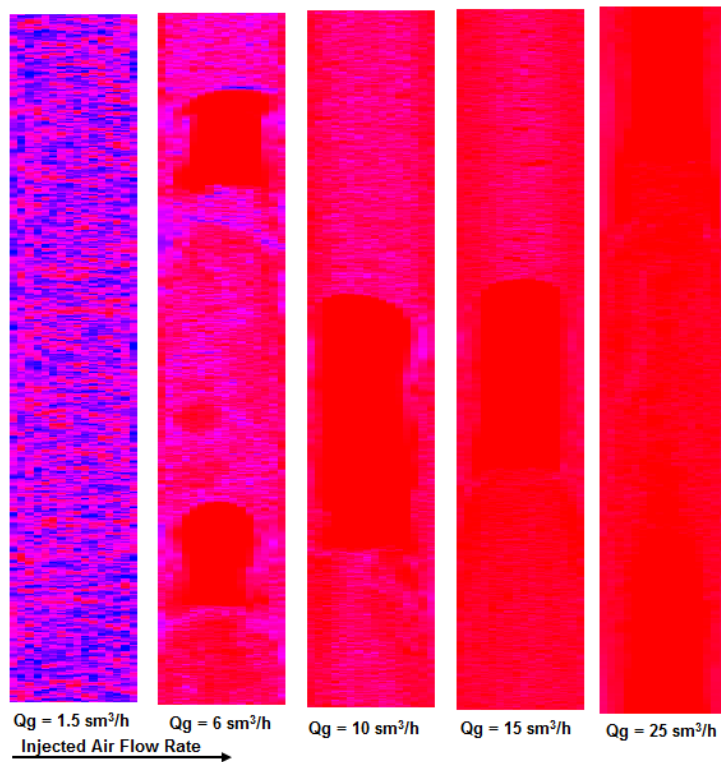
(b)

Figure 5-32: Visualization of WMS data from air/oil/water flow at U$_{sm}$ = 0.25 m/s (WC = 0.8) and different U$_{sg}$, a) Cross-sectional images, b) Slice views.

(a)

Qg = 1.5 sm³/h   Qg = 6 sm³/h   Qg = 10 sm³/h   Qg = 15 sm³/h   Qg = 25 sm³/h

Injected Air Flow Rate →
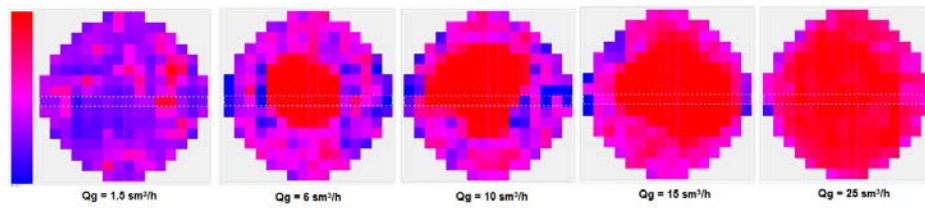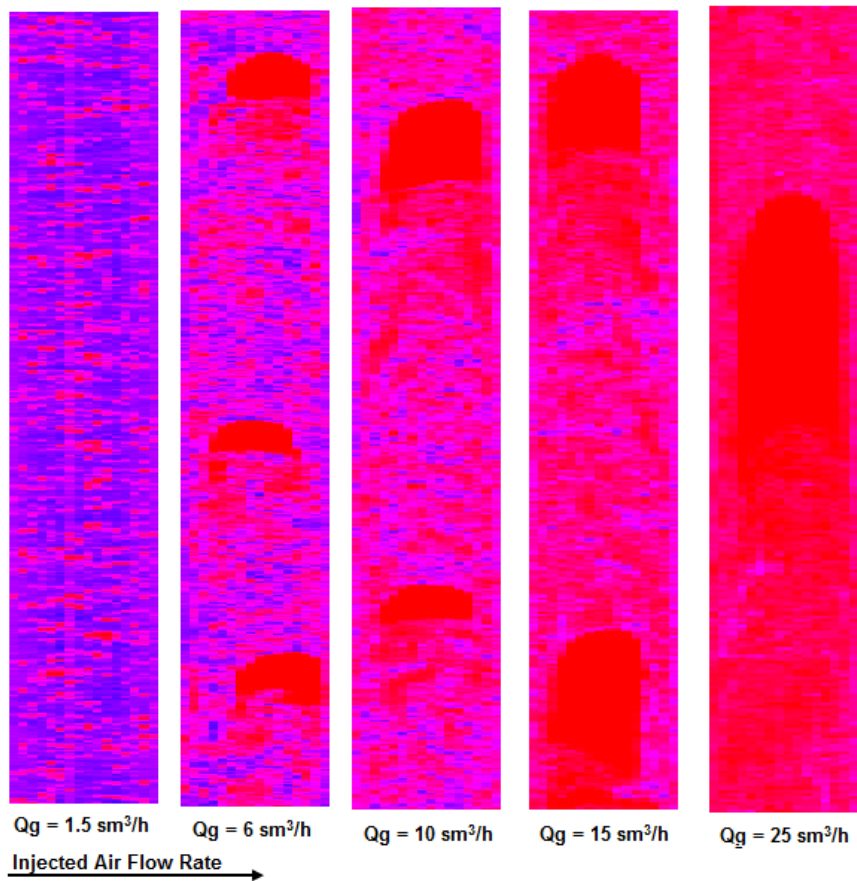
(b)

Figure 5-33: Visualization of WMS data from air/oil/water flow at mixture liquid superficial velocity of 1 m/s (WC = 0.8) different air superficial velocities, a) Cross-sectional images, b) Slice views

CHAPTER SIX

6 CONCLUSIONS AND FUTURE WORK

This chapter provides the main conclusions gained from this research work and the recommendations for further work.

In line with the aims and objectives, this thesis was able to achieve the following conclusions:

An extensive literature review discussing the techniques of gas-lift in oils wells and in subsea riser systems was carried out. Within this review, the thesis also reviewed investigations into two and three phase flows characteristics in vertical pipes. The former includes gas-liquid and liquid-liquid flows whilst the latter includes liquid/liquid flows under riser base gas injection.

- **Gas-liquid two-phase flows:**

As previously mentioned, the thesis discussed in details a test investigation into two-phase flow using air-water in the vertical riser. The one objective of this test was to investigate the characteristics of the two phase flow whilst scrutinizing the collection of data of the used instrumentations' response to comprehensive multiphase flow conditions.

The results showed high correlation between the hard gamma and soft gamma void fraction and the capacitance WMS void fraction results were consistent with gamma voids (hard and soft) at lower gas superficial velocities. However, at higher gas superficial velocities, the capacitance WMS void fractions were slightly higher than the gamma measurements probably due to the difference in the performances of the devices at high void fraction.

The flow pattern of air-water two-phase flow at each flow condition was identified by using different methods. The flow regimes identified under the tested flow conditions in this study were within Bubbly, bubbly/slug transition (spherical bubbly), slug, churn and annular flows. The visualization by the WMS was consistent with measurements of using time traces (WMS cross-sectional void and gamma counts) and PDF techniques.

The WMS was also able to provide useful information about cross-sectional void distributions. At lower injected air flows (where flows were indicated as bubbly and bubbly/slug transition flows) the obtained WMS void distribution data show a flattened profile around the pipe centre with a slight air decrease at the pipe wall (almost intermediate peak distribution). Also, with the flow conditions at fixed liquid superficial velocities of 0.25 and 0.5 m/s the void profiles appear to have a more flattened profile around the pipe centre compared to the higher water flows of 1, 1.5 and 2 m/s. As air and water superficial velocities increase, the void fraction profiles gradually become core-peaking void profile. A further increase in injected gas superficial velocity, leads to forming a clear core-peaking profile (maximum values of void fraction are around the pipe centre). No wall-peaking void distribution was identified for all tested flow conditions of air-water flow under riser base gas injection.

In terms of pressure gradient behaviour along the vertical riser, there is a decrease in the total pressure gradient due to an increase in injected gas superficial velocity, which suggests an increase in the effectiveness of the gas lifting. Also, the rate of drop in total pressure gradient at the lower injected gas superficial velocities is higher than that for higher gas superficial velocities. On the other hand, the determined frictional pressure gradient was found to increase as the injected gas superficial velocity increased.

The entrance effect on the multiphase flow characteristics in the 52 mm ID vertical riser was also studied for the air-water system. The new technique of using a WMS based on capacitance measurements was employed to obtain comprehensive information of the flow regime, void fraction fluctuation and phase distribution at the top of the riser. The considered results for the two inlet configurations exhibited differences in flow patterns and average void fraction values and distributions inside the riser. This dissimilarity is due to the effect of flow behaviour in the horizontal flowline that influences the vertical riser behaviour when gas is introduced through the horizontal flowline. These findings show that, in some multiphase applications that utilise gas-lift or gas injection, the location of the injection point has an impact on the flow patterns and phase fraction measurements and distributions.

A comparison between the capacitance and conductive wire-mesh measurements for air-water flow has been carried out at the top of the 52 mm vertical riser. The obtained results show that the main cross-sectional void fraction values measured by conductive WMS and capacitance WMS are close with only a small percentage difference. In terms of flow pattern, the obtained results show that both instruments predict similar flow regime signatures. Slight differences between conductive void distributions and the capacitance void distributions were observed. These differences clearly appear towards the pipe wall. Thus, deeper investigations including comparisons with another reliable tomography instruments are suggested to be carried out in the future.

The qualitative and quantitative results provided by the capacitance WMS for air-water tests in the vertical riser showed that the WMS is a valuable technique and encouraging when used for investigating multiphase flows, which are very common in the oil industry.

- **Liquid-liquid two-phase flow:**

The experimental results for the oil-water mixture flow show that the mixture density and total pressure gradient across the vertical riser increases with increasing input WC and vice versa. Also, the total pressure gradient increases with increasing total mixture flow (oil plus water flow rate). This increase was expected and can be explained by the fact that the hydrostatic pressure gradient is directly proportional to mixture density and frictional pressure increases with increasing liquid mixture flow in the system.

Efforts were made to calculate the slippage between oil and water (slip ratio) and interesting results were found; at the lower mixture velocities, the difference between continuous and dispersed phase velocities gradually decreases as the flow approaches the phase inversion. At higher mixture superficial velocity, when both fluids tend to be more homogenized, the slip ratio values are close to unity (fluids move approximately at the same velocity).

From the pressure gradient data that measured along the vertical riser sections for higher mixture oil-water flowrates of 1, 1.5 and 2 m/s, there is a relatively

increase (peak) in the total pressure gradient around the point of the 0.42 input WC, indicating the occurrence of the phase inversion point. The peak in the measured total pressure gradient was used as an indication of the phase inversion point. For the opposite experiments route starting from pure water to pure oil continuous the phase inversion point took place at a slightly higher input WC of 0.45 (i.e. a step forward of 3% in the phase fraction was observed between the two experimental routes).

An attempt to use capacitance WMS, for the possibility of extracting useful qualitative and quantitative information about the oil-water upflow characteristics inside the vertical riser, was carried out during the experiments of oil-water flow in the current study.

The successfully acquired qualitative results of the visualization and cross section phase distributions show that at lower oil fractions higher amounts of the oil phase tend to flow near to the pipe wall, whereas higher water concentration appears around the pipe centre. As the mixture superficial velocity increases, the flow appears to become gradually homogeneous but it still shows slightly higher oil fraction moves near the pipe wall and still greater water moves around the centre with some oil phase flowing within. The chordal phase distribution results were consistent with the corresponding visualization results. However, oil fraction profiles for the lower mixture superficial velocities are not a uniform (shown as asymmetrical) oil distribution over the pipe's cross section. At higher oil fraction (typically input oil fraction = 55%, i.e. 45% input water cut, where phase inversion point took place in the tests' direction from water continuous to oil continuous), the average chordal oil concentration profile started to show a core-peaking distribution, compared with the lower oil fraction at the same mixture superficial velocity. This also supported what was observed from the obtained WMS reconstructed images (cross-sectional and slice views) at these flow conditions.

Further more, the PDFs corresponding to the time series of the obtained average cross-sectional oil volume fraction data were also generated for several mixture flow conditions. It was found that the broadening and amplitude of the

PDF's peak indicate the homogeneity level of the mixture in the riser. i.e. at the lower mixture superficial velocity of 0.25 & 0.5 m/s where the flow was observed to be a dispersed flow with less homogeneity, the PDFs shape was characterised as a shorter, broader, single peak. At higher superficial velocities of 1 & 1.5 m/s where the flow was indicated to be more homogeneous, the PDF geometry displays a narrower peak with higher amplitude. Also, the PDF shape is significantly influenced by the occurrence of phase inversion. The change in the PDF's character is attributed to the possible effect of the WMS signals by the different mixture chracteristic that forms at the phase inversion point.

The promising findings for the WMS data in oil-water flows and particularly at phase inversion could lead to a better understanding of the local phase distributions during inversion after further investigation is carried out in the future.

- **<u>Liquid-liquid with riser base gas injection:</u>**

Based on the PDFs' flow patterns identification technique, the wide-ranging flow rates of the tested air injection were able to form several types of flow regimes for air-oil-water flows in the vertical riser section. Thus, in addition to the transition regions' patterns, Bubbly, bubbly/slug transition, slug flow, slug/churn flow, churn flow and churn to annular flow regimes were characterised.

In terms of pressure gradient behaviour, it was found that total pressure gradient for oil/water flow with gas injection was always lower than that of oil-water without gas injection. Total pressure gradient decreases with increasing air injection rate at the constant water cut. This is because of the decrease in the mixture density when the air bubbles aerate the liquid mixture and thus make it lighter. Accordingly, total pressure gradient decreases as hydrostatic pressure gradient decreases with density, which is the principle behind the gas-lift technique.

At the constant gas injection flowrate in the riser, the total pressure gradient gradually increases with raising water cuts up to a water cut of 42% (the phase inversion point), where the pressure gradient were found to be still higher than

others. Then the pressure gradients, at the same rate of air injection and increasing water cut were observed to be gradually dropping. Consequently, outside phase inversion, the gas reduces the pressure gradient, and the gas-lift technique can be effective. However, the gas lifting efficiency still shows more improvement after the phase inversion point than before the inversion point. The decrease of mixture viscosity due to increased water cut after phase inversion is the main reason for this behaviour.

In terms of the phase inversion point, the lower injection of gas does not affect the WC at phase inversion. However, it has shown a slight shift forward at the highest gas flow rates where the flow was indicated as churn and churn to annular flow.

In terms of void fraction, it was found that the measured mean void fraction reaches its lowest value at the phase inversion point. These void fraction results were found to consistent with previously published results.

Attempts are also made to use the capacitance WMS to acquire qualitative information about the characteristics of air-oil-water three-phase flow inside the riser under different flow conditions. The WMS was only able to discriminate between two media with different permittivity values in coloured images. It was almost discrimination between air and water/oil mixture. Different flow patterns (bubble, slug, churn and annular flows) were identified. These results are almost in agreement with the PDFs' results that corresponding to gamma meter counts for the same flow conditions.

Future recommendations

There are a number of areas that can further enhance the quality of the research work described in this thesis. Some recommendations for further investigation are given as follows:

1- From the experiments of air/liquid flows carried out in the 52 mm diameter riser and discussed in Chapters 4 and 5, the WMS was only placed at the top of the riser and as a consequence only measurements at the riser top part were possible to be performed. In order to study the flow development along the vertical riser using the features of the data obtained from WMS, further work should look at placing the WMS at different heights along the vertical riser. This will also provide the opportunity of comparing the characteristics of the flow at several locations which would add a greater understanding of multiphase flow behaviour in vertical pipes.

2- Further experimental investigation using the WMS to study the bubble size distribution and breakup at water continuous flow, oil continuous flow and at the phase inversion point could provide interesting information about the inversion process and about influence of gas injection on gas lift efficiency.

3- In order to investigate gas-lifting in the three-phase facility, it is recommended to establish a pressure driven force system to drive the liquids to the riser instead of using pump force. The idea of a design pressurised vessel to drive fluids to the system could emanate from pressure driven conditions as found in real oil production systems.

4- Validating the experimental results of air-oil-water flow under riser base gas injection with appropriate numerical simulations will be beneficial to any further work.

REFERENCES

Abdulkadir, M. (2011), "Experimental and computational fluid dynamics (CFD) studies of gas/liquid flow in bends", PhD thesis, University of Nottingham, UK

Ali, S.F. (2009), "Two Phase Flow in Large Diameter Vertical Riser", School of Engineering, Cranfield University

Angeli, P. (1996), "Liquid-liquid dispersed flows in horizontal pipes", University of London.

Anon (2005), "Production Technology manual", Institute of Petroleum Engineering, Heriot-Watt University

Arirachakaran, S., Oglesby, K. D., Malinowsky, M. S., Shoham, O. and Brill, J. P. (1989), "An Analysis of Oil/Water Flow Phenomena in Horizontal Pipes", Society of Petroleum Engineers (SPE), Oklahoma City, Oklahoma.

Arubi, T. M. (2011), "Multiphase Flow Measurement Using Gamma-Based Techniques", PhD thesis, School of Engineering, Cranfield University, UK

Blaney, S. (2008), "Gamma Radiation Methods for Clamp-on Multiphase Flow Metering", PhD thesis, Cranfield University, UK

Blaney, S. and Yeung, H. (2007), "Gamma Radiation Methods for Cost-Effective Multiphase Flow Metering", 13th International Conference on Multiphase Production Technology, Edinburgh, UK

Blaney, S. and Yeung, H. (2008), "Investigation of the exploitation of a fast-sampling single gamma densitometer and pattern recognition to resolve the superficial phase velocities and liquid phase water cut of vertically upward multiphase flows", Flow Measurement and Instrumentation, vol. 19, no. 2, pp. 57-66.

Boyun G., William C. L., Ghalambor A. (2007), "Petroleum Production Engineering a Computer-Assisted Approach", Elsevier Science & Technology Books.

Brauner, N. and Ullmann, A. (2002), "Modelling of phase inversion phenomenon in two-phase pipe flows", International Journal of Multiphase Flow, vol. 28, no. 7, pp. 1177-1204.

Brown, K.E. (1967), "Gas lift theory and practice: including a review of petroleum engineering fundamentals", Prentice-Hall, Englewood Cliffs, N.J.

Clarke, S. I. and Sawistowski, H. (1978), "Phase inversion of stirred liquid/liquid dispersions under mass transfer conditions", Trans. IChemE, vol. 56, pp. 50-55

Costigan, G. and Whalley, P.B. (1997), "Slug flow regime identification from dynamic void fraction measurements in vertical air-water flows", International Journal of Multiphase Flow, vol. 23, no. 2, pp. 263-282.

Da Silva, M.J., Schleicher, E. and Hampel, U. (2007), "Capacitance wire-mesh sensor for fast measurement of phase fraction distributions", Measurement Science and Technology, vol. 18, no. 7, pp. 2245-2251

Da Silva, M.J., dos Santos, E., Hampel, U., Rodriguez, I. H. and Rodriguez, O. (2011), "Phase fraction distribution measurement of oil-water flow with capacitance wire mesh sensor". Measurement Science and Technology, 22:104020.

Da Silva, M.J., Thiele, S., Abdulkareem, M., Azzopardi, B.J. and Hampel, U. (2010), "High-resolution gas-oil two-phase flow visualization with a capacitance wire-mesh sensor", Flow Measurement and Instrumentation, vol. 21, no. 3, pp. 191-197

Da Silva, M.J. and Hampel, U. (2013), "Capacitance wire-mesh sensor applied for the visualization of three-phase gas-liquid-liquid flows", Flow Measurement and Instrumentation, vol. 34, no. 0, pp. 113-117.

Descamps, M., Oliemans, R.V.A., Ooms, G., Mudde, R.F. and Kusters, R. (2006), "Influence of gas injection on phase inversion in an oil/water flow through a vertical tube", International Journal of Multiphase Flow, vol. 32, no. 3, pp. 311-322.

Descamps, M., Oliemans, R.V.A., Ooms, G. and Mudde, R.F. (2007), "Experimental investigation of three-phase flow in a vertical pipe: Local characteristics of the gas phase for gas-lift conditions", International Journal of Multiphase Flow, vol. 33, no. 11, pp. 1205-1221.

Dong, F., Liu, X., Deng, X., Xu, D. and Xu, L. (2001), "Identification of two-phase flow regimes in horizontal, inclined and vertical pipes", Measurement Science and Technology, vol. 12, no. 8, pp. 1069-1075

Dong, F., Xu, Y., Qiao, X. and Xu, L. (2005), "Void fraction measurement for two-phase flow using electrical resistance tomography", Canadian Journal of Chemical Engineering, vol. 83, no. 1, pp. 19-23.

Dykesteen, E., et al, (2005), 'Handbook of Multiphase Metering', Norwegian Society of Oil and Gas Measurement, NFOGM, Revision 2.

Flores, J. G., Chen, X. T., Sarica, C. and Brill, J. P. (1999), "Characterization of Oil-Water Flow Patterns in Vertical and Deviated Wells", SPE Production & Operations, vol. 14, no. 2

Hapanowicz, J. (2010), "Phase inversion in liquid-liquid pipe flow", Flow Measurement and Instrumentation, vol. 21, no. 3, pp. 284-291

Helmholtz-Zentrum Dresden-Rossendorf (HZDR), (2012), "Wire Mesh Sensor System CAP200 Manual", Version 1.4, Teletronic Rossendorf GmbH

Hernandez-Perez, V. (2008), "Gas-liquid two-phase flow in inclined pipes", PhD thesis, University of Nottingham, UK.

Hewitt, G.F. (1982), "Handbook of multiphase systems, Chapter 2: Flow Regimes" Hemisphere, Washington, USA.

Hewitt, G.F., and Roberts, D.N., (1969), "Studies of Two-Phase Flow Patterns by Simultaneous X-ray and Flash Photography", AERE-M 2159, HMSO, Harwell

Hill, T.J. (1990), "Gas injection at riser base solves slugging, flow problems", Oil and Gas Journal, vol. 88, no. 9, pp. 88-92

Hu, B. (2006), "Experimental and theoretical investigation of phase inversion in liquid-liquid dispersions", PhD thesis, Department of Chemical Engineering, University College London, UK

Hu, B. and Angeli, P. (2006), "Phase inversion and associated phenomena in oil-water vertical pipeline flow". Can. J. Chem. Eng., 84(1): 94-107

Ioannou, K. and Angeli, P. (2005), "Phase inversion in dispersed liquid-liquid flows", Experimental Thermal and Fluid Science, vol. 29, no. 3, pp. 331-339

Jansen, F.E., Shoham, O. and Taitel, Y. (1996), "The elimination of severe slugging-experiments and modeling", International Journal of Multiphase Flow, vol. 22, no. 6, pp. 1055-1072

Jayawardena, S.S., Zabaras, G.J. and Dykhno, L.A., (2007), "The Use of Subsea Gas Lift in Deep water Applications", Offshore Technology Conference, Houston, Texas, U.S.A

Jones Jr., O.C. and Zuber, N. (1975), "The interrelation between void fraction fluctuations and flow patterns in two-phase flow", International Journal of Multiphase Flow, vol. 2, no. 3, pp. 273-306

Kumara, S., Halvorsen, B.M. and Melaaen, M.C. (2010), "Single-beam gamma densitometry measurements of oil/water flow in horizontal and slightly inclined pipes", International Journal of Multiphase Flow, vol. 36, no. 6, pp. 467-480

Luhning, R.W. and Sawistowski, H. (1971), "Phase inversion in stirred liquid-liquid systems", Proceeding of the International Solvent Extraction Conference, the Hague, pp. 873-887, Society of Chemical Industry, London.

Mandhane, J.M., Gregory, G.A. and Aziz, K. (1974), "A flow pattern map for gas-liquid flow in horizontal pipes", International Journal of Multiphase Flow, vol. 1, no. 4, pp. 537-553

Morgan, R.G., Markides, C.N., Hale, C.P., Hewitt, G.F., 2012. Horizontal liquid–liquid flow characteristics at low superficial velocities using laser-induced fluorescence. Int. J. Muliphase Flow 43, 101–117

Morgan R.G, Markides CN, Zadrazil I and Hewitt G.F (2013), "Characteristics of horizontal liquid-liquid flows in a circular pipe using simultaneous high-speed laser-induced fluorescence and particle velocimetry", Int. J. Multiphase Flow, Vol. 49, ISSN: 0301 - 9322, Pages: 99 -118

Nädler, M. and Mewes, D., (1995), "Intermittent three-phase flow of oil, water and gas in horizontal pipes", Proc. 5th Int. Offshore and Polar Eng. Conf. (ISOPE-5), the Hague.

Nädler, M. and Mewes, D. (1997), "Flow induced emulsification in the flow of two immiscible liquids in horizontal pipes", Int. J. Multiphase Flow, vol. 23(1): pp. 55-68.

Ngan, K.H. (2010), "Phase Inversion in dispersed liquid-liquid pipe flow", PhD thesis, University College London, UK.

Olerni, C. and Wang, M., (2013), "Measurement of air distribution and void fraction of an upwards air-water flow using electrical resistance tomography and a wire-mesh sensor", Measurement Science & Technology, vol. 24, no. 3, pp. 1.

Omebere-Iyari, N.K. and Azzopardi, B.J. (2007), "A Study of Flow Patterns for Gas/Liquid Flow in Small Diameter Tubes", Chemical Engineering Research and Design, vol. 85, no. 2, pp. 180-192.

Piela, K., Delfos, R., Ooms, G., Westerweel, J. and Oliemans, R.V.A., (2008), "On the phase inversion process in an oil-water pipe flow", International Journal of Multiphase Flow, vol. 34, no. 7, pp. 665-677

Piela, K., Delfos, R., Ooms, G., Westerweel, J., Oliemans, R.V.A. and Mudde, R.F. (2006), "Experimental investigation of phase inversion in an oil/water flow through a horizontal pipe loop", International Journal of Multiphase Flow, vol. 32, no. 9, pp. 1087-1099.

Pietruske, H. and Prasser, H. (2007), "Wire-mesh sensors for high-resolving two-phase flow studies at high pressures and temperatures", Flow Measurement and Instrumentation, vol. 18, no. 2, pp. 87-94

Pots, B. I. M., Bromilow, I. G. and Konijn, M. J. W. F. (1985), "Severe Slug Flow in Offshore Flow-line/Riser Systems", Proceedings 4th Middle East Oil Show, Manama, Bahrain

Prasser, H-M., Bottger, A. and Zschau, J., (1998), "A new electrode-mesh tomography for gas/liquid flows", Flow Measurement and Instrumentation, vol. 9, no. 2, pp. 111-119.

Rodriguez, I.H., Yamaguti, H.K.B., de Castro, M.S., Da Silva, M.J. and Rodriguez, O.M.H. (2011), "Slip ratio in dispersed viscous oil/water pipe flow", Experimental Thermal and Fluid Science, vol. 35, no. 1, pp. 11-19.

Serizawa A. (1988), "Phase distribution in two-phase flow Transient Phenomena in Multiphase Flow", pp. 179-224, Hemisphere, Washington

Szalinski, L., Abdulkareem, L.A., Da Silva, M.J., Thiele, S., Beyer, M., Lucas, D., Hernandez-Perez, V., Hampel, U. and Azzopardi, B.J. (2010), "Comparative study of gas/oil and gas/water two-phase flow in a vertical pipe", Chemical Engineering Science, vol. 65, no. 12, pp. 3836-3848

Takács, G. (2005), "Gas lift manual, Handbook", PennWell, Tulsa, Okla

Wang, W., Ngan, K.H., Angeli, P. and Gong, J., (2009), "Effect of glycerol on the binary coalescence of water drops in stagnant oil phase", Chemical Engineering Research and Design, Vol. 87, no. 12, pp. 1640-1648

Wang, W. and Gong, J. (2009), "Experiment Research of Phase Inversion in Mineral Oil Water Two-Phase Flow in Horizontal Pipe", Journal of Energy Resources Technology, vol. 131

Xu, J., Wu, Y. and Chang, Y. (2009), "Influence of Gas Injection on the In-Situ Oil Fraction of an Oil-Water Flow in Horizontal Pipes", Chemical Engineering & Technology, vol. 32, no. (12), pp.1922-1928

Xu, J., Li, D., Guo, J. and Wu, Y. (2010), "Investigations of phase inversion and frictional pressure gradients in upward and downward oil/water flow in vertical pipes", International Journal of Multiphase Flow, vol. 36, no. 11-12, pp. 930-939.

Xu, J., Zhang, J., Liu, H. and Wu, Y. (2012), "Oil/gas/water three-phase upward flow through a vertical pipe: Influence of gas injection on the pressure gradient", International Journal of Multiphase Flow, vol. 46, no. 0, pp. 1-8.

Xu, X. X., (2007), "Study on oil–water two-phase flow in horizontal pipelines", Journal of Petroleum Science and Engineering, Vol. 59, pp.43 - 58

Yeh, G. C., Haynie Jr., F. H. and Moses, R. A. (1964), "Phase-volume relationship at the point of phase inversion in liquid dispersions", AIChE J., vol. 10, no. 2, pp. 260-265

Yeo, L. Y., Perez de Ortiz, E. S., Hewitt, G. F. (2000). Phase inversion and associated phenomena. Multiphase Science and Technology, 12(1): 51-116.

Yeung, H. and Lao, L., (2013), "Cranfield University Three-Phase Test Facility Operating Manual", Cranfield University, Cranfield, UK

Zangana, M.H.S (2011), "Film Behaviour of Vertical Gas-Liquid Flow in a Large Diameter Pipe", PhD thesis, University of Nottingham, UK

Zhao, D., Guo, L., Hu, X., Zhang, X. and Wang, X. (2006), "Experimental study on local characteristics of oil/water dispersed flow in a vertical pipe", International Journal of Multiphase Flow, vol. 32, no. 10-11, pp. 1254-1268

APPENDICES

Appendix A

Appendix A-1 Calibration Certificate of Brookfield Viscometer)

Certificate of Viscometer Calibration

Certificate No.

12/S58075

Customer

CRANFIELD UNIVERSITY

Model/Serial No.

Calibration Date

LVDVI PRIME   AP6524698

31 JAN 2012

This instrument has been serviced and calibrated to conform to the calibration specifications for the Brookfield Viscometer. Calibration has been determined and traceable to National Institute of Standards and Technology (NIST) standards with the following Reference Instruments and Viscosity Standard Oil.

Reference Instrument

Model

LVT-MAS

Serial No.

206544

Viscosity Standard
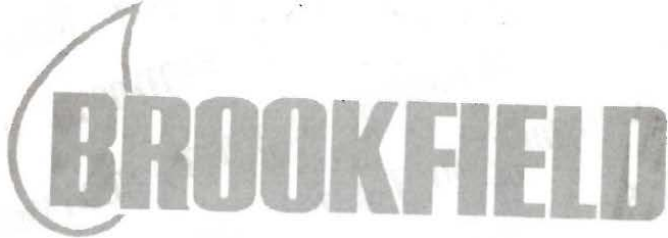
NIST Fluid

S-2000

Lot No.

09201

Reference Temperature Sensor

Model

FLUKE 52

Serial No.

T-83109

Calibration of this instrument will be accurate to within 1% of its full-scale range when operated according to calibration conditions as specified in the Brookfield Viscometer Instruction Manual. It will reproduce to within 0.2% of its full-scale range for any combination of spindle and speed.
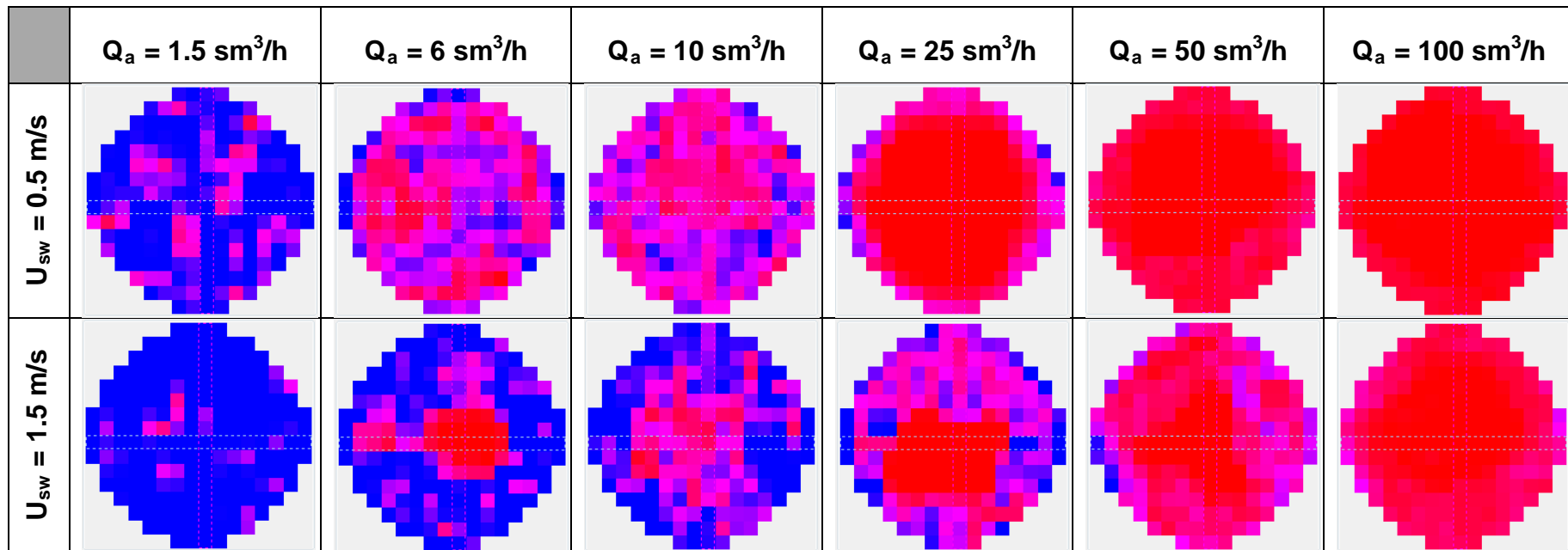
Brookfield
Engineer

TERRY HUNT

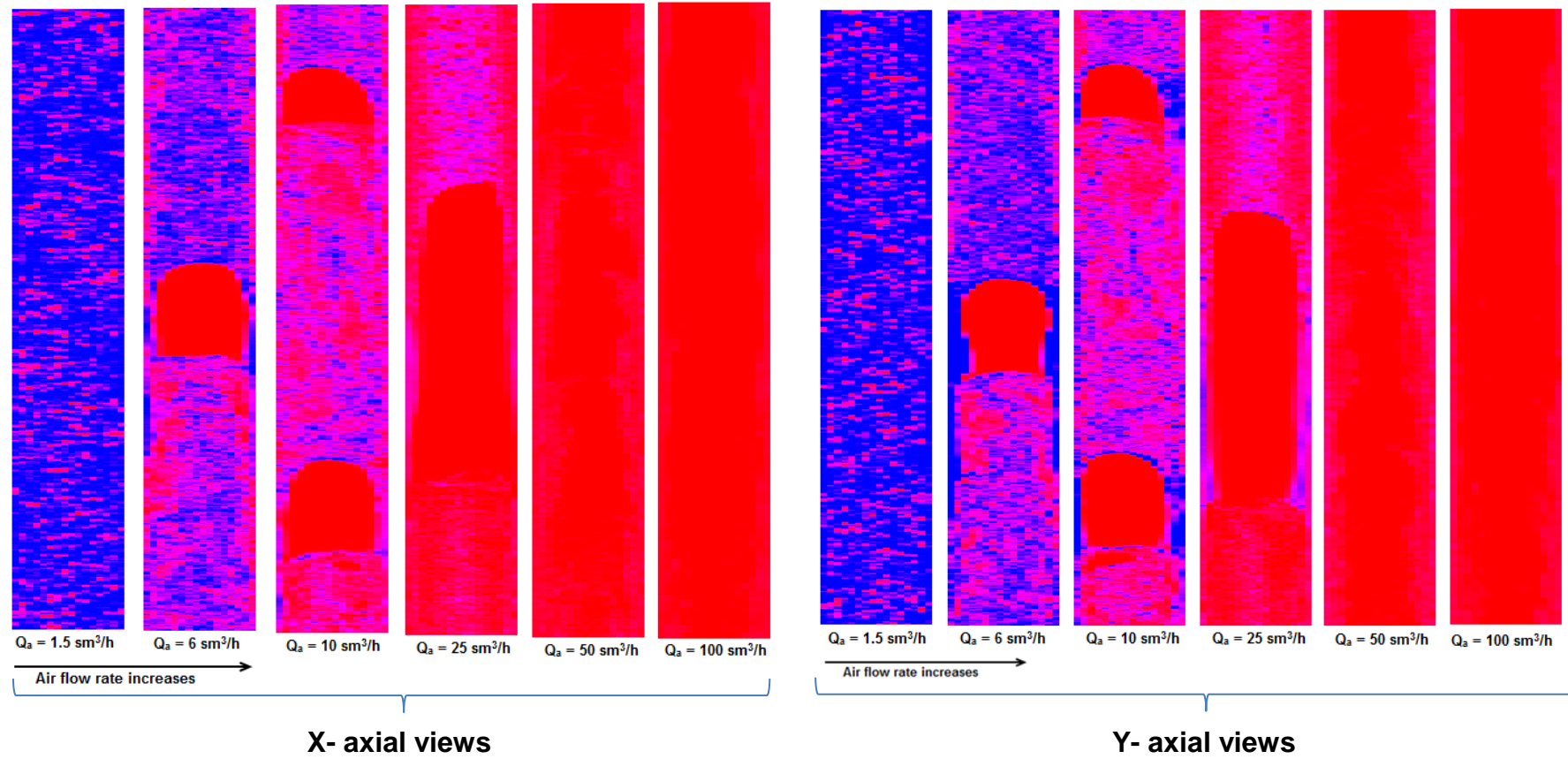BROOKFIELD

Appendix A-2: (Design Drawing for the 16 x 16 WMS)
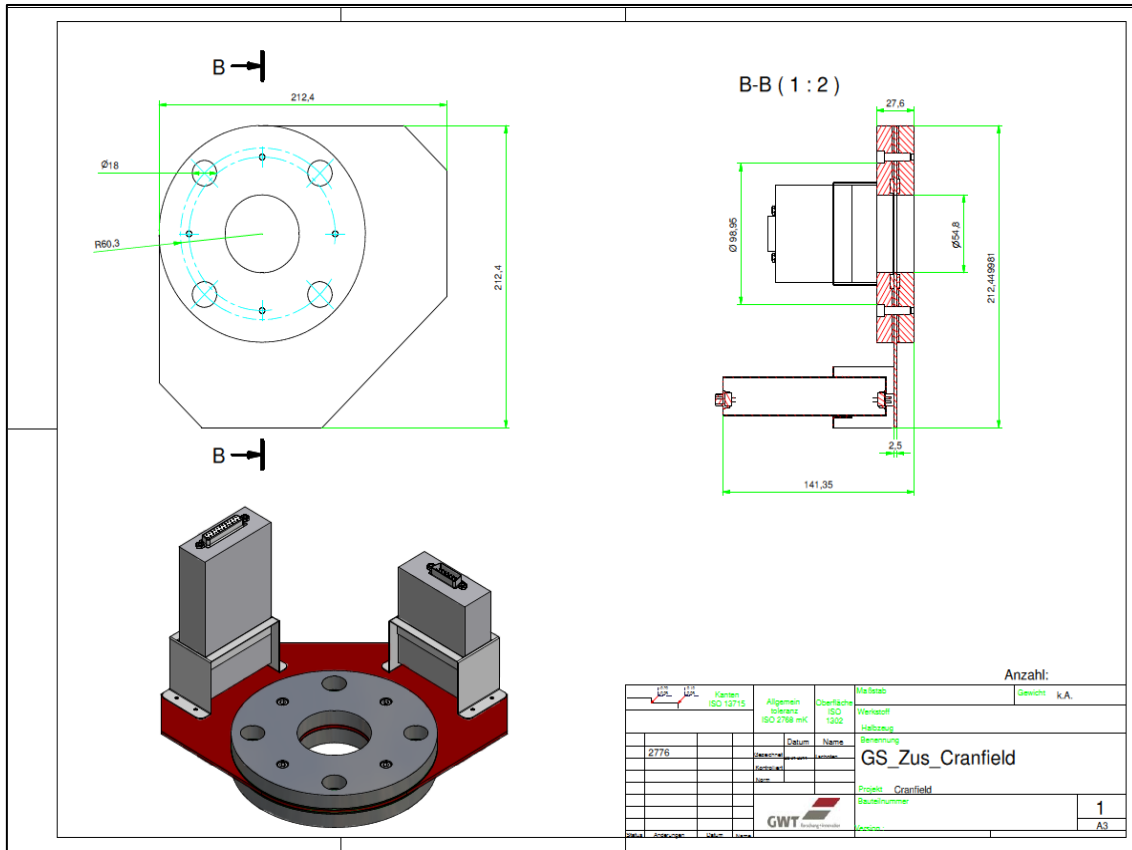
Appendix B: Wire-mesh Sensor Visualization (Output images)
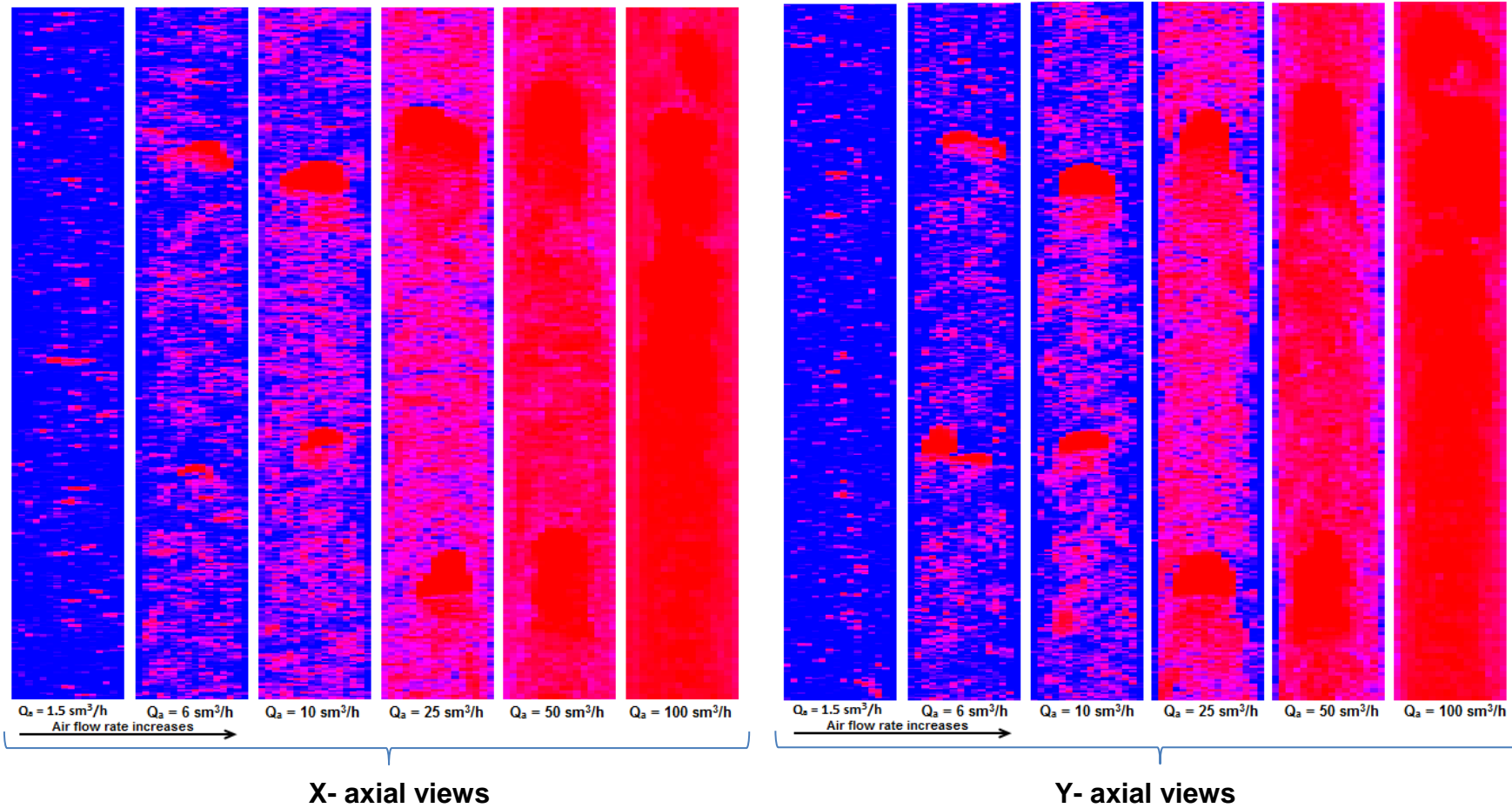
1- Air-Water Two-Phase Flow:

	$Q_a = 1.5$ sm^3/h	$Q_a = 6$ sm^3/h	$Q_a = 10$ sm^3/h	$Q_a = 25$ sm^3/h	$Q_a = 50$ sm^3/h	$Q_a = 100$ sm^3/h
$U_{sw} = 0.5$ m/s						
$U_{sw} = 1.5$ m/s						

(Cross-sectional Images)

Constant superficial liquid velocity U_{sw} = 0.5 m/s

X- axial views

Y- axial views

(Slice views)

Constant superficial liquid velocity U$_{sw}$ = 1.5 m/s

X- axial views   Y- axial views

(Slice views)

177

2- Oil-Water Two-Phase Flow:

Constant mixture liquid superficial velocity U_{sm} = 0.5 m/s

10% Oil cut   20% Oil cut   30% Oil cut   40% Oil cut

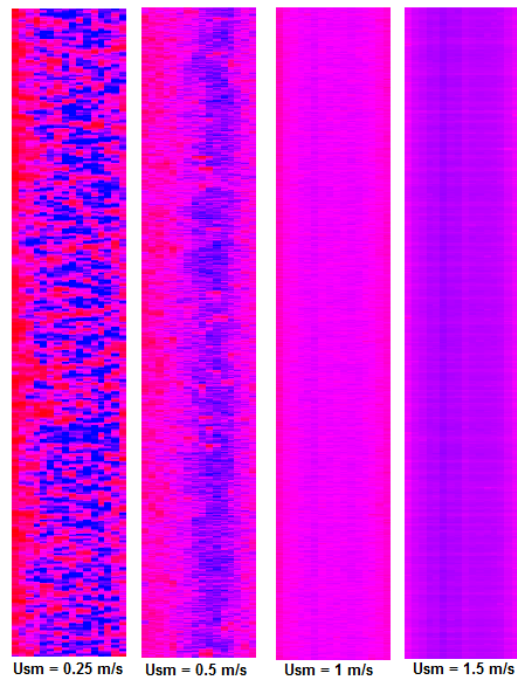**X- axial views**

10% Oil cut   20% Oil cut   30% Oil cut   40% Oil cut
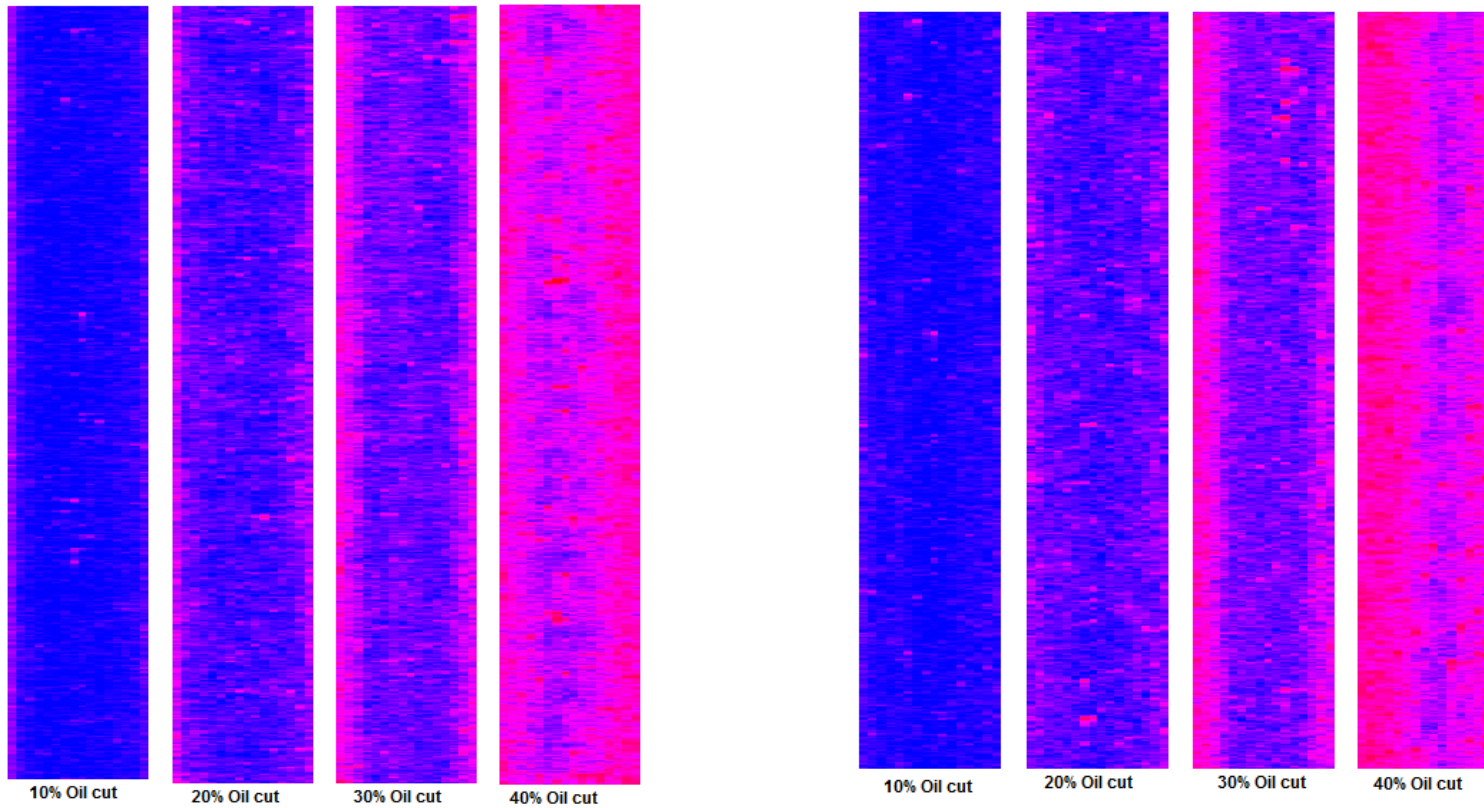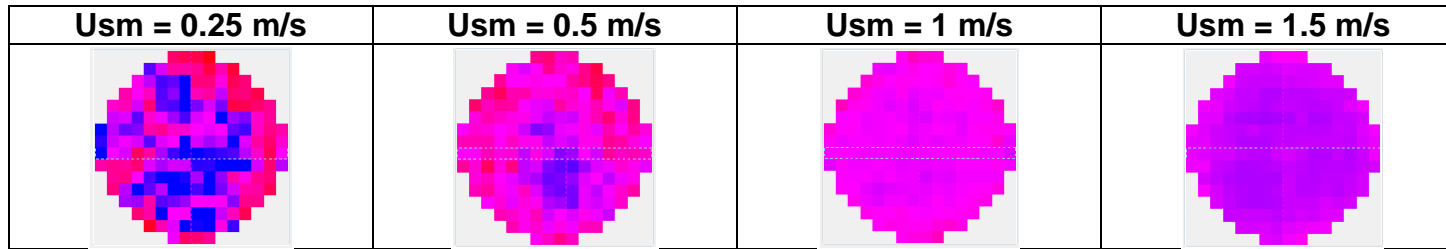
Y- axial views

(Axial slice views)

Constant input water cut of 0.6 and different mixture superficial velocities:

Usm = 0.25 m/s	Usm = 0.5 m/s	Usm = 1 m/s	Usm = 1.5 m/s

Usm = 0.25 m/s　　Usm = 0.5 m/s　　Usm = 1 m/s　　Usm = 1.5 m/s

X-slice views

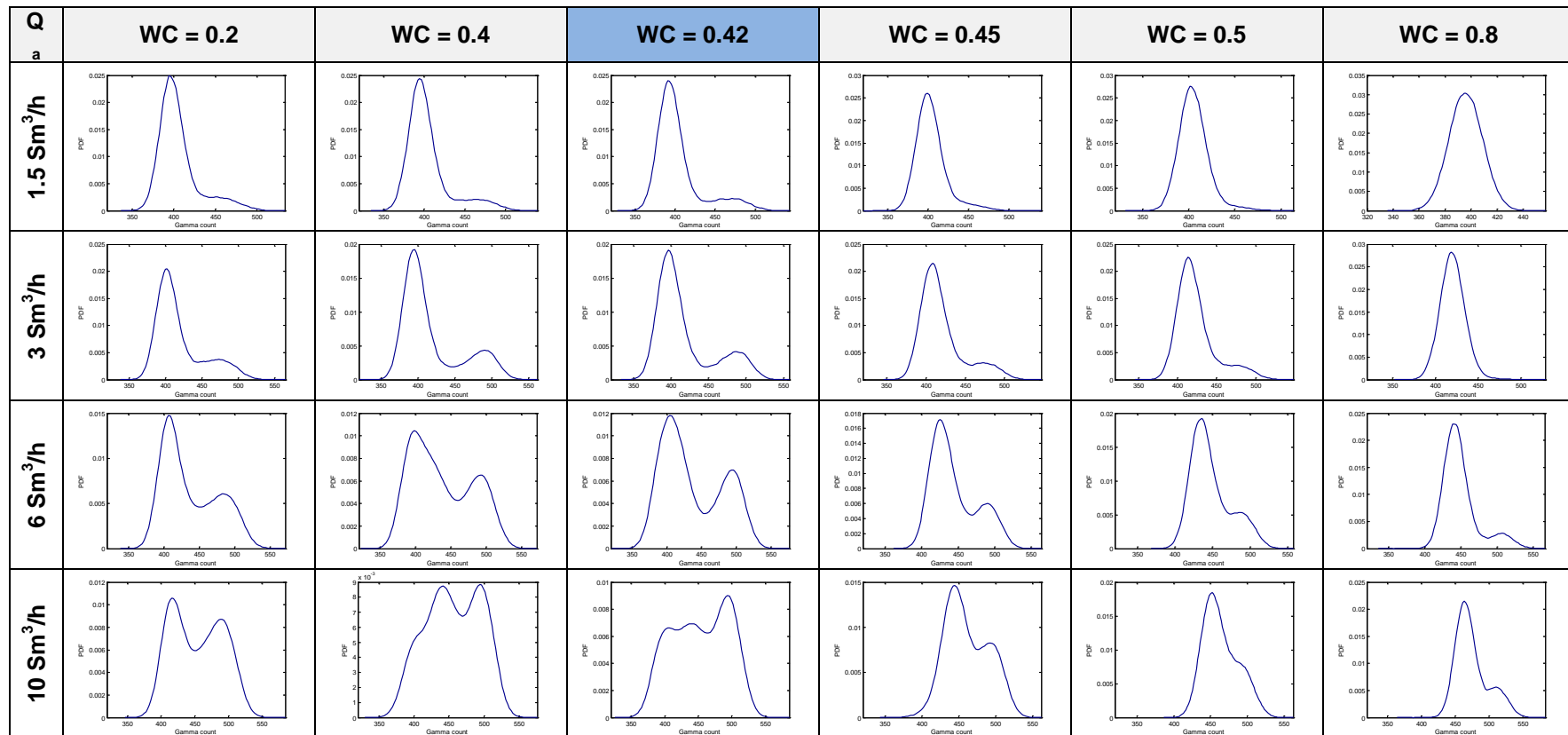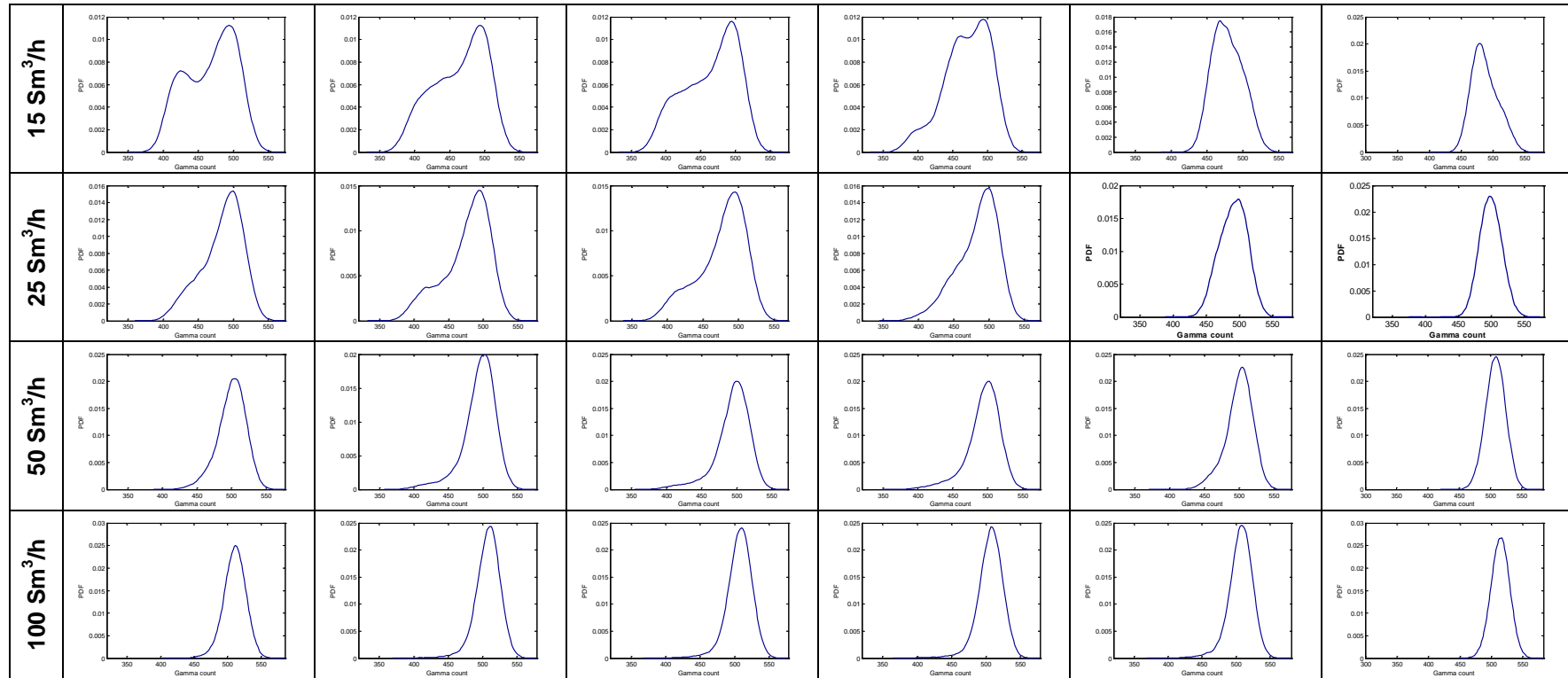Usm = 0.25 m/s　　Usm = 0.5 m/s　　Usm = 1 m/s　　Usm = 1.5 m/s
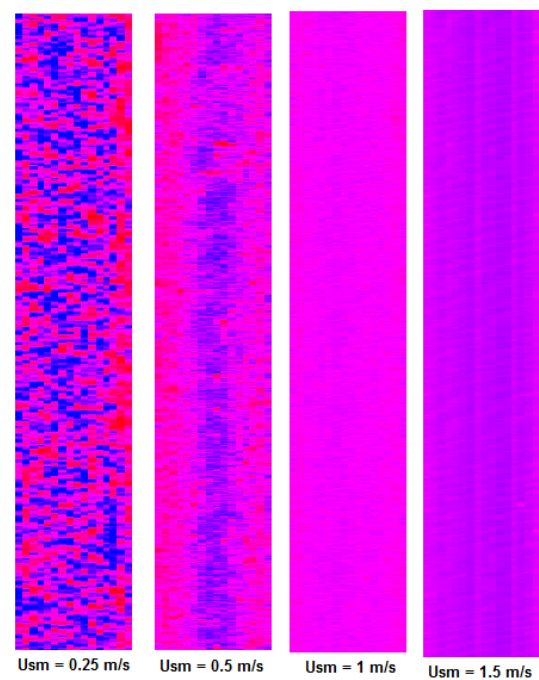
Y-slice views

Appendix C (PDF of Gamma Count for Air-Oil-Water flow)

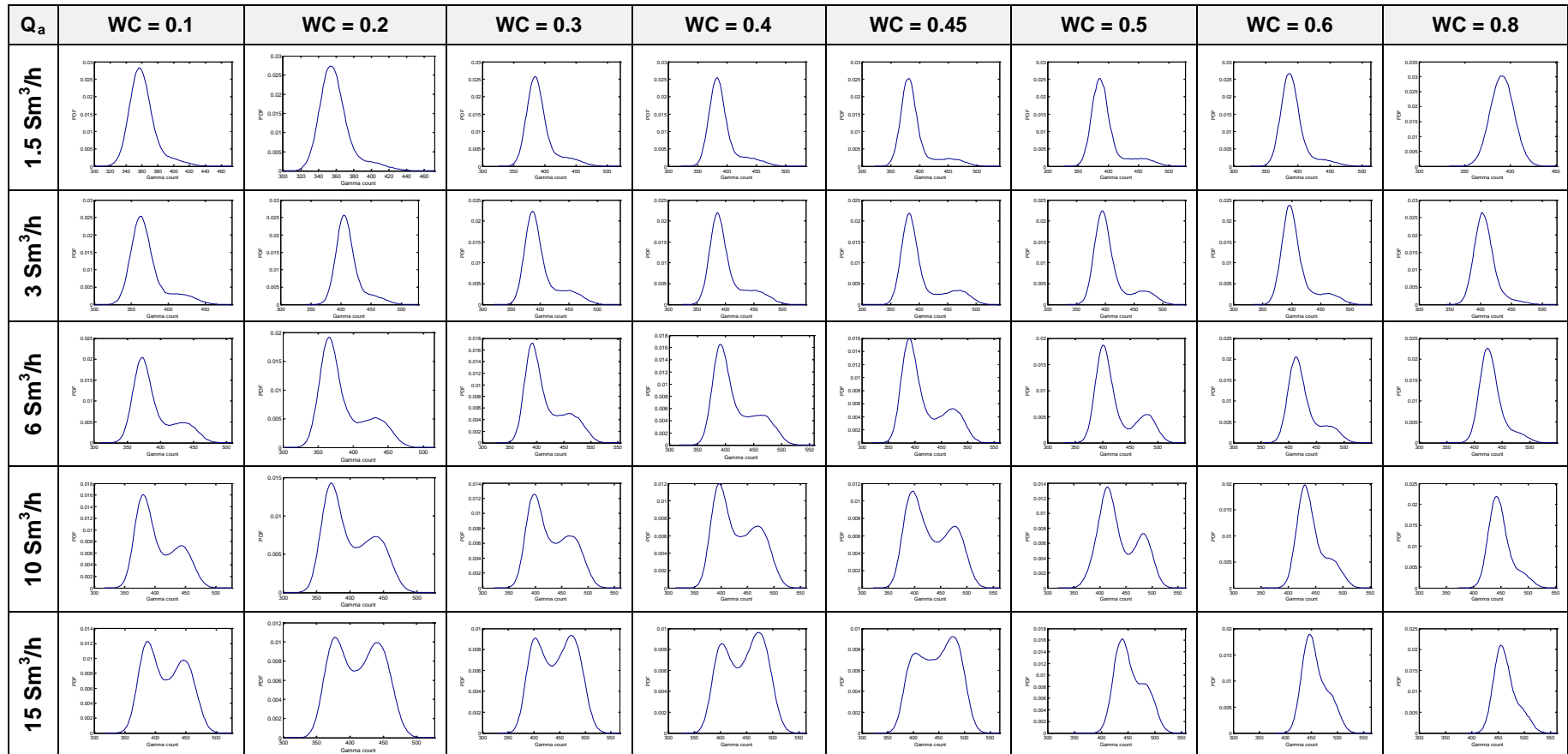## Appendix C-1 (Experiments at mixture liquid superficial velocity of 0.25 m/s)

Table 6-1: PDF profiles of gamma count signals for air-oil-water flow tests at mixture liquid superficial velocity of 0.25 m/s

Appendix C-2 (Experiments at mixture liquid superficial velocity of 0.5 m/s)

Table 6-2: PDF profiles of gamma count signals for air-oil-water flow tests at mixture liquid superficial velocity of 0.5 m/s
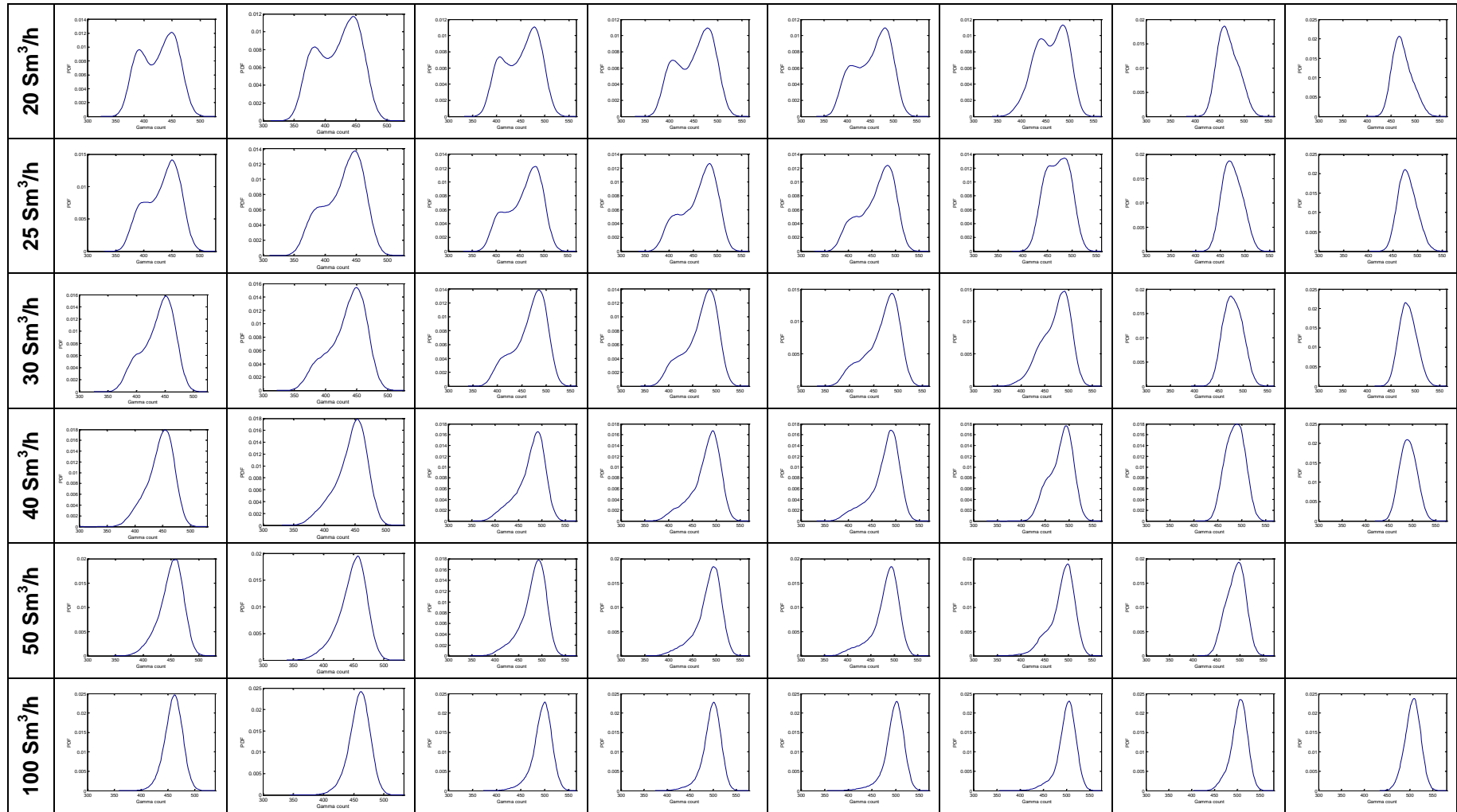
Appendix C-3 (Experiments at mixture liquid superficial velocity of 1 m/s)

Table 6-3: PDF profiles of gamma count signals for air-oil-water flow tests at mixture liquid superficial velocity of 1 m/s

The table shows a 9×3 grid of probability density function (PDF) plots. Columns are labeled by water cut (WC) values and rows by gas flow rate (Q_a).

Q_a	WC = 0.1	WC = 0.2	WC = 0.3	WC = 0.4	WC = 0.42	WC = 0.45	WC = 0.5	WC = 0.6	WC = 0.8
30 Sm³/h									
50 Sm³/h									
100 Sm³/h									